NASA/CR—2007-214678

Experimental Investigation of Transition to Turbulence as Affected by Passing Wakes: Effects of High FSTI and Increased Rod Spacing

Richard W. Kaszeta, Terrence W. Simon, Nan Jiang, and Federico Ottaviani
University of Minnesota, Minneapolis, Minnesota

March 2007

NASA STI Program . . . in Profile

Since its founding, NASA has been dedicated to the advancement of aeronautics and space science. The NASA Scientific and Technical Information (STI) program plays a key part in helping NASA maintain this important role.

The NASA STI Program operates under the auspices of the Agency Chief Information Officer. It collects, organizes, provides for archiving, and disseminates NASA's STI. The NASA STI program provides access to the NASA Aeronautics and Space Database and its public interface, the NASA Technical Reports Server, thus providing one of the largest collections of aeronautical and space science STI in the world. Results are published in both non-NASA channels and by NASA in the NASA STI Report Series, which includes the following report types:

- TECHNICAL PUBLICATION. Reports of completed research or a major significant phase of research that present the results of NASA programs and include extensive data or theoretical analysis. Includes compilations of significant scientific and technical data and information deemed to be of continuing reference value. NASA counterpart of peer-reviewed formal professional papers but has less stringent limitations on manuscript length and extent of graphic presentations.

- TECHNICAL MEMORANDUM. Scientific and technical findings that are preliminary or of specialized interest, e.g., quick release reports, working papers, and bibliographies that contain minimal annotation. Does not contain extensive analysis.

- CONTRACTOR REPORT. Scientific and technical findings by NASA-sponsored contractors and grantees.

- CONFERENCE PUBLICATION. Collected papers from scientific and technical conferences, symposia, seminars, or other meetings sponsored or cosponsored by NASA.

- SPECIAL PUBLICATION. Scientific, technical, or historical information from NASA programs, projects, and missions, often concerned with subjects having substantial public interest.

- TECHNICAL TRANSLATION. English-language translations of foreign scientific and technical material pertinent to NASA's mission.

Specialized services also include creating custom thesauri, building customized databases, organizing and publishing research results.

For more information about the NASA STI program, see the following:

- Access the NASA STI program home page at *http://www.sti.nasa.gov*

- E-mail your question via the Internet to *help@sti.nasa.gov*

- Fax your question to the NASA STI Help Desk at 301–621–0134

- Telephone the NASA STI Help Desk at 301–621–0390

- Write to:
  NASA Center for AeroSpace Information (CASI)
  7115 Standard Drive
  Hanover, MD 21076–1320

NASA/CR—2007-214678

Experimental Investigation of Transition to Turbulence as Affected by Passing Wakes: Effects of High FSTI and Increased Rod Spacing

Richard W. Kaszeta, Terrence W. Simon, Nan Jiang, and Federico Ottaviani
University of Minnesota, Minneapolis, Minnesota

Prepared under Cooperative Agreement NCC3–652

National Aeronautics and
Space Administration

Glenn Research Center
Cleveland, Ohio 44135

March 2007

Acknowledgments

This project was supported by NASA Glenn Research Center, Cooperative Agreement NCC3–652. The technical monitor was Dr. David E. Ashpis. His guidance, thorough review and coordination of researchers on the NASA LP Turbine Program are greatly appreciated. Support was also from the National Science Foundation Research Fellowship Fund and the University of Minnesota Graduate School, Graduate Research Fellowship, and Dissertation Fellowship Funds. Special thanks go also to Professor Ralph Volino of the U.S. Naval Academy and Dr. William Solomon of General Electric Company for their help on spectral measurements and turbulence intermittency calculations. The authors would like to also thank Mr. Bob Nelson and Mr. Patrick Nelsen at the Mechanical Engineering Department Research Shop for their excellent help with fabrication of the test facility.

This work was sponsored by the Fundamental Aeronautics Program at the NASA Glenn Research Center.

Level of Review: This material has been technically reviewed by NASA technical management.

Available from

NASA Center for Aerospace Information
7115 Standard Drive
Hanover, MD 21076–1320

National Technical Information Service
5285 Port Royal Road
Springfield, VA 22161

Available electronically at http://gltrs.grc.nasa.gov

Executive Summary

Experimental results from a study of the effects of passing wakes upon laminar-to-turbulent transition in a low-pressure turbine passage are presented. The test section geometry is designed to simulate the effects of unsteady wakes resulting from rotor-stator interaction upon laminar-to-turbulent transition in turbine blade boundary layers and separated flow regions over suction surfaces. Single-wire, thermal anemometry techniques are used to measure time-resolved and phase-averaged, wall-normal profiles of velocity, turbulence intensity and intermittency at multiple streamwise locations over the turbine airfoil suction surface. The Reynolds number based on suction surface length and stage exit velocity is 50,000. This study compares a previously documented base case flow[1] having an approach flow turbulence intensity of 2.5% and a wake passing Strouhal number of 0.792 to two additional cases: one having an increased rod spacing case having a wake passing Strouhal number of 0.396, and another having an elevated approach flow turbulence intensity of 10%. From these data, the effects of increased rod spacing and elevated $FSTI$ upon transition and separation processes in the near-wall flow are documented. The results show that a decreased wake passing Strouhal number results in an earlier separation with a larger separation bubble, while the elevated $FSTI$ results in earlier separation, but with a shorter, thinner, separation bubble. The data and animations are included in an accompanying CD–ROM.

[1]Kaszeta, R.W.; and Simon T.W.: Experimental Investigation of Transition to Turbulence as Affected by Passing Wakes. NASA/CR—2002-212104, 2002.

Contents

List of Figures **ix**

List of Tables **xvii**

Nomenclature **xix**

Chapter 1 Introduction **1**

1.1 Motivation 1

1.2 The Present Study 2

Chapter 2 Experimental Test Facility **5**

2.1 The Experimental Facility 5

2.1.1 Instrumentation 6

2.2 Experimental Procedure 6

2.2.1 Experimental Uncertainty 7

Chapter 3 Documentation of Flow Parameters **13**

3.1 Operating Parameters 13

3.2 Approach Flow Uniformity 14

3.2.1 Low-FSTI Cases 14

3.2.2 High-FSTI Case 15
3.3 Turbulence Quantities 22
3.3.1 Low-FSTI Cases 22
3.3.2 High-FSTI Case 24
3.4 Wake Characterization 32
3.4.1 Low-FSTI Cases 32
3.4.2 High-FSTI Case 32
3.5 Pressure Profiles 35

Chapter 4 The Increased Wake Spacing Case Results 41
4.1 Introduction 41
4.2 Experimental Results 41
4.2.1 General Features 42
4.2.2 Separation Points 43
4.2.3 Transition Onset 46
4.2.4 Narrower Wakes 47
4.2.5 Slightly Stronger Wakes 47
4.2.6 Thicker Boundary Layer 47
4.2.7 Larger Separation Bubble 47
4.2.8 Distinct Wakes 48

Chapter 5 High-FSTI Results 91
5.1 Introduction 91
5.2 Experimental Results 91
5.2.1 Separation Points 92
5.2.2 Transition Onset 93
5.2.3 Stronger Wakes 93

5.2.4 Less Response of the Boundary Layer to Freestream Influences 93
5.2.5 Less "Calming" of the Flow as the Wake Passes 94
5.2.6 Earlier Reattachment 94
5.2.7 Merging Wakes 94

Chapter 6 Conclusions **127**

6.1 General Significance and Applicability of the Results 127
6.2 Specific Conclusions: Increased Wake Spacing Case 127
6.3 Specific Conclusions: High-FSTI Case 128
6.4 Considerations for Further Study 128

References **130**

Appendix A Facility Geometry **135**

Appendix B Source Code Listings **139**

B.1 automate2.c 141
B.2 p09.m 146
B.3 p09inter.m 147
B.4 sp09.m 152
B.5 sp09inter.m 153
B.6 hp09.m 157
B.7 hp09inter.m 159
B.8 lengthscale.m 163

Appendix C CD Animations and Figures **165**

C.1 Digital Copy of this Report 165
C.2 ASCII-Tabulated Data 165
C.3 Multidimensional Visualizations 166

C.4 Case Comparison Visualizations 166
C.5 Wake Generator Movies 166

List of Figures

2.1 Cross-sectional view of the wake generator. 9

2.2 PAK-B airfoil geometry 10

2.3 Turbulence grids used $FSTI = 10\%$. Blowing grid on the left and square passive grid on the right. 11

2.4 Blown jet grid 12

3.1 Cross-sectional view of the wake generator passage 17

3.2 Inlet flow 2-D single-sensor hot-wire survey, low-$FSTI$ cases 18

3.3 Inlet flow velocity and turbulence intensity distributions, low-$FSTI$ cases . 19

3.4 Inlet flow 2-D single-sensor hot-wire survey, high-$FSTI$ case 20

3.5 Inlet flow velocity and turbulence intensity distributions, high-$FSTI$ case . 21

3.6 Power spectral distributions of turbulence, low-$FSTI$ cases 28

3.7 Power spectral distributions of turbulence, plotted in energy coordinates, low-$FSTI$ cases 29

3.8 Power spectral distributions of turbulence, high-$FSTI$ case 30

3.9 Power spectral distributions of turbulence, plotted in energy coordinates, high-$FSTI$ case 31

3.10 Ensemble-average velocity and TI of 600 wakes, base case 33

3.11 Ensemble-average velocity and TI of 225 wakes, increased wake spacing case 34

3.12 Ensemble-average velocity and TI of 600 wakes, base case 36

3.13 Ensemble-average velocity and TI of 440 wakes, high-$FSTI$ case 37

3.14 Pressure Coefficient Distribution at $Re_{L_{ss}} = 50{,}000$ and $TI = 2.5\%$ 39

3.15 Pressure Coefficient Distribution at $Re_{L_{ss}} = 50{,}000$ and $TI = 10\%$ 39

4.1 Approximate wall shear stress, base case 49

4.2 Approximate wall shear stress, increased wake spacing case 49

4.3 Velocity, $\tilde{u}$, (m/s), at station 4 ($s/L_{ss} = 31.36\%$) 50

4.4 Velocity rms, $\widetilde{u_{rms}}$, (m/s), at station 4 ($s/L_{ss} = 31.36\%$) 50

4.5 Turbulence Intensity, $\widetilde{TI}$, at station 4 ($s/L_{ss} = 31.36\%$) 51

4.6 Intermittency, $\tilde{\gamma}$, at station 4 ($s/L_{ss} = 31.36\%$) 51

4.7 Velocity, $\tilde{u}$, (m/s), at station 5 ($s/L_{ss} = 37.35\%$) 52

4.8 Velocity rms, $\widetilde{u_{rms}}$, (m/s), at station 5 ($s/L_{ss} = 37.35\%$) 52

4.9 Turbulence Intensity, $\widetilde{TI}$, at station 5 ($s/L_{ss} = 37.35\%$) 53

4.10 Intermittency, $\tilde{\gamma}$, at station 5 ($s/L_{ss} = 37.35\%$) 53

4.11 Velocity, $\tilde{u}$, (m/s), at station 6 ($s/L_{ss} = 43.34\%$) 54

4.12 Velocity rms, $\widetilde{u_{rms}}$, (m/s), at station 6 ($s/L_{ss} = 43.34\%$) 54

4.13 Turbulence Intensity, $\widetilde{TI}$, at station 6 ($s/L_{ss} = 43.34\%$) 55

4.14 Intermittency, $\tilde{\gamma}$, at station 6 ($s/L_{ss} = 43.34\%$) 55

4.15 Velocity, $\tilde{u}$, (m/s), at station 7 ($s/L_{ss} = 49.33\%$) 56

4.16 Velocity rms, $\widetilde{u_{rms}}$, (m/s), at station 7 ($s/L_{ss} = 49.33\%$) 56

4.17 Turbulence Intensity, $\widetilde{TI}$, at station 7 ($s/L_{ss} = 49.33\%$) 57

4.18 Intermittency, $\tilde{\gamma}$, at station 7 ($s/L_{ss} = 49.33\%$) 57

4.19 Velocity, $\tilde{u}$, (m/s), at station 8 ($s/L_{ss} = 55.33\%$) 58

4.20 Velocity rms, $\widetilde{u_{rms}}$, (m/s), at station 8 ($s/L_{ss} = 55.33\%$) 58

4.21 Turbulence Intensity, $\widetilde{TI}$, at station 8 ($s/L_{ss} = 55.33\%$) 59

4.22 Intermittency, $\tilde{\gamma}$, at station 8 ($s/L_{ss} = 55.33\%$) 59

4.23 Velocity, $\tilde{u}$, (m/s), at station 9 ($s/L_{ss} = 61.32\%$) 60

4.24 Velocity rms, $\widetilde{u_{rms}}$, (m/s), at station 9 ($s/L_{ss} = 61.32\%$) 60

4.25 Turbulence Intensity, $\widetilde{TI}$, at station 9 ($s/L_{ss} = 61.32\%$) 61

4.26 Intermittency, $\tilde{\gamma}$, at station 9 ($s/L_{ss} = 61.32\%$) 61

4.27 Velocity, $\tilde{u}$, (m/s), at station 10 ($s/L_{ss} = 70.31\%$) 62

4.28 Velocity rms, $\widetilde{u_{rms}}$, (m/s), at station 10 ($s/L_{ss} = 70.31\%$) 62

4.29 Turbulence Intensity, $\widetilde{TI}$, at station 10 ($s/L_{ss} = 70.31\%$) 63

4.30 Intermittency, $\tilde{\gamma}$, at station 10 ($s/L_{ss} = 70.31\%$) 63

4.31 Velocity, $\tilde{u}$, (m/s), at station 11 ($s/L_{ss} = 76.11\%$) 64

4.32 Velocity rms, $\widetilde{u_{rms}}$, (m/s), at station 11 ($s/L_{ss} = 76.11\%$) 64

4.33 Turbulence Intensity, $\widetilde{TI}$, at station 11 ($s/L_{ss} = 76.11\%$) 65

4.34 Intermittency, $\tilde{\gamma}$, at station 11 ($s/L_{ss} = 76.11\%$) 65

4.35 Velocity, $\tilde{u}$, (m/s), at station 12 ($s/L_{ss} = 84.00\%$) 66

4.36 Velocity rms, $\widetilde{u_{rms}}$, (m/s), at station 12 ($s/L_{ss} = 84.00\%$) 66

4.37 Turbulence Intensity, $\widetilde{TI}$, at station 12 ($s/L_{ss} = 84.00\%$) 67

4.38 Intermittency, $\tilde{\gamma}$, at station 12 ($s/L_{ss} = 84.00\%$) 67

4.39 Velocity, $\tilde{u}$, (m/s), at station 13 ($s/L_{ss} = 93.49\%$) 68

4.40 Velocity rms, $\widetilde{u_{rms}}$, (m/s), at station 13 ($s/L_{ss} = 93.49\%$) 68

4.41 Turbulence Intensity, $\widetilde{TI}$, at station 13 ($s/L_{ss} = 93.49\%$) 69

4.42 Intermittency, $\tilde{\gamma}$, at station 13 ($s/L_{ss} = 93.49\%$) 69

4.43 Phase average velocity $\tilde{u}(y, \theta)$ at station 4 ($s/L_{ss} = 31.36\%$), presented as a function of θ, base case. 70

4.44 Phase average velocity $\tilde{u}(y, \theta)$ at station 4 ($s/L_{ss} = 31.36\%$), presented as a function of θ, increased wake spacing case. 71

4.45 Phase average velocity $\tilde{u}(y, \theta)$ at station 5 ($s/L_{ss} = 37.35\%$), presented as a function of θ, base case. 72

4.46 Phase average velocity $\tilde{u}(y, \theta)$ at station 5 ($s/L_{ss} = 37.35\%$), presented as a function of θ, increased wake spacing case. 73

4.47 Phase average velocity $\tilde{u}(y,\theta)$ at station 6 ($s/L_{ss} = 43.34\%$), presented as a function of θ, base case. 74

4.48 Phase average velocity $\tilde{u}(y,\theta)$ at station 6 ($s/L_{ss} = 43.34\%$), presented as a function of θ, increased wake spacing case. 75

4.49 Phase average velocity $\tilde{u}(y,\theta)$ at station 7 ($s/L_{ss} = 49.33\%$), presented as a function of θ, base case. 76

4.50 Phase average velocity $\tilde{u}(y,\theta)$ at station 7 ($s/L_{ss} = 49.33\%$), presented as a function of θ, increased wake spacing case. 77

4.51 Phase average velocity $\tilde{u}(y,\theta)$ at station 8 ($s/L_{ss} = 55.33\%$), presented as a function of θ, base case. 78

4.52 Phase average velocity $\tilde{u}(y,\theta)$ at station 8 ($s/L_{ss} = 55.33\%$), presented as a function of θ, increased wake spacing case. 79

4.53 Phase average velocity $\tilde{u}(y,\theta)$ at station 9 ($s/L_{ss} = 61.32\%$), presented as a function of θ., base case 80

4.54 Phase average velocity $\tilde{u}(y,\theta)$ at station 9 ($s/L_{ss} = 61.32\%$), presented as a function of θ, increased wake spacing case. 81

4.55 Phase average velocity $\tilde{u}(y,\theta)$ at station 10 ($s/L_{ss} = 70.31\%$), presented as a function of θ, base case. 82

4.56 Phase average velocity $\tilde{u}(y,\theta)$ at station 10 ($s/L_{ss} = 70.31\%$), presented as a function of θ, increased wake spacing case. 83

4.57 Phase average velocity $\tilde{u}(y,\theta)$ at station 11 ($s/L_{ss} = 76.11\%$), presented as a function of θ, base case. 84

4.58 Phase average velocity $\tilde{u}(y,\theta)$ at station 11 ($s/L_{ss} = 76.11\%$), presented as a function of θ, increased wake spacing case. 85

4.59 Phase average velocity $\tilde{u}(y,\theta)$ at station 12 ($s/L_{ss} = 84.00\%$), presented as a function of θ, base case. 86

4.60 Phase average velocity $\tilde{u}(y,\theta)$ at station 12 ($s/L_{ss} = 84.00\%$), presented as a function of θ, increased wake spacing case. 87

4.61 Phase average velocity $\tilde{u}(y,\theta)$ at station 13 ($s/L_{ss} = 93.49\%$), presented as a function of θ, base case. 88

4.62 Phase average velocity $\tilde{u}(y,\theta)$ at station 13 ($s/L_{ss} = 93.49\%$), presented as a function of θ, increased wake spacing case. 89

5.1 Approximate wall shear stress, base case 95
5.2 Approximate wall shear stress, high-$FSTI$ case 95
5.3 Velocity, $\tilde{u}$, (m/s), at station 4 ($s/L_{ss} = 31.36\%$) 96
5.4 Velocity rms, $\widetilde{u_{rms}}$, (m/s), at station 4 ($s/L_{ss} = 31.36\%$) 96
5.5 Turbulence Intensity, $\widetilde{TI}$, at station 4 ($s/L_{ss} = 31.36\%$) 97
5.6 Intermittency, $\tilde{\gamma}$, at station 4 ($s/L_{ss} = 31.36\%$) 97
5.7 Velocity, $\tilde{u}$, (m/s), at station 5 ($s/L_{ss} = 37.35\%$) 98
5.8 Velocity rms, $\widetilde{u_{rms}}$, (m/s), at station 5 ($s/L_{ss} = 37.35\%$) 98
5.9 Turbulence Intensity, $\widetilde{TI}$, at station 5 ($s/L_{ss} = 37.35\%$) 99
5.10 Intermittency, $\tilde{\gamma}$, at station 5 ($s/L_{ss} = 37.35\%$) 99
5.11 Velocity, $\tilde{u}$, (m/s), at station 6 ($s/L_{ss} = 43.34\%$) 100
5.12 Velocity rms, $\widetilde{u_{rms}}$, (m/s), at station 6 ($s/L_{ss} = 43.34\%$) 100
5.13 Turbulence Intensity, $\widetilde{TI}$, at station 6 ($s/L_{ss} = 43.34\%$) 101
5.14 Intermittency, $\tilde{\gamma}$, at station 6 ($s/L_{ss} = 43.34\%$) 101
5.15 Velocity, $\tilde{u}$, (m/s), at station 7 ($s/L_{ss} = 49.33\%$) 102
5.16 Velocity rms, $\widetilde{u_{rms}}$, (m/s), at station 7 ($s/L_{ss} = 49.33\%$) 102
5.17 Turbulence Intensity, $\widetilde{TI}$, at station 7 ($s/L_{ss} = 49.33\%$) 103
5.18 Intermittency, $\tilde{\gamma}$, at station 7 ($s/L_{ss} = 49.33\%$) 103
5.19 Velocity, $\tilde{u}$, (m/s), at station 8 ($s/L_{ss} = 55.33\%$) 104
5.20 Velocity rms, $\widetilde{u_{rms}}$, (m/s), at station 8 ($s/L_{ss} = 55.33\%$) 104
5.21 Turbulence Intensity, $\widetilde{TI}$, at station 8 ($s/L_{ss} = 55.33\%$) 105
5.22 Intermittency, $\tilde{\gamma}$, at station 8 ($s/L_{ss} = 55.33\%$) 105
5.23 Velocity, $\tilde{u}$, (m/s), at station 9 ($s/L_{ss} = 61.32\%$) 106
5.24 Velocity rms, $\widetilde{u_{rms}}$, (m/s), at station 9 ($s/L_{ss} = 61.32\%$) 106
5.25 Turbulence Intensity, $\widetilde{TI}$, at station 9 ($s/L_{ss} = 61.32\%$) 107
5.26 Intermittency, $\tilde{\gamma}$, at station 9 ($s/L_{ss} = 61.32\%$) 107

5.27 Velocity, $\tilde{u}$, (m/s), at station 10 ($s/L_{ss} = 70.31\%$) 108

5.28 Velocity rms, $\widetilde{u_{rms}}$, (m/s), at station 10 ($s/L_{ss} = 70.31\%$) 108

5.29 Turbulence Intensity, $\widetilde{TI}$, at station 10 ($s/L_{ss} = 70.31\%$) 109

5.30 Intermittency, $\tilde{\gamma}$, at station 10 ($s/L_{ss} = 70.31\%$) 109

5.31 Velocity, $\tilde{u}$, (m/s), at station 11 ($s/L_{ss} = 76.11\%$) 110

5.32 Velocity rms, $\widetilde{u_{rms}}$, (m/s), at station 11 ($s/L_{ss} = 76.11\%$) 110

5.33 Turbulence Intensity, $\widetilde{TI}$, at station 11 ($s/L_{ss} = 76.11\%$) 111

5.34 Intermittency, $\tilde{\gamma}$, at station 11 ($s/L_{ss} = 76.11\%$) 111

5.35 Velocity, $\tilde{u}$, (m/s), at station 12 ($s/L_{ss} = 84.00\%$) 112

5.36 Velocity rms, $\widetilde{u_{rms}}$, (m/s), at station 12 ($s/L_{ss} = 84.00\%$) 112

5.37 Turbulence Intensity, $\widetilde{TI}$, at station 12 ($s/L_{ss} = 84.00\%$) 113

5.38 Intermittency, $\tilde{\gamma}$, at station 12 ($s/L_{ss} = 84.00\%$) 113

5.39 Velocity, $\tilde{u}$, (m/s), at station 13 ($s/L_{ss} = 93.49\%$) 114

5.40 Velocity rms, $\widetilde{u_{rms}}$, (m/s), at station 13 ($s/L_{ss} = 93.49\%$) 114

5.41 Turbulence Intensity, $\widetilde{TI}$, at station 13 ($s/L_{ss} = 93.49\%$) 115

5.42 Intermittency, $\tilde{\gamma}$, at station 13 ($s/L_{ss} = 93.49\%$) 115

5.43 Phase average velocity $\tilde{u}(y, \theta)$ at station 4 ($s/L_{ss} = 31.36\%$), presented as a function of θ, high-$FSTI$ case. 116

5.44 Phase average velocity $\tilde{u}(y, \theta)$ at station 5 ($s/L_{ss} = 37.35\%$), presented as a function of θ, high-$FSTI$ case. 117

5.45 Phase average velocity $\tilde{u}(y, \theta)$ at station 6 ($s/L_{ss} = 43.34\%$), presented as a function of θ, high-$FSTI$ case. 118

5.46 Phase average velocity $\tilde{u}(y, \theta)$ at station 7 ($s/L_{ss} = 49.33\%$), presented as a function of θ, high-$FSTI$ case. 119

5.47 Phase average velocity $\tilde{u}(y, \theta)$ at station 8 ($s/L_{ss} = 55.33\%$), presented as a function of θ, high-$FSTI$ case. 120

5.48 Phase average velocity $\tilde{u}(y, \theta)$ at station 9 ($s/L_{ss} = 61.32\%$), presented as a function of θ, high-$FSTI$ case. 121

5.49 Phase average velocity $\tilde{u}(y,\theta)$ at station 10 ($s/L_{ss} = 70.31\%$), presented as a function of θ, high-$FSTI$ case. 122

5.50 Phase average velocity $\tilde{u}(y,\theta)$ at station 11 ($s/L_{ss} = 76.11\%$), presented as a function of θ, high-$FSTI$ case. 123

5.51 Phase average velocity $\tilde{u}(y,\theta)$ at station 12 ($s/L_{ss} = 84.00\%$), presented as a function of θ, high-$FSTI$ case. 124

5.52 Phase average velocity $\tilde{u}(y,\theta)$ at station 13 ($s/L_{ss} = 93.49\%$), presented as a function of θ, high-$FSTI$ case. 125

A.1 Wake generator dimensions and geometry 136

A.2 Turbine passage dimensions and geometry 137

C.1 ACSII File Format 167

List of Tables

1.1 Summary of various cases with or without wakes 4

2.1 Profile locations on the suction surface 8

2.2 Wall-normal measurement locations 8

3.1 Turbulence quantities for the inlet flow with a suction surface length Reynolds number, $Re_{L_{ss}}$, of 50,000 and a freestream turbulence intensity, TI, of 2.5% . 26

3.2 Turbulence quantities for the inlet flow with $Re_{L_{ss}} = 50{,}000$ and $TI = 10\%$. 26

3.3 Turbulence quantities for the steady inlet flow with $Re_{L_{ss}} = 50{,}000$ and $TI = 2.5\%$ 27

3.4 Turbulence quantities for the steady inlet flow with $Re_{L_{ss}} = 50{,}000$ and $TI = 10\%$ 27

A.1 Wake generator and turbine passage dimensions 138

B.1 Included programs 140

C.1 Description of ASCII data files 167

C.2 Visualization animations, base case 168

C.3 Visualization animations, increased wake spacing case 169

C.4 Visualization animations, high-FSTI case 170

C.5 Comparison animations, increased wake spacing case 171

C.6 Comparison animations, high-FSTI case 172

Nomenclature

C_p	Pressure coefficient
d	Wake generator rod diameter
E_u	Power density function of u'
E_v	Power density function of v'
E_w	Power density function of w'
f	Frequency
$FSTI$	Freestream turbulence intensity
k	Turbulent kinetic energy, $0.5(\overline{u'u' + v'v' + w'w'})$
L	True chord length
L_r	Rod spacing along sled axis
L_u	Energy length scale
L_x	Axial chord length
L_z	Airfoil span length
L_{ss}	Suction surface length
l	Distance along the blade's true chord
ℓ_1	Inlet channel width
ℓ_2	Wake generator streamwise length
ℓ_3	Wake generator upstream flap length
ℓ_4	Wake generator downstream flap length
ℓ_5	Suction surface bleed slot width

ℓ_6	Pressure surface bleed slot width
ℓ_7	Distance from the inlet plane to the point mid-span between the leading edges
M	Number of data points used in the autocorrelation
N	Number of data points in the sample
P	Airfoil pitch
P_s	Static pressure
P_t	Total pressure
$P_{s,exit}$	Static pressure at passage exit
$Q_{u,i}$	Auto-correlation of u' at point i
$Re_{L_{ss}}$	Reynolds number based on suction surface length, L_{ss}, and passage exit velocity
S	Wake Strouhal number, fL_x/u_x
s	Distance along the blade's suction surface
T	Wake passing period
t	Time
TI	Turbulence intensity
u	Streamwise component of velocity
u_r	Rod velocity
u_x	Axial component of inlet velocity
U_{fs}	Freestream velocity, velocity at the edge of the near-wall viscous zone
v	Wall-normal component of velocity
w	Spanwise component of velocity
x	Axial distance from blade leading edge
y	Normal distance from the suction surface
z	Spanwise distance from the measurement plane

Greek:

β_1	Airfoil inlet angle
β_2	Airfoil outlet angle

ϵ	Dissipation of turbulence kinetic energy
γ	Turbulence intermittency
λ	Taylor microscale
$\Lambda_{u,x}$	Integral length scale of u' in streamwise direction
$\Lambda_{v,x}$	Integral length scale of v' in streamwise direction
$\Lambda_{w,x}$	Integral length scale of w' in streamwise direction
μ	Viscosity
ν	Kinematic viscosity
τ_w	Wall shear stress, $\mu \left.\frac{\partial u}{\partial y}\right\|_{y=0}$
θ	Momentum thickness, Phase Angle

Sub/Superscripts:

$\bar{}$	Time-average
$\tilde{}$	Phase-average
$'$	Fluctuation about mean value
rms	Root mean square of quantity

Chapter 1

Introduction

1.1 Motivation

Low Pressure Turbines (LPT) are commonly used in the aerospace industry, primarily to provide input shaft power for fan and compressor components of turbine engines. Turbine design engineers seek to develop engines of increased efficiency and decreased weight, while reducing cost. The LPT has been shown to be a component worthy of attention in this endeavor. Key to such improvement is a better understanding of low-Reynolds number flow transition and separation.

Though transition to turbulence has been studied for many years, transition in LP turbine engines, with elevated disturbance levels and periodic unsteadiness is less well documented. High levels of freestream turbulence present in the engine cause earlier transition and such transition can prevent separation in spite of the adverse pressure gradient imposed on the boundary layer on the trailing portion of the suction surface of a turbine airfoil. It has been observed by a number of researchers that disturbances in the external boundary layer can trigger transition phenomena in the near-wall boundary layer. One such work was done by Dietz (1999), who investigated the receptivity of a boundary layer to harmonic disturbances in the freestream.

Thus, blades in such an environment may be designed for higher loading if the effects of passing wakes and elevated turbulence on bypass transition are properly included in the design. In a seminal paper on this topic, Mayle (1991) observed in 1991 that the majority of the experimental work which is focused upon laminar-to-turbulent transition has been

conducted under lower turbulence and steady flow conditions. However, the actual flow present in turbine engines has turbulence levels of $12 - 15\%$, with significant unsteadiness due to wakes (Heitland (2000)). Mayle suggested that investigations should be conducted to document the effects of wakes on transition over turbine airfoil surfaces. Since 1991, considerable progress on the topic has ensued, as will be discussed.

1.2 The Present Study

A review of research on transition in LP turbines is presented by Simon and Kaszeta (2000). While some experimental data which document the flow field and transition in turbomachinery flows exist, much of the research has been conducted under steady flow conditions. Of the unsteady-flow experimental studies, the majority presented only surface measurements, such as surface pseudo-shear stress through the use of hot-film sensors, or were conducted in more simplified geometries. Few in-flow measurements of turbine passages have been presented. Howell et al. (2001) measured unsteady boundary layer behavior in two high-lift and one ultra-high-lift LP turbines using surface mounted hot film sensors. Regions of wake-induced transition, natural transition and calming in the boundary layer were identified and effects of passing wakes on these regions were discussed. Wolff et al. (2000) presented velocity profiles and surface-mounted hot-film pseudo-shear-stress distributions near the trailing edge of an LP turbine blade in a turbine cascade. Some profile measurements were given in Halstead et al. (1997), but focus was on attached-flow transition. Similarly, boundary layer profiles over a curved plate disturbed by wakes were presented in Schobeiri et al. (1995). Kaszeta et al. (2003, 2005) analyzed the experimental data with the aid of the skewness of pseudo shear stress measured by using hot film surface sensors. A more detailed review of recent bypass transition work can be found in Jiang and Simon (2003a).

Previously, Kaszeta and Simon (2002) and Kaszeta et al. (2001) presented wall-normal boundary layer profiles of velocity, turbulence intensity and intermittency, using a modified version of the cascade simulator used in Qiu (1996), Qiu and Simon (1997) and Simon et al. (2000). A linear wake generator, modified from a design developed by Yuan (1999), was used to introduce periodic wakes into the flow upstream of the turbine blade leading edges, simulating the wakes created by rotor-stator interaction. The wake generator operated by sliding a rack of rods through the flow development section. Through the use of a photo-gate mounted on the sliding rack, the rods' positions could be recorded, allowing ensemble averaging of individual wakes and their influence on the LP turbine near-wall flow. By ana-

lyzing these results, ensemble averaged, wall-normal profiles of velocity, turbulence intensity and turbulence intermittency were presented for a series of locations on the turbine passage suction surface. Both the experimental geometry and the results are amenable to comparison with wake-disturbed, LP turbine computational works, such as those of Dorney et al. (2000), Wu and Durbin (2000a,b) and Suzen and Huang (2000). The application of algebraic transition models for such computation was discussed by Jiang and Simon (2003a,b, 2004)

The results presented in Kaszeta and Simon (2002) showed that one of the most significant effects of the introduction of wakes to the turbine passage was an overall increase in the level of turbulence. Kaszeta and Simon (2002) noted that the introduction of wakes disturbed the flow enough that the between-wake turbulence level was boosted to 5%, from the *FSTI* of 2.5% upstream of their wake generator. This suggests that low-Reynolds number, LP turbine flow background turbulence levels are more than 2.5%. Thus, the case presented in Kaszeta and Simon (2002) was repeated with an elevated level of *FSTI* in the flow upstream of the wake generator of 10%. The results are presented and discussed herein.

The wakes presented in Kaszeta and Simon (2002) have dimensionless Strouhal number small enough that the wakes were spaced together tightly enough that the turbulence intensity and velocity between wakes did not return to the level seen when no wakes were present. Thus, a variation of this case with a greater wake spacing would allow a study of the calming and re-growth of boundary layers expected with a longer period between wakes. This allows documentation of such a flow and indicates the conditions that would exist if fewer airfoils were utilized in a particular half-stage. Important to this are the effects of temporal acceleration associated with passing wakes, as discussed by Jiang and Simon (2003c, 2005). The current document presents results from a case in which the spacing between rods has been doubled or (the wake Strouhal number has been halved) from that of the Kaszeta and Simon (2002) study.

The objectives of this study are as follows:

1. Document the development of boundary layers in a simulated turbine passage under the influence of rod-generated wakes using the flow conditions of Kaszeta and Simon (2002) but with an increased rod spacing. For the case chosen, the rod spacing, L_r/P, is 2.0, effectively doubling the wake period, T, from that of Kaszeta and Simon (2002) without affecting the rod velocity to approach flow velocity ratio.

2. Document the development of boundary layers in a simulated turbine passage under

the influence of rod-generated wakes using the same flow conditions as Kaszeta and Simon (2002), but with an elevated level of $FSTI$ in the flow approaching the wake generator of 10%.

3. By comparing these data with the previous data reported by Kaszeta and Simon (2002), one can identify the effects of increased rod spacing and elevated approach flow $FSTI$ upon the transition and separation processes present on the suction surface of the low-pressure turbine airfoil.

4. By comparison of these data with previous data reported by Simon et al. (2000) one can identify the effects of wakes. Table 1.1 indicated the various cases which could be used in this comparison study.

Table 1.1: Summary of various cases with or without wakes

Cases	$TI(\%)$	WakeL_r/P	Primary Sources of Documentation
Base case	2.5	1.0	Kaszeta and Simon (2002)
No-wake Comparison	2.5	No-wake	Simon et al. (2000)
High TI Case	10	1.0	This report
Increased Spacing Case	2.5	2.0	This report
No-wake, High TI Comparison	10	No-wake	Simon et al. (2000)

Chapter 2

Experimental Test Facility

2.1 The Experimental Facility

The experimental facility, shown in Fig. 2.1, consists of a low-speed wind tunnel, a wake generator and a turbine blade passage simulator. The wake generator was designed by Yuan (1999) to simulate wakes emerging from upstream turbine stages in a low pressure turbine. It consists of a moving sled assembly which contains a series of 0.635 cm (0.25 in) stainless steel rods that simulate vane wakes, spaced at 80% of the blade chord length (the same pitch as the test airfoil pitch). The rods are located 79.4 mm upstream from the leading edges of the airfoils. The airfoil shape used for the turbine passage is the PAK-B blade profile released to research by Pratt and Whitney. The turbine passage geometry is described in Figure 2.2. Note that this facility uses a single pressure surface, a single suction surface, and leading edge bleed slots to simulate a single turbine passage.

A more complete description of the facility can be found in Kaszeta and Simon (2002) or Kaszeta (2000). However, to produce the correct flow conditions for the data sets presented here, minor modifications to the facility were required.

For the increased rod spacing case, the wake generator was modified to double the spacing of the wake generating rods by removing every other rod in the wake generating sled. Effectively, this doubles the rod spacing, L_r, resulting in a doubling of the wake period, T, while leaving the rod speed, u_r, unchanged.

For the high-$FSTI$ case, the rods removed from the wake generator were re-installed to restore the original number and spacing. To increase the approach flow turbulence intensity,

two minor modifications to the turbulence generation grid used in Kaszeta and Simon (2002) were required. To achieve a *FSTI* of 10%, the combination of a passive bar grid and a blowing grid is used, shown in Figure 2.3. A bar grid composed of a series of 1.27 cm × 1.27 cm square wooden bars, arranged to form a mesh of open squares, sized 1.27 cm × 1.91 cm, was inserted at the entrance of the flow development section (approximately 1 m upstream of the inlet plane shown in Figure 2.1). This grid provides an overall flow blockage of approximately 63% and elevates the *FSTI* in the approach flow to approximately 6%.

To further elevate the *FSTI* of the approach flow, the static rod grid used in Kaszeta and Simon (2002) was replaced with a blown jet grid, consisting of nine stainless steel tubes, 0.95 cm OD, with each rod having five pairs of 0.8 mm holes angled at ±60° to the downstream direction. These nine tubes (shown in Figure 2.4)are evenly spaced at vertical intervals of 6.745 cm. To each of the tubes high pressure air is supplied. By pressuring the manifold to 13.5 kPa above the approach flow, the blown jet grid produces enough additional turbulence to elevate the flow *FSTI* upstream of the wake generator to approximately 10%. Documentation of the approach flow turbulence for both the increased spacing and the high-*FSTI* cases is presented in Chapter 3. The complete turbine cascade geometry is described in Appendix A.

2.1.1 Instrumentation

A TSI model IFA-100 hot-wire anemometer bridge was used for velocity measurements. The anemometer was calibrated against a Pitot tube under low-turbulence conditions using the same wind tunnel and velocity range as the experiment. The anemometer's output was low-pass filtered at 20 kHz using the bridge's built-in filters. The anemometer's output was sampled at 100 kHz using an IOtech ADC-488/8SA analog-to-digital converter. With an approach flow of approximately 3 m/s, spectral measurements indicated that these filtering and sampling rates were sufficiently high to resolve the turbulence frequencies present in the flow.

2.2 Experimental Procedure

Wall-normal profiles were collected at 10 streamwise locations along the suction surface, stations p04 through p13, listed in Table 2.1, at 30 different wall-normal distances ranging from $y = 0.1$ mm to $y = 16.5$ mm, unevenly spaced with steps ranging from $\Delta y = 0.1$ mm

near the wall to $\Delta y = 1\,\text{mm}$ approaching the freestream. The y values used for this study are listed in Table 2.2. The near-wall velocity results were corrected for conduction errors using the technique describe by Wills (1962).

The wake generator was run to create a series of wakes. Each series of wakes was decomposed into individual wakes from signals provided from a photogate (a high-speed infrared diode/transistor combination) mounted on the wake generator. The photogate signals when each rod has entered the channel upstream of the turbine passage. Each wake was then further decomposed into 45 segments, each representing 2.22% of the wake's wake period. The segments from each of the wakes were then ensemble-averaged to obtain the phase-averaged velocity, $\tilde{u}$, and the rms velocity fluctuation, $\widetilde{u_{rms}}$. Additionally, the raw velocity signals were processed using the Turbulent Event Recognition Algorithm (TERA) of Falco and Gendrich (1990), as modified by Walker and Solomon (1992), to obtain turbulence intermittencies, and the phase average intermittency, $\tilde{\gamma}$ was calculated from these values. A full discussion of the TERA algorithm used in this study is in Kaszeta and Simon (2002). These measurements were taken at 30 y-positions and at 10 s-positions (p04 to p13). No data were collected at p01, since it is the leading edge of the blade, and no profiles were collected at stations p02 and p03 since it is difficult to correctly locate the probe's nearness to the wall due to geometric constraints. Further, since they are far upstream of transition, information from these profiles is of little utility.

2.2.1 Experimental Uncertainty

Using standard thermal anemometry error estimation techniques, the level of uncertainty (with 95% confidence) of the velocity measurements was determined to be $\delta u/u \approx 4.7\%$, quite acceptable for measurement of boundary layer profiles. This analysis applies to attached boundary layer flow measurements with local turbulence intensity values of less than 25%. In some cases, one or both of these requirements were violated and such data are only approximate. These cases are discussed in detail in Kaszeta and Simon (2002).

Table 2.1: Profile locations on the suction surface

Tap No.	x (cm)	x/L_x (%)	l (cm)	l/L (%)	s (cm)	s/L_{ss} (%)
p01	0.00	0.00	0	0.00	0.00	0.00
p02	0.41	3.94	0.07	0.61	0.79	5.19
p03	2.17	20.98	1.08	9.45	3.02	19.78
p04	3.90	37.62	2.48	21.70	4.79	31.36
p05	4.80	46.35	3.36	29.40	5.71	37.35
p06	5.65	54.59	4.28	37.45	6.62	43.34
p07	6.43	62.04	5.18	45.32	7.54	49.33
p08	7.10	68.54	6.04	52.84	8.45	55.33
p09	7.67	74.08	6.88	60.19	9.37	61.32
p10	8.40	81.13	8.05	70.43	10.74	70.31
p11	8.83	85.23	8.78	76.82	11.63	76.11
p12	9.38	90.55	9.73	85.13	12.83	84.00
p13	10.02	96.71	10.87	95.10	14.28	93.49

Table 2.2: Wall-normal measurement locations

Station	y
1	0.010 cm
2	0.020 cm
3	0.030 cm
4	0.050 cm
5	0.070 cm
6	0.090 cm
7	0.120 cm
8	0.150 cm
9	0.180 cm
10	0.220 cm

Station	y
11	0.260 cm
12	0.300 cm
13	0.350 cm
14	0.400 cm
15	0.450 cm
16	0.510 cm
17	0.570 cm
18	0.630 cm
19	0.700 cm
20	0.770 cm

Station	y
21	0.840 cm
22	0.920 cm
23	1.000 cm
24	1.080 cm
25	1.170 cm
26	1.260 cm
27	1.350 cm
28	1.450 cm
29	1.550 cm
30	1.650 cm

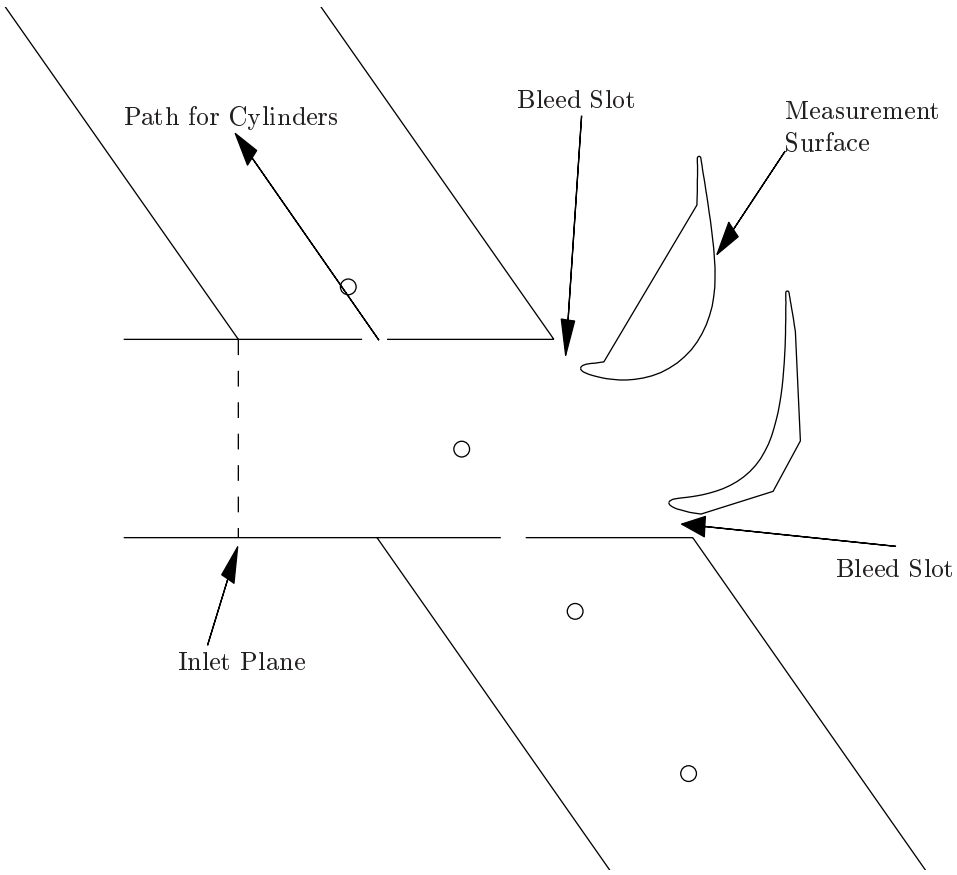

Figure 2.1: Cross-sectional view of the wake generator.

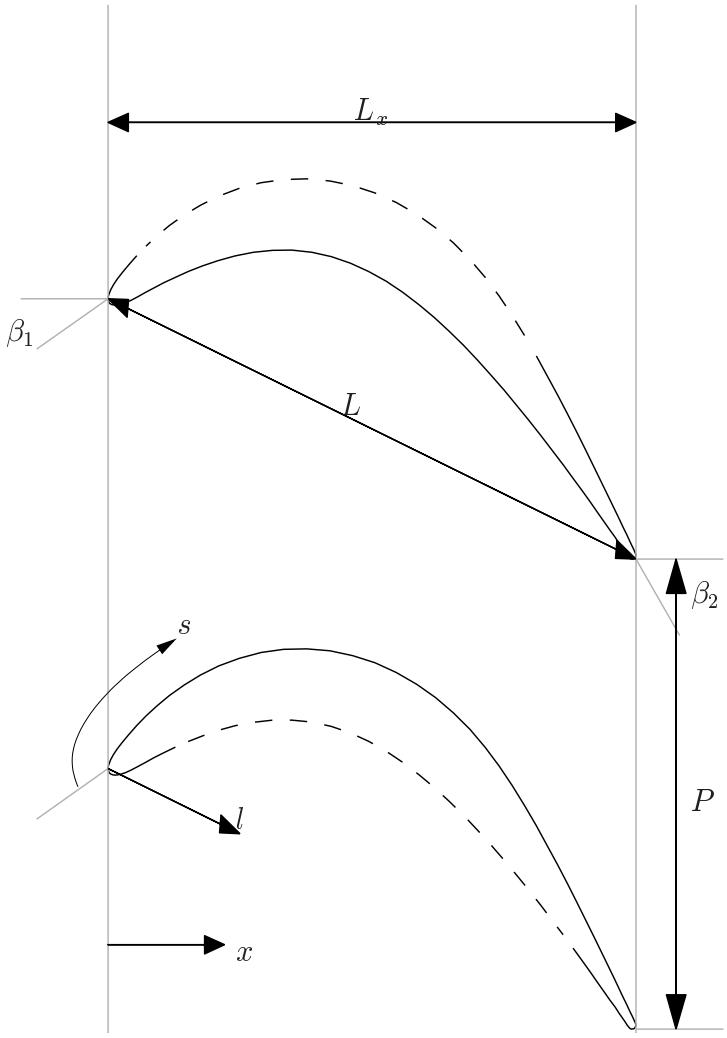

Chord length, L:	114.3 mm
Axial chord length, L_x:	103.57 mm
Suction surface length, L_{ss}:	152.76 mm
Axial chord to chord ratio, L_x/L:	0.906
Pitch to chord ratio, P/L:	0.8
Aspect ratio (span/chord), L_z/L:	6.0
Blade inlet angle, β_1:	35°
Blade outlet angle, β_2:	−60°
Rod velocity to axial velocity ratio, u_r/u_x:	∼0.70
Rod spacing to airfoil pitch ratio, L_r/P, (Original Case):	1.0
Rod spacing to airfoil pitch ratio, L_r/P, (Increased Spacing Case):	2.0

Figure 2.2: PAK-B airfoil geometry

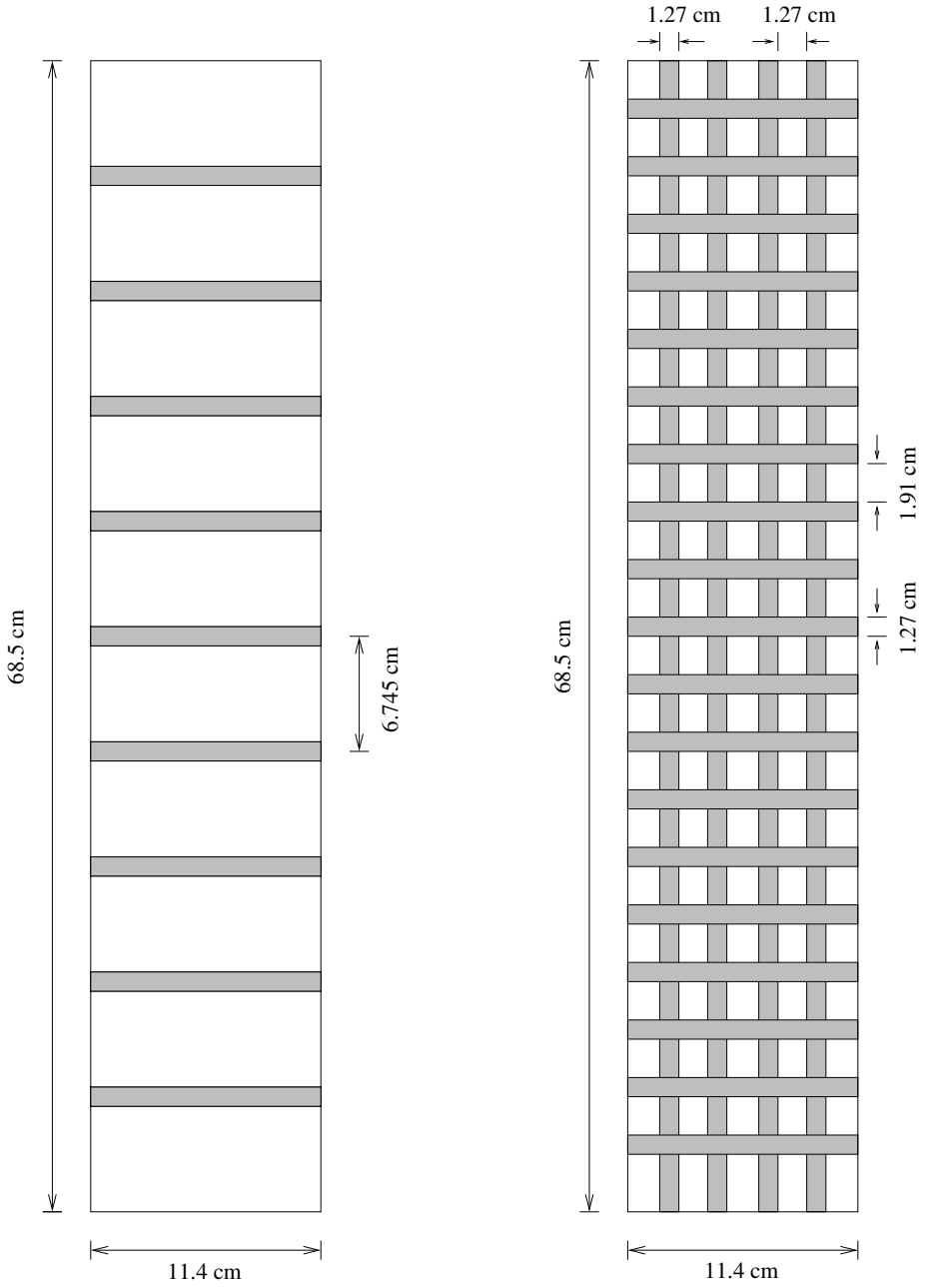

Figure 2.3: Turbulence grids used $FSTI = 10\%$. Blowing grid on the left and square passive grid on the right.

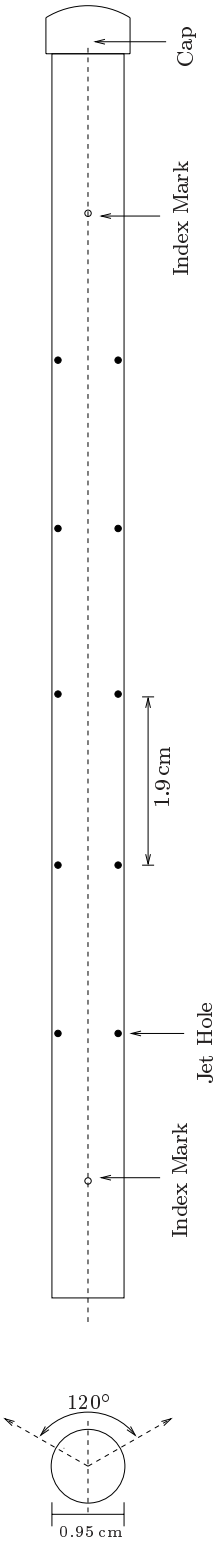

Figure 2.4: Blown jet grid

Chapter 3

Documentation of Flow Parameters

3.1 Operating Parameters

The test facility is designed to produce flow conditions simulating a low pressure turbine. As discussed in section 2.1, the experimental facility is capable of operating over a large range of inlet parameters. Particularly, the facility can operate with suction surface length Reynolds numbers ranging from $Re_{L_{ss}} = 25{,}000$ to 300,000 and with free-stream turbulence intensities ranging from 0.5 to 10%. However, the wake generator has an operating speed range corresponding to approximately $Re_{L_{ss}} = 25{,}000$ to 62,500.

Based upon this constraint and an interest in investigating the low portion of the Reynolds number range, operating conditions for the with-wake study of $Re_{L_{ss}} = 50{,}000$ and turbulence intensity of 2.5% were chosen as the base case to this study. This case is fully described by Kaszeta and Simon (2002). A case without wakes taken from the works of Simon et al. (2000) serves as a no-wake comparison case to the base case of this experiment. A comparison of the two displays the effects of wakes on the flow when all else is equal. This no-wake case showed both separation and boundary layer transition. The complete documentation of it is presented in Simon et al. (2000).

For the increased wake spacing case presented in this report, the approach flow conditions used in the base case presented in Kaszeta and Simon (2002) were imposed. The only difference is that every other rod in the wake generating sled was removed. A comparison of this case with the base case displays the effects of rod spacing when all else is equal.

For the elevated-$FSTI$ case presented in this report, it was necessary to modify the

facility to elevate the approach flow *FSTI* to 10%. A comparison of this case with the base case shows the effects of turbulence intensity of the flow approaching the wake generating rods. A comparison of this case with a no-wake case of the same conditions but without wakes documented in Simon et al. (2000) shows the effect of adding wakes when the background turbulence is elevated.

Documentation of the approach flow uniformity, turbulence quantities and pressure distribution over the blades when the wakes are not present, are presented below for both low-*FSTI* cases (the base and increased spacing cases) and for the high-*FSTI* case. Refer to Simon et al. (2000) for documentation of the approach flow for the earlier study without wakes.

3.2 Approach Flow Uniformity

3.2.1 Low-*FSTI* Cases

Based upon the turbine passage simulator geometry (Figure 3.1), the desired operating Reynolds number of $Re_{Lss} = 50{,}000$ corresponds to an inlet velocity of nominally $u_x = 3.03\,{}^{\mathrm{m}}/_{\mathrm{s}}$, and a wake generating sled velocity of

$$u_r = 0.7u_x = 2.12\,{}^{\mathrm{m}}/_{\mathrm{s}}. \tag{3.1}$$

Using the original rod spacing of 91.44 mm, the wake passing frequency is 23.18 Hz, and with the increased rod spacing of 182.88 mm, the frequency becomes 11.59 Hz. With an axial chord length, L_x, of 103.57 mm, this spacing and sled velocity yields a wake Strouhal number, S, of 0.792 for the original rod spacing case and 0.396 for the increased rod spacing case. The inlet turbulence intensity of 2.5% was achieved by the use of the passive rod grid, discussed in Kaszeta and Simon (2002).

The freestream uniformity plots of the approach velocity and turbulence level were measured using two single-sensor anemometer surveys of the approach flow: a coarse two-dimensional survey across the entire flow development section and a detailed one-dimensional survey along the mid-span plane. Both were taken at the inlet plane, shown as a dashed line on Figure 3.1. It is located 18.25 cm upstream from the mid-span point between the leading edges of the airfoils. Additionally, a series of surveys with a triple-sensor anemometer probe was used to document the inlet turbulence parameters.

The two-dimensional survey results along the inlet plane for this case were presented in Kaszeta and Simon (2002), but are presented again in Figure 3.2. The largest deviations in uniformity are due to the side-walls' boundary layers. Examining the velocity distribution, Figure 3.2(a), we can see that the velocity varies between 93.3% and 104.1% of the mean inlet value. However, if we restrict ourselves to the region of interest (between the leading edges), the maximum deviation from the mean velocity drops to less than 4%. Figure 3.2(b) shows the turbulence intensity distribution at the same location. Including the near-wall region, the turbulence intensity, TI, ranges from 2.86% near the center of the channel to over 7.5% in the boundary layer. However, if we restrict ourselves to the region between the leading edges, the flow turbulence intensity is nearly uniform, varying from 3.00% to 3.02%.

To more fully document the upstream flow, a second, high-resolution, 1-D survey is taken of the inlet plane at the z-plane where the boundary layer measurements on the airfoils are taken. These results are shown in Figure 3.3, in which $\bar{u}$ is the time-averaged velocity, and $\bar{\bar{u}}$ is the spatial average of $\bar{u}$ in the channel. The locations of the leading edges of both the pressure surface and suction surface are shown in the figures. Note that the profiles are nearly uniform in the region of interest between the leading edges. Also note that, due to slight leakage through the hot-wire access hole and possible blockage by the probe stem, there is some slight error in the pressure side profile data (note the slight scatter in the data), so it may be more desirable to treat the pressure surface half inlet flow as being a mirror image of the suction surface flow. From these plots, using the suction-side half-flow, we can report a nominal average velocity of 3.03 $^{\mathrm{m}}/_{\mathrm{s}}$, and a turbulence intensity of 3%, which decays to approximately 2.5% by the time the flow reaches the test section leading edge.

From the profile data at the inlet plane, a momentum boundary layer thickness on the side wall upstream of the suction surface, θ, of 0.1464 cm was calculated.

3.2.2 High-*FSTI* Case

Like the low-*FSTI* case, the operating state for this case corresponds to an inlet velocity of nominally $u_x = 3.03$ $^{\mathrm{m}}/_{\mathrm{s}}$, and a wake generating sled velocity of 2.12 m/s. Using the original rod spacing of 91.44 mm, the wake passing frequency is 23.18 Hz. Using an axial chord length, L_x, of 103.57 mm, the wake Strouhal number, S, is 0.792. The inlet turbulence intensity of 10% was achieved by the use of a combination of a static square bar grid and a blown grid, as discussed in section 2.1.

For the high-*FSTI* case, the freestream uniformities of the approach velocity and tur-

bulence level were measured at the inlet plane, shown as a dashed line on Figure 3.1 and located 18.25 cm upstream from the mid-span point between the airfoil leading edges.

The two-dimensional survey results along the inlet plane for the high-*FSTI* case are shown in Figure 3.4. The largest deviations in uniformity are due to the side-walls' boundary layers. Examining the velocity distribution, Figure 3.4(a), we can see that the velocity varies between 85.36% and 102.9% of the mean inlet value. However, if we restrict ourselves to the region of interest (between the leading edges), the maximum deviation from the mean velocity drops to less than 3%.

Similarly, Figure 3.4(b) shows the turbulence intensity distribution at the same location. Including the near-wall region, the turbulence intensity ranges from 10.6% near the center of the channel to over 16% in the boundary layer. However, if we restrict ourselves to the region between the leading edges, the flow turbulence intensity is nearly uniform, varying from 10% to 12%.

Like the low-*FSTI* case, a second, high-resolution, 1-D survey was taken of the inlet plane at the same z location as that where the airfoil boundary layer measurements were taken. These results are shown in Figure 3.5, in which $\bar{u}$ is the time-averaged velocity, and $\bar{\bar{u}}$ is the spatial average of $\bar{u}$ in the channel. The locations of the leading edges of both the pressure surface and suction surface are shown in the figures. Note that the profiles are nearly uniform in the region of interest, between the leading edges. From these plots, we can report a nominal average velocity of 3.04 m/s, and a turbulence intensity of 10.5%, which is projected to decay to approximately 9.75% at the test section leading edge.

From the profile data at the inlet plane, a momentum boundary layer thickness on the side wall upstream of the suction surface of $\theta = 0.1685$ cm was calculated.

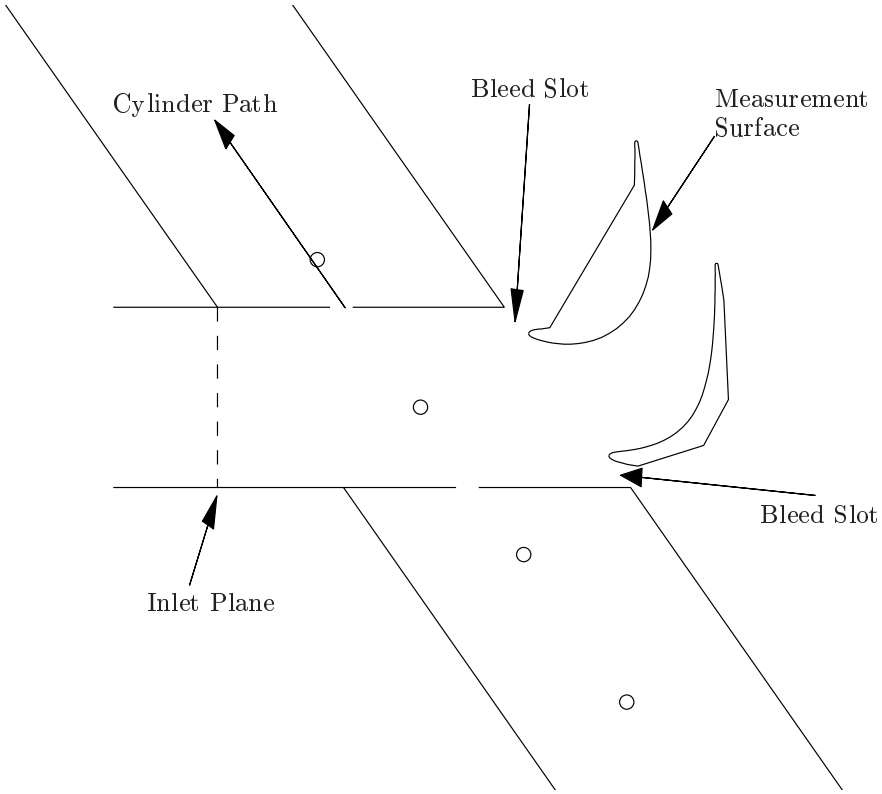

Figure 3.1: Cross-sectional view of the wake generator passage, showing the inlet plane location

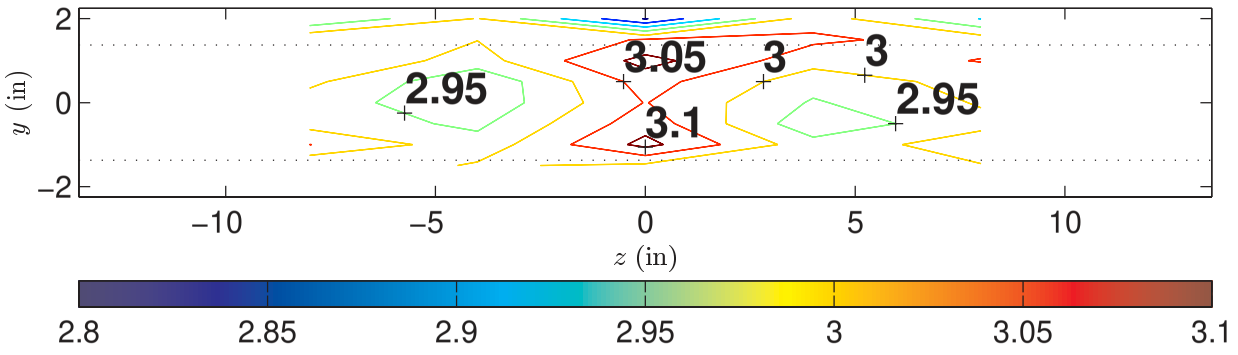

(a) $\bar{u}(y, z)$

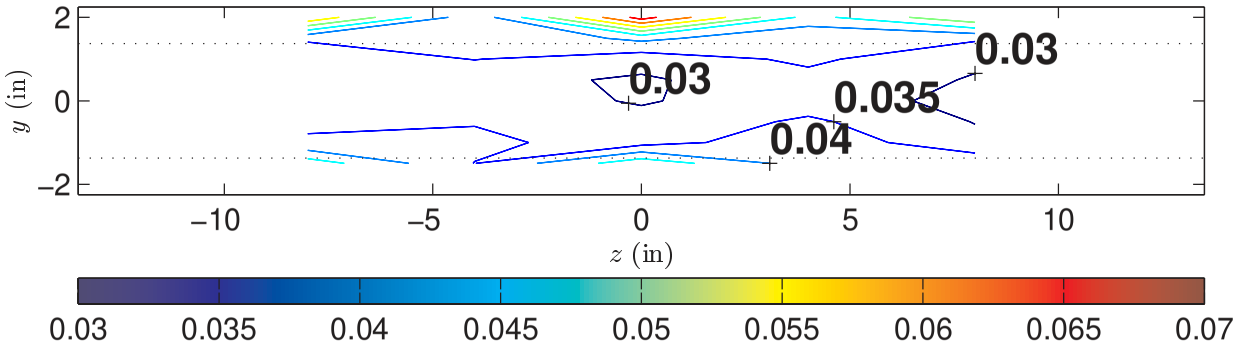

(b) $TI(y, z)$

Figure 3.2: Inlet flow 2-D single-sensor hot-wire survey, low-*FSTI* cases. The dotted lines indicate the location of the test section airfoil leading edges

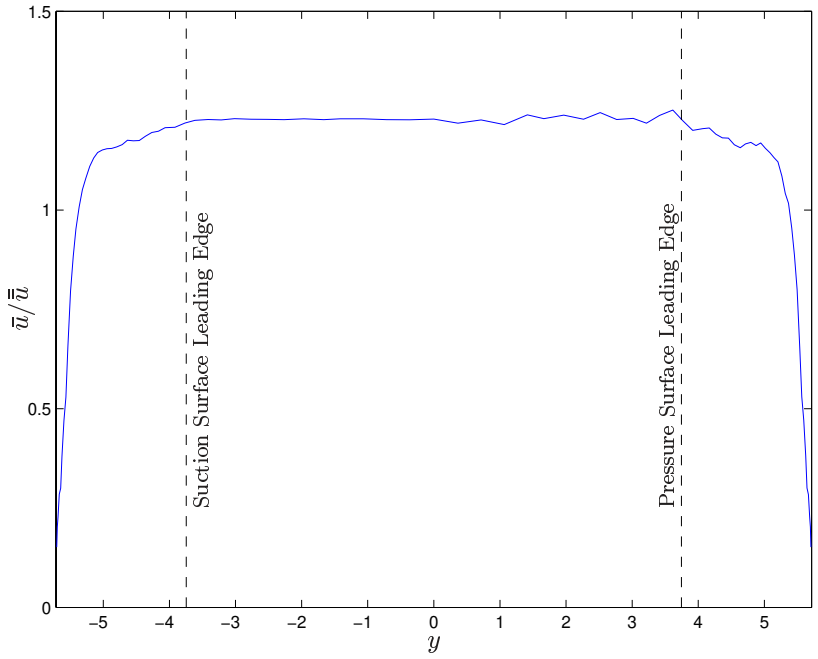

(a) Mean Velocity, $\bar{u}/\bar{\bar{u}}$

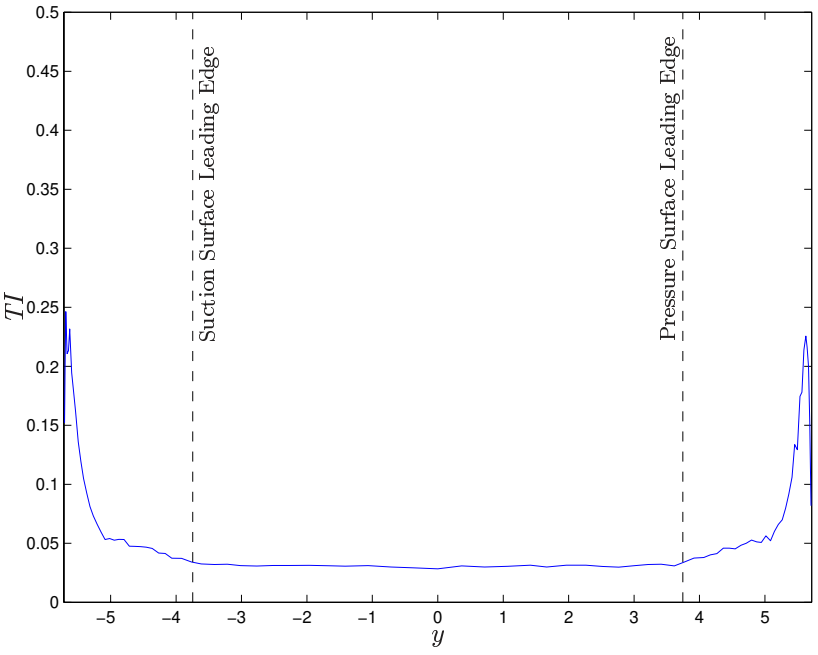

(b) Turbulence Intensity TI

Figure 3.3: Inlet flow velocity and turbulence intensity distributions, low-$FSTI$ cases

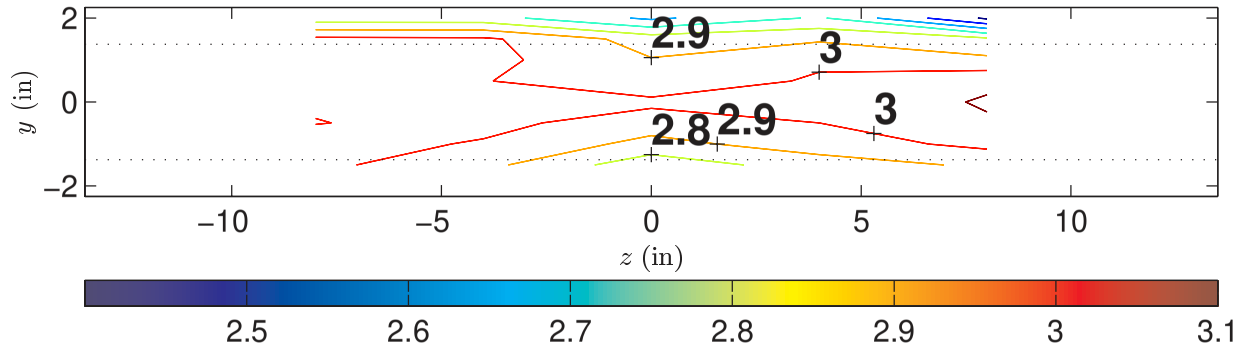

(a) $\bar{u}(y, z)$

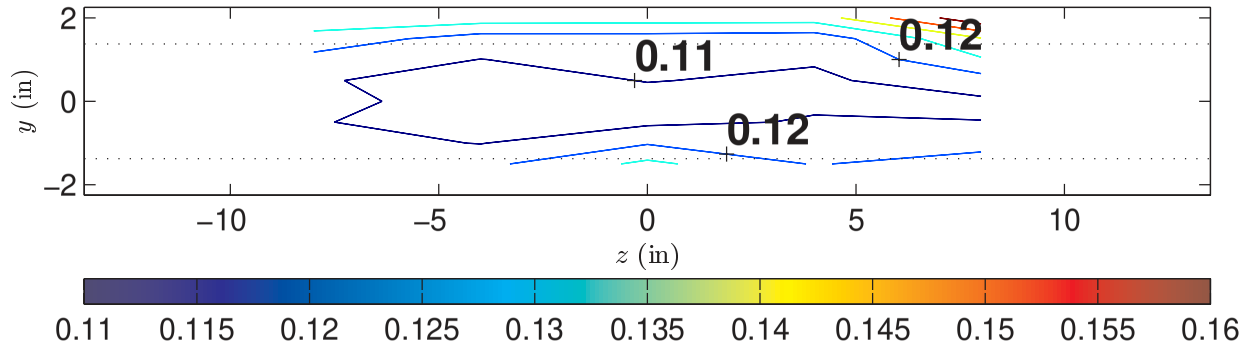

(b) $TI(y, z)$

Figure 3.4: Inlet flow 2-D single-sensor hot-wire survey, high-$FSTI$ case. The dotted lines indicate the location of the test section airfoil leading edges

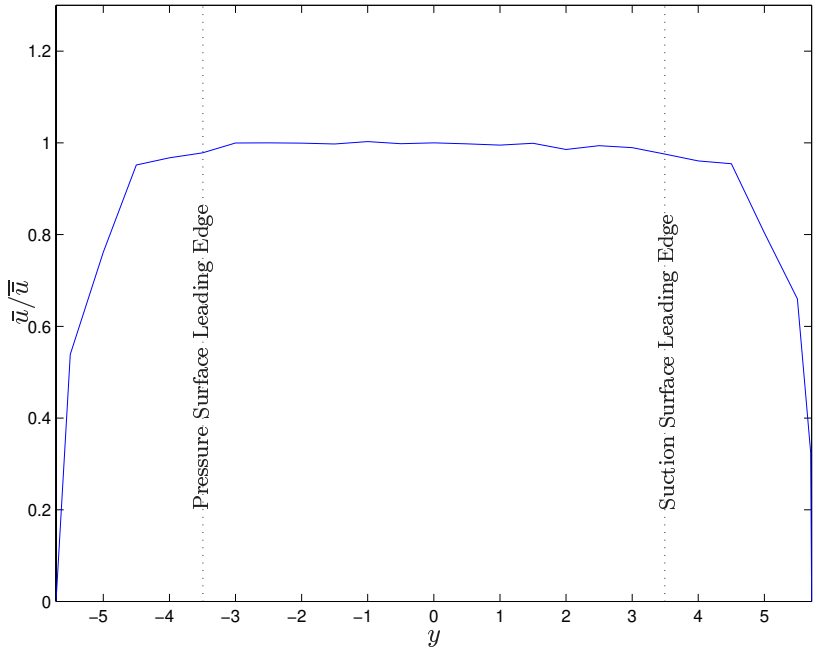

(a) Mean Velocity, $\bar{u}/\bar{\bar{u}}$

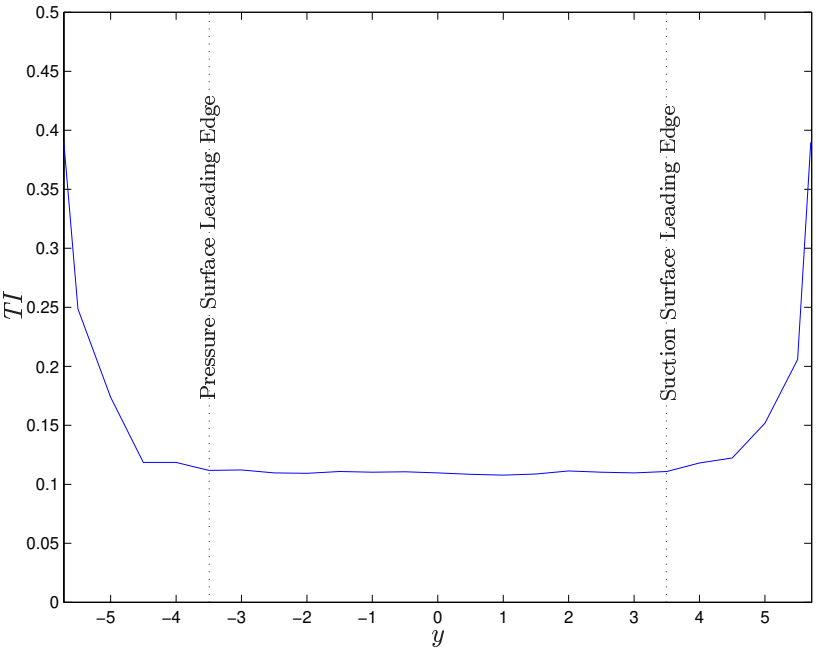

(b) Turbulence Intensity TI

Figure 3.5: Inlet flow velocity and turbulence intensity distributions, high-$FSTI$ case

3.3 Turbulence Quantities

3.3.1 Low-*FSTI* Cases

In order to document the turbulence scales upstream of the wake generator, one-dimensional power spectra of u', v', and w' were measured using a triple-sensor anemometer probe. These power spectral measurements were collected at the same location as the single-wire surveys in the previous section, 18.25 cm upstream of the turbine passage inlet. The power spectral measurements were collected by sampling 2,097,152 (2^{21}) data points at 2 kHz (low-pass filtered at 500 kHz), for a total sampling time of 17.47 minutes. The power spectral distribution were computed using MATLAB, using the script `lengthscale.m` included in Appendix B. Details of such measurements are given in Kaszeta and Simon (2002).

The power spectra are presented in Figure 3.6. In Figure 3.7, they are plotted versus energy coordinates. From these data, the integral length scales of the flow, $\Lambda_{u,x}$, $\Lambda_{v,x}$, and $\Lambda_{w,x}$, are calculated. Using relations developed by Hinze (1975), the integral length scales are calculated by extrapolating the PSD values in Figure 3.6 to f=0 and using the relations given below. Where the spectra don't display a zero derivative at the lowest frequency, extrapolation was not possible and the minimum frequency value was taken as the $f = 0$ value.

$$\Lambda_{u,x} = \frac{\bar{u}E_u(f=0)}{4u'^2_{rms}} \tag{3.2a}$$

$$\Lambda_{v,x} = \frac{\bar{u}E_v(f=0)}{4v'^2_{rms}} \tag{3.2b}$$

$$\Lambda_{w,x} = \frac{\bar{u}E_w(f=0)}{4w'^2_{rms}}. \tag{3.2c}$$

From these results, integral length scales of $\Lambda_{u,x} = 4.44$ cm, $\Lambda_{v,x} = 1.21$ cm, and $\Lambda_{w,x} = 0.99$ cm were calculated.

For comparison, the integral length scales are calculated also by using the autocorrelation of the velocity signal. From Hinze:

$$\Lambda_{u,x} = \frac{1}{u'^2_{rms}} \int_0^\infty Q_u(x)dx = \frac{\bar{u}}{u'^2_{rms}} \int_0^\infty Q_u(t)dt = \frac{\bar{u}}{u'^2_{rms}} \sum_{i=1}^{N} Q_{u,i} \tag{3.3}$$

where $Q_{u,i}$, the auto-correlation of u', is calculated using

$$Q_{u,i} = \sum_{j=1}^{N-i} u_j u_{i+j} \Delta t. \tag{3.4}$$

Combining Eqn. 3.3 and Eqn. 3.4, we obtain

$$\Lambda_{u,x} = \frac{\bar{u}\Delta t}{{u'}^2_{rms}} \sum_{i=1}^{M} \sum_{j=1}^{N-1} u_j u_{i+j}. \tag{3.5a}$$

Similarly, equations for $\Lambda_{v,x}$ and $\Lambda_{w,x}$ can be derived:

$$\Lambda_{v,x} = \frac{\bar{u}\Delta t}{{v'}^2_{rms}} \sum_{i=1}^{M} \sum_{j=1}^{N-1} v_j v_{i+j} \tag{3.5b}$$

$$\Lambda_{w,x} = \frac{\bar{u}\Delta t}{{w'}^2_{rms}} \sum_{i=1}^{M} \sum_{j=1}^{N-1} w_j w_{i+j} \tag{3.5c}$$

where N is the number of data points in the signal and M is the number of data points after which the autocorrelation has had its first zero-crossing. Using this technique, integral length scales of $\Lambda_{u,x} = 4.19\,\text{cm}$, $\Lambda_{v,x} = 1.04\,\text{cm}$, and $\Lambda_{w,x} = 1.04\,\text{cm}$ were calculated, reasonably consistent with the PSD-derived values.

Similarly, the spectra in Figure 3.6 can be used to estimate the turbulence dissipation rate, ϵ, by fitting a $-5/3$ sloped line to the power spectrum in the inertial subrange and using the Kolmogoroff spectrum law (Hinze, 1975):

$$E_u(f) = 0.6545\pi^{-2/3}\epsilon^{2/3}(\bar{u})^{2/3}(2f)^{-5/3}. \tag{3.6}$$

yielding a value of ϵ of $0.049\,\text{m}^2/\text{s}^3$. Note that the line shown in Figure 3.6 is a $-5/3$ sloped line provided for reference. The line used for this calculation would parallel it.

Also, the dissipation, ϵ, can be calculated directly by measuring the turbulent kinetic energy, k, at two streamwise locations, simplifying the k-ϵ equations, assuming one-dimensional, isotropic flow:

$$U_{fs}\frac{\partial k}{\partial x} = -\epsilon. \tag{3.7}$$

By measuring k at two locations in the flow which are sufficiently close to assume linearity but sufficiently separated to minimize error, we can estimate $\partial k/\partial x$ using finite differences. Calculating k at the measurement plane used above and at a point 10.16 cm upstream of the measurement plane, we can estimate ϵ to be $0.050\,{}^{\mathrm{m}^2}/_{\mathrm{s}^3}$, reasonably consistent with our results obtained from the PSD.

Once calculated, ϵ can then be used to calculate both the energy length scale, L_u, and the Taylor microscale, λ:

$$L_u = 1.5\frac{\left(u'_{rms}\right)^3}{\epsilon} \tag{3.8}$$

$$\lambda = \left(\frac{15\nu u'^2_{rms}}{\epsilon}\right)^{1/2}. \tag{3.9}$$

Using these relations, $\epsilon = 0.049\,{}^{\mathrm{m}^2}/_{\mathrm{s}^3}$, $L_u = 1.25\,\mathrm{cm}$, and $\lambda = 5.05\,\mathrm{mm}$. The turbulence quantities of the flow are summarized in Table 3.1.

3.3.2 High-*FSTI* Case

In order to document the turbulence scales upstream of the wake generator in the high-*FSTI* configuration, another set of power spectral measurements was collected at the same location as for the low-*FSTI* cases presented in section 3.3.1.

The power spectra for the high-*FSTI* case are presented in Figure 3.8. In Figure 3.9, they are plotted versus energy coordinates. From these data, the integral length scales of the flow, $\Lambda_{u,x}$, $\Lambda_{v,x}$, and $\Lambda_{w,x}$, are calculated. Using Eqn. 3.2, integral length scales of $\Lambda_{u,x} = 5.55\,\mathrm{cm}$, $\Lambda_{v,x} = 1.57\,\mathrm{cm}$, and $\Lambda_{w,x} = 1.67\,\mathrm{cm}$ were calculated.

For comparison, the integral length scales are calculated from the autocorrelations. Using Eqn. 3.3, integral length scales of $\Lambda_{u,x} = 5.75\,\mathrm{cm}$, $\Lambda_{v,x} = 1.29\,\mathrm{cm}$, and $\Lambda_{w,x} = 1.38\,\mathrm{cm}$ were calculated, reasonably consistent with the PSD-derived values.

The spectra in Figure 3.8 are used to estimate the turbulence dissipation rate, ϵ, by fitting a $-5/3$ sloped line to the power spectrum and using Eqn. 3.6, yielding a value of ϵ of $6.426\,{}^{\mathrm{m}^2}/_{\mathrm{s}^3}$.

The calculated value of ϵ is used to calculate both the energy length scale, L_u, and the Taylor microscale, λ. Using Eqn. 3.8, $L_u = 0.7844\,\mathrm{cm}$ and $\lambda = 2.075\,\mathrm{mm}$. The turbulence quantities of the flow for the high-*FSTI* case are summarized in Table 3.2. Note that these

values, particularly the length scale, $\Lambda_{u,x}$, and the dissipation, ϵ, are significantly higher than the values reported for the the same nominal flow by Simon et al. (2000). The authors hypothesize that these differences are due to the difficulty of exactly matching turbulence length scales using a blown grid for turbulence generation. For comparison, quantities from Simon et al. (2000) are provided in Tables 3.3 and 3.4.

Table 3.1: Turbulence quantities for the inlet flow with a suction surface length Reynolds number, $Re_{L_{ss}}$, of 50,000 and a freestream turbulence intensity, TI, of 2.5%

Quantity:	**Value:**
Turbulence Length Scale, $\Lambda_{u,x}$ from PSD:	4.44 cm
Turbulence Length Scale, $\Lambda_{v,x}$ from PSD:	1.21 cm
Turbulence Length Scale, $\Lambda_{w,x}$ from PSD:	0.99 cm
Turbulent Dissipation, ϵ, from PSD:	$0.049\ {}^{m^2}/_{s^3}$
Energy Length Scale, L_u:	1.25 cm
Taylor Microscale, λ:	5.05 mm

Table 3.2: Turbulence quantities for the inlet flow with $Re_{L_{ss}} = 50{,}000$ and $TI = 10\%$

Quantity:	**Value:**
Turbulence Length Scale, $\Lambda_{u,x}$ from PSD:	5.55 cm
Turbulence Length Scale, $\Lambda_{v,x}$ from PSD:	1.57 cm
Turbulence Length Scale, $\Lambda_{w,x}$ from PSD:	1.67 cm
Turbulent Dissipation, ϵ, from PSD:	$6.426\ {}^{m^2}/_{s^3}$
Energy Length Scale, L_u:	0.7844 cm
Taylor Microscale, λ:	2.075 mm

Table 3.3: Turbulence quantities for the steady inlet flow with $Re_{L_{ss}} = 50{,}000$ and $TI = 2.5\%$, from Simon et al. (2000)

Quantity:	**Value:**
Turbulence Length Scale, $\Lambda_{u,x}$:	4.27 cm
Turbulence Length Scale, $\Lambda_{v,x}$:	1.03 cm
Turbulence Length Scale, $\Lambda_{w,x}$:	1.03 cm
Turbulent Dissipation, ϵ:	$0.05\,{}^{\mathrm{m}^2}/_{\mathrm{s}^3}$
Energy Length Scale, L_u:	1.37 cm
Taylor Microscale, λ:	5.19 mm

Table 3.4: Turbulence quantities for the steady inlet flow with $Re_{L_{ss}} = 50{,}000$ and $TI = 10\%$, from Simon et al. (2000)

Quantity:	**Value:**
Turbulence Length Scale, $\Lambda_{u,x}$:	2.82 cm
Turbulence Length Scale, $\Lambda_{v,x}$:	1.37 cm
Turbulence Length Scale, $\Lambda_{w,x}$:	1.52 cm
Turbulent Dissipation, ϵ:	$2.77\,{}^{\mathrm{m}^2}/_{\mathrm{s}^3}$
Energy Length Scale, L_u:	1.36 cm
Taylor Microscale, λ:	2.84 mm

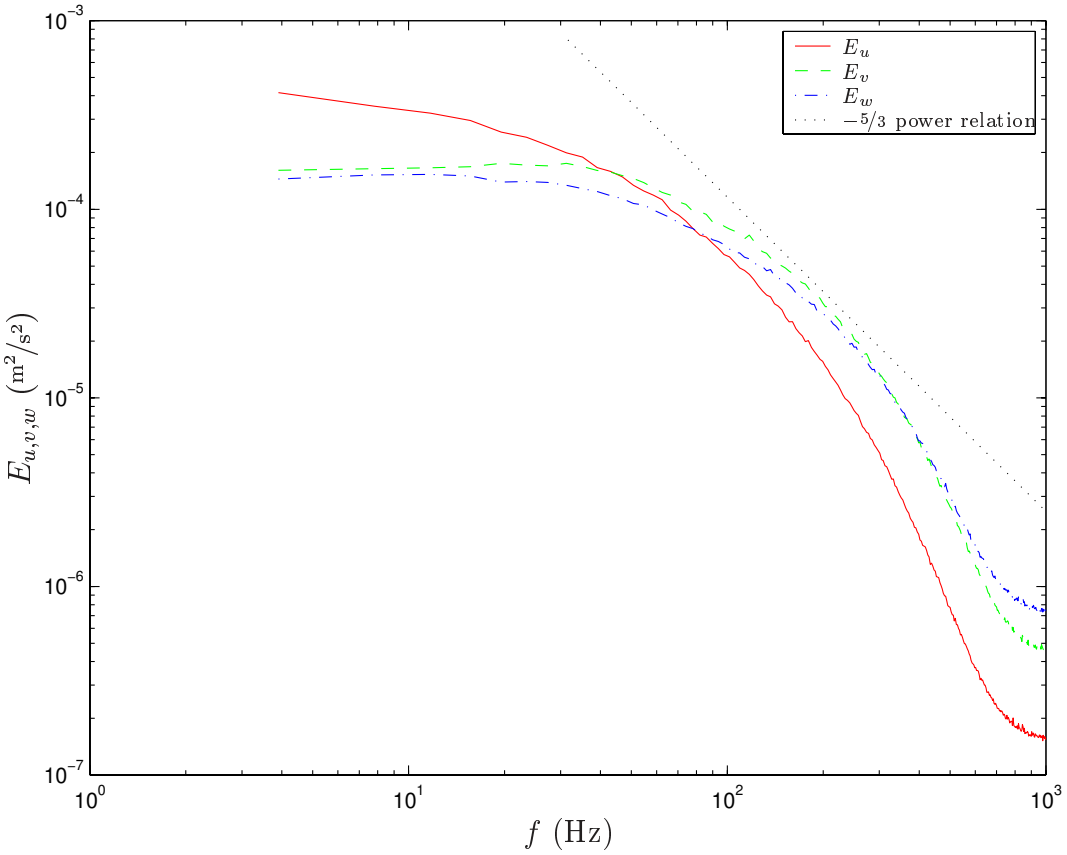

Figure 3.6: Power spectral distributions of turbulence in the x, y, and z directions at the inlet plane, low-$FSTI$ cases

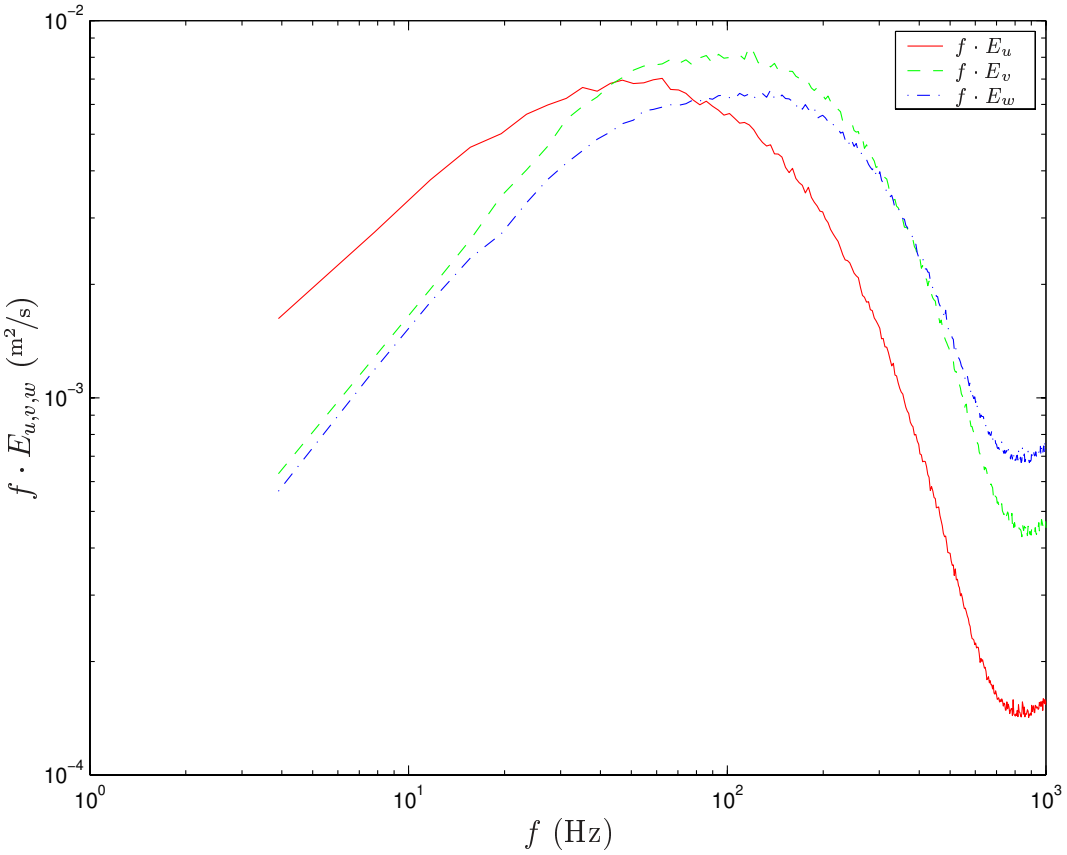

Figure 3.7: Power spectral distributions of turbulence in the x, y, and z directions at the inlet plane, plotted in energy coordinates, low-$FSTI$ cases

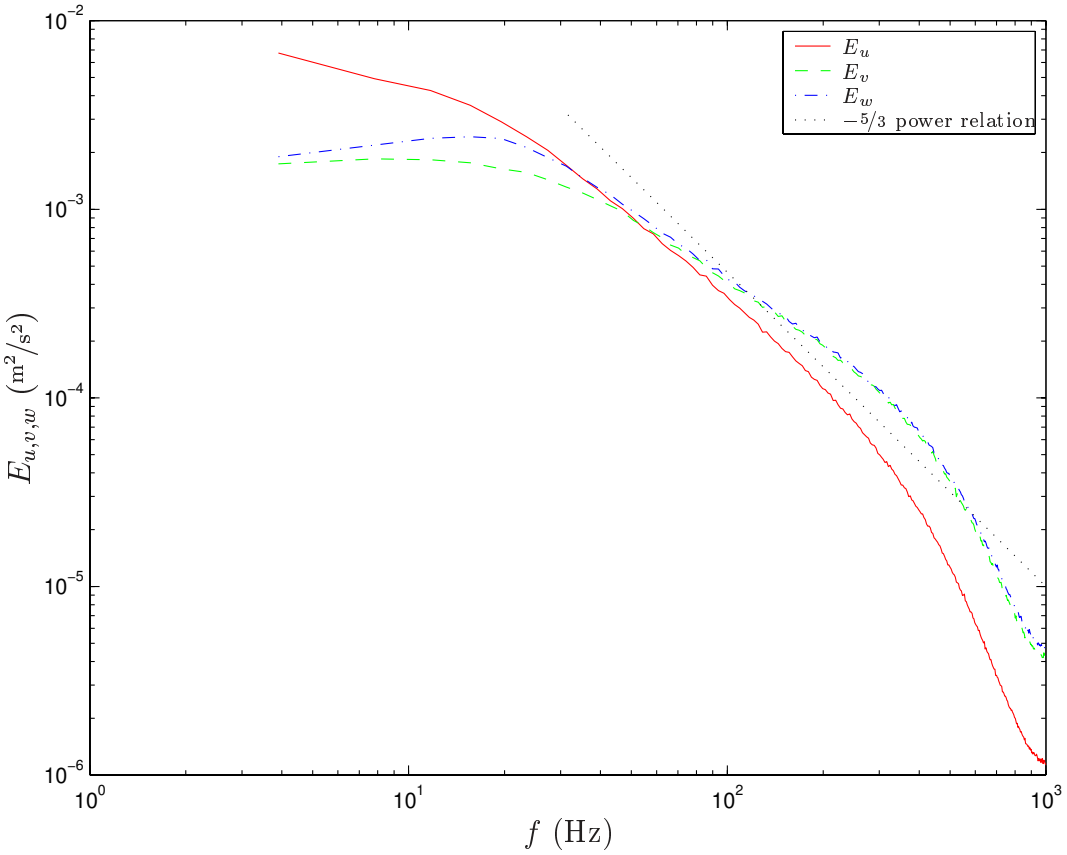

Figure 3.8: Power spectral distributions of turbulence in the x, y, and z directions at the inlet plane, high-$FSTI$ case

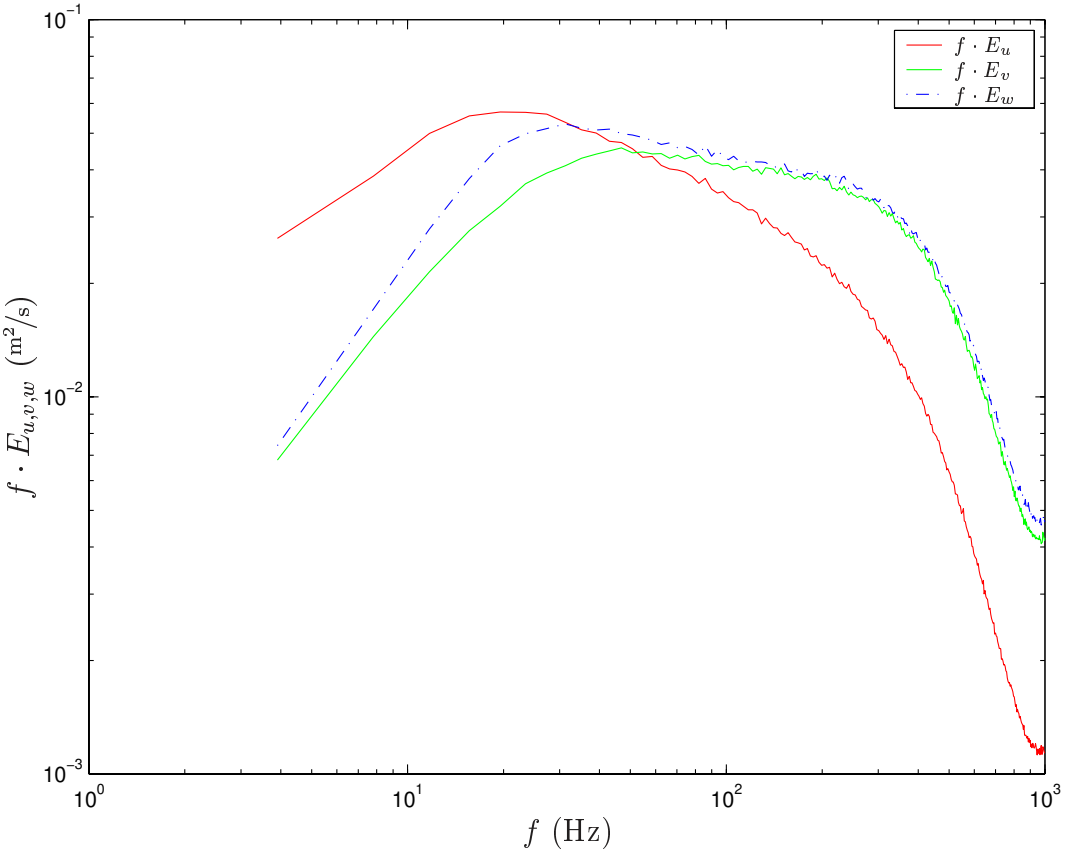

Figure 3.9: Power spectral distributions of turbulence in the x, y, and z directions at the inlet plane, plotted in energy coordinates, high-$FSTI$ case

3.4 Wake Characterization

3.4.1 Low-*FSTI* Cases

Figures 3.10 and 3.11 document the incoming wakes generated by our wake generator for the base case, and the increased wake spacing case, respectively.

Briefly, the base case was with very broad wakes, having a minimum velocity of approximately 87.5% of the mean value and a peak turbulence level of 17.5% (see Figures 3.10(a) and 3.10(b)). Since the wakes are broad, they merge rapidly, creating a nearly sinusoidal flow, (Figure 3.10(a)). There is no quiescent, steady flow period between wakes where the flow returns to the background turbulence level.

For the increased wake spacing case, every other rod was removed to create wakes of similar nature, but allowing the flow twice as much time to recover from the wakes' perturbations. Examining Figure 3.11, we can see that for the increased wake spacing case, the wakes are much narrower, and for approximately half of the wake period, the flow is essentially steady. However, the wakes also have a larger velocity deficit than in the base case, with a minimum velocity of approximately 80% of the mean velocity. Similarly, the wakes also have a higher level of turbulence associated with them, with a peak turbulence level of approximately 25%. We should note, however, that, like the base case, the background turbulence level never returns to the *FSTI* level of 2.5% seen upstream of the wake generator, so the presence of wakes in the flow still causes a significant increase in the overall level of free-stream turbulence in the flow, even in the between-wake portion of the flow.

In summary, for the increased wake spacing case, the wakes are narrower, but stronger, and allow the flow to return to near-steady conditions between the wakes.

3.4.2 High-*FSTI* Case

Figures 3.12 and 3.13 document the incoming wakes generated by our wake generator for the base (low-*FSTI*) base case and the high-*FSTI* case, respectively.

The incoming wakes for the high-*FSTI* case (see Figs. 3.13(a) and 3.13(b)) show a similar wake to the base case—the minimum velocity of the wake is approximately 87.5% of the mean value. However, the higher-*FSTI* approach flow results in an overall increase in turbulence level: while the base case wakes' *TI* values range from approximately 5% between

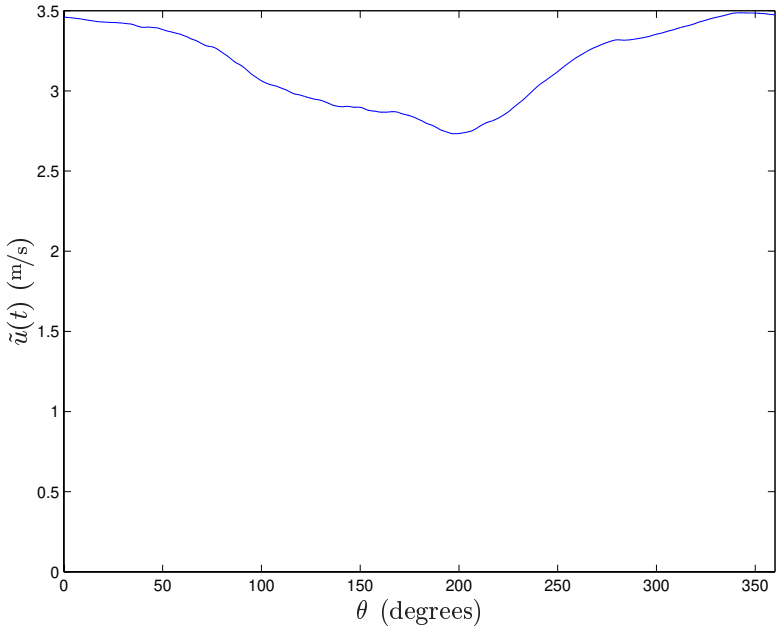

(a) $\tilde{u}(t)$

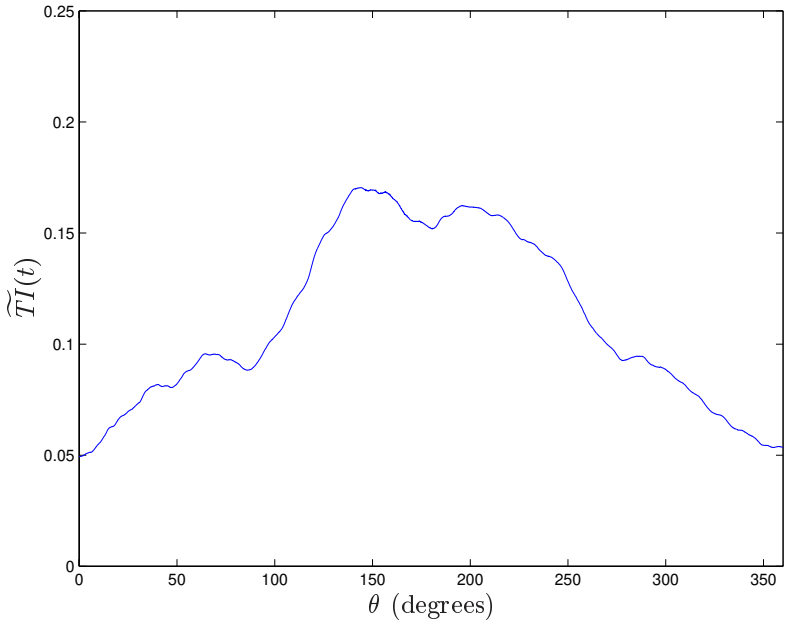

(b) $\widetilde{TI}(t)$

Figure 3.10: Ensemble-average velocity and TI of 600 wakes, taken at the midpoint between the leading edges of the pressure and suction surfaces, base case

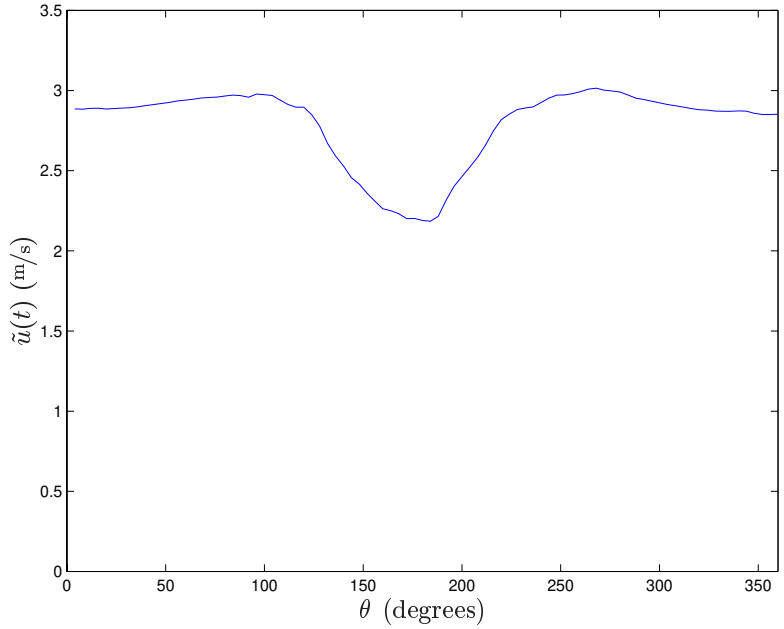

(a) $\tilde{u}(t)$

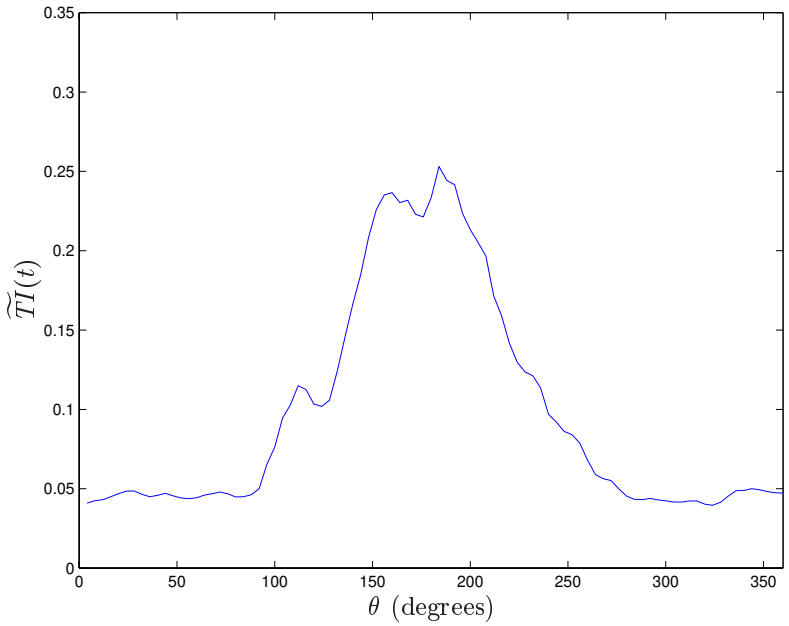

(b) $\widetilde{TI}(t)$

Figure 3.11: Ensemble-average velocity and TI of 225 wakes, taken at the midpoint between the leading edges of the pressure and suction surfaces, increased wake spacing case.

the wakes to 17.5% in the middle of the wakes, the high-*FSTI* wakes' *TI* values range from 10% between wakes to 25% at the middle of the wake. Thus, the increase of the approach flow *FSTI* resulted in a corresponding increase in the overall turbulence level throughout the wake passing period.

Additionally, the shapes of the wakes' velocity profiles in Figures 3.12(a) and 3.13(a) are slightly different. For the low-*FSTI* wakes, the velocity profile of the wake initially shows a gradual deceleration of the flow ($0 < \theta < 200°$), followed by a more rapid acceleration of the flow after the rod passes ($200° < \theta < 350°$). However, in the high-*FSTI* wakes, the velocity profile of the wake initially shows a strong deceleration of the flow ($0 < \theta < 140°$), followed by a more gradual acceleration of the flow after the rod passes ($140° < \theta < 315°$). Additionally, the high-*FSTI* case wakes appear to be slightly narrower in time, allowing the flow a longer period ($140° < \theta < 315°$) to recover from the wake passage.

3.5 Pressure Profiles

In order to assure that the general flow pattern in this facility matches both the design angle of attack and the steady flow studies presented by Simon et al. (2000), the pressure bleed slots in the facility were adjusted, so that at steady state:

1. The incoming flow to the passage stagnates as closely as possible to the leading edge stagnation line at pressure tap p01, to assure the proper angle of attack.

2. The static pressure distribution measured over the 13 pressure taps located on the suction surface matches the pressure distribution of Simon et al. (2000) for the same $Re_{L_{ss}}$ and *FSTI*.

After the facility's bleed slots were adjusted, the local static pressure was measured at each of the 13 pressure stations. From these measurements, the local pressure coefficient at each station was calculated,

$$C_p = -\frac{P_t - P_s}{P_t - P_{s,exit}} \tag{3.10}$$

where P_t is the total pressure, P_s is the local static pressure, and $P_{s,exit}$ is the static pressure downstream of the test section as computed from $P_{s,inlet}$, the flow exit area to inlet area ratio, and the assumption of inviscid flow. This calculation assumes that the flow leaves the passage at the blade exit camber angle, β_2.

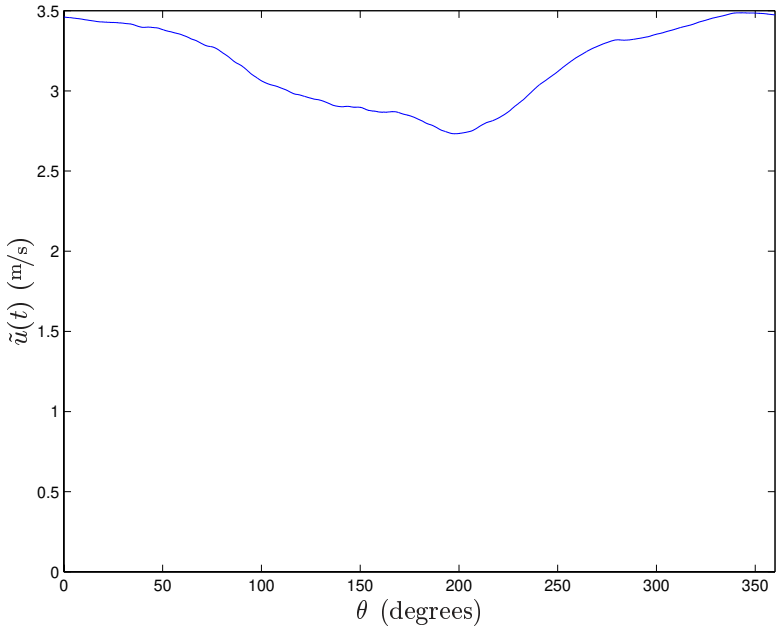

(a) $\tilde{u}(t)$

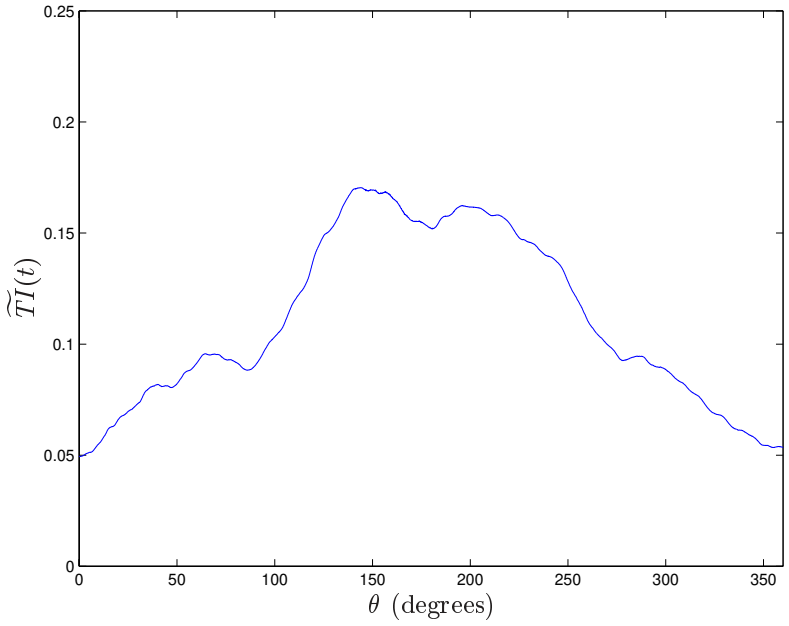

(b) $\widetilde{TI}(t)$

Figure 3.12: Ensemble-average velocity and TI of 600 wakes, taken at the midpoint between the leading edges of the pressure and suction surfaces, base case

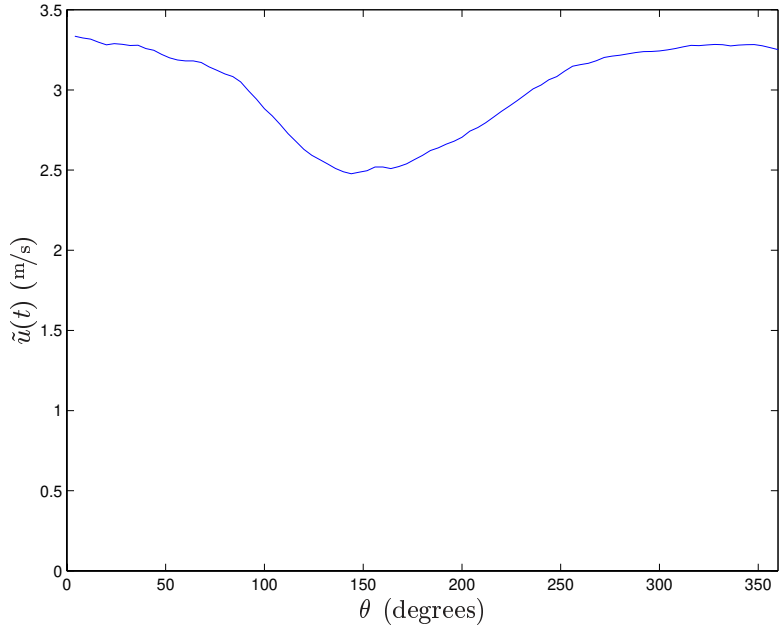

(a) $\tilde{u}(t)$

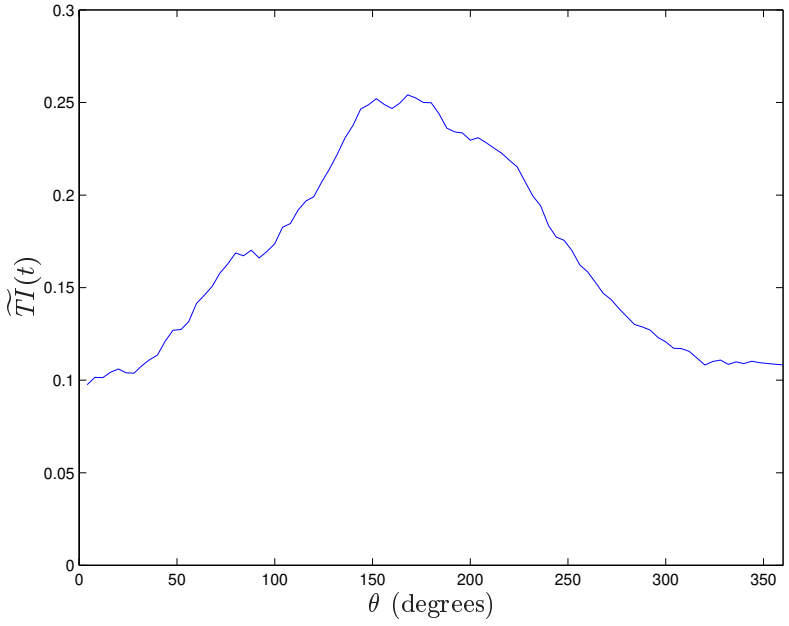

(b) $\widetilde{TI}(t)$

Figure 3.13: Ensemble-average velocity and TI of 440 wakes, taken at the midpoint between the leading edges of the pressure and suction surfaces (high-$FSTI$ case).

The measured values of C_p, as well as those reported by Simon et al. (2000) and the High-Re design C_p distribution for the PAK-B airfoil are shown for the low-$FSTI$ and high-$FSTI$ cases, in Figures 3.14 and 3.15, respectively.

Examining the low-$FSTI$ cases, Figure 3.14, one sees that the measured C_p distribution for the current study closely matches the C_p distribution reported by Simon et al. (2000), suggesting that, despite facility modifications, the steady flow through the turbine passage is essentially the same. It is also useful to note that, starting at $x/L_x = 60\%$, the pressure profile begins to vary significantly from the design calculation profile, suggesting that the boundary layer is beginning to rapidly thicken and the flow is beginning to separate. Between this location and $x/L_x = 96\%$, it appears that the flow has separated, possibly re-attaching just before the trailing edge of the airfoil. These results are supported by the velocity profiles presented by Simon et al. (2000).

Examining the high-$FSTI$ case, Figure 3.15, we can see a similar distribution as that seen in Figure 3.14. However, the pressure profile for the high-$FSTI$ case agrees with the design calculation profile until $x/L_x = 70\%$, suggesting that the boundary layer separates further downstream than in the low-$FSTI$ cases. The measured pressure distributions again match the design calculation values starting at $x/L_x = 90\%$, suggesting that the high-$FSTI$ flow re-attaches farther upstream than does the low-$FSTI$ flow. Additionally, comparing the C_p values of Simon et al. (2000) to the present study, we see close agreement, suggesting that for the high-$FSTI$ case, our flow parameters are similar to those presented by Simon et al. (2000).

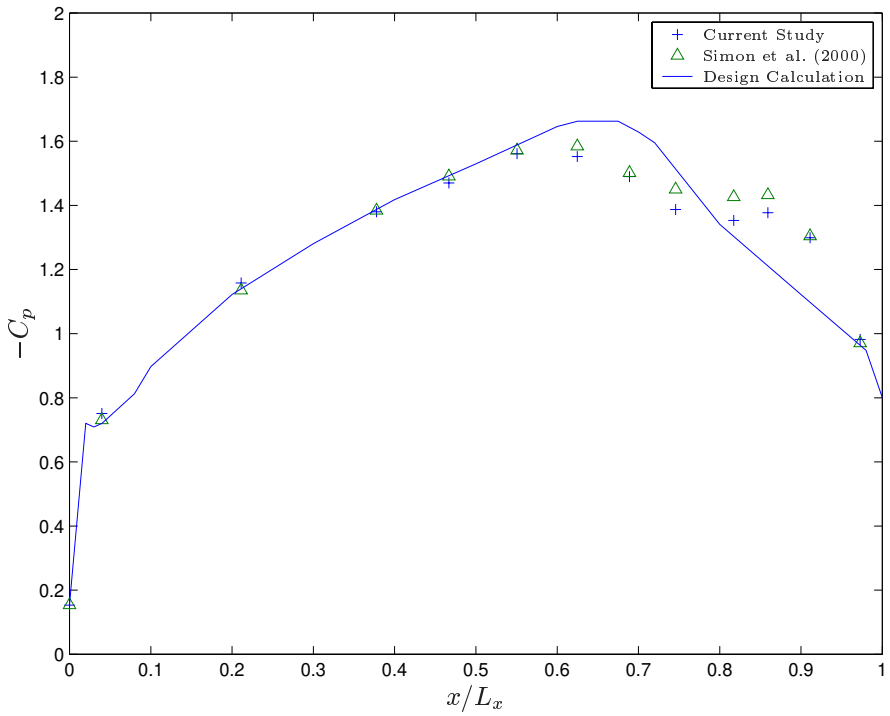

Figure 3.14: Pressure Coefficient Distribution at $Re_{L_{ss}} = 50{,}000$ and $TI = 2.5\%$

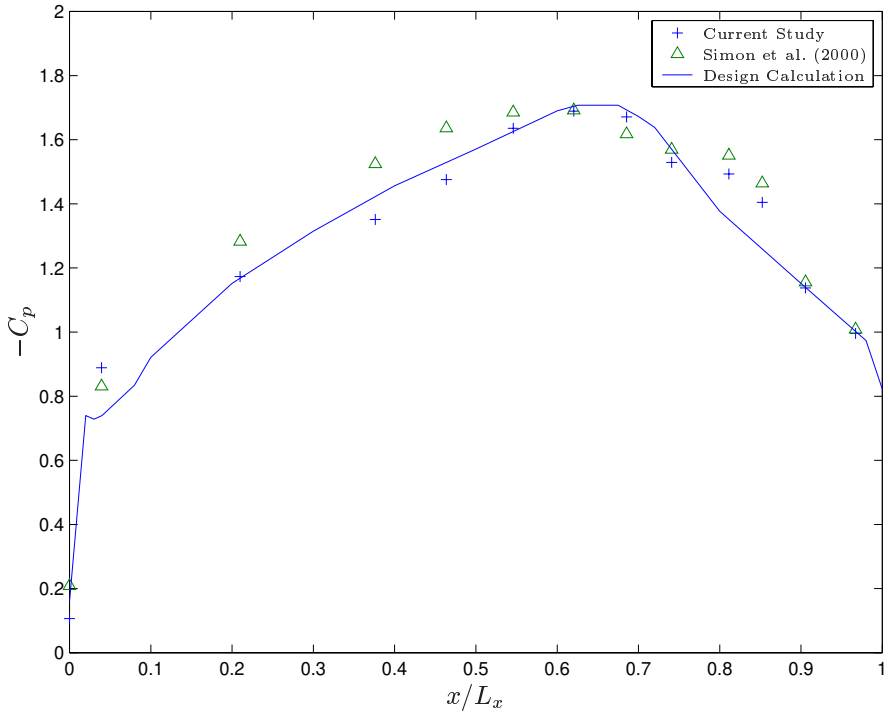

Figure 3.15: Pressure Coefficient Distribution at $Re_{L_{ss}} = 50{,}000$ and $TI = 10\%$

Chapter 4

The Increased Wake Spacing Case Results

4.1 Introduction

In this chapter, we present a repeat of the base case documented in Kaszeta and Simon (2002), but with every other rod of the wake generator removed. This case will hereafter be referred to as the "increased wake spacing case."

The data for this case were collected for stations 4 ($s/L_{ss} = 31.36\%$) through 13 ($s/L_{ss} = 93.49\%$). Stations 2 ($s/L_{ss} = 5.19\%$) and 3 ($s/L_{ss} = 19.78\%$) were omitted since it is difficult to correctly locate the probe relative to the wall. Because the boundary layers are very thin at these locations, accurate wall location is crucial and measurements with uncertain positioning are of little utility.

4.2 Experimental Results

Due to the periodic unsteady nature of this flow, the results of the experiment are presented as phase-averaged quantities.

The boundary-layer data for stations 4 through 13 are presented in Figures 4.3 through 4.42, with the increased wake spacing case data presented alongside the base case data taken at the same locations. Profiles of velocity, velocity rms, turbulence intensity, and intermittency are presented. It is important for the reader to keep in mind that since the

rod period is doubled, each of the increased wake spacing plots represents twice as much physical time as the corresponding base case plot.

The data are presented in order of measurement station number. For each, the data are first presented as a series of pseudo-color plots representing the velocity, velocity rms, the turbulence intensity, and the intermittency. Examples of each of these plots are given in Figure 4.3 ($\tilde{u}(y,\theta)$), Figure 4.4 ($\widetilde{u_{rms}}(y,\theta)$), Figure 4.5 ($\widetilde{TI}(y,\theta)$), and Figure 4.6 ($\tilde{\gamma}(y,\theta)$). For each of these figures, the horizontal axis represents a single wake, presented as the phase angle, θ, while the vertical axis represents the wall-normal distance, y. Thus, each figure represents the ensemble average of the series of wakes at a fixed location on the suction surface. Each figure for a specific quantity, such as Figures 4.5, 4.9, 4.13, etc., are presented with the same scale. At times this leads to rather uneventful plots for certain positions on the airfoil, an example is the $\widetilde{TI}$ plot of Figure 4.5.

Additionally, for stations 4 through 13, the ensemble-average velocity data are presented again in Figures 4.43 through 4.62, with each quantity represented as a series of plots showing the wall-normal distribution of each quantity at times during the wake-passing period. Examples of each of these plots are shown in Figure 4.51 and Figure 4.52 for the base case and increased spacing case, respectively. For each axes corresponding to a fixed value of θ, the horizontal axis designates the plotted quantity and the vertical axis represents the wall-normal distance, y. Presenting the data in this fashion allows easier visualization of the near-wall values of the velocity and the overall shape of the boundary layer velocity profile than possible with the color contour plots. This format is particularly useful when looking for regions of separated flow.

4.2.1 General Features

In general, the increased wake spacing case produces a similar flow field to the base case. This is because the most dominant influence is the pressure profile as established by the airfoil shape. The introduction of wakes in a steady flow greatly disturbs the flow and creates several interesting flow phenomena, especially on the turbine blade suction surface. These phenomena are discussed as follow:

- The wakes, which create a velocity deficit in the flow field, add a temporal acceleration and deceleration effect to the flow. This effect is combined with the spatial acceleration that the flow undergoes as a result of the turbine airfoil and passage geometry. But, the spatial acceleration term, $u\,\frac{\partial u}{\partial x}$, is also influenced by the passing wakes by virtue of the change in

u due to the wakes. This temporal acceleration was discussed by Jiang and Simon (2003c, 2005).

- Additionally, the velocity deficit introduced by the wakes is associated with a oscillating pressure field created by the entrance and departure of rods within the channel upstream the turbine passage. The pressure fluctuation moves at sonic velocity, much faster than the flow itself. Due to the different speeds at which pressure fluctuations and velocity wakes travel along the turbine passage, their effects on the flow field interact differently at different streamwise positions.

- The periodic oscillation of the velocity approaching the turbine passage results in an oscillation in the angle of attack of the flow approaching the airfoil. Thus, the development of the boundary layer is affected, and changes accordingly as a function of time. Though not measured directly, the pressure distribution over the surface would respond accordingly to the changes in approach angle.

- The turbulence associated with the wakes is convected downstream along the turbine passage. This increases the turbulence level and can accelerate transition to turbulence.

- Separation points and transition onset points are time dependent. The high disturbance within the wakes can trigger earlier transition, while transition can delay separation.

- Attached flow transition and separated flow transition are both found in this case but at different times during the wake passing cycle.

- The wider temporal spacing of the wakes allows a much longer period for the boundary layer to recover from the wakes' perturbations and resume a boundary layer development that is more like that of the steady-flow case documented in Simon et al. (2000).

We can summarize the differences between the base case and increased wake spacing case as follows:

4.2.2 Separation Points

At lower Reynolds numbers, LP turbine flows are subject to separation. For example, the steady state results reported by Qiu (1996) for $Re_{Lss} = 50,000$, $FSTI = 2.5\%$ and the present airfoil and passage geometry indicated that under these conditions, the boundary layer separated from the suction surface at approximately 53% of the suction surface length. Note that the approach flow (to the wake generators) turbulence intensity values for the base

case and the increased wake spacing case are approximately 2.5%. Qiu (1996) also recorded separation at 54% of the suction surface length for a case of $Re_{L_{ss}} = 50,000$,$FSTI = 10\%$ and the present airfoil and passage geometry. Note that the wake turbulence levels in the base case and the increased wake spacing case are both approximately 10%.

In the base case, the flow was also found to separate, although the introduction of wakes into this flow greatly changed the flow turbulence and instantaneous pressure gradients (Kaszeta and Simon (2002)). The difference was that the separation points moved back and forward along the suction surface in the region $53\% < s/L_{ss} < 59\%$ during the wake passing cycle. As the wake arrived in this region, deceleration due to wake arrival created inflectional boundary layer profiles and the flow separated from the wall. When the wake passed, the flow accelerated, separation was suppressed and the separation point moved downstream with the wake. Movement of the separation point stopped at $s/L_{ss} = 59\%$, while the wake continued moving downstream. Before the flow fully recovered from the passage of the wake, the leading edge of the next wake arrived. It made the flow decelerate again which caused the separation point to move upstream to $s/L_{ss} = 53\%$. Then the process was repeated.

Similar characteristics of the flow behavior are shown in the increased wake spacing case. However the separation points move within the region $51\% < s/L_{ss} < 60\%$ during the wake passing cycle (Kaszeta et al. (2003)). The flow upstream of $s/L_{ss} = 49.33\%$ does not separate at any time within the wake passing cycle (see Figures 4.44, 4.46, 4.48 and 4.50). From the velocity profiles in the boundary layer at $s/L_{ss} = 55.33\%$ (Figure 4.52), we can see the flow is separating or in the separation region. That means the most upstream separation point is in the region $49.33\% < s/L_{ss} < 55.33\%$. By comparing the velocity profiles in the boundary layer at $s/L_{ss} = 55.33\%$ and $s/L_{ss} = 61.32\%$ at $\theta = 224^\circ$ (see Figures 4.52 and 4.54), we can conclude that the flow is separating in the region $55.33\% < s/L_{ss} < 61.32\%$. By checking the intermittency profiles (Figures 4.22 and 4.26), we found that the wake is passing this region in the freestream.

The base case flowfield shows clear evidence of transient separation at station 9 (see the thick, low-velocity, near-wall region in the velocity plot at $\theta = 200^\circ$ in Figure 4.23(a), the inflectional profile at $\theta = 200^\circ$ in Figure 4.53, and the corresponding low-rms, near-wall regional in the rms plot in Figure 4.24(a)), and has completely separated by station 11 (Figures 4.31(a), 4.57, and 4.32(a)). Due to the decrease in the overall level of turbulence and the increased recovery time between wakes before the next free-stream flow acceleration begins, the flow shows evidence of separation earlier in the cycle in the increased wake spacing

case, with transient separation starting at station 8 (Figures 4.19(b), 4.52, and 4.20(b)), and complete separation occurring by station 10 (Figures 4.27(b), 4.55, and 4.28(b)).

Additionally, from the near-wall distributions of the ensemble-average velocity, $\tilde{u}(y, \theta)$, we can calculate an estimate of the wall shear stress on the suction surface. The first two points on the ensemble-average wall-normal velocity profile are used to approximate the value of the near-wall shear stress,

$$\tau_w = \mu \left. \frac{\partial u}{\partial y} \right|_{y=0} . \tag{4.1}$$

The approximated surface shear stress distributions for the base case and the increased wake spacing case are presented in Figures 4.1 and 4.2, respectively.

Examining the base case in Figure 4.1, we can see evidence of separation as an abrupt drop-off in surface shear stress, ranging from $s/L_{ss} \approx 0.55$ to $s/L_{ss} \approx 0.7$ as the wakes pass. Similarly, evidence of reattachment can be seen as an increase in surface shear stress, ranging from $s/L_{ss} \approx 0.8$ to $s/L_{ss} \approx 0.95$, although the change in shear stress for reattachment is smaller than that seen for separation.

However, in the increased-spacing case (Figure 4.2), the location of the abrupt drop-off in shear stress occurs starting at $s/L_{ss} \approx 0.45$, suggesting that separation is occurring farther upstream. From Figure 4.2, no clear evidence of an increase in surface shear stress near the trailing edge can be seen, so no conclusions about reattachment can be made from this presentation of the data. It appears, however,that reattachment is delayed in this case.

These data must be used with caution, since the uncertainties in the measurements are quite high ($\sim 30\%$) in some of the more severe locations. Additionally, the use of hot-wire anemometry to measure velocities means that for high-TI and reversing flow, the measured velocity (and hence the calculated shear stress) can be incorrect. We will be able to identify regions of low wall shear stress but we cannot measure the directions or magnitudes of near-zero values with accuracy. Essentially, when $|\tau_w| < 0.05\,\mathrm{Pa}$, we can merely say that it is low, without accurately quantifying it. Previous measurements in the steady flow (Simon et al., 2000) showed that separation and reattachment points taken from such shear stress distribution maps which were computed from near-wall flow velocities differed, somewhat, from separation and reattachment points taken directly from surface shear stress direction measurements. Ideally, the location of separation should be determined using surface measurement techniques, such as surface-mounted hot films. The ink-dot technique

used in the steady-flow cases cannot be used in the unsteady flow.

4.2.3 Transition Onset

In the increased wake spacing case, we can see evidence of separated flow transition and attached flow transition. The transition onset points are time-dependent, as affected by the passing wake. Transition onset is observed upstream of separation in the period $248^\circ < \theta < 268^\circ$, while in the period $272^\circ < \theta < 332^\circ$, separated flow transition is observed (Kaszeta et al. (2003)). We define the obvious but small elevation of u_{rms} as transition onset, like yellow part in the boundary layer in Figure 4.12(b) (at $\theta = 200^\circ$). By comparing Figure 4.8(b) and Figure 4.12(b), we can say the earliest transition onset point is between $37.35\% < s/L_{ss} < 43.34\%$, which is more upstream than the separation points. The disturbance from the freestream is the reason for early transition. The passing wake is overhead at this time (see Figure 4.14). We also notice that the flow is relaminarized after $\theta = 225^\circ$ at $s/L_{ss} = 43.34\%$ (see Fig 4.14b). But the downstream flow is transitioning or turbulent (see Figures 4.16(b) and 4.20(b)). This means the transition is moving downstream with the passing wake. After $\theta = 300^\circ$, the flow is relaminarized at $s/L_{ss} = 61.32\%$ (see Figure 4.24(b)) while the flow downstream is transitioning or turbulent (see Figures 4.28(b) and 4.32(b)). This means transition onset is between $61.32\% < s/L_{ss} < 70.31\%$, which is downstream of the separation point.

Compared to the base case, the increased wake spacing case has a shorter turbulent strip. For example, at $s/L_{ss} = 55.33\%$, the flow is in transition or turbulent from $\theta = 180^\circ$ to 260° in the increased wake spacing case (see Figure 4.20(b)), while in the base case the flow is turbulent or turbulent-like from $\theta = 120^\circ$ to 330° (see Figure 4.20(b)). Again, the reason is the disturbance of the freestream overhead. In the base case, the freestream is much more disturbed due to a broader passing wake (see Figure 4.22(a)). But in the increased wake spacing case, the wake is narrower and during most of the wake passing cycle, the flow is recovering (see Figure 4.22).

For both cases, the transitioning flow or turbulent flow can thin the boundary layer, retarding separation but with a lag in time. For instance, the boundary layer is thinnest at $\theta = 250^\circ$ at $s/L_{ss} = 55.33\%$ (see Figure 4.19(b)). The flow in the boundary layer experienced transition or turbulence just before this time (see Figure 4.20(b)). We can see a clear correlation from the figures. This is how the passing wake can affect the separation point.

4.2.4 Narrower Wakes

By examining the boundary layer velocity profiles, we can see that in the pre-separation flowfield, the boundary layer has had adequate time to recover from the wake passage. For example, if at station 6 we compare the base case data (Figure 4.11(a)) and the increased spacing data (Figure 4.11(b)), we can see that in the base case, the boundary layer never fully recovers from one wake to the next, while in the increased wake spacing case, from $\theta = 35^\circ$ to 125° the boundary layer is invariant with time, suggesting that the flow has fully recovered from the passing of the previous wake. Similar conclusions can be drawn by examining the velocity rms (Figure 4.12), the TI (Figure 4.13), and the intermittency (Figure 4.14) plots.

4.2.5 Slightly Stronger Wakes

The wakes in the increased wake spacing case have a slightly larger velocity deficit associated with them. As a result of this, the response of the boundary layer to a passing wake is stronger. For example, comparing velocity profiles at station 8, Figures 4.19(a) and 4.19(b), we can see that in the increased wake spacing case, the thickening/thinning of the near-wall boundary layer is much more pronounced ($175^\circ < \theta < 325^\circ$) than with the base case ($100^\circ < \theta < 350^\circ$). This is probably due to the flow having the opportunity to fully recover from the passage of each wake before the arrival of the next wake.

4.2.6 Thicker Boundary Layer

Referring to the velocity plots in Figures 4.19(a) and 4.19(b), since the flow has an opportunity to recover from each passing wake, the boundary layer has the opportunity to undergo boundary layer streamwise development as though the wakes were not present. As a result of this, the increased wake spacing case shows a slightly thicker boundary layer near the end of the acceleration period which begins with the wake passing.

4.2.7 Larger Separation Bubble

Similarly, the separation bubble in the increased wake spacing case is much thicker than the bubble seen in the base case. Comparing the velocity profiles at the thickest portion of the separation bubble, station 11 for the base case (Figure 4.31(a)) and station 12 for the increased wake spacing case (Figure 4.35(b)), we can see that the bubble in the increased

spacing case is more than twice as thick as that of the base case.

4.2.8 Distinct Wakes

Examining the intermittency distributions in the base case, we can see that the wakes are close enough that in the freestream, the flow never returns to a laminar-like state (see the elevated intermittency regions between the wakes in the base case in Figures 4.6(a), 4.22(a) and 4.38(a)). For the equivalent locations, the increasing spacing case data show that the freestream flow has had an opportunity to return to laminar-like flow (see the near-zero intermittency regions between the wakes in the increased wake spacing case in Figures 4.6(b), 4.22(b) and 4.38(b)). Similarly, the between-wake regions of the base case generally have higher turbulence levels than in the increased spacing case (compare Figures 4.19(a) and 4.19(b)).

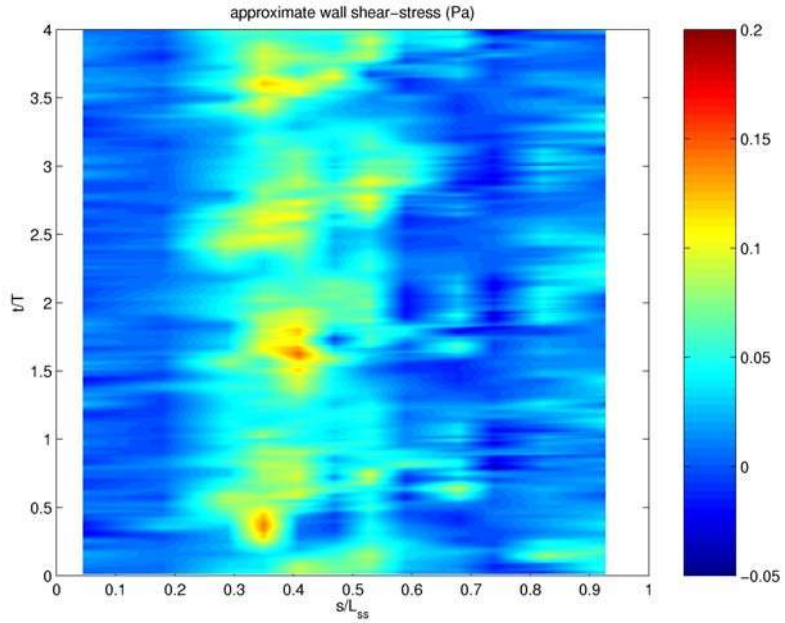

Figure 4.1: Approximate wall shear stress obtained from the ensemble-averaged velocity profiles, base case

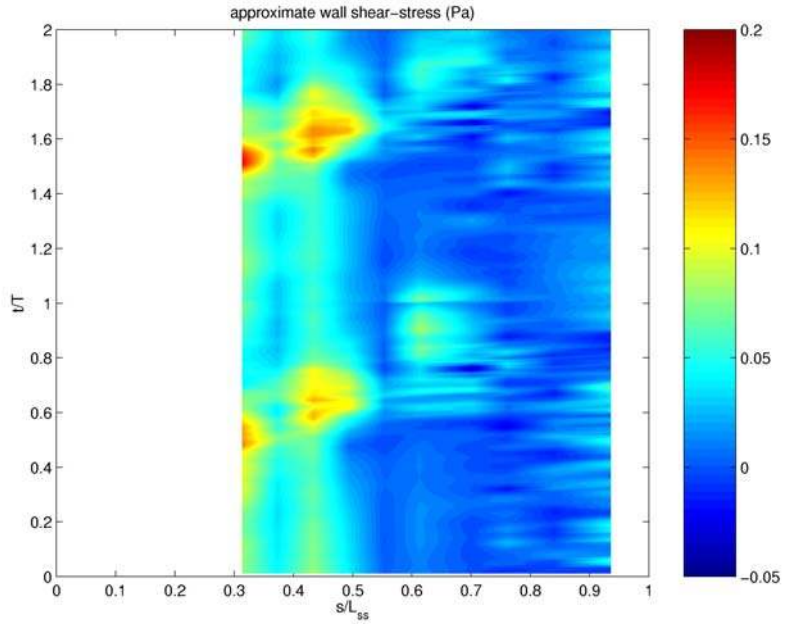

Figure 4.2: Approximate wall shear stress obtained from the ensemble-averaged velocity profiles, increased wake spacing case

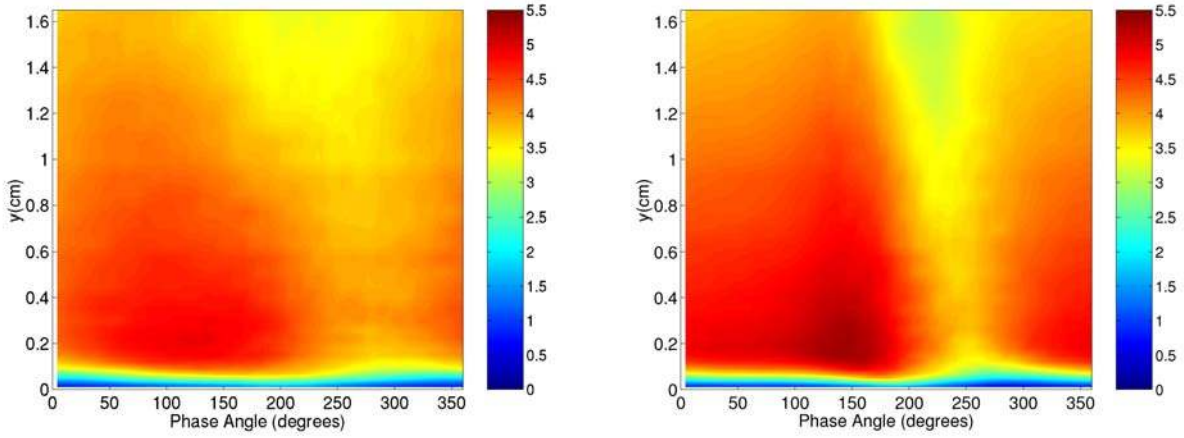

(a) Base Case (b) Increased Wake Spacing Case

Figure 4.3: Velocity, $\tilde{u}$, (m/s), at station 4 ($s/L_{ss} = 31.36\%$)

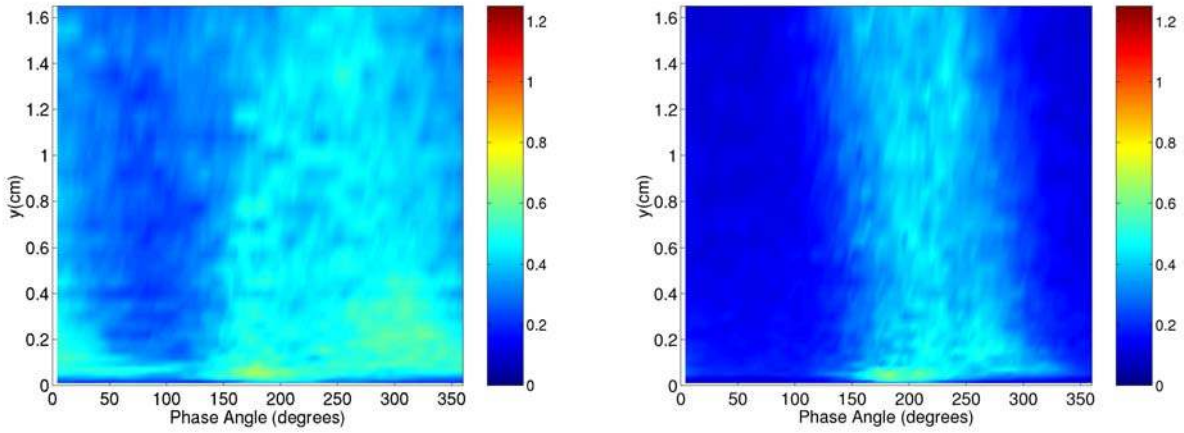

(a) Base Case (b) Increased Wake Spacing Case

Figure 4.4: Velocity rms, $\widetilde{u_{rms}}$, (m/s), at station 4 ($s/L_{ss} = 31.36\%$)

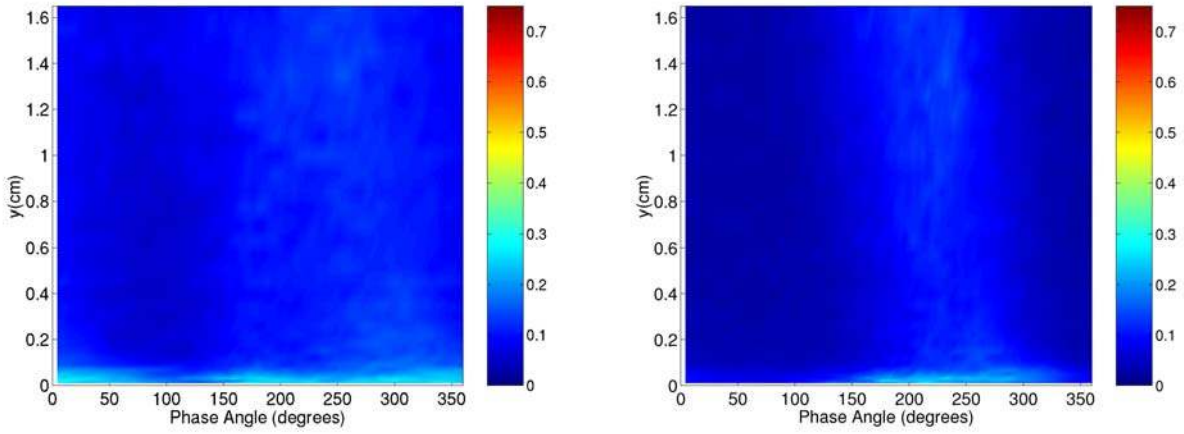

(a) Base Case (b) Increased Wake Spacing Case

Figure 4.5: Turbulence Intensity, $\widetilde{TI}$, at station 4 ($s/L_{ss} = 31.36\%$)

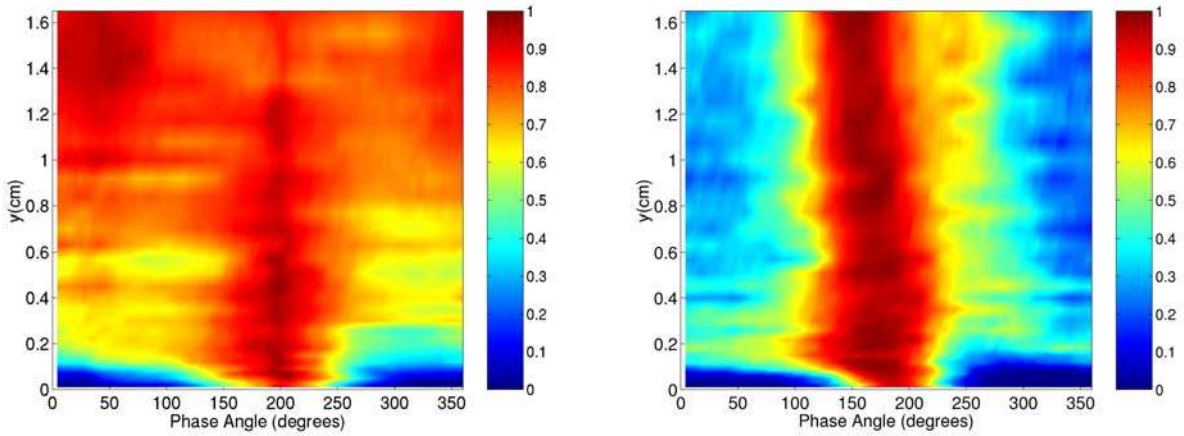

(a) Base Case (b) Increased Wake Spacing Case

Figure 4.6: Intermittency, $\tilde{\gamma}$, at station 4 ($s/L_{ss} = 31.36\%$)

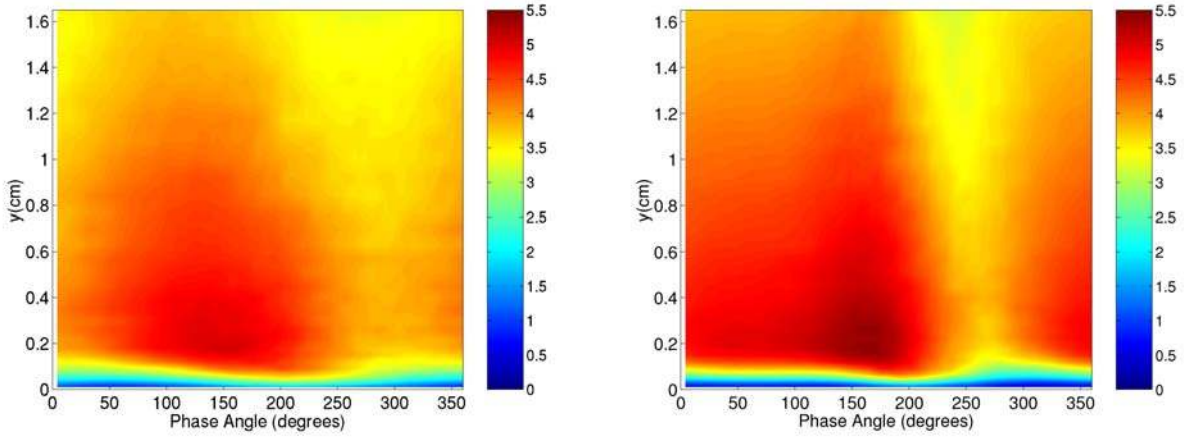

(a) Base Case (b) Increased Wake Spacing Case

Figure 4.7: Velocity, $\tilde{u}$, (m/s), at station 5 ($s/L_{ss} = 37.35\%$)

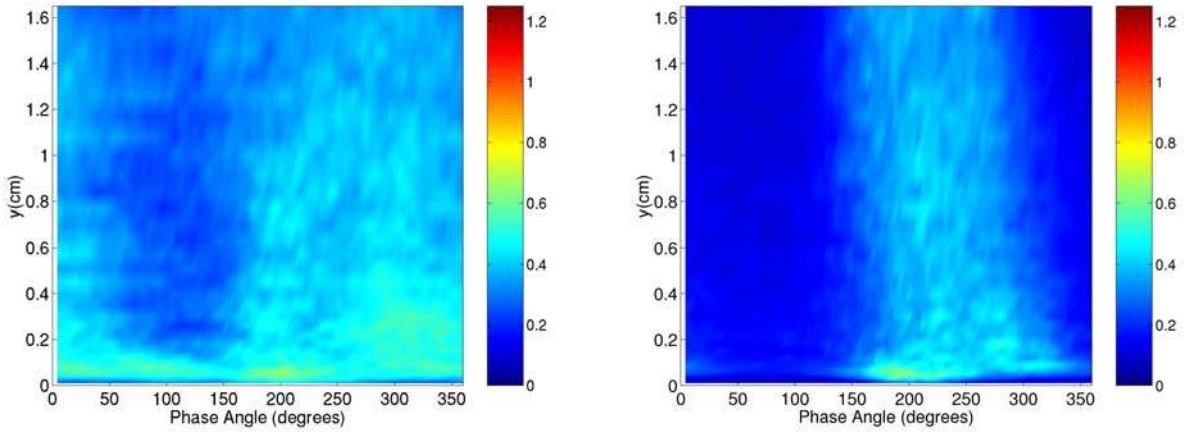

(a) Base Case (b) Increased Wake Spacing Case

Figure 4.8: Velocity rms, $\widetilde{u_{rms}}$, (m/s), at station 5 ($s/L_{ss} = 37.35\%$)

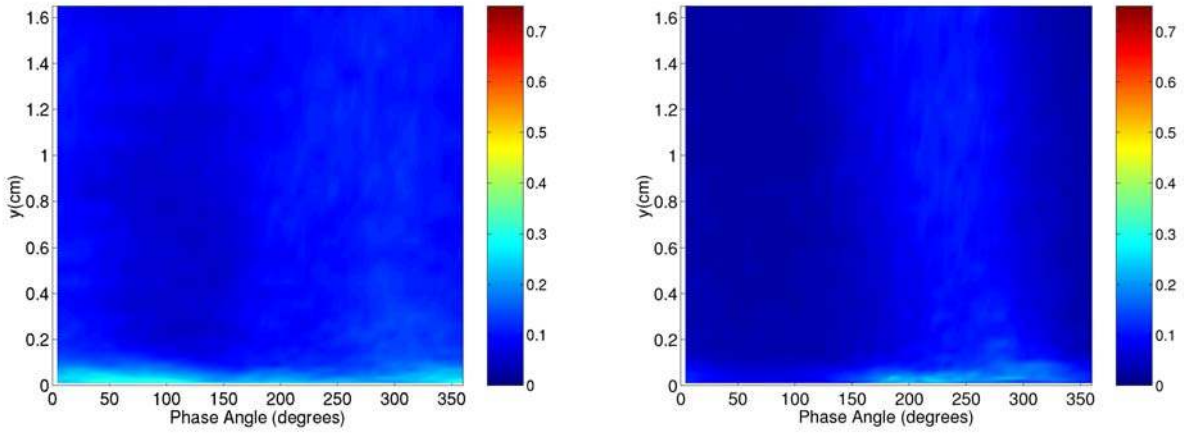

(a) Base Case

(b) Increased Wake Spacing Case

Figure 4.9: Turbulence Intensity, $\widetilde{TI}$, at station 5 ($s/L_{ss} = 37.35\%$)

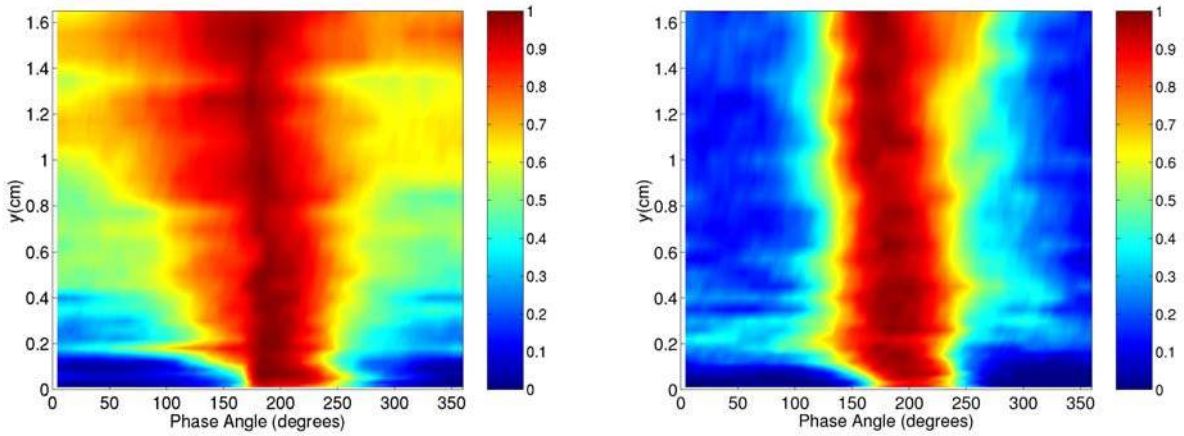

(a) Base Case

(b) Increased Wake Spacing Case

Figure 4.10: Intermittency, $\tilde{\gamma}$, at station 5 ($s/L_{ss} = 37.35\%$)

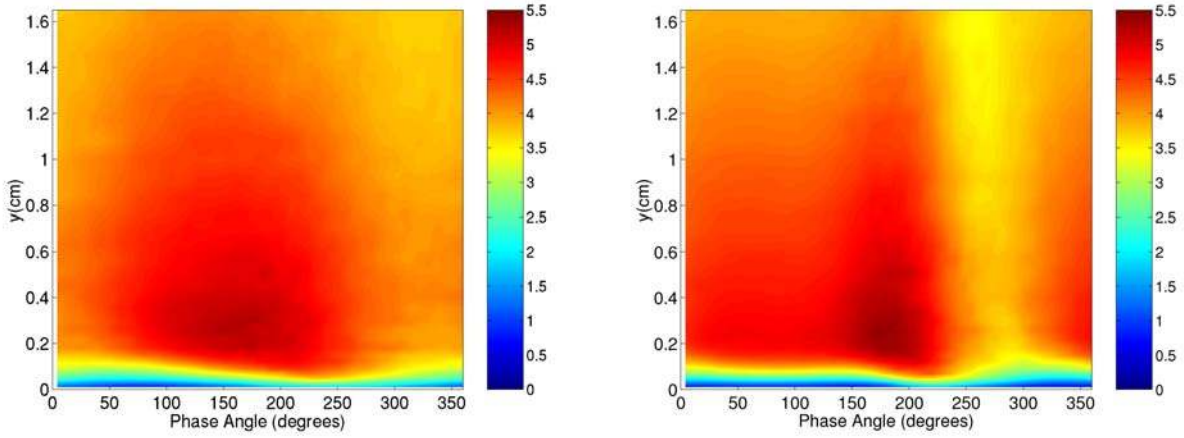

(a) Base Case (b) Increased Wake Spacing Case

Figure 4.11: Velocity, $\tilde{u}$, (m/s), at station 6 ($s/L_{ss} = 43.34\%$)

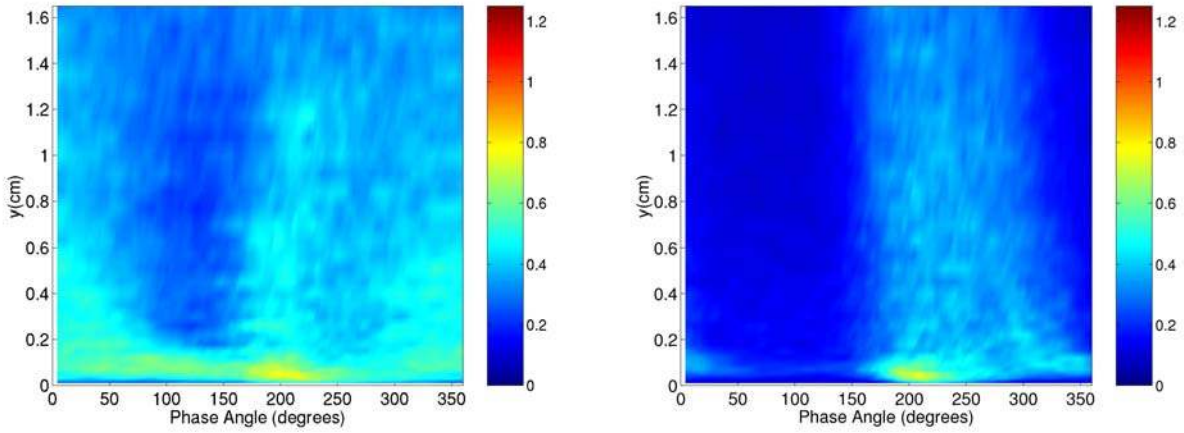

(a) Base Case (b) Increased Wake Spacing Case

Figure 4.12: Velocity rms, $\widetilde{u_{rms}}$, (m/s), at station 6 ($s/L_{ss} = 43.34\%$)

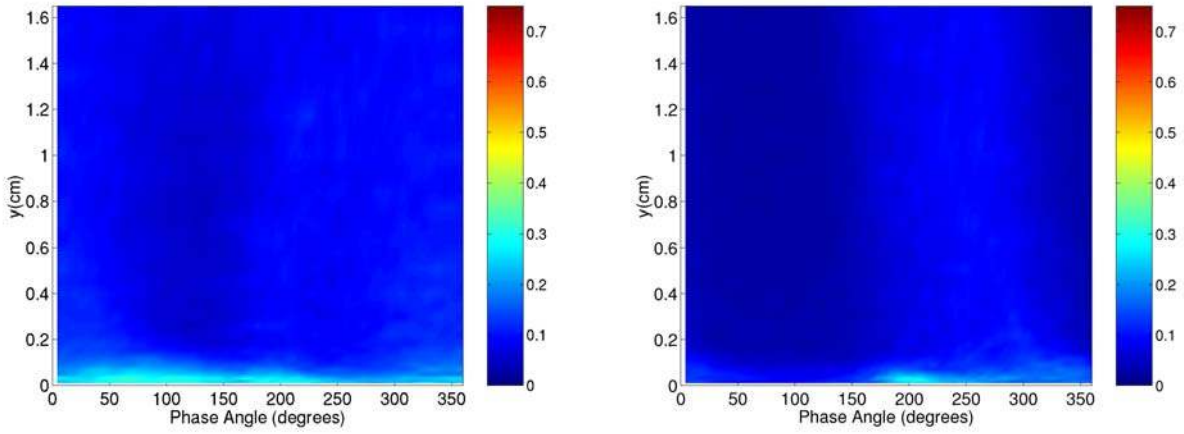

(a) Base Case (b) Increased Wake Spacing Case

Figure 4.13: Turbulence Intensity, $\widetilde{TI}$, at station 6 ($s/L_{ss} = 43.34\%$)

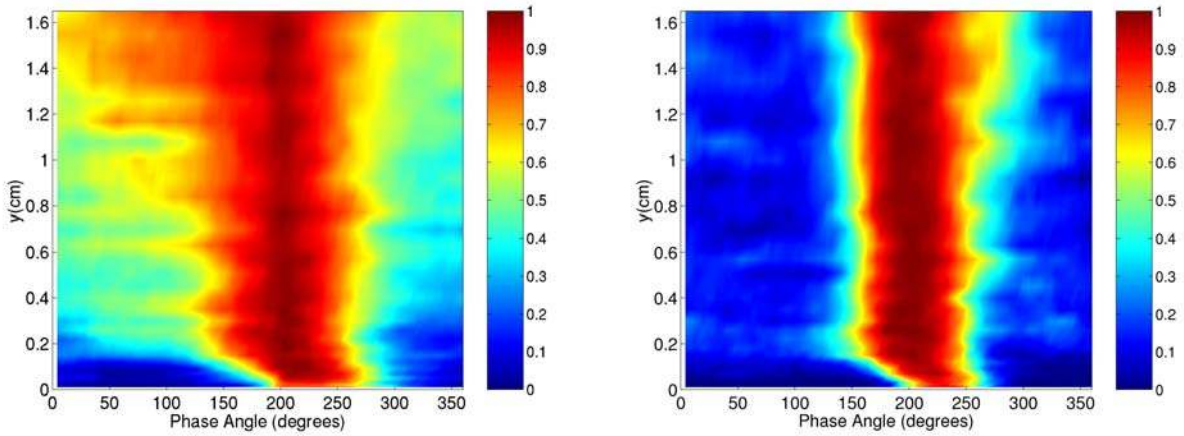

(a) Base Case (b) Increased Wake Spacing Case

Figure 4.14: Intermittency, $\tilde{\gamma}$, at station 6 ($s/L_{ss} = 43.34\%$)

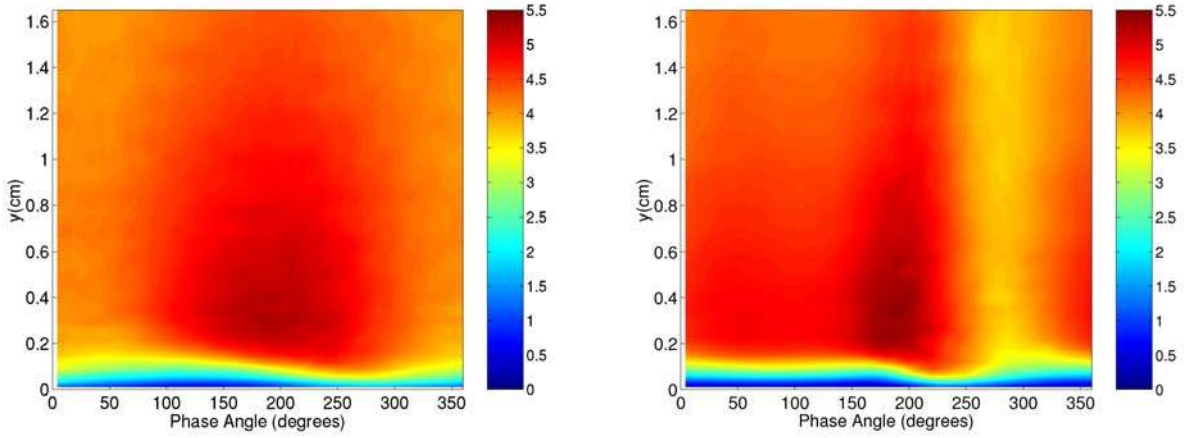

(a) Base Case (b) Increased Wake Spacing Case

Figure 4.15: Velocity, $\tilde{u}$, (m/s), at station 7 ($s/L_{ss} = 49.33\%$)

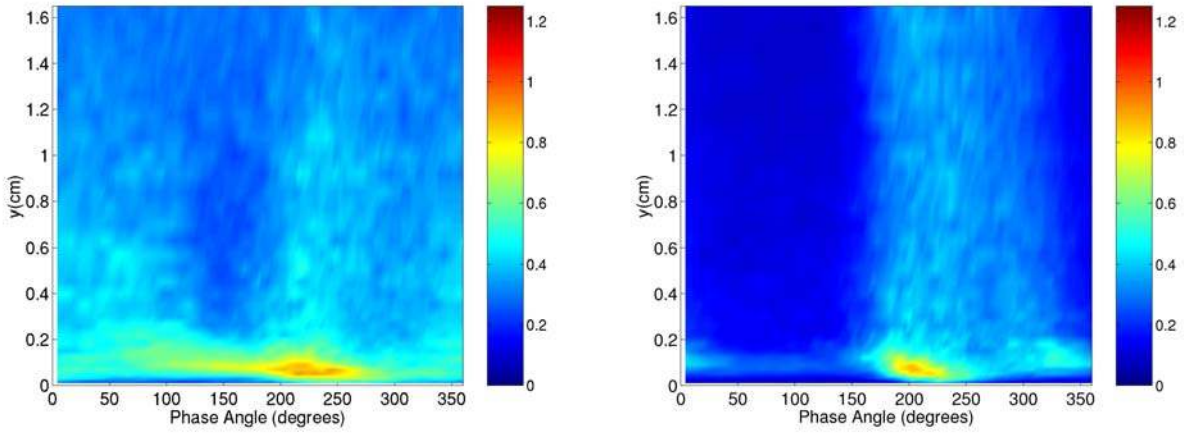

(a) Base Case (b) Increased Wake Spacing Case

Figure 4.16: Velocity rms, $\widetilde{u_{rms}}$, (m/s), at station 7 ($s/L_{ss} = 49.33\%$)

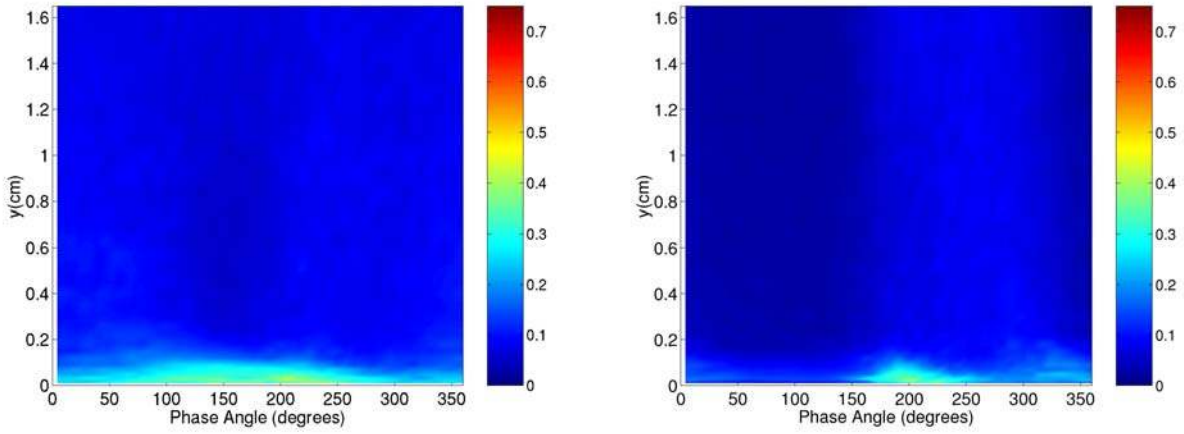

(a) Base Case (b) Increased Wake Spacing Case

Figure 4.17: Turbulence Intensity, $\widetilde{TI}$, at station 7 ($s/L_{ss} = 49.33\%$)

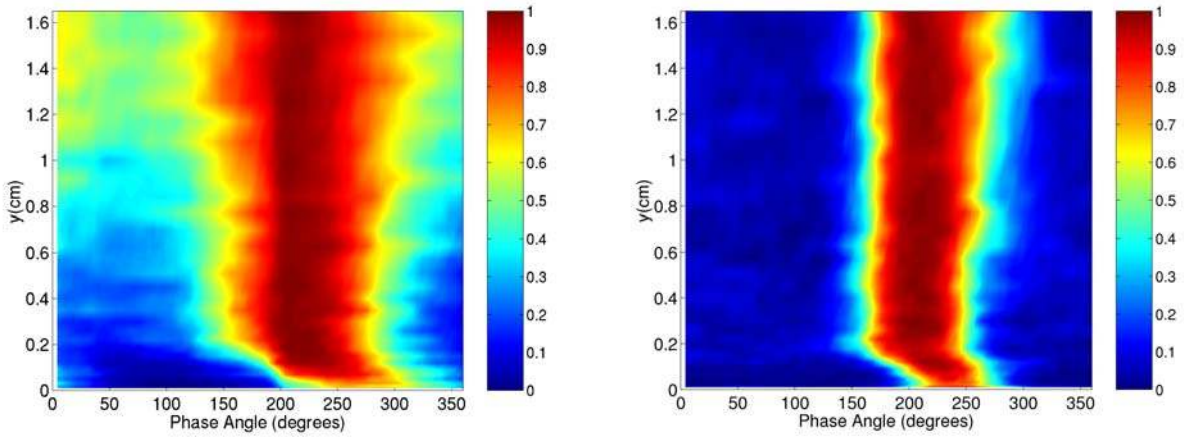

(a) Base Case (b) Increased Wake Spacing Case

Figure 4.18: Intermittency, $\tilde{\gamma}$, at station 7 ($s/L_{ss} = 49.33\%$)

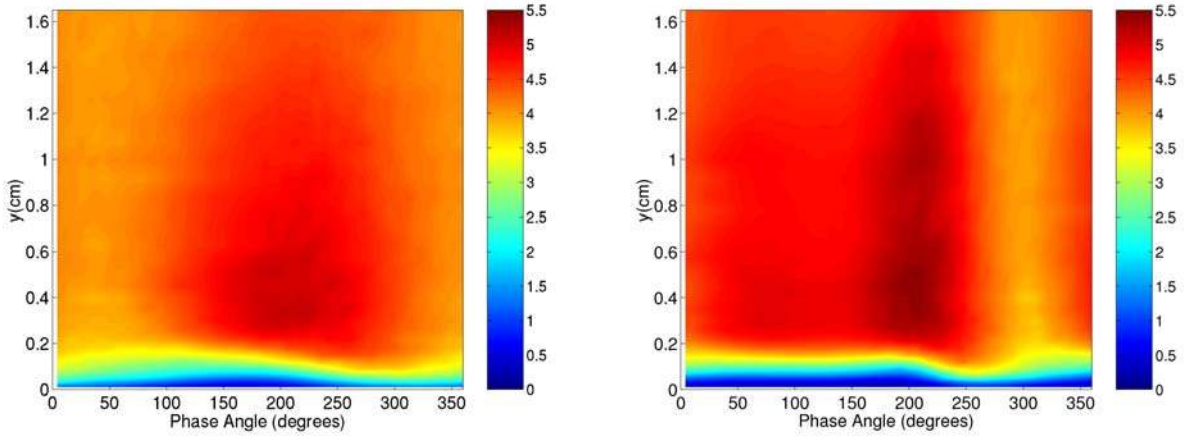

(a) Base Case (b) Increased Wake Spacing Case

Figure 4.19: Velocity, $\tilde{u}$, (m/s), at station 8 ($s/L_{ss} = 55.33\%$)

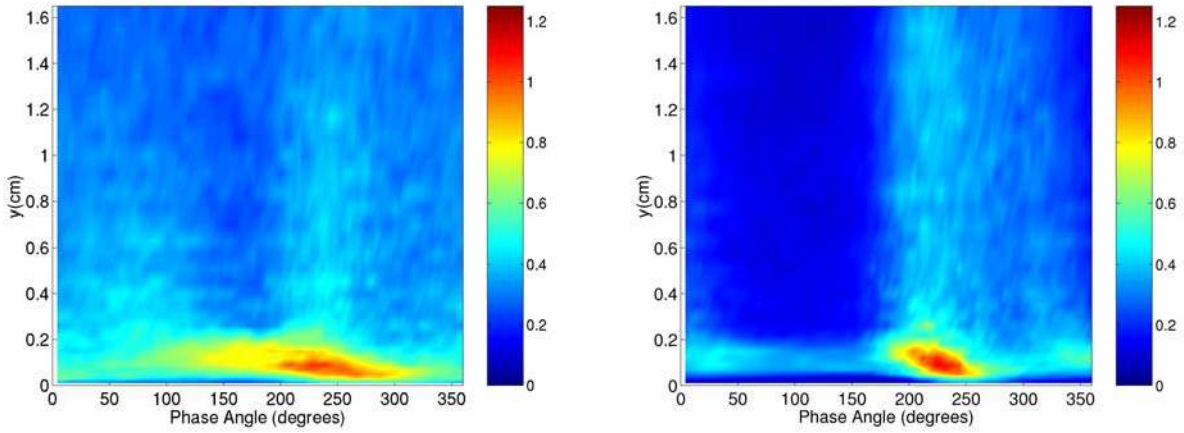

(a) Base Case (b) Increased Wake Spacing Case

Figure 4.20: Velocity rms, $\widetilde{u_{rms}}$, (m/s), at station 8 ($s/L_{ss} = 55.33\%$)

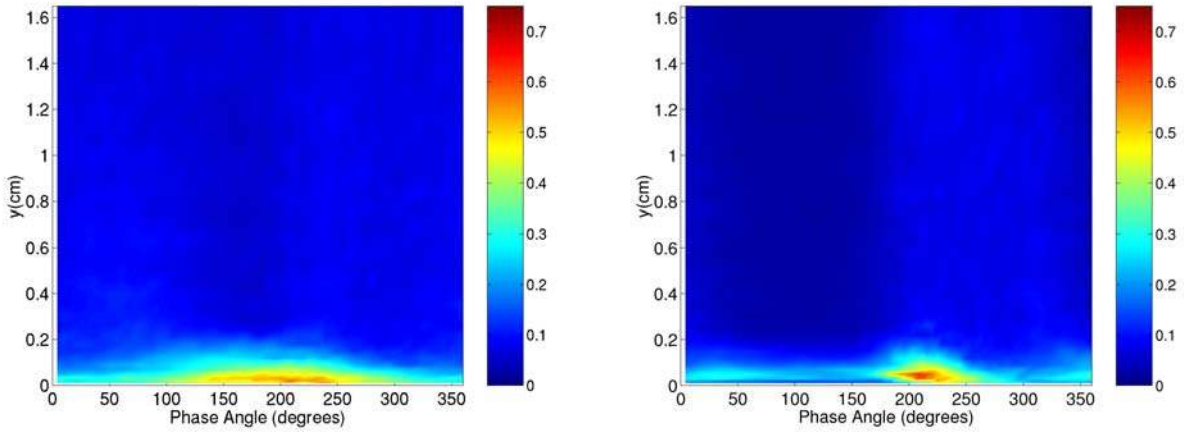

(a) Base Case (b) Increased Wake Spacing Case

Figure 4.21: Turbulence Intensity, $\widetilde{TI}$, at station 8 ($s/L_{ss} = 55.33\%$)

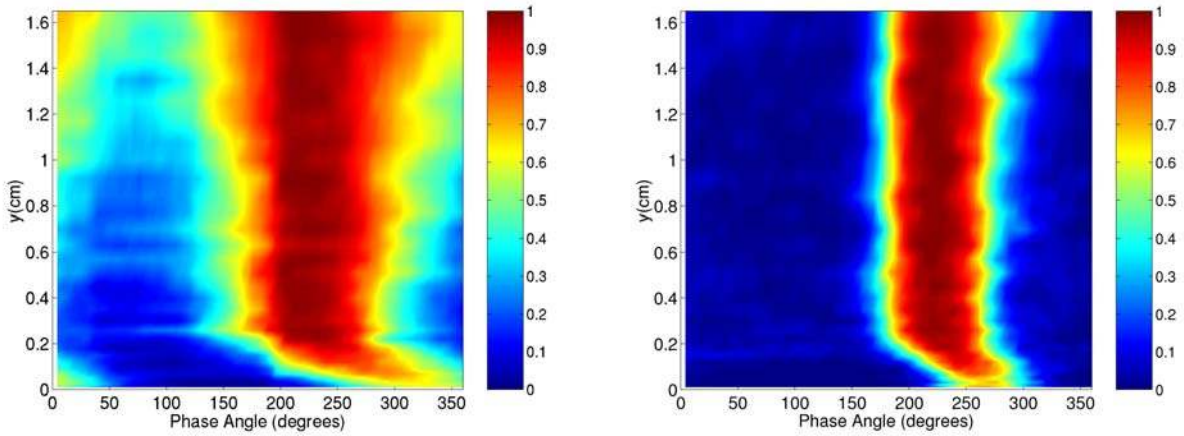

(a) Base Case (b) Increased Wake Spacing Case

Figure 4.22: Intermittency, $\tilde{\gamma}$, at station 8 ($s/L_{ss} = 55.33\%$)

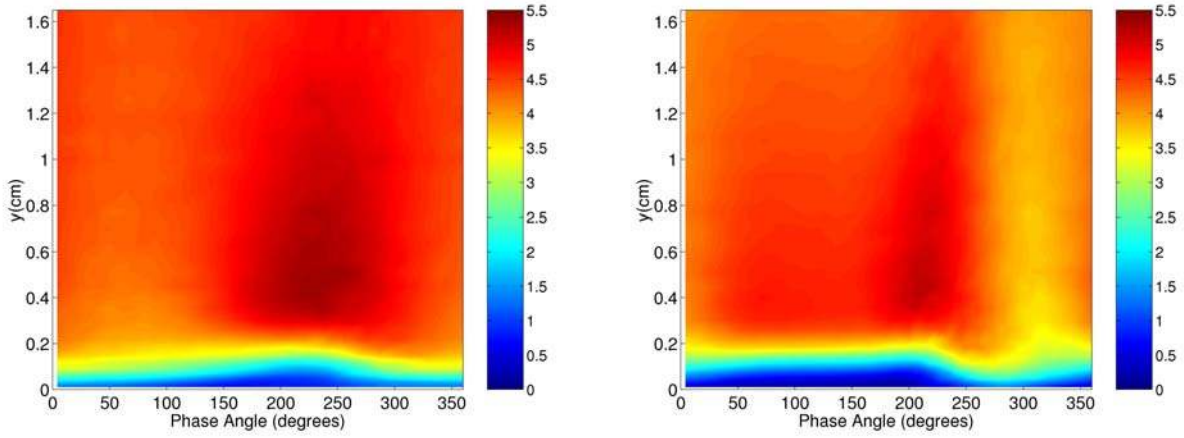

(a) Base Case (b) Increased Wake Spacing Case

Figure 4.23: Velocity, $\tilde{u}$, (m/s), at station 9 ($s/L_{ss} = 61.32\%$)

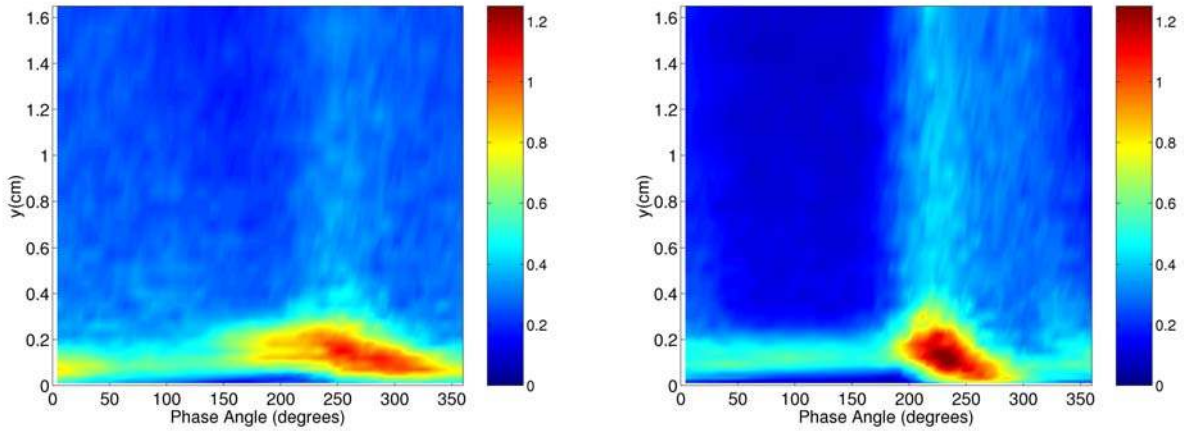

(a) Base Case (b) Increased Wake Spacing Case

Figure 4.24: Velocity rms, $\widetilde{u_{rms}}$, (m/s), at station 9 ($s/L_{ss} = 61.32\%$)

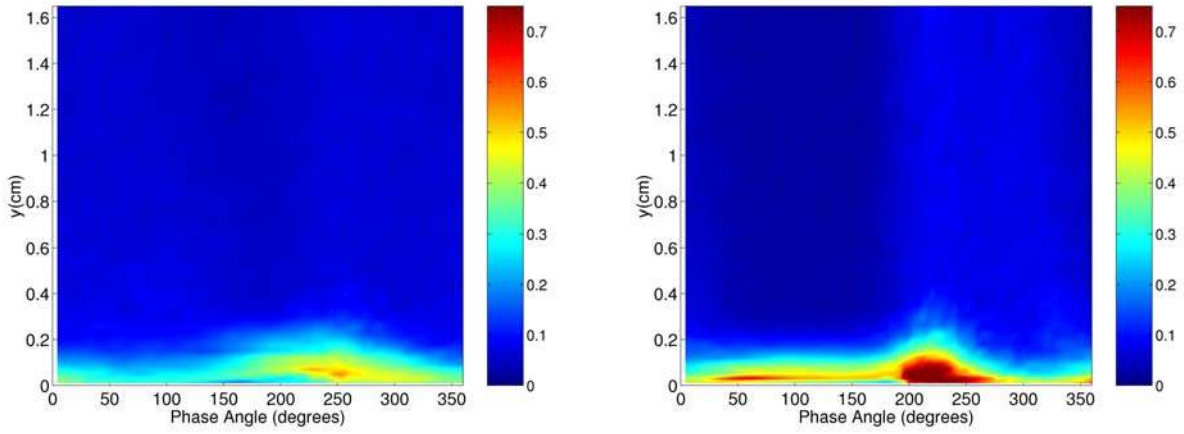

(a) Base Case (b) Increased Wake Spacing Case

Figure 4.25: Turbulence Intensity, $\widetilde{TI}$, at station 9 ($s/L_{ss} = 61.32\%$)

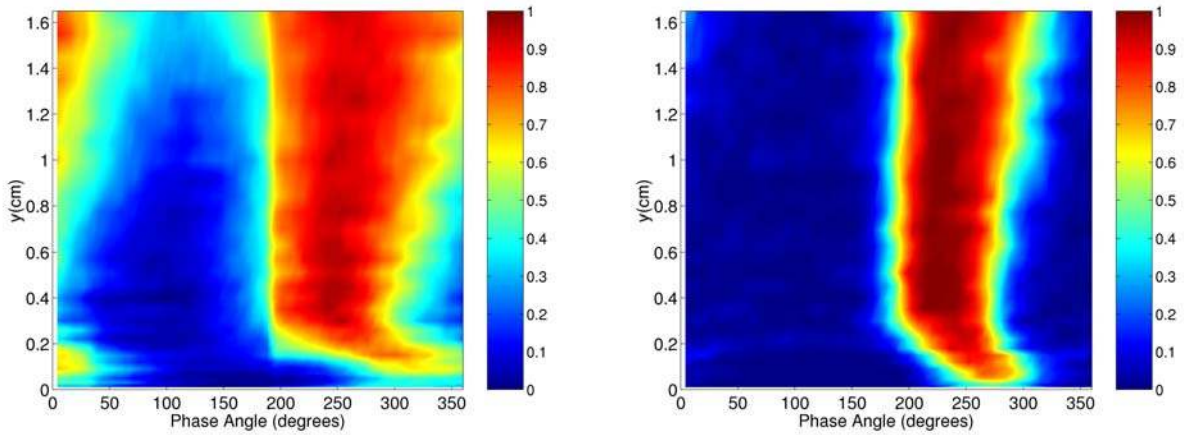

(a) Base Case (b) Increased Wake Spacing Case

Figure 4.26: Intermittency, $\tilde{\gamma}$, at station 9 ($s/L_{ss} = 61.32\%$)

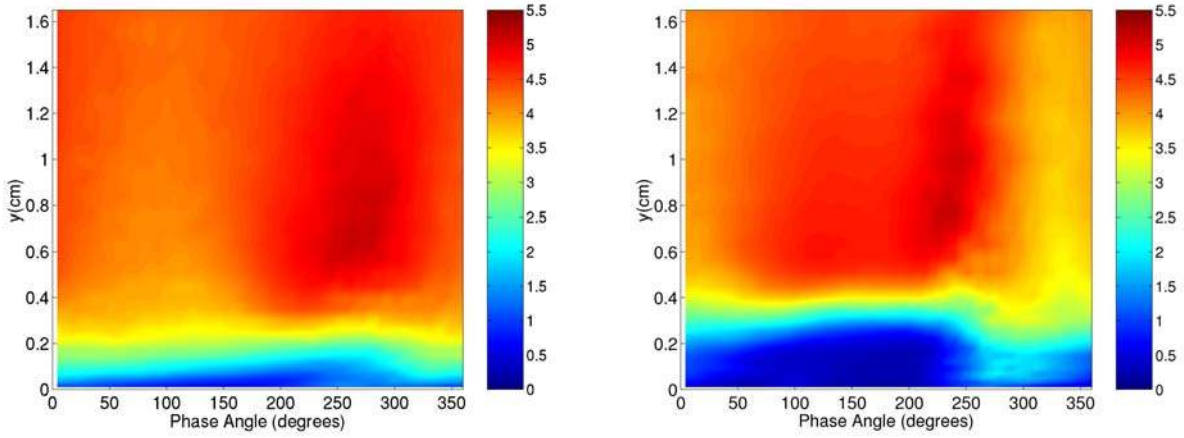

(a) Base Case

(b) Increased Wake Spacing Case

Figure 4.27: Velocity, $\tilde{u}$, (m/s), at station 10 ($s/L_{ss} = 70.31\%$)

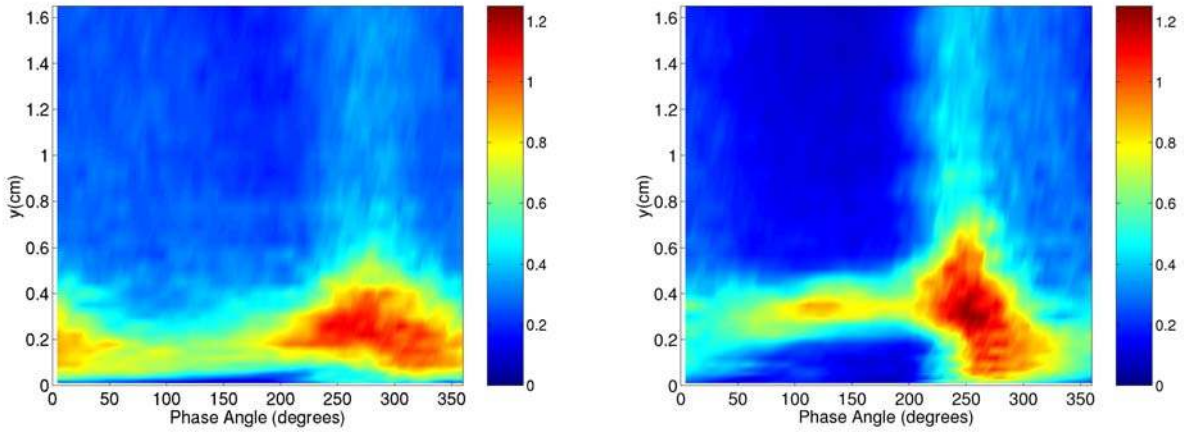

(a) Base Case

(b) Increased Wake Spacing Case

Figure 4.28: Velocity rms, $\widetilde{u_{rms}}$, (m/s), at station 10 ($s/L_{ss} = 70.31\%$)

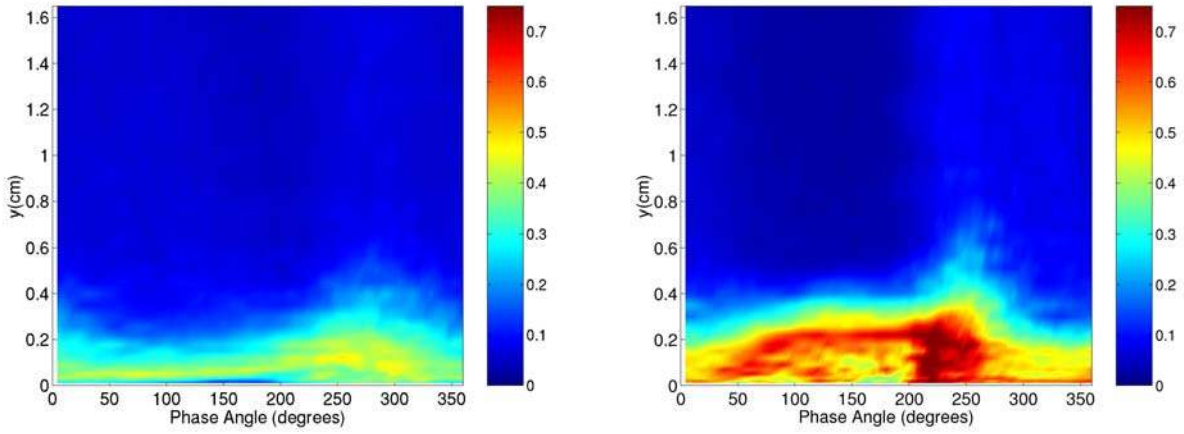

(a) Base Case (b) Increased Wake Spacing Case

Figure 4.29: Turbulence Intensity, $\widetilde{TI}$, at station 10 ($s/L_{ss} = 70.31\%$)

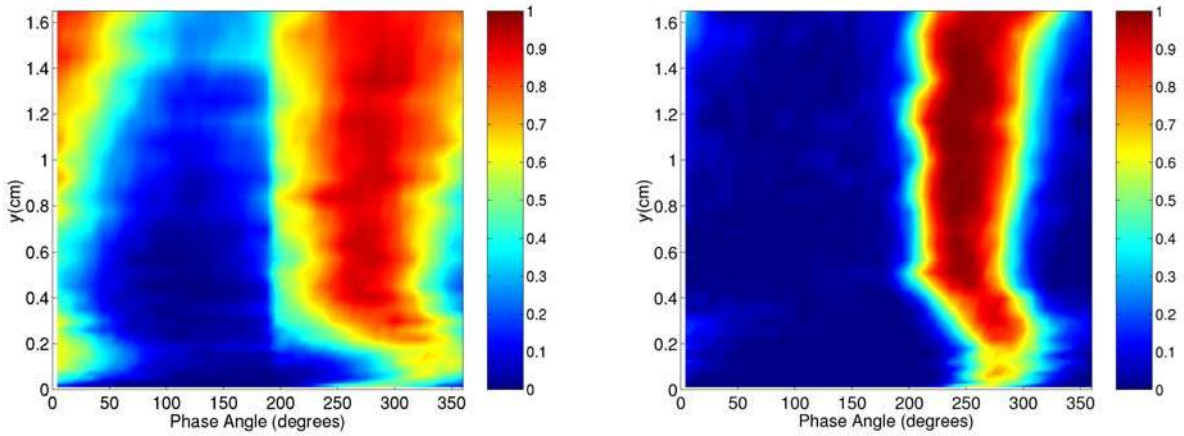

(a) Base Case (b) Increased Wake Spacing Case

Figure 4.30: Intermittency, $\tilde{\gamma}$, at station 10 ($s/L_{ss} = 70.31\%$)

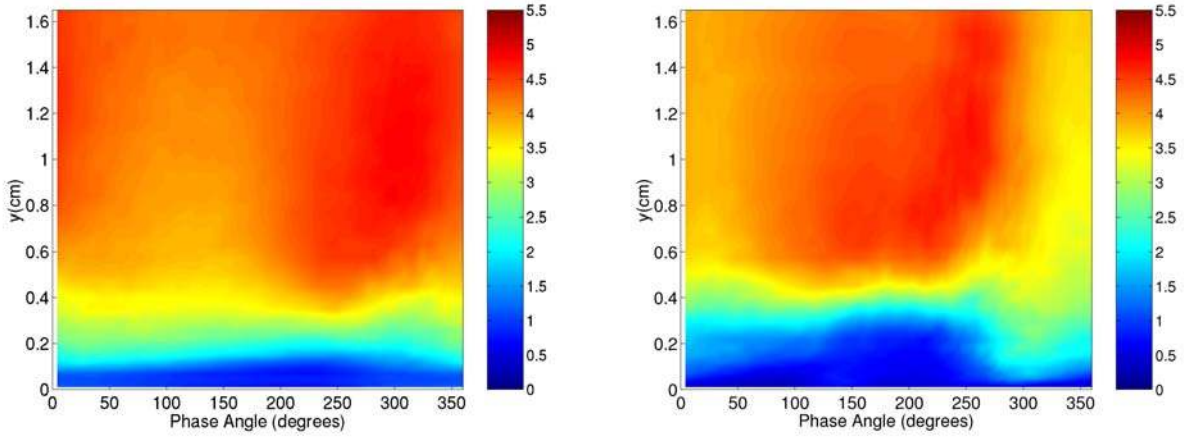

(a) Base Case (b) Increased Wake Spacing Case

Figure 4.31: Velocity, $\tilde{u}$, (m/s), at station 11 ($s/L_{ss} = 76.11\%$)

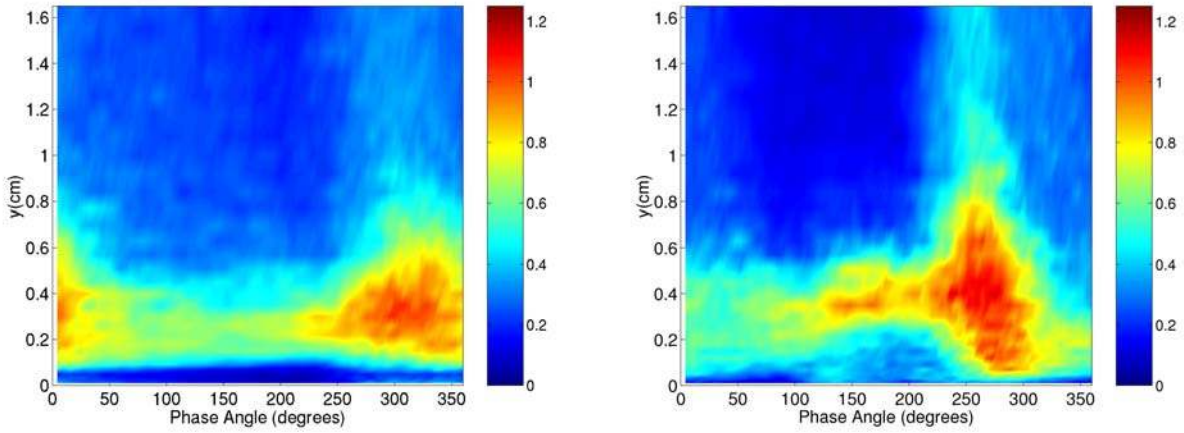

(a) Base Case (b) Increased Wake Spacing Case

Figure 4.32: Velocity rms, $\widetilde{u_{rms}}$, (m/s), at station 11 ($s/L_{ss} = 76.11\%$)

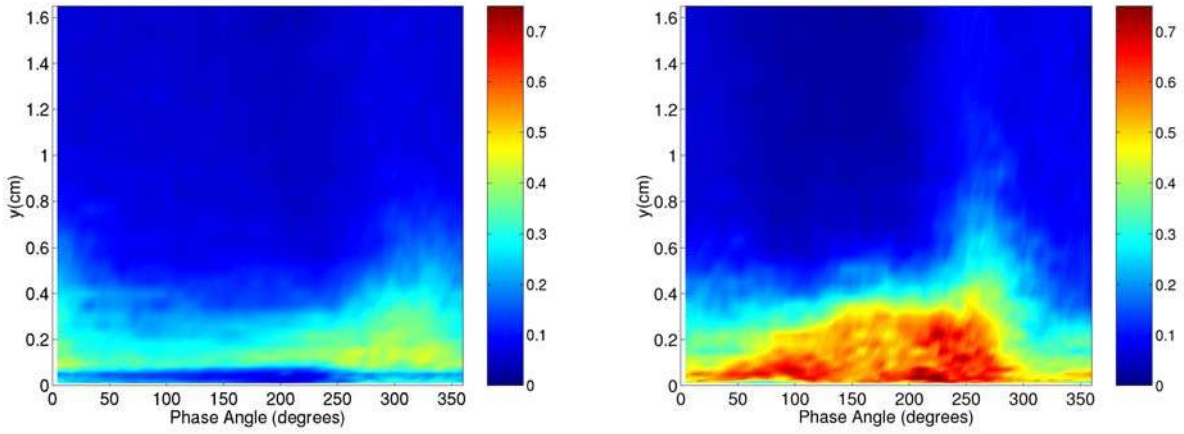

(a) Base Case (b) Increased Wake Spacing Case

Figure 4.33: Turbulence Intensity, $\widetilde{TI}$, at station 11 ($s/L_{ss} = 76.11\%$)

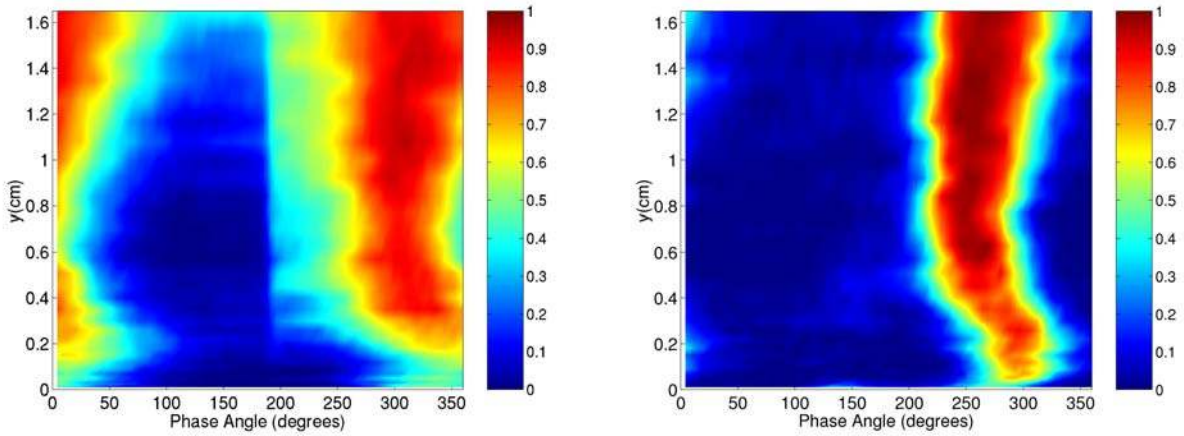

(a) Base Case (b) Increased Wake Spacing Case

Figure 4.34: Intermittency, $\tilde{\gamma}$, at station 11 ($s/L_{ss} = 76.11\%$)

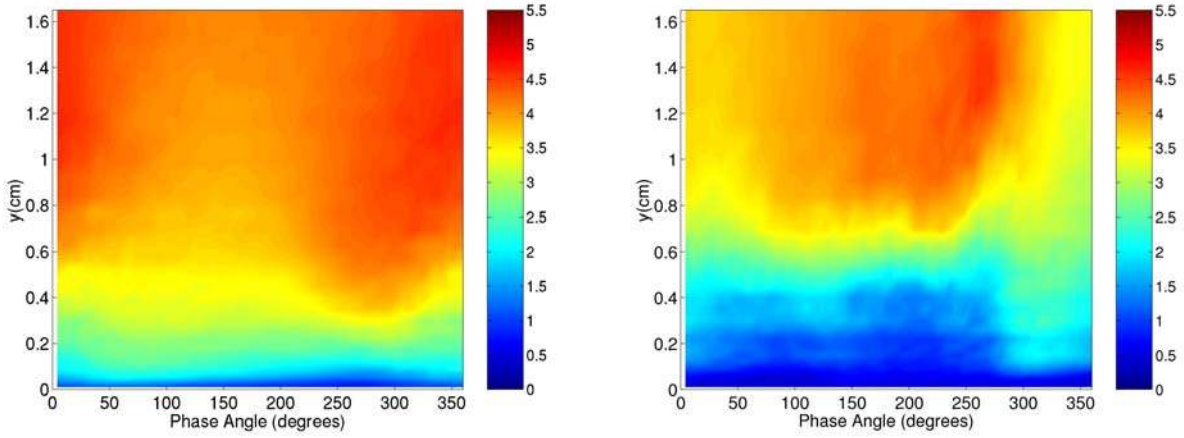

(a) Base Case

(b) Increased Wake Spacing Case

Figure 4.35: Velocity, $\tilde{u}$, (m/s), at station 12 ($s/L_{ss} = 84.00\%$)

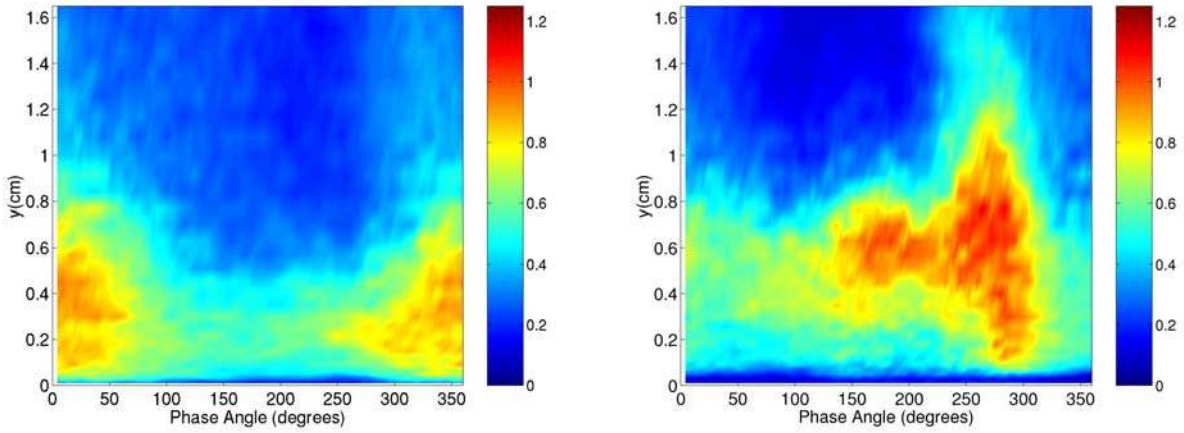

(a) Base Case

(b) Increased Wake Spacing Case

Figure 4.36: Velocity rms, $\widetilde{u_{rms}}$, (m/s), at station 12 ($s/L_{ss} = 84.00\%$)

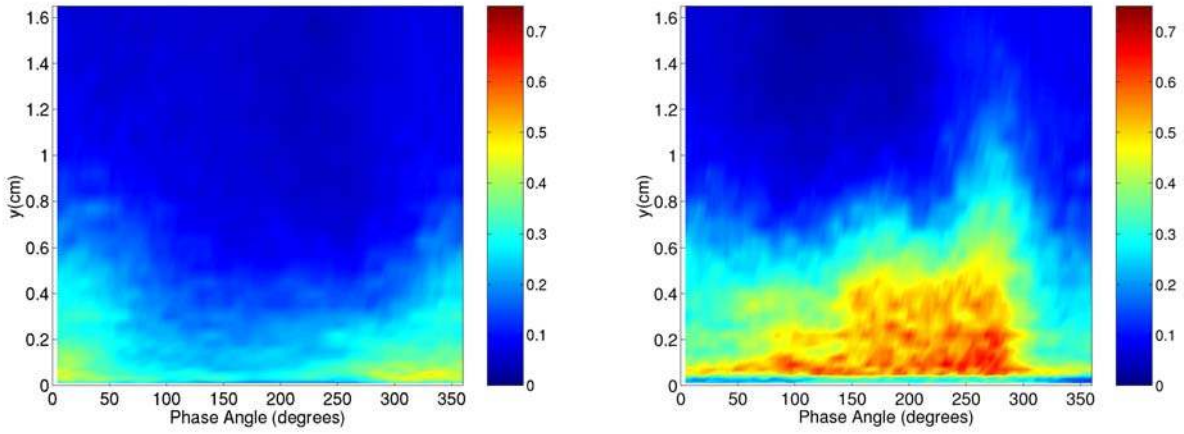

(a) Base Case (b) Increased Wake Spacing Case

Figure 4.37: Turbulence Intensity, $\widetilde{TI}$, at station 12 ($s/L_{ss} = 84.00\%$)

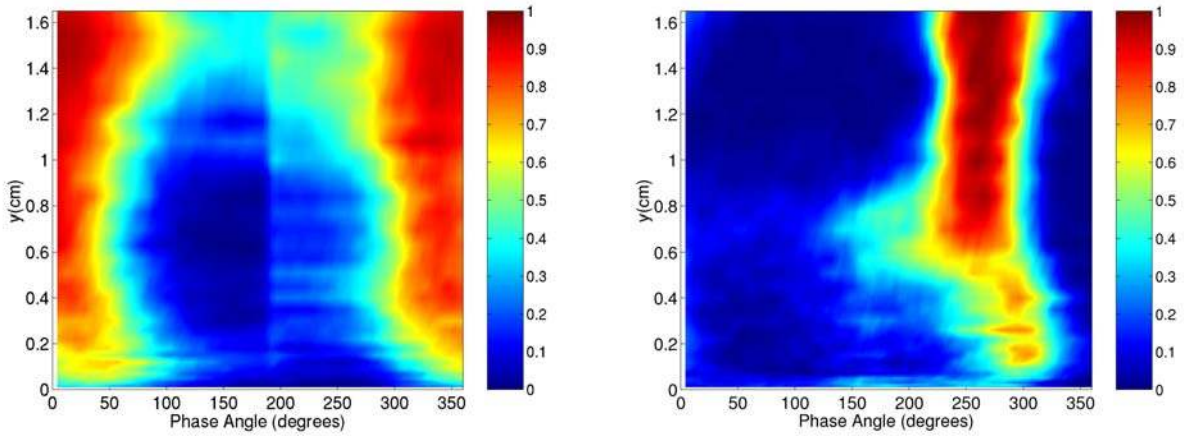

(a) Base Case (b) Increased Wake Spacing Case

Figure 4.38: Intermittency, $\tilde{\gamma}$, at station 12 ($s/L_{ss} = 84.00\%$)

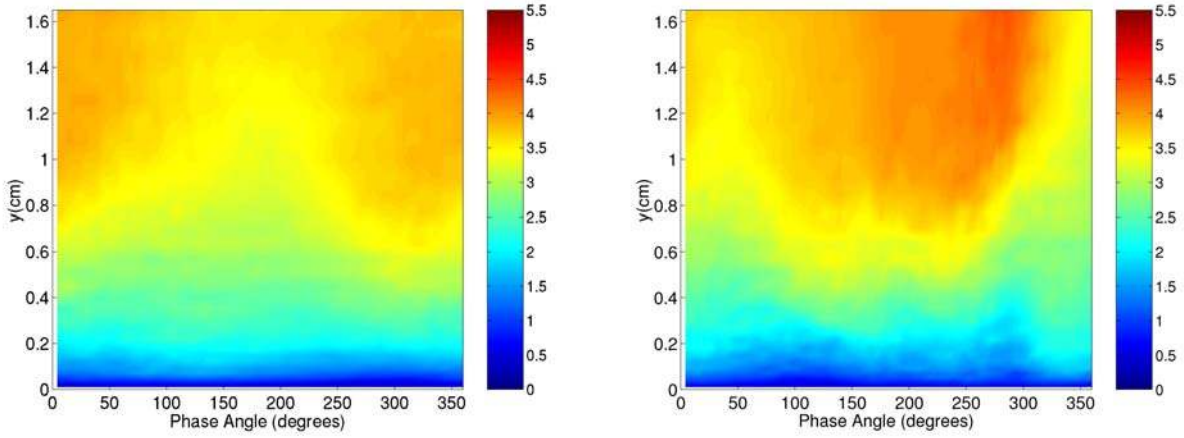

(a) Base Case (b) Increased Wake Spacing Case

Figure 4.39: Velocity, $\tilde{u}$, (m/s), at station 13 ($s/L_{ss} = 93.49\%$)

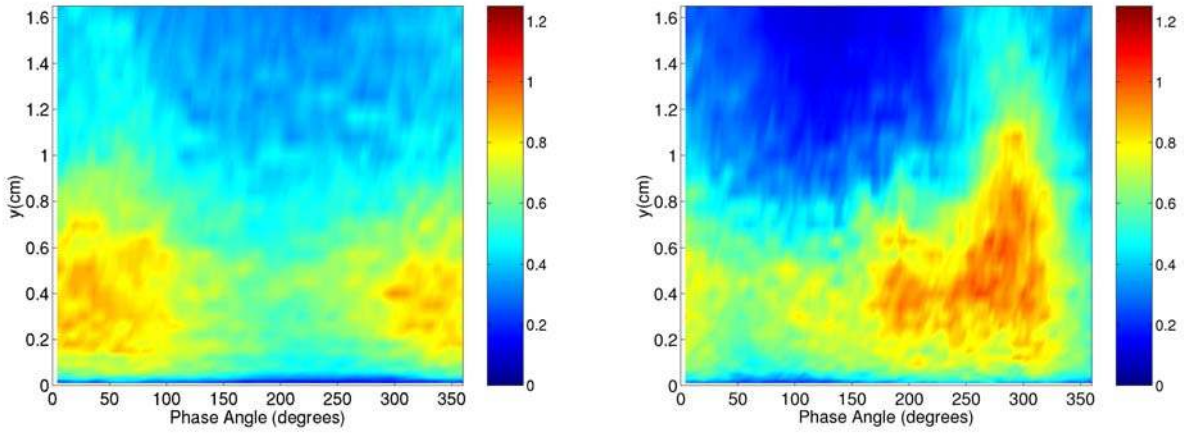

(a) Base Case (b) Increased Wake Spacing Case

Figure 4.40: Velocity rms, $\widetilde{u_{rms}}$, (m/s), at station 13 ($s/L_{ss} = 93.49\%$)

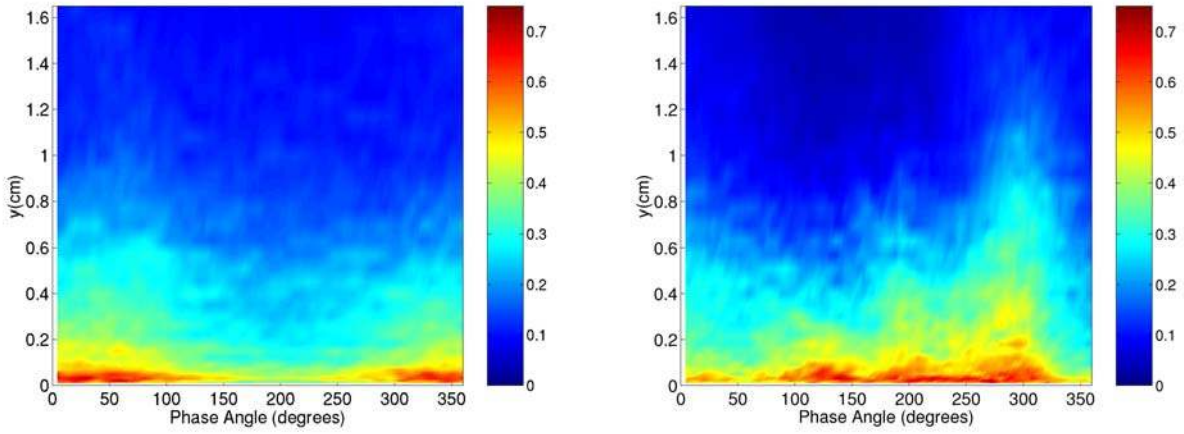

(a) Base Case (b) Increased Wake Spacing Case

Figure 4.41: Turbulence Intensity, $\widetilde{TI}$, at station 13 ($s/L_{ss} = 93.49\%$)

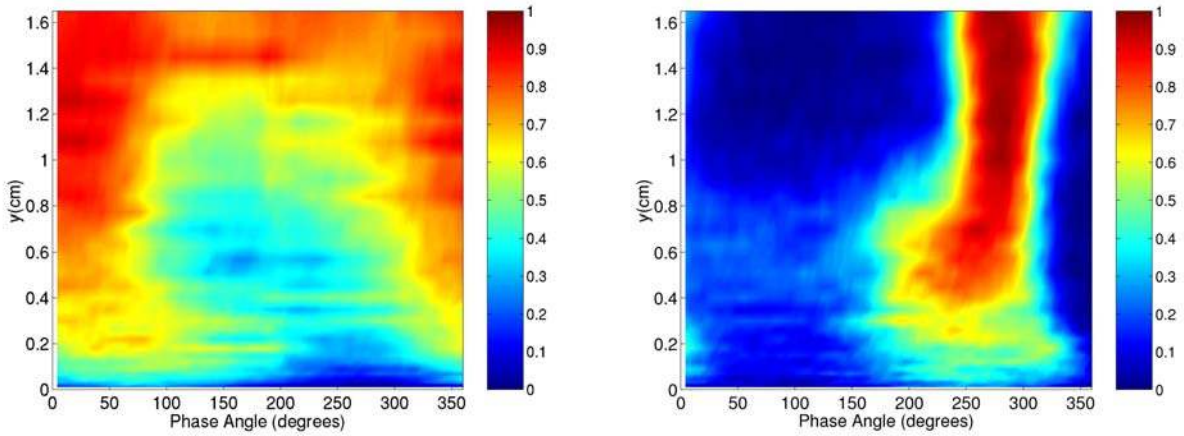

(a) Base Case (b) Increased Wake Spacing Case

Figure 4.42: Intermittency, $\tilde{\gamma}$, at station 13 ($s/L_{ss} = 93.49\%$)

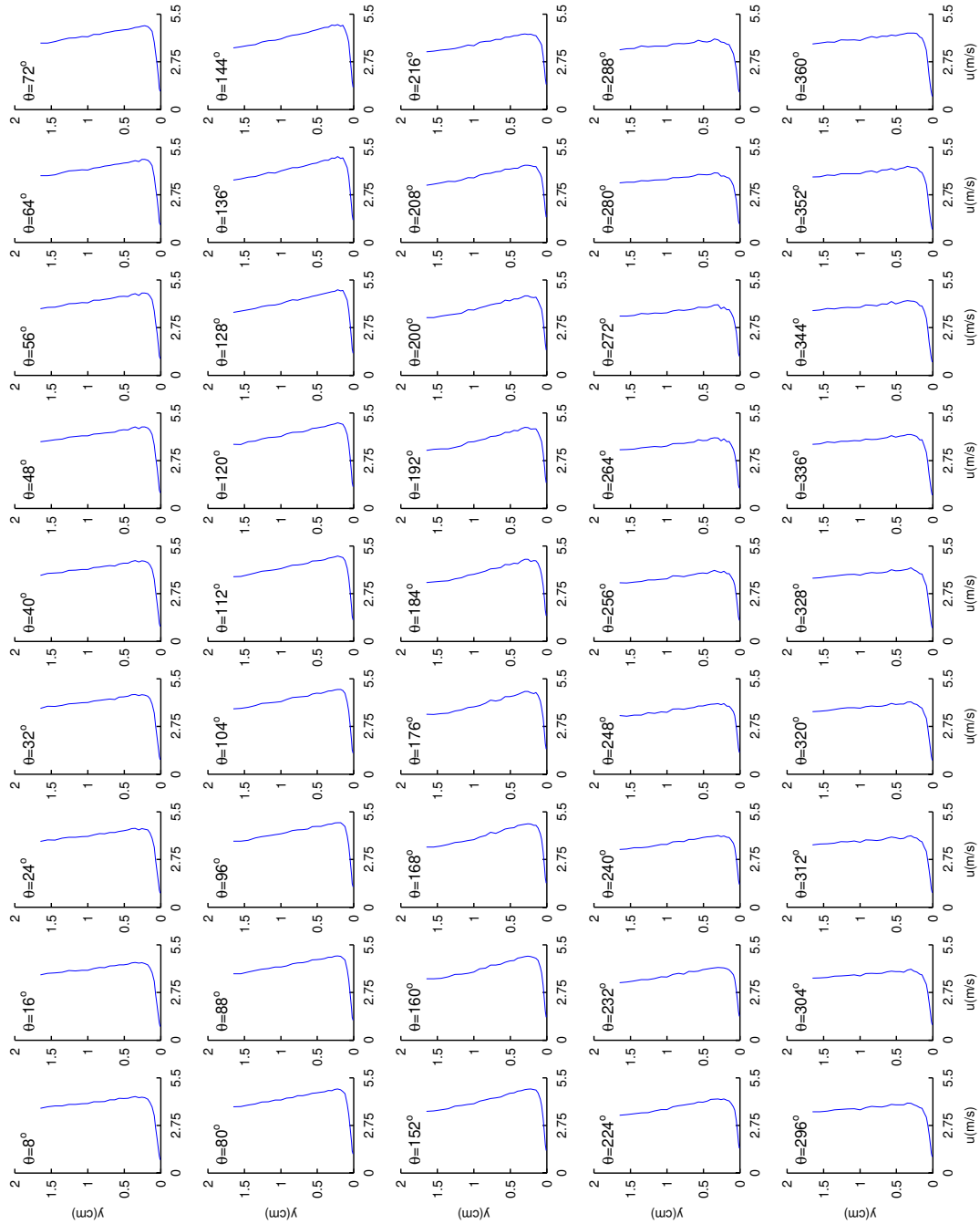

Figure 4.43: Phase average velocity $\tilde{u}(y, \theta)$ at station 4 ($s/L_{ss} = 31.36\%$), presented as a function of θ, base case.

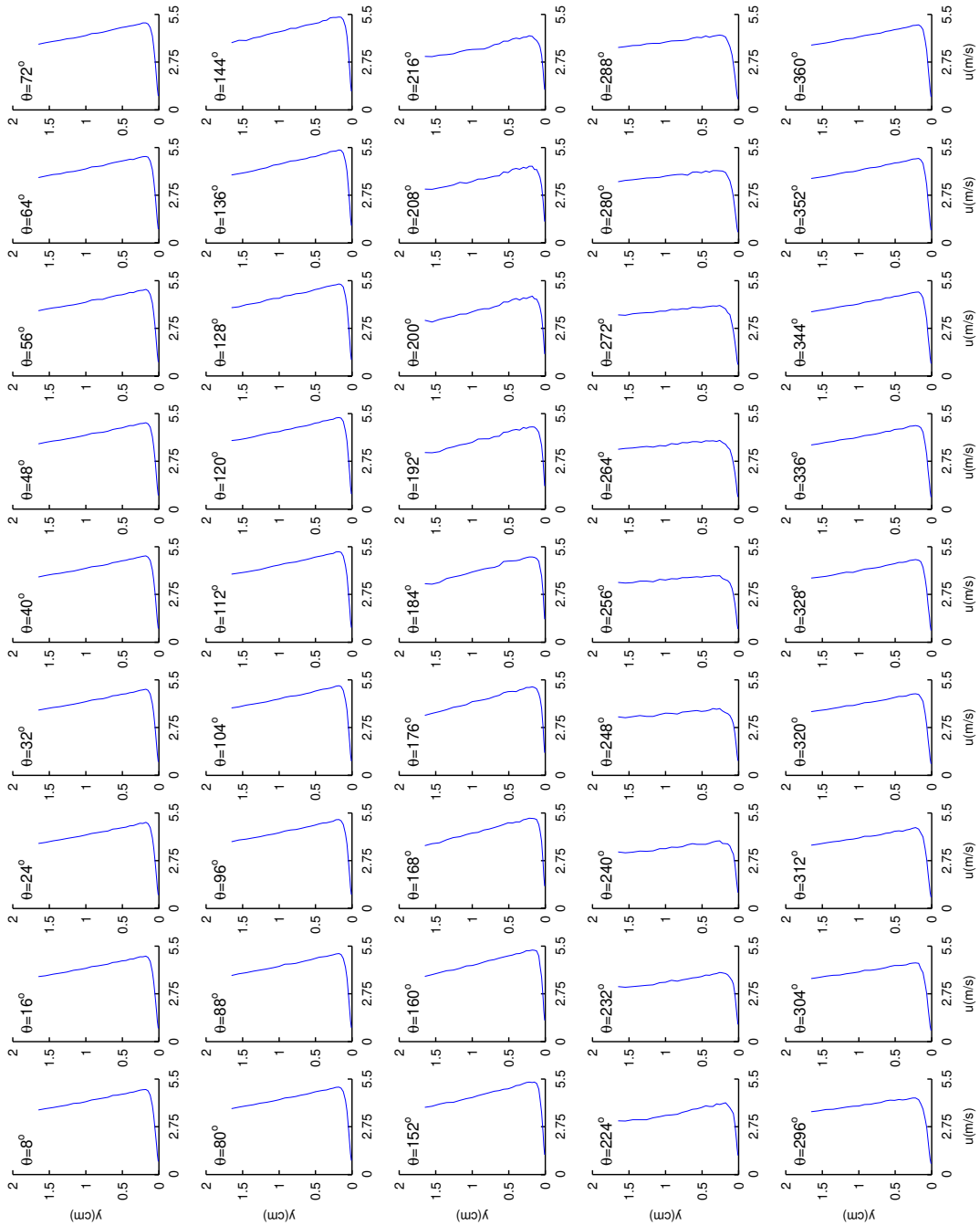

Figure 4.44: Phase average velocity $\tilde{u}(y, \theta)$ at station 4 $(s/L_{ss} = 31.36\%)$, presented as a function of θ, increased wake spacing case.

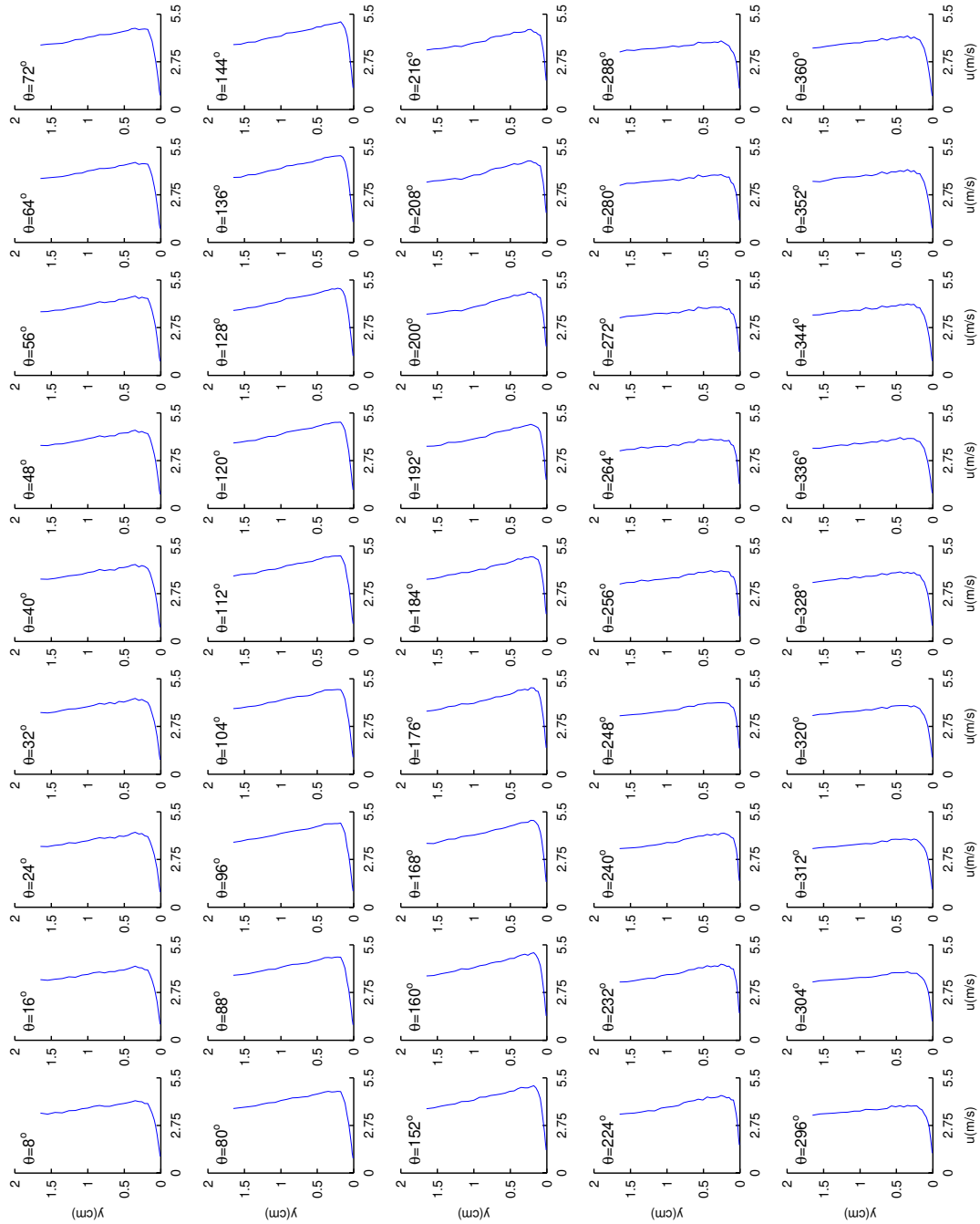

Figure 4.45: Phase average velocity $\tilde{u}(y, \theta)$ at station 5 ($s/L_{ss} = 37.35\%$), presented as a function of θ, base case.

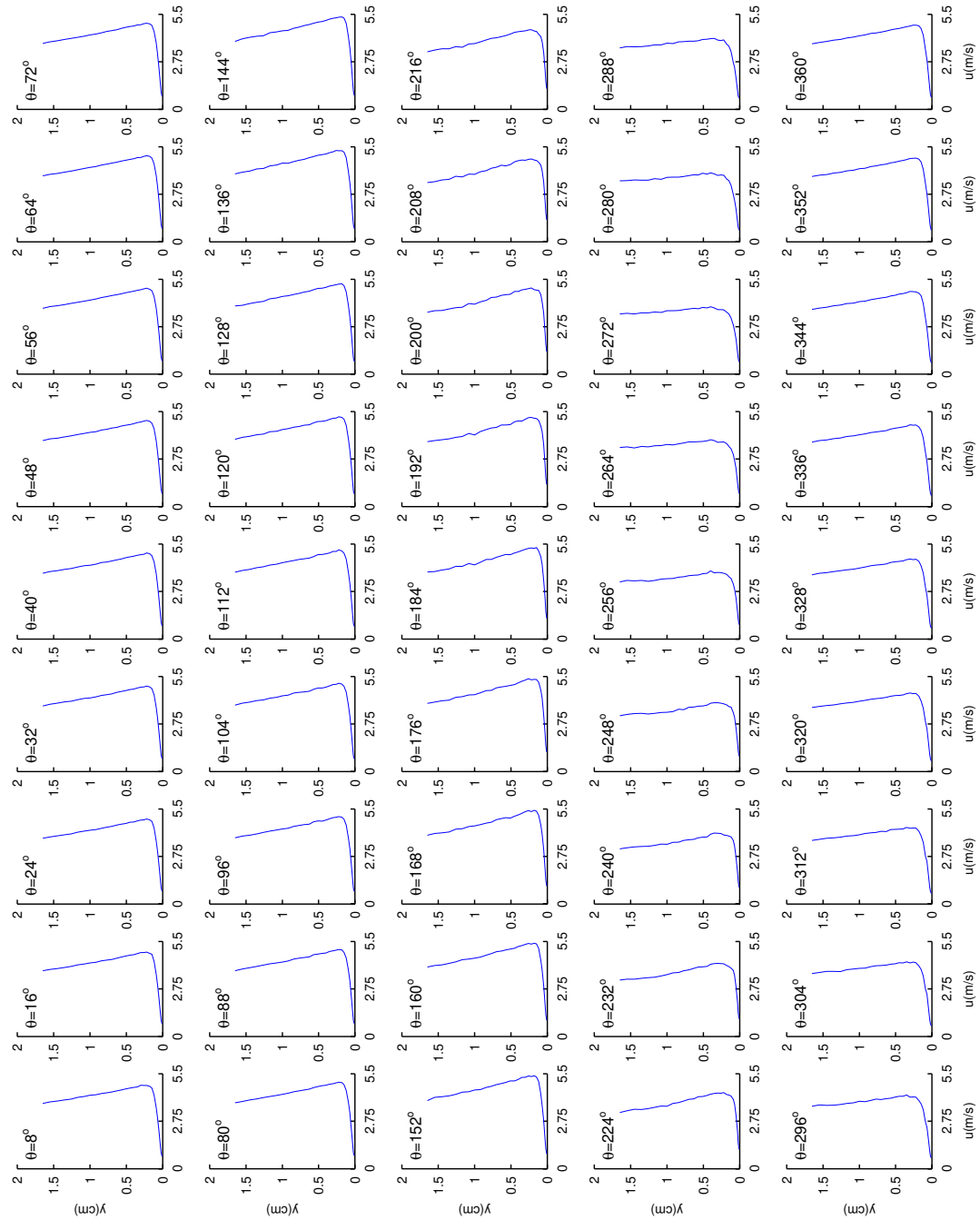

Figure 4.46: Phase average velocity $\tilde{u}(y, \theta)$ at station 5 $(s/L_{ss} = 37.35\%)$, presented as a function of θ, increased wake spacing case.

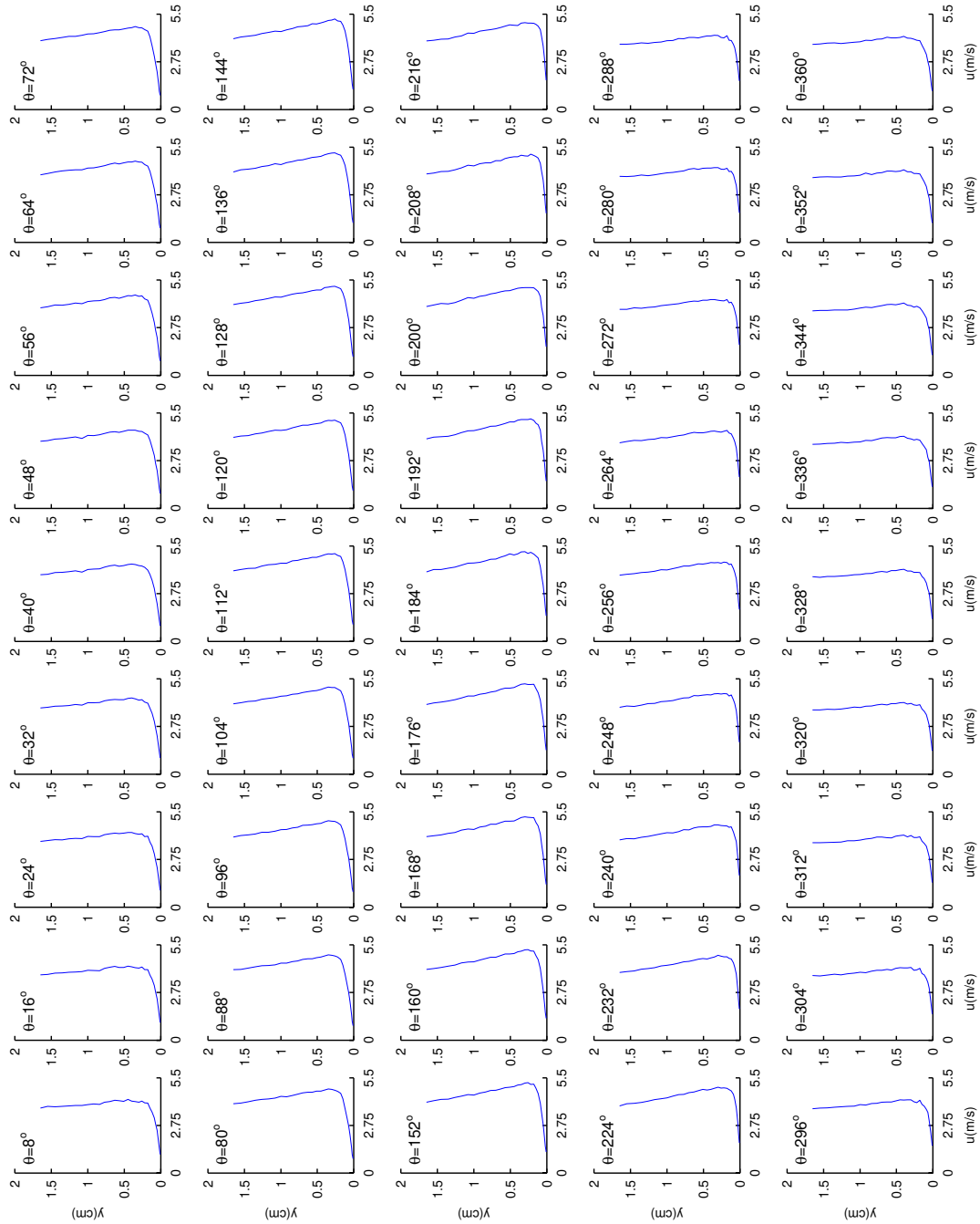

Figure 4.47: Phase average velocity $\tilde{u}(y, \theta)$ at station 6 ($s/L_{ss} = 43.34\%$), presented as a function of θ, base case.

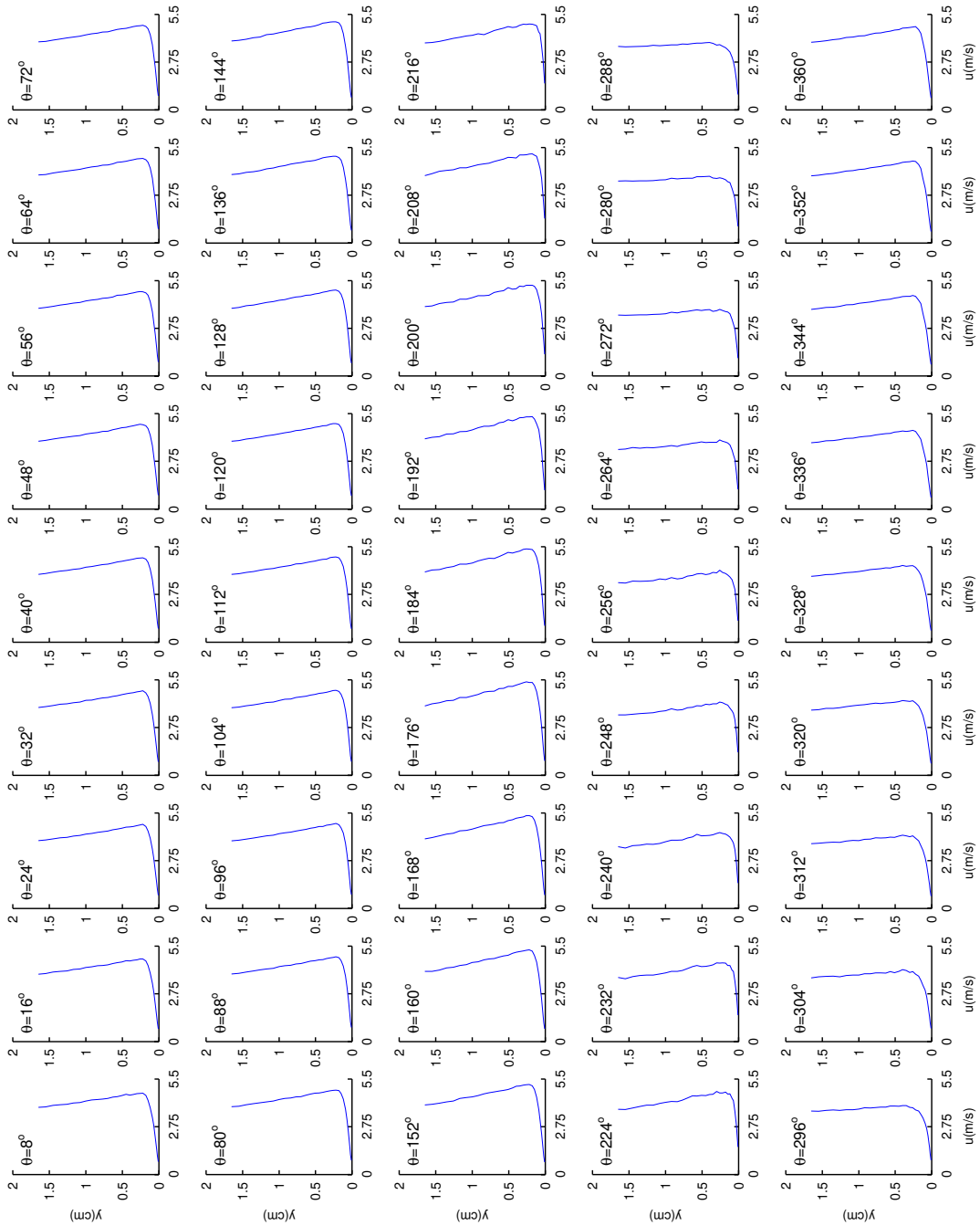

Figure 4.48: Phase average velocity $\tilde{u}(y, \theta)$ at station 6 $(s/L_{ss} = 43.34\%)$, presented as a function of θ, increased wake spacing case.

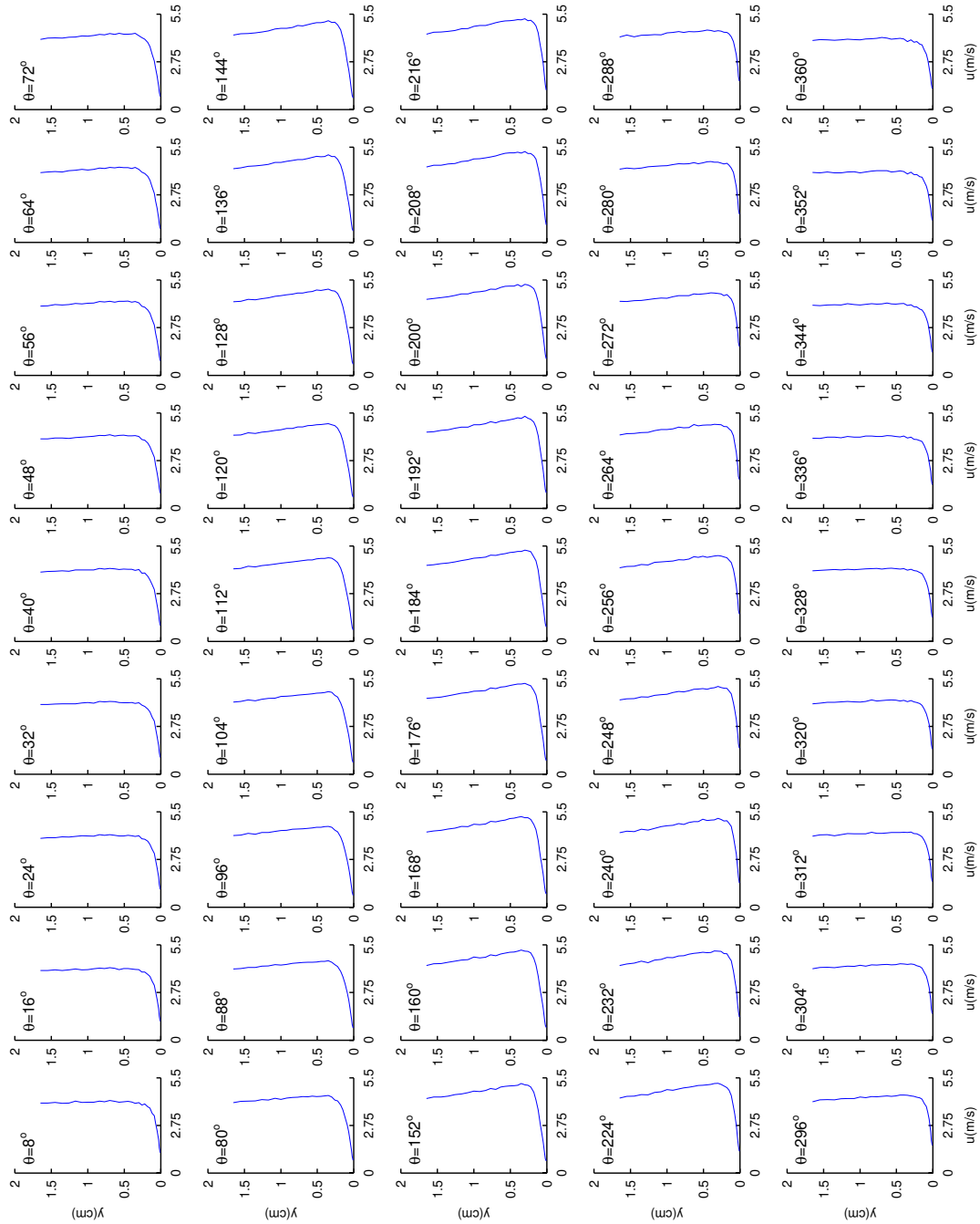

Figure 4.49: Phase average velocity $\tilde{u}(y, \theta)$ at station 7 ($s/L_{ss} = 49.33\%$), presented as a function of θ, base case.

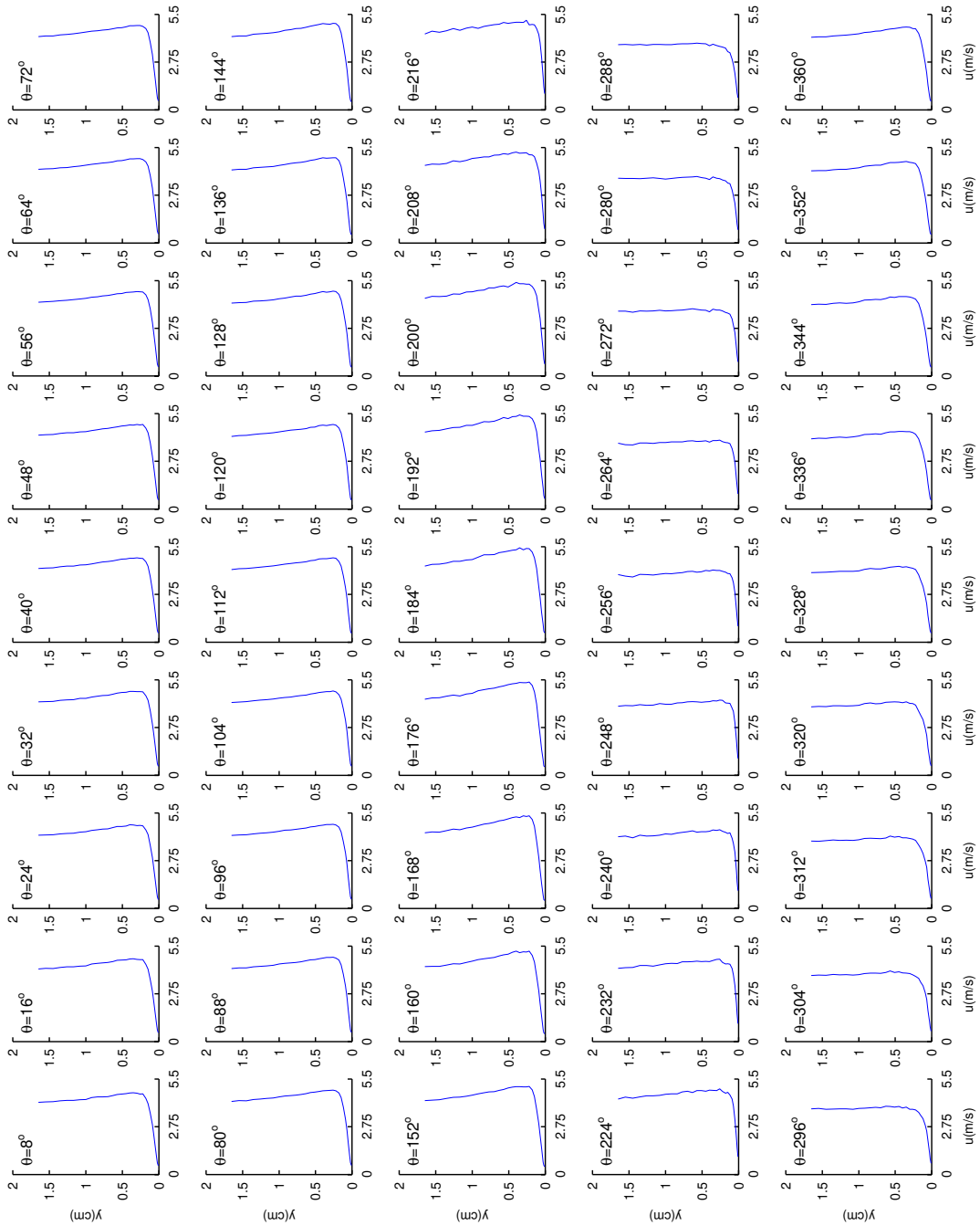

Figure 4.50: Phase average velocity $\tilde{u}(y, \theta)$ at station 7 ($s/L_{ss} = 49.33\%$), presented as a function of θ, increased wake spacing case.

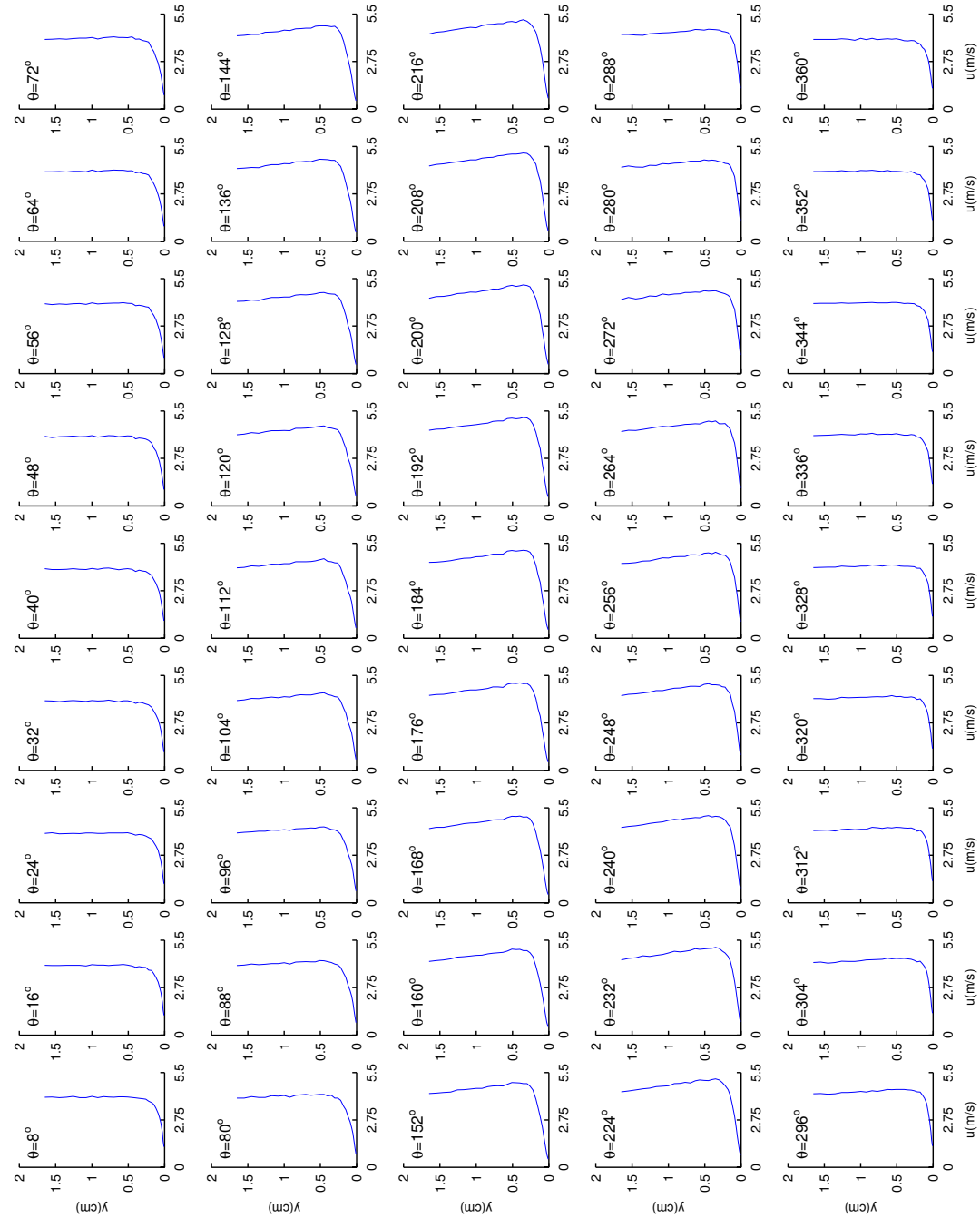

Figure 4.51: Phase average velocity $\tilde{u}(y, \theta)$ at station 8 ($s/L_{ss} = 55.33\%$), presented as a function of θ, base case.

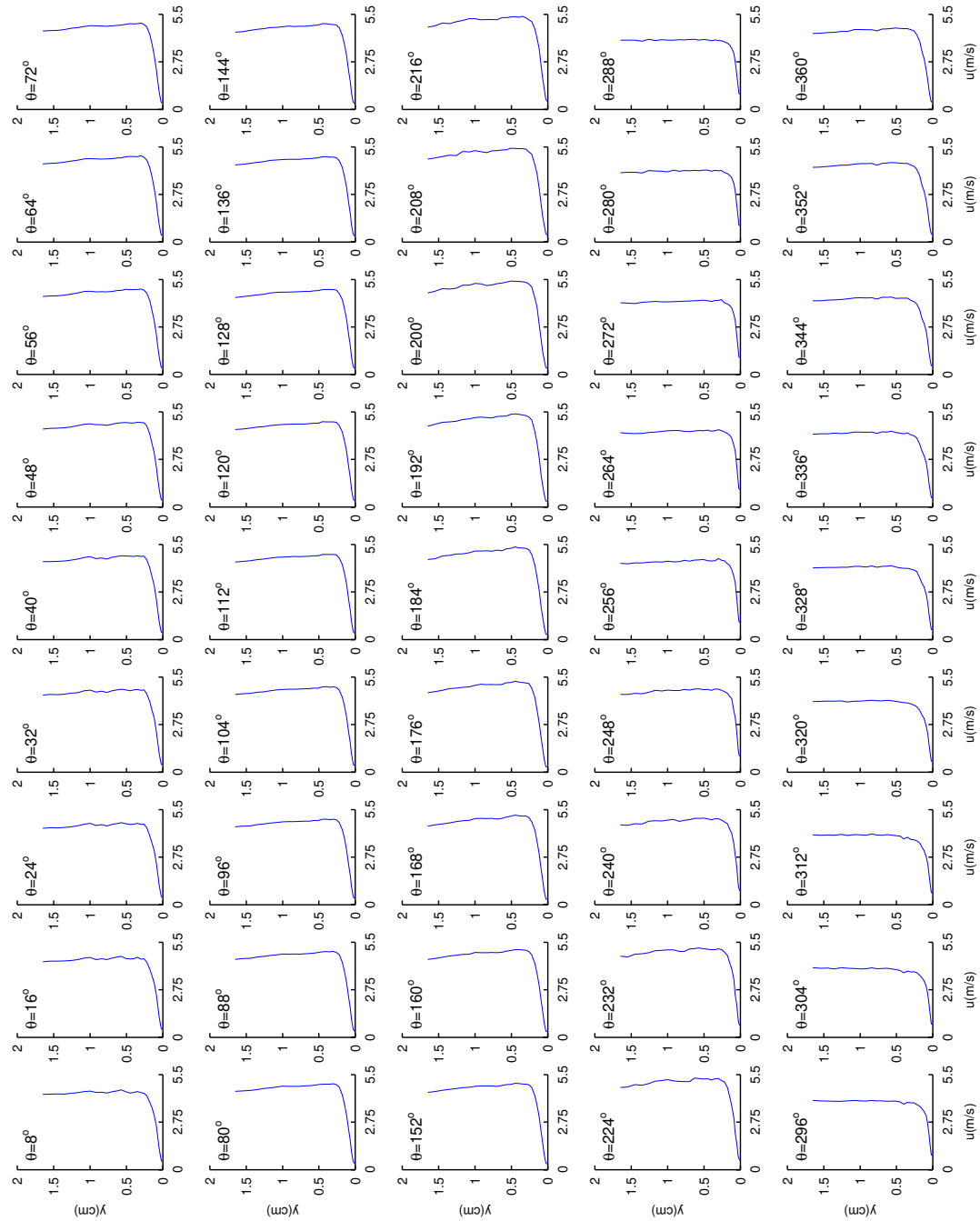

Figure 4.52: Phase average velocity $\tilde{u}(y, \theta)$ at station 8 $(s/L_{ss} = 55.33\%)$, presented as a function of θ, increased wake spacing case.

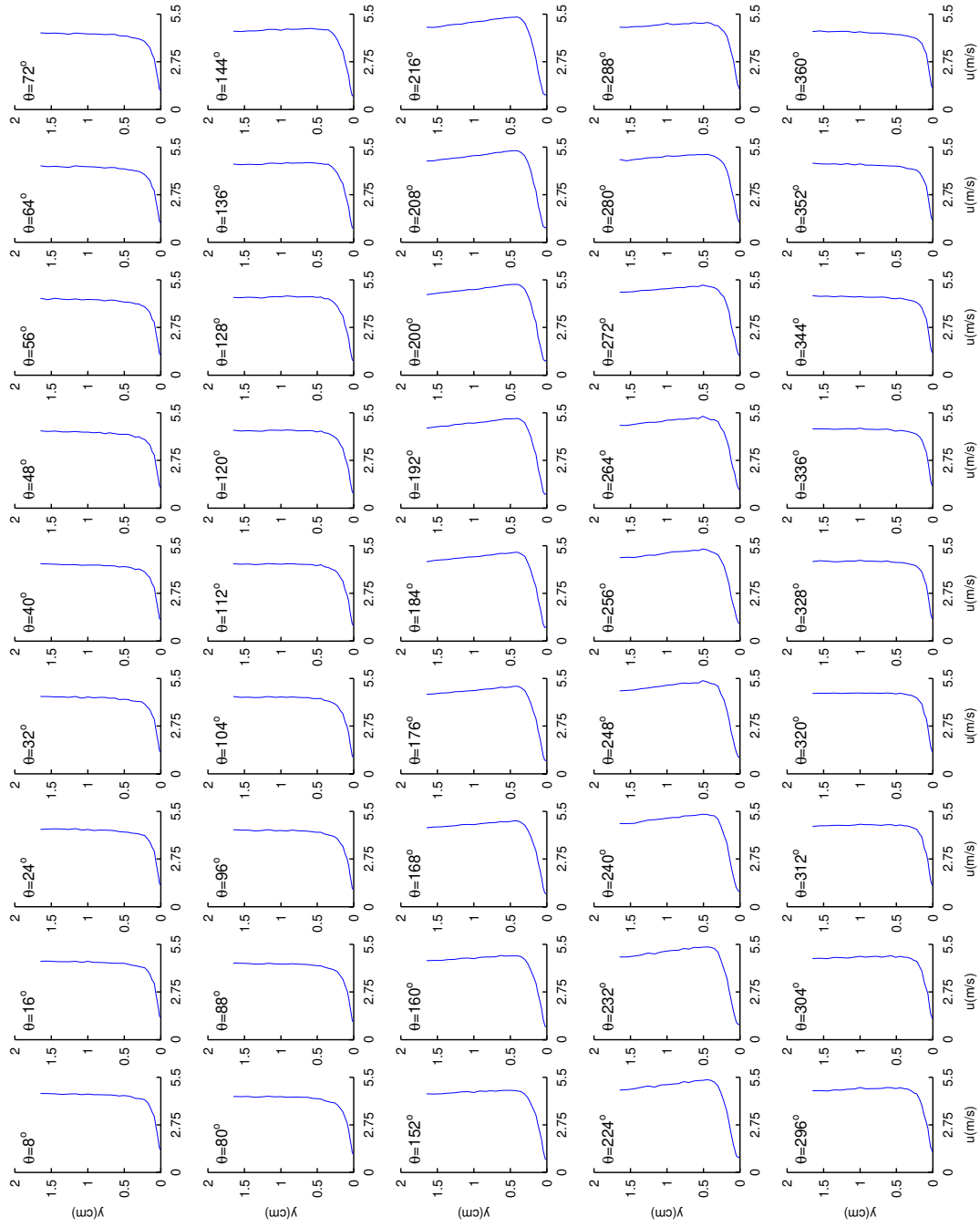

Figure 4.53: Phase average velocity $\tilde{u}(y, \theta)$ at station 9 ($s/L_{ss} = 61.32\%$), presented as a function of θ., base case

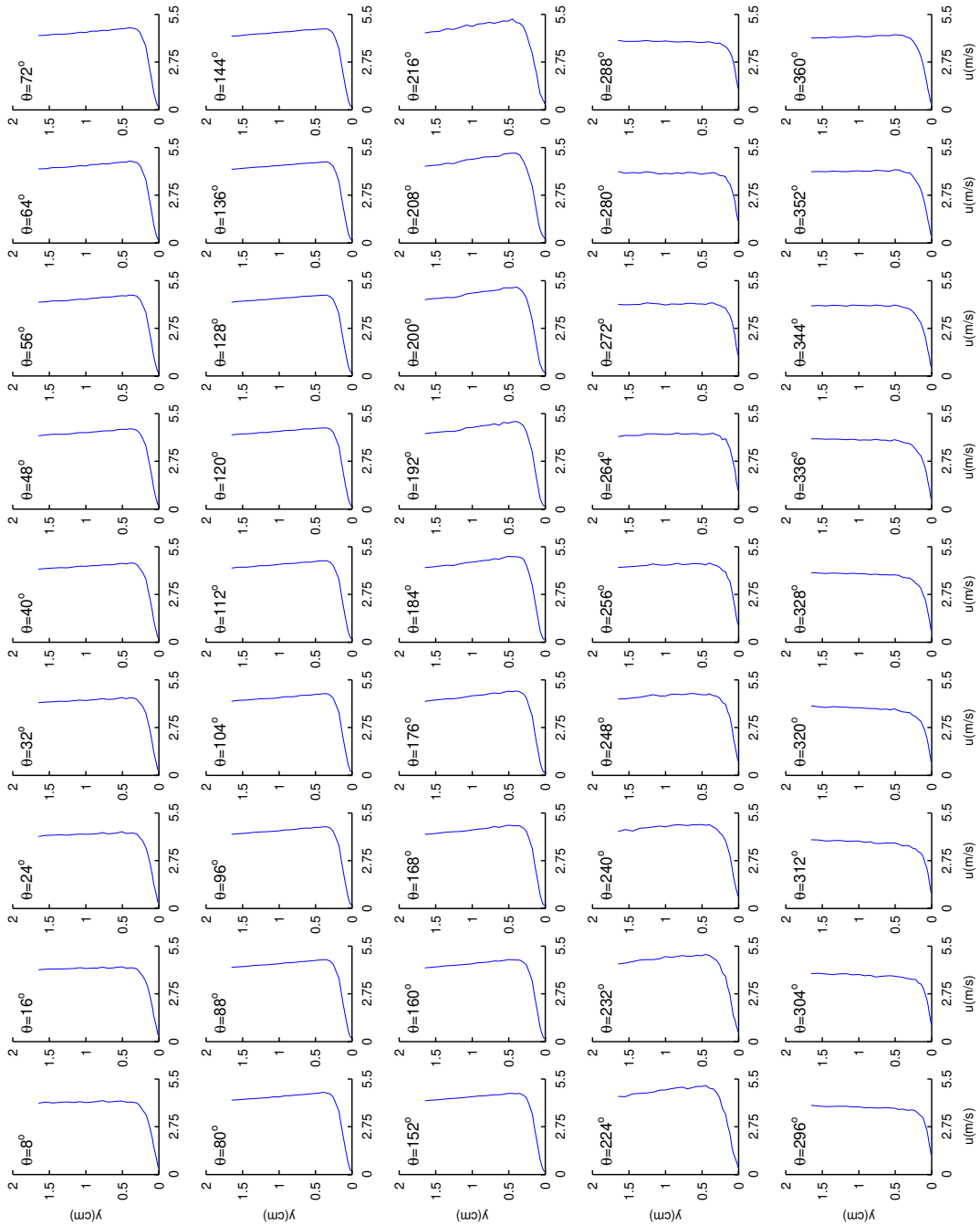

Figure 4.54: Phase average velocity $\tilde{u}(y, \theta)$ at station 9 $(s/L_{ss} = 61.32\%)$, presented as a function of θ, increased wake spacing case.

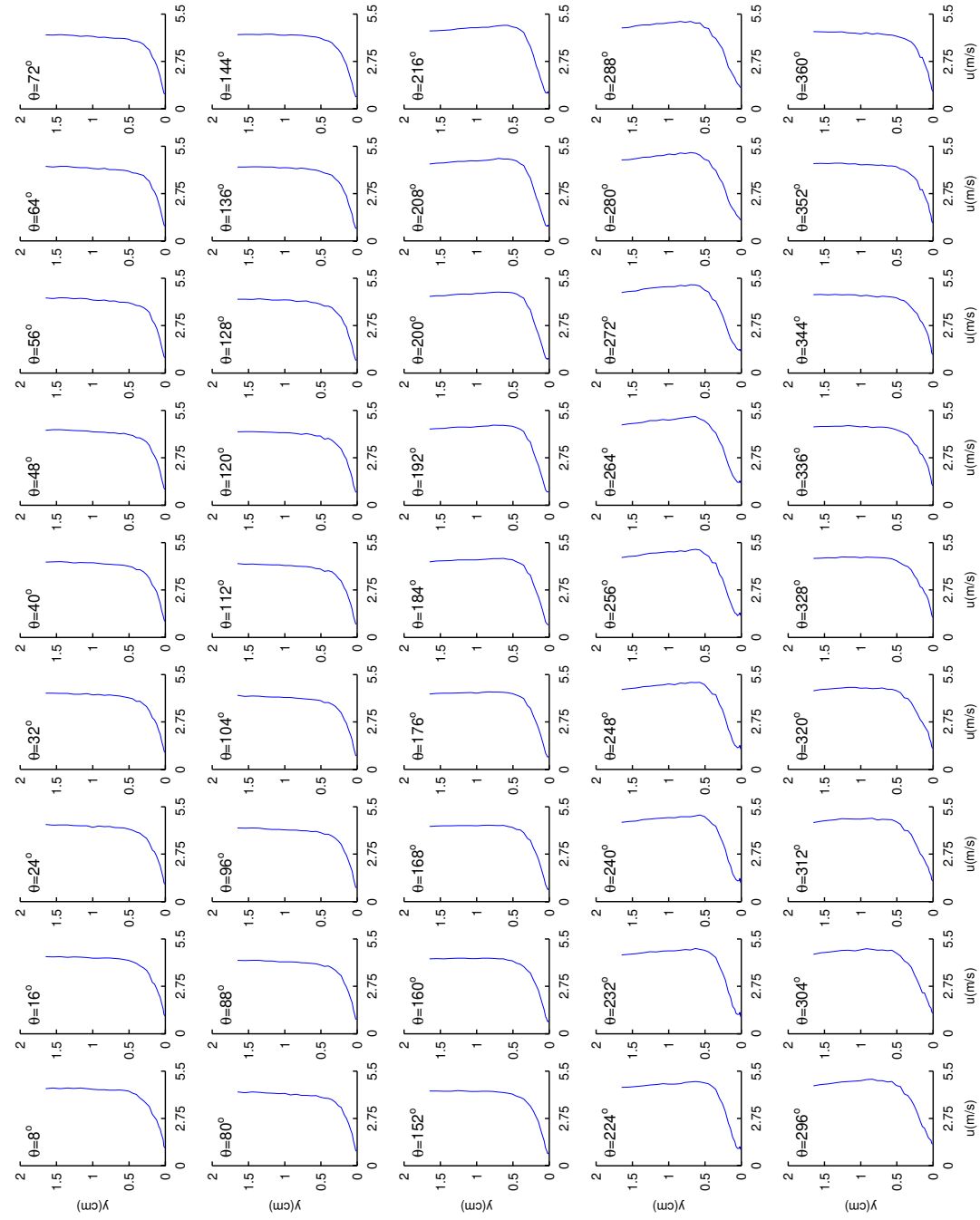

Figure 4.55: Phase average velocity $\tilde{u}(y, \theta)$ at station 10 ($s/L_{ss} = 70.31\%$), presented as a function of θ, base case.

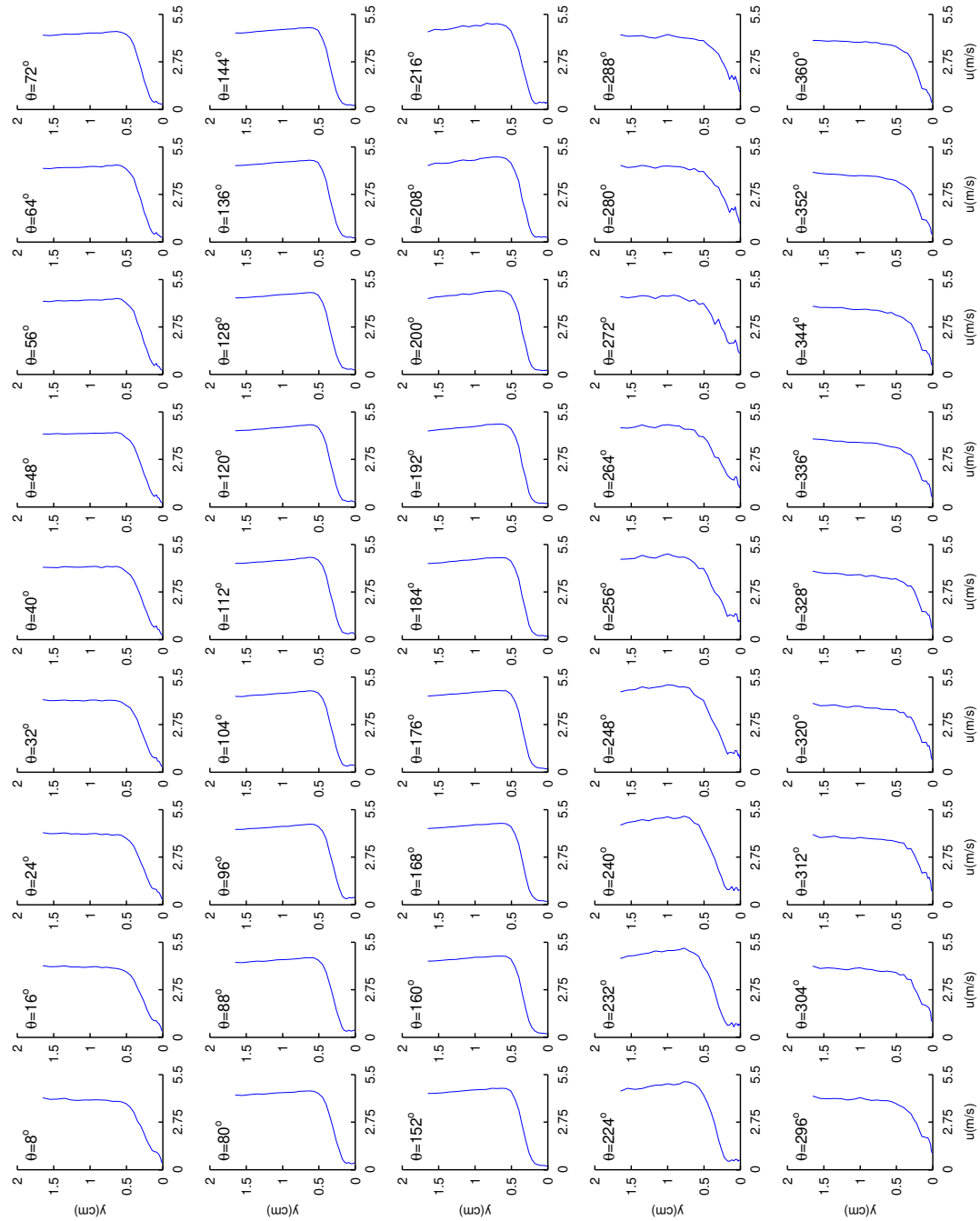

Figure 4.56: Phase average velocity $\tilde{u}(y, \theta)$ at station 10 ($s/L_{ss} = 70.31\%$), presented as a function of θ, increased wake spacing case.

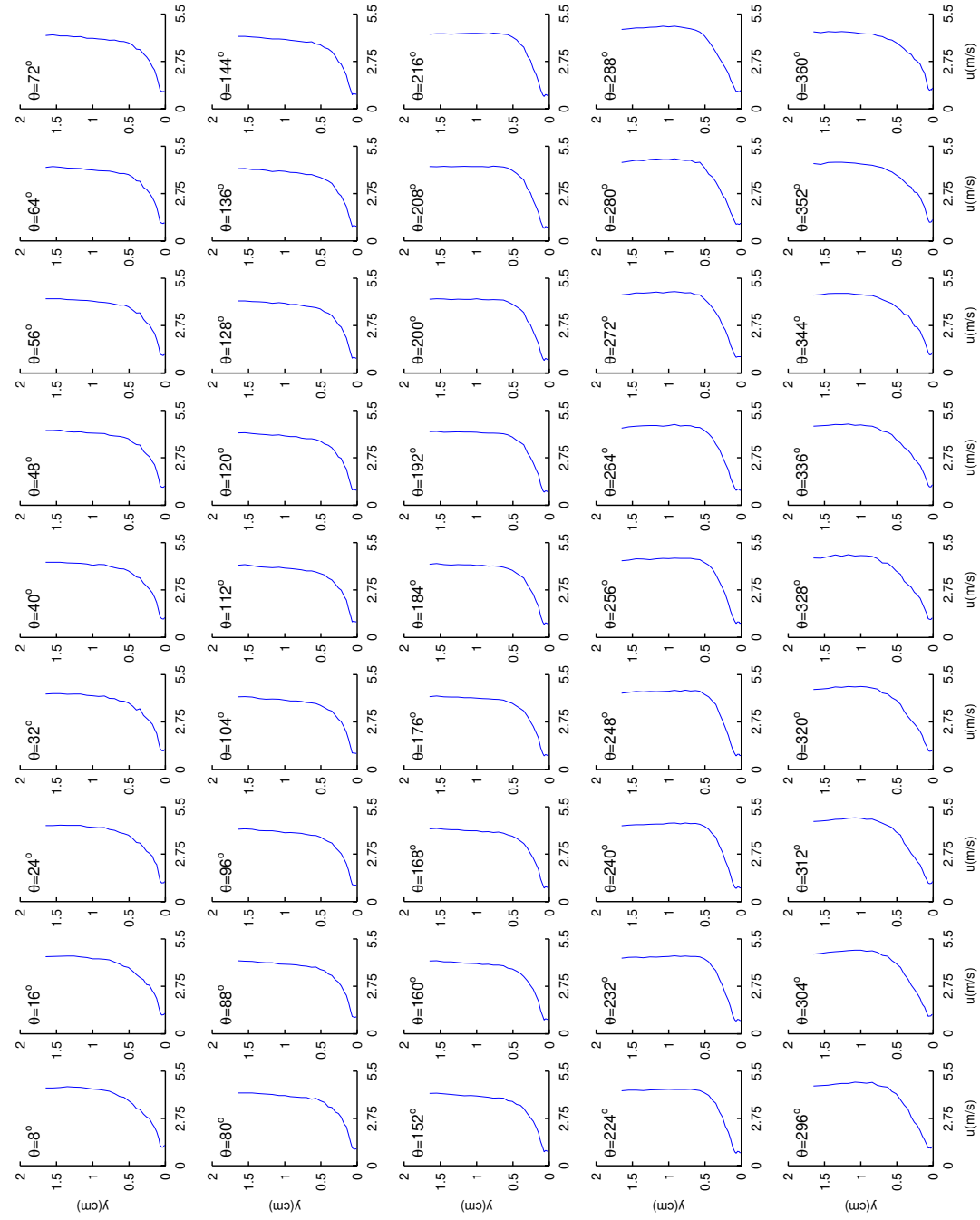

Figure 4.57: Phase average velocity $\tilde{u}(y, \theta)$ at station 11 ($s/L_{ss} = 76.11\%$), presented as a function of θ, base case.

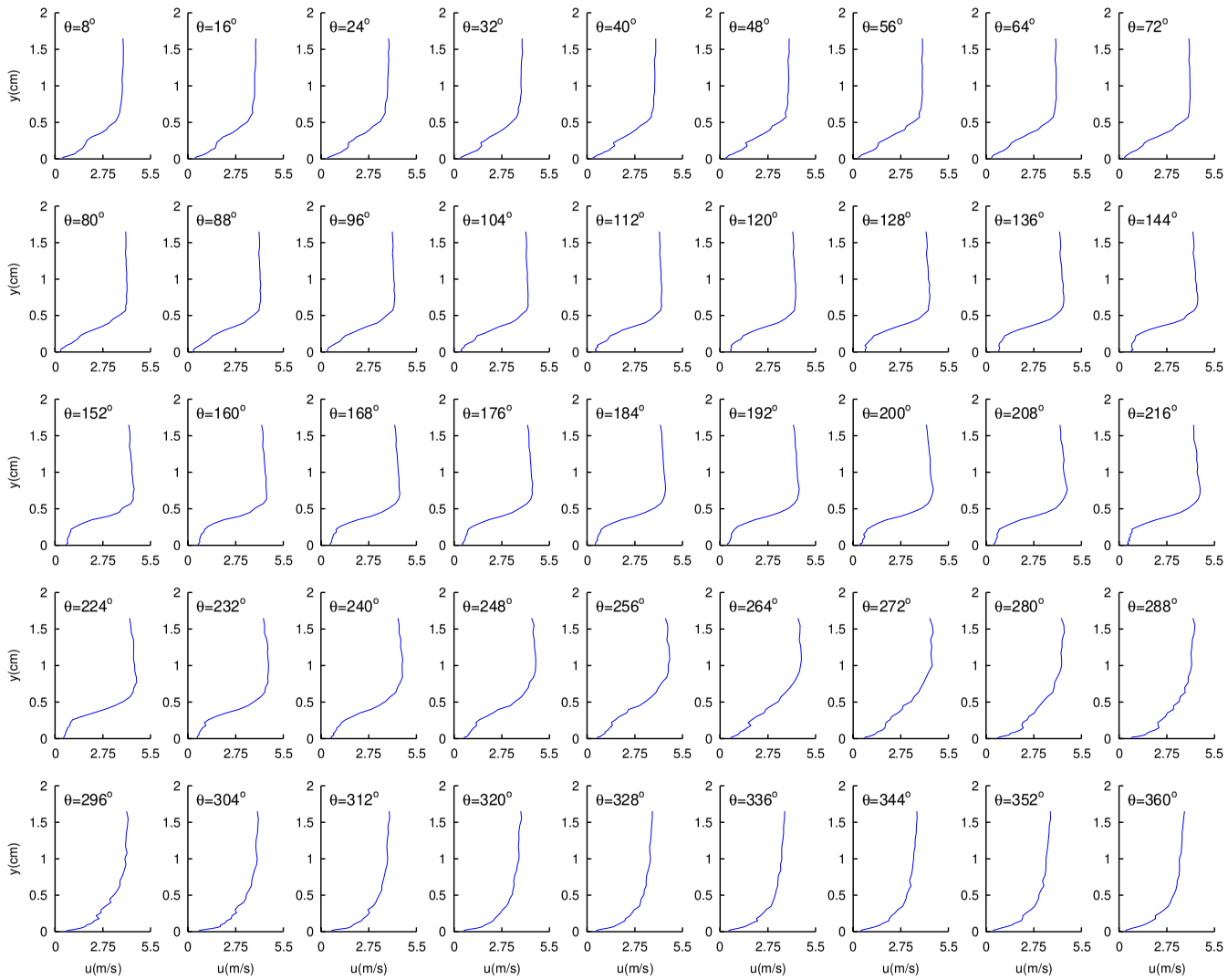

Figure 4.58: Phase average velocity $\tilde{u}(y, \theta)$ at station 11 ($s/L_{ss} = 76.11\%$), presented as a function of θ, increased wake spacing case.

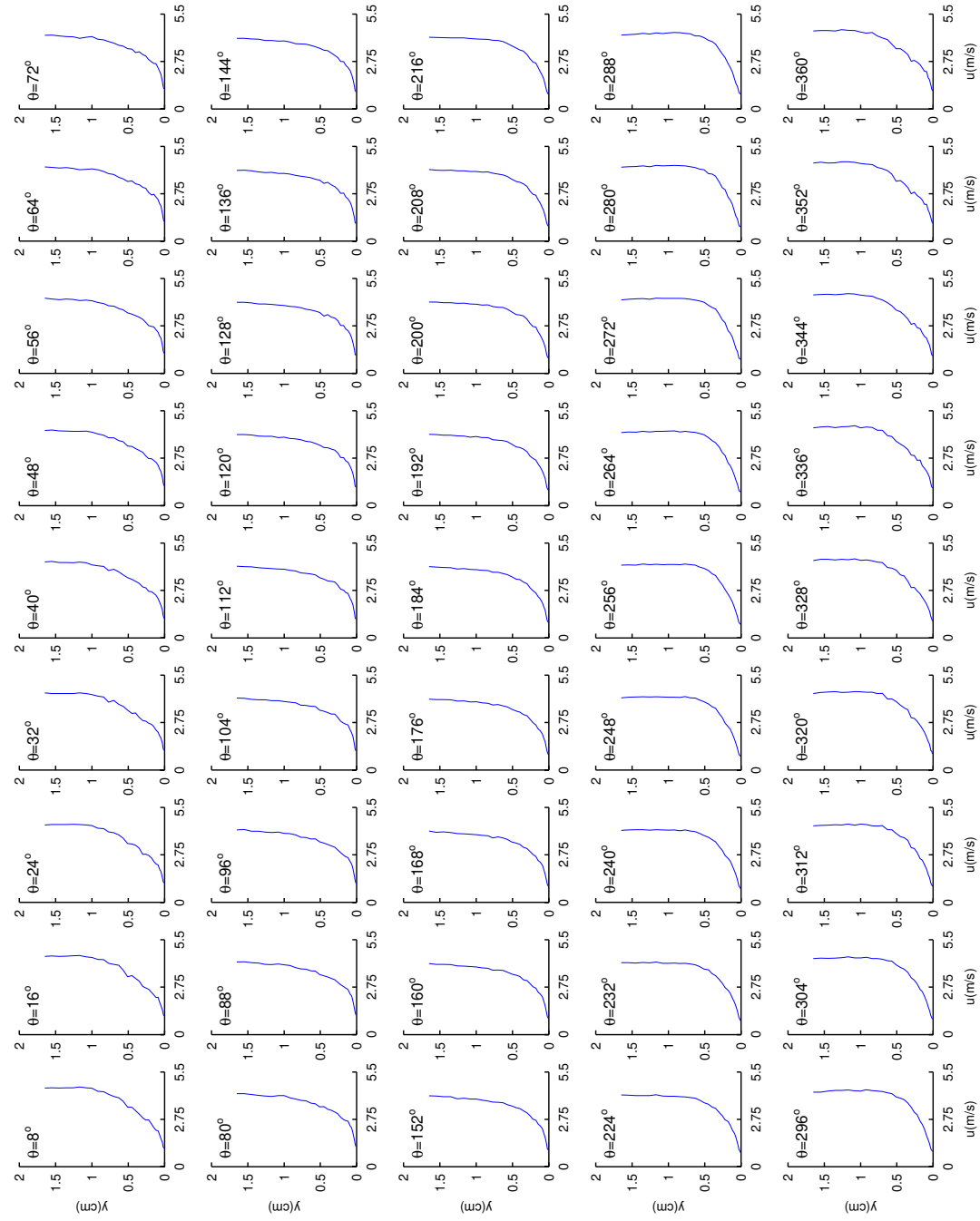

Figure 4.59: Phase average velocity $\tilde{u}(y, \theta)$ at station 12 ($s/L_{ss} = 84.00\%$), presented as a function of θ, base case.

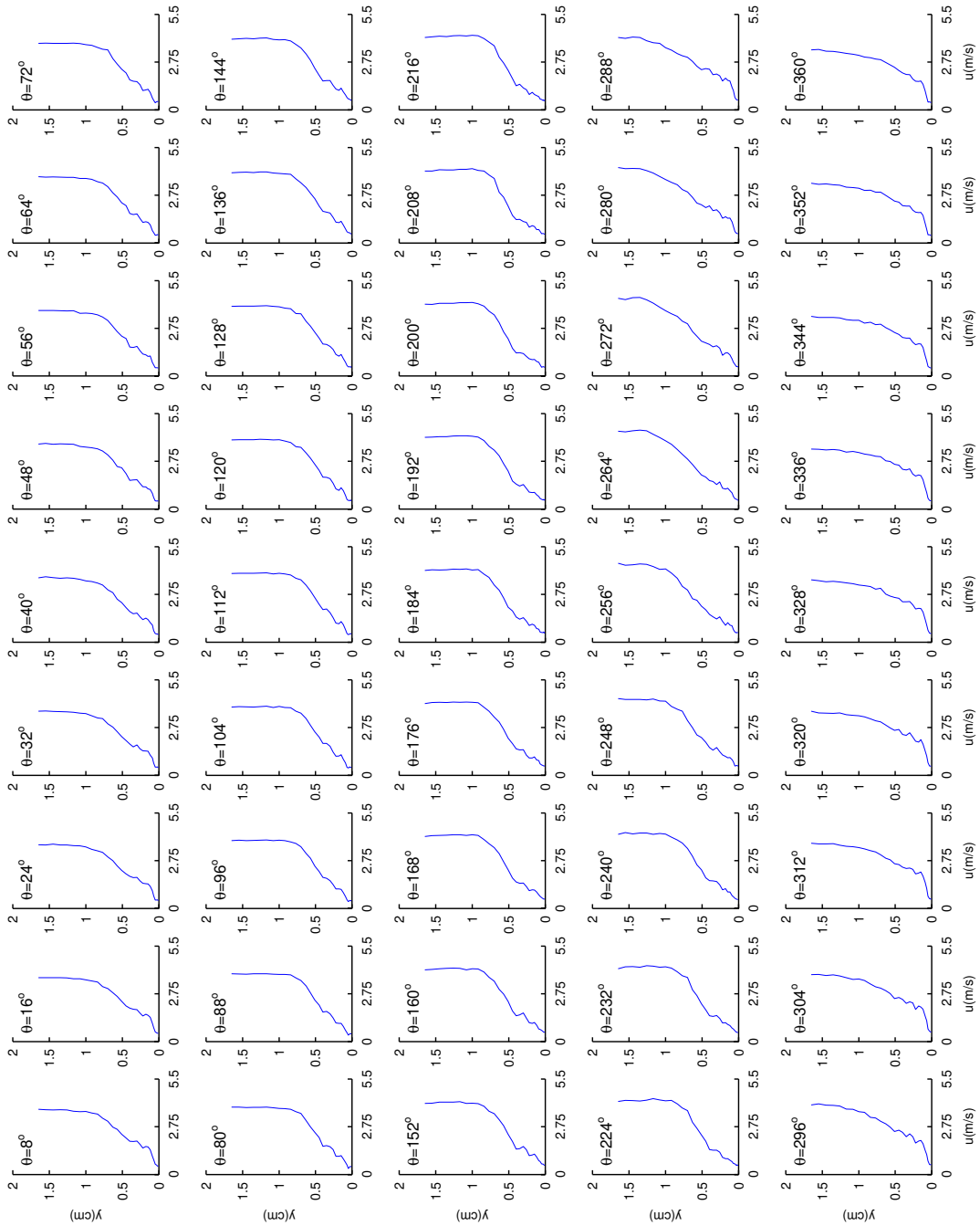

Figure 4.60: Phase average velocity $\tilde{u}(y, \theta)$ at station 12 ($s/L_{ss} = 84.00\%$), presented as a function of θ, increased wake spacing case.

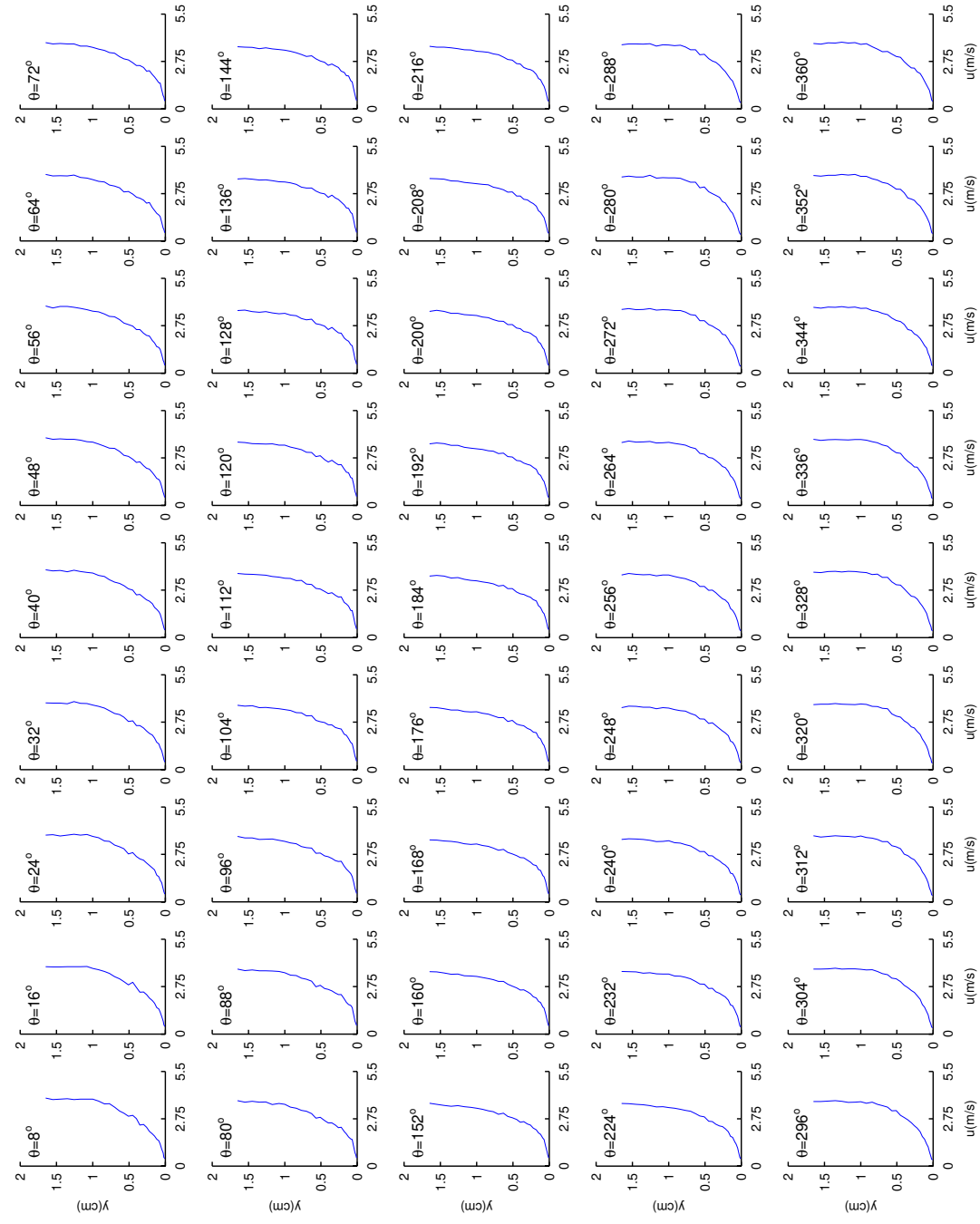

Figure 4.61: Phase average velocity $\tilde{u}(y, \theta)$ at station 13 ($s/L_{ss} = 93.49\%$), presented as a function of θ, base case.

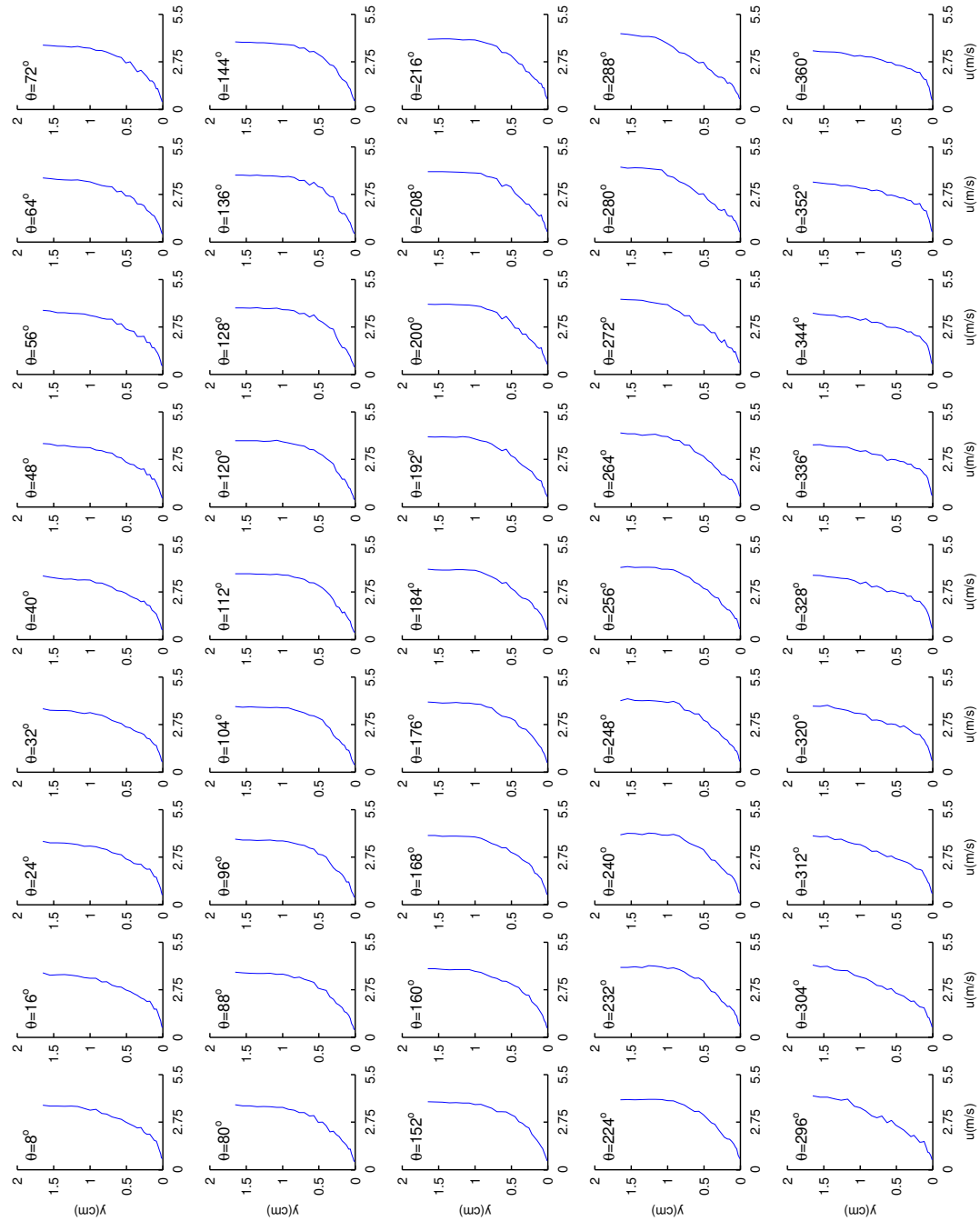

Figure 4.62: Phase average velocity $\tilde{u}(y, \theta)$ at station 13 ($s/L_{ss} = 93.49\%$), presented as a function of θ, increased wake spacing case.

Chapter 5

High-*FSTI* Results

5.1 Introduction

In this chapter, we present a case which is a repeat of the base case documented in Kaszeta and Simon (2002), but with the *FSTI* upstream of the wake generator elevated from 2.5% to 10%. This case will hereafter be referred to as the "high-*FSTI* case." This case uses the same rod spacing as the base case.

The high-*FSTI* case data were collected for stations 4 ($s/L_{ss} = 31.36\%$) through 13 ($s/L_{ss} = 93.49\%$). Stations 2 ($s/L_{ss} = 5.19\%$) and 3 ($s/L_{ss} = 19.78\%$) were omitted since it was difficult to correctly locate the probe relative to the wall. Because the boundary layers are very thin at these locations, accurate wall location is crucial and measurements with uncertain positioning are of little utility.

5.2 Experimental Results

The boundary-layer data for stations 4 through 13 are presented in Figures. 5.3 through 5.42, with the high-*FSTI* data presented alongside the base case data taken at the same locations. Profiles of velocity, velocity rms, turbulence intensity, and intermittency are presented.

The data are presented in order of pressure tap number. For each pressure tap location, the data are first presented as a series of pseudo-color plots representing the velocity, velocity rms, turbulence intensity, and intermittency. Examples of each of these plots are given in Figure 5.3 ($\tilde{u}(y,\theta)$), Figure 5.4 ($\widetilde{u_{rms}}(y,\theta)$), Figure 5.5 ($\widetilde{TI}(y,\theta)$), and Figure 5.6 ($\tilde{\gamma}(y,\theta)$).

For each of these figures, the horizontal axis is the phase angle, θ, over one wake-passing period, while the vertical axis is the wall-normal distance, y. Each figure represents the ensemble average of 140 wakes at a fixed location on the suction surface. Note that since both cases have the same wake spacing, the $0 < \theta < 360^{\circ}$ intervals on these plots represent the same physical time.

Additionally, for stations 4 through 13, the ensemble-average velocity data are presented again in Figures 5.43 through 5.52, with each quantity now represented as a series of plots showing the wall-normal distribution of each quantity at times during the wake-passing period. An examples of this style of plot is shown in Figure 5.47. For each axes corresponding to a fixed value of θ, the horizontal axis designates the plotted quantity and the vertical axis represents the wall-normal distance, y. Unlike the pseudo-color plots, presenting the data in this fashion allows the near-wall values of the velocity and the overall shape of the boundary layer velocity profile to be more easily visualized. This is particularly useful when looking for regions of separated flow.

In general, the high-*FSTI* case produces a similar flow field to the base low-*FSTI* case (see Section 4.2.1). However, the combination of an overall higher level of turbulence with the slightly different wake shape for the high-*FSTI* case results in some significant differences between these cases.

5.2.1 Separation Points

The separation characteristics of this flow are similar to those of the base case and the increased wake spacing case. However, in this case, separation has moved slightly downstream over most of the wake passing cycle, to the region $53\% < s/L_{ss} < 63\%$. By checking the velocity profiles in the boundary layer, we find that the flow begins to show signs of separation at $s/L_{ss} = 55.33\%$ (see Figure 5.47). The flow does not separate upstream of $s/L_{ss} = 49.33\%$ during the whole wake passing cycle (see Figures 5.43, 5.44, 5.45 and 5.46).

The high FSTI case has a shorter separation bubble than the base case. The flow is reattached at $s/L_{ss} = 84.00\%$ in the high FSTI case (see Figure 5.51). While in the base case, the flow is still separated at $s/L_{ss} = 93.49\%$ during part of the wake passing cycle (see Figure 4.61). Separation is suppressed by the high disturbance level and the stronger acceleration of the free stream.

5.2.2 Transition Onset

In the high FSTI case, both attached flow transition and separated flow transition are found. For example, at $\theta = 320°$, we can see obvious increase in u_{rms} in the near wall region at $s/L_{ss} = 55.33\%$ (see Figure 5.20(b)) compared with the u_{rms} in the near wall region at $s/L_{ss} = 49.33\%$ (see Figure 5.16(b)). At this time, transition begins between $49.33\% < s/L_{ss} < 55.33\%$. We also can see a rise in u_{rms} near this location. Thus we assign transition onset to be at this location. At this time in the wake passing period, separation is observed between $55.33\% < s/L_{ss} < 61.32\%$ (see Figures 5.47 and 5.48). During the wake passing cycle, transition sometimes begins downstream of separation. For instance, at $\theta = 104°$, transition begins between $61.32\% < s/L_{ss} < 70.31\%$ (see Figures 5.24(b) and 5.28(b)) and separation is between $55.33\% < s/L_{ss} < 61.32\%$ (see Figures 5.47 and 5.48). In this case, a larger portion of the passing cycle is transitional than that in the base case or the increased wake spacing case.

5.2.3 Stronger Wakes

We can see that the high-*FSTI* wakes are stronger at any given measurement station. For example, examining the velocity fluctuations shown for station 4 in Figure 5.3, we can see that the wake in the freestream of the high-*FSTI* case (Figure 5.3(b)) has a larger velocity deficit (lower values of $\tilde{u}$) than that of the low-*FSTI* case (Figure 5.3(a)).

5.2.4 Less Response of the Boundary Layer to Freestream Influences

When examining the base case data, it was observed that the boundary layer would respond to changes in the freestream velocity by a thickening and thinning of the boundary layer. Examining the velocity distributions shown for stations 8 and 9 in Figures 5.19 and 5.23, respectively, we can see that for the high-*FSTI* flow (Figures 5.19(b) and 5.23(b)), the response of the boundary layer to changes in the freestream velocity is reduced from that seen for the low-*FSTI* case (Figures 5.19(a) and 5.23(a)), even though the freestream changes in velocity are larger for the high-*FSTI* case. This conclusion is drawn by observing the change of thickness of the near-wall, low-velocity region. Apparently, with increased turbulence, the near-wall flow is less influenced by the temporal pressure gradients associated with the passing wakes.

5.2.5 Less "Calming" of the Flow as the Wake Passes

Examining the distribution of velocity rms shown for the base case at a representative location, station 4, Figure 5.4(b), we can observe that as the wake passes and the freestream flow accelerates from $50^\circ < \theta < 150^\circ$, the flow is calmed, resulting in a noticeable decrease in the velocity rms values outside of the boundary layer ($y > 0.1\,\mathrm{cm}$). However, for the corresponding location in the high-*FSTI* flow, Figure 5.4(b), we see no such decrease in velocity rms, suggesting that the *FSTI* level is high enough to keep the flow from being calmed between wakes. Again, the high-*FSTI* results in less sensitivity to temporal acceleration. Similar results can be seen for stations 5 through 7.

5.2.6 Earlier Reattachment

The base case flowfield appears to reattach at station 12 (as seen in the *TI* distribution in Figure 5.37(a)). However, it appears that the elevated *FSTI* levels of the high-FSTI case result in earlier reattachment; partially re-attaching at station 10 (see the *TI* distribution in Figure 5.29(b)), and fully re-attaching by station 11 (see the *TI* distribution in Figure 5.33(b)). This is in agreement with the literature that shows a shorter separation bubble in the case of higher *FSTI* due to quicker transition to turbulence.

Examining the surface shear stress for the base case in Figure 5.1, we can see evidence of reattachment ranging from $s/L_{ss} \approx 0.8$ to $s/L_{ss} \approx 0.95$. In the high-*FSTI* case in Figure 5.2, a fairly abrupt increase in shear stress occurs starting at $s/L_{ss} \approx 0.75$, reinforcing the evidence that the high-*FSTI* case reattaches sooner than does the base case.

5.2.7 Merging Wakes

For both the base and high-*FSTI* cases, the wakes are sufficiently broad in time that they tend to merge (for example, look at the $\tilde{\gamma}$ distribution in Figure 5.22). However, in the high-*FSTI* flows, the elevated turbulence level of the freestream appears to broaden the wakes somewhat. Examining the $\tilde{\gamma}$ distribution in Figure 5.22(b), we can see that the freestream flow never recovers from the wake passage, while in the base case the flow recovers slightly between wakes (see the near-zero $\tilde{\gamma}$ values in the freestream between the wakes in Figure 5.22(a)).

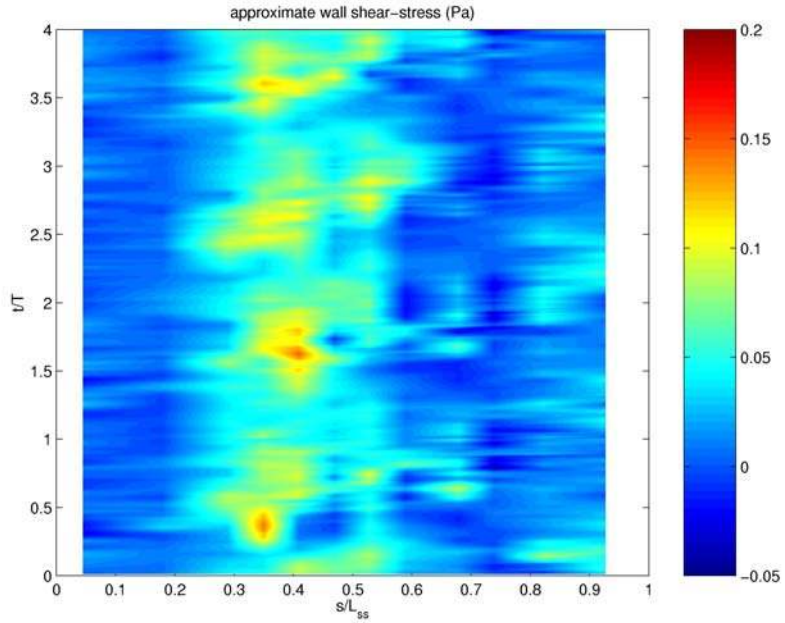

Figure 5.1: Approximate wall shear stress obtained from the ensemble-averaged velocity profiles, base case

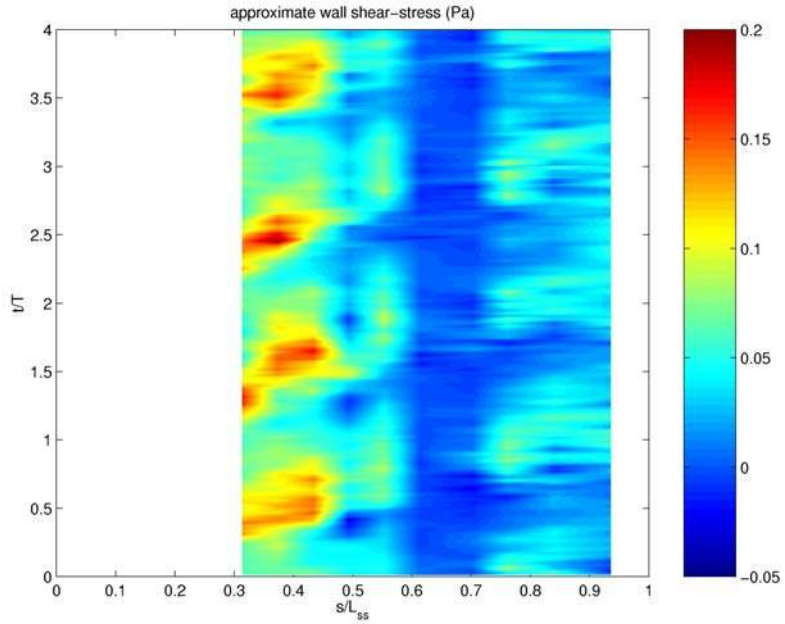

Figure 5.2: Approximate wall shear stress obtained from the ensemble-averaged velocity profiles, high-$FSTI$ case

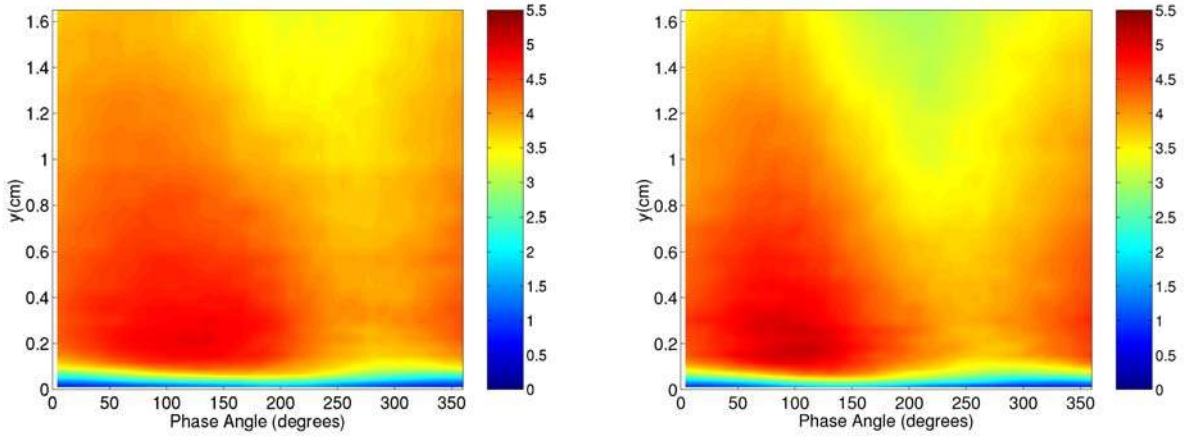

(a) Base Case (b) High-$FSTI$ Case

Figure 5.3: Velocity, $\tilde{u}$, (m/s), at station 4 ($s/L_{ss} = 31.36\%$)

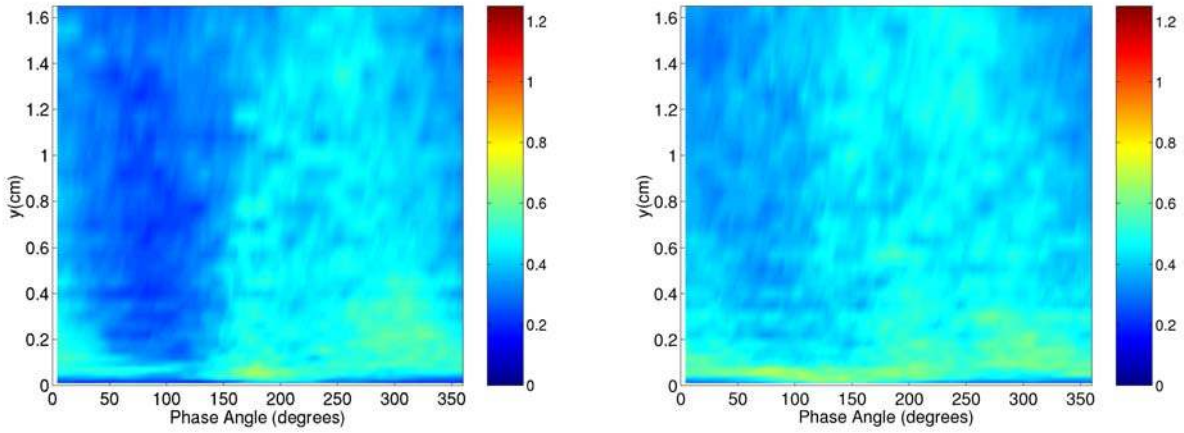

(a) Base Case (b) High-$FSTI$ Case

Figure 5.4: Velocity rms, $\widetilde{u_{rms}}$, (m/s), at station 4 ($s/L_{ss} = 31.36\%$)

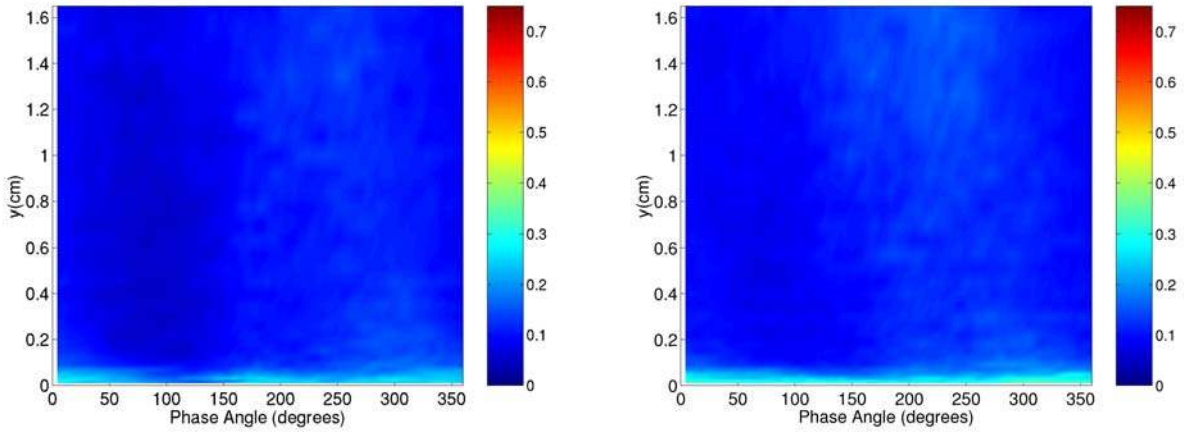

(a) Base Case

(b) High-$FSTI$ Case

Figure 5.5: Turbulence Intensity, $\widetilde{TI}$, at station 4 ($s/L_{ss} = 31.36\%$)

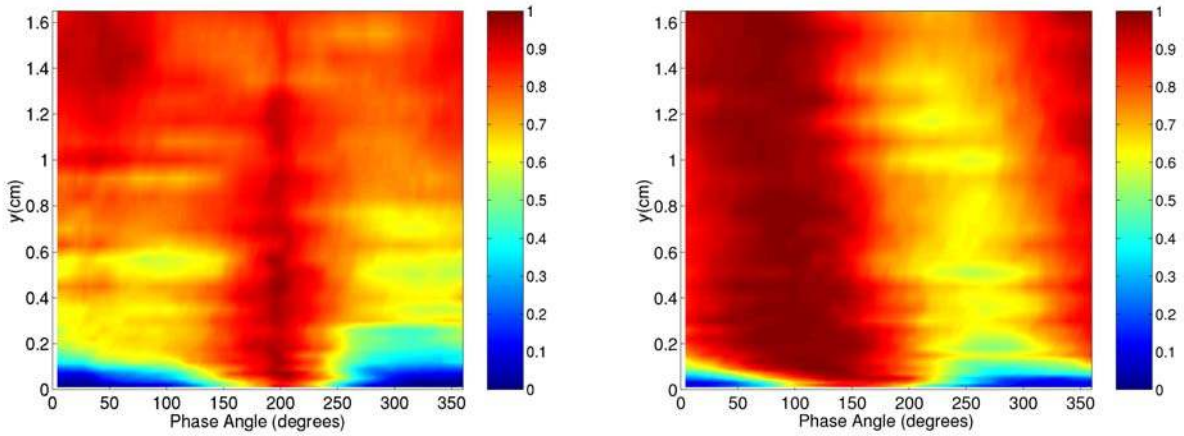

(a) Base Case

(b) High-$FSTI$ Case

Figure 5.6: Intermittency, $\tilde{\gamma}$, at station 4 ($s/L_{ss} = 31.36\%$)

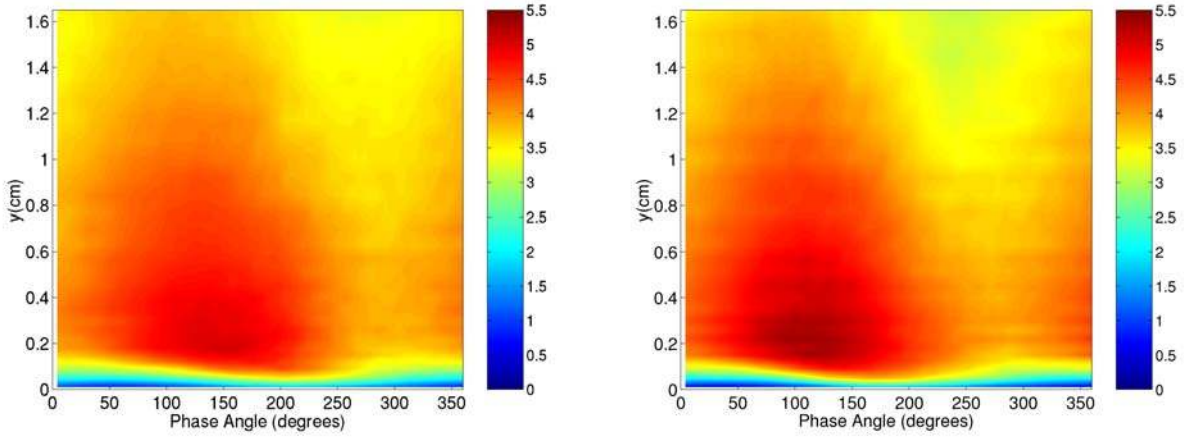

(a) Base Case (b) High-$FSTI$ Case

Figure 5.7: Velocity, $\tilde{u}$, (m/s), at station 5 ($s/L_{ss} = 37.35\%$)

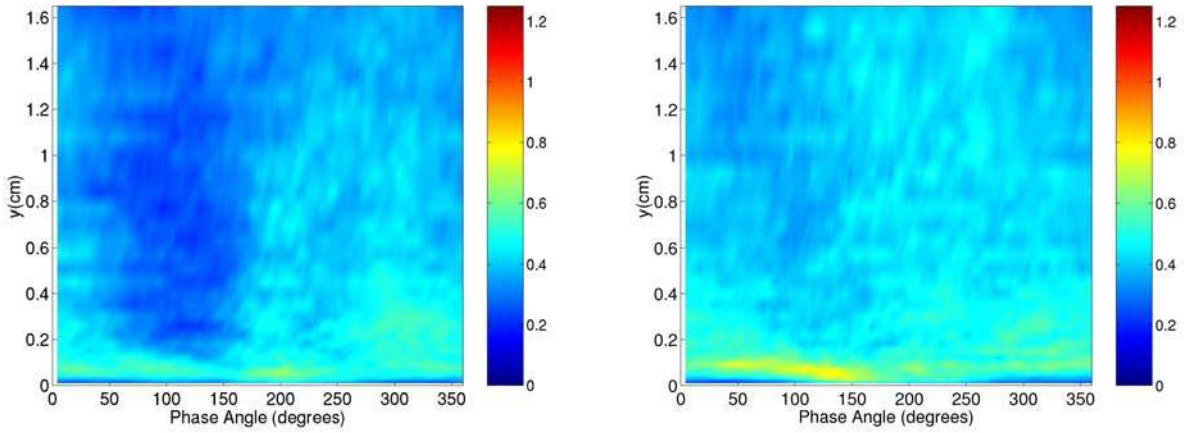

(a) Base Case (b) High-$FSTI$ Case

Figure 5.8: Velocity rms, $\widetilde{u_{rms}}$, (m/s), at station 5 ($s/L_{ss} = 37.35\%$)

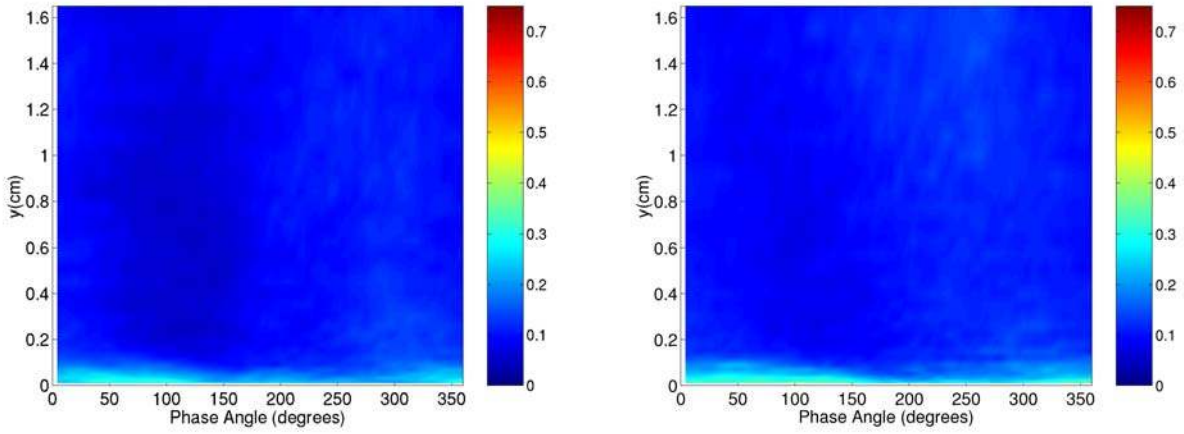

(a) Base Case

(b) High-$FSTI$ Case

Figure 5.9: Turbulence Intensity, $\widetilde{TI}$, at station 5 ($s/L_{ss} = 37.35\%$)

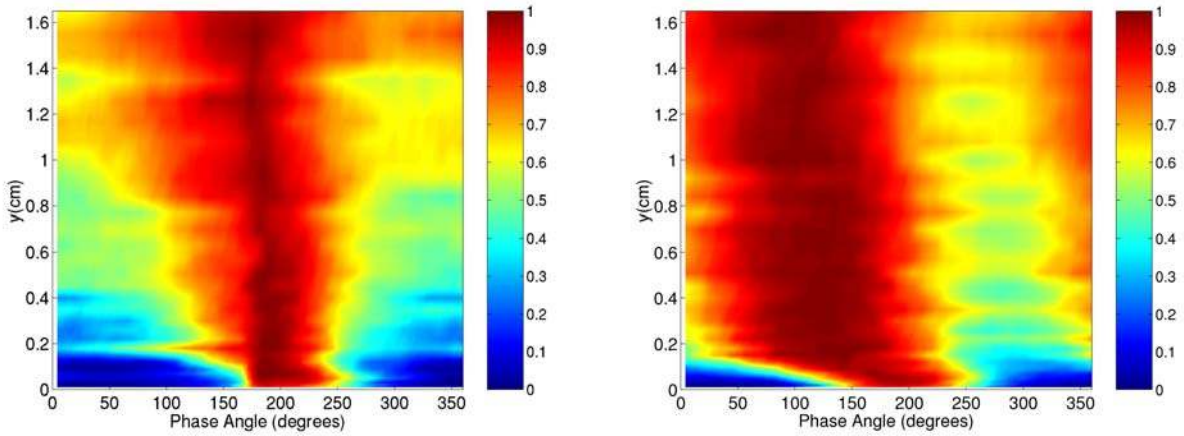

(a) Base Case

(b) High-$FSTI$ Case

Figure 5.10: Intermittency, $\tilde{\gamma}$, at station 5 ($s/L_{ss} = 37.35\%$)

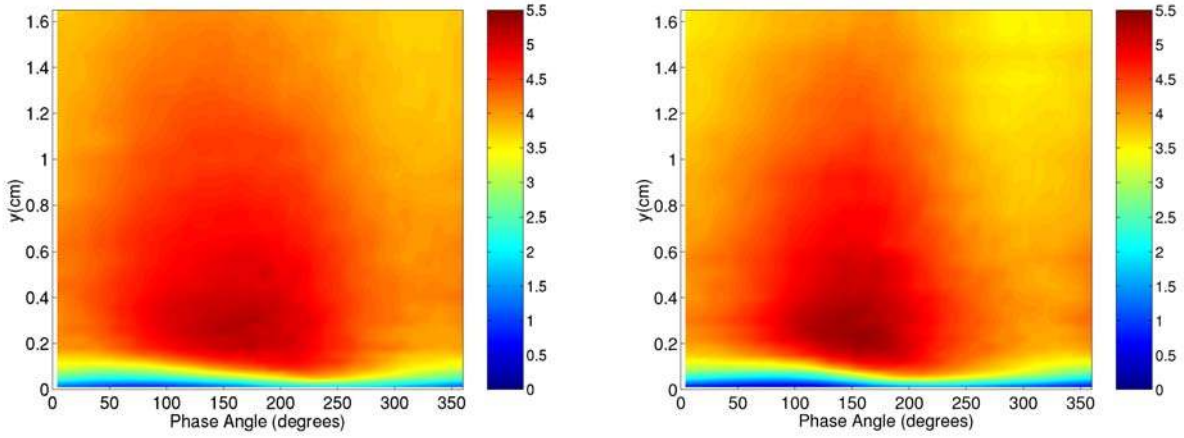

(a) Base Case (b) High-$FSTI$ Case

Figure 5.11: Velocity, $\tilde{u}$, (m/s), at station 6 ($s/L_{ss} = 43.34\%$)

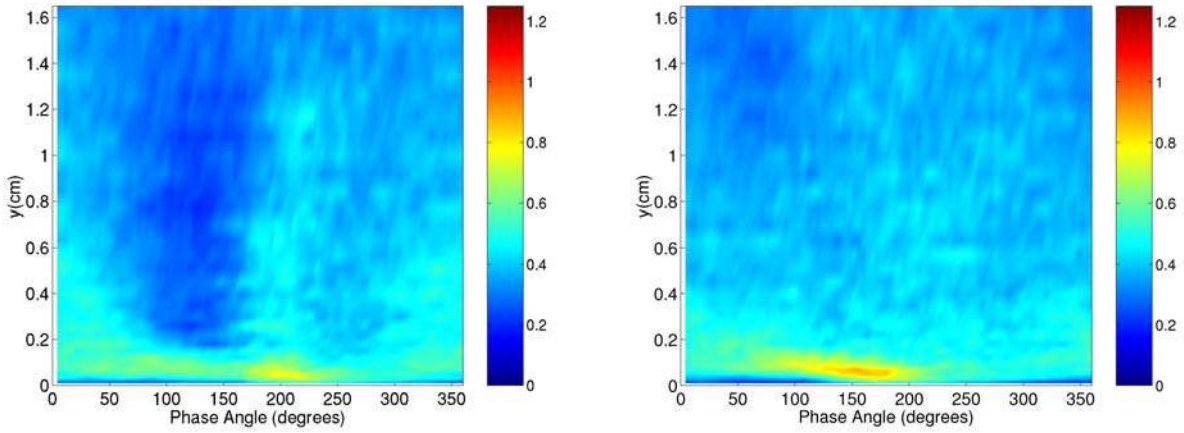

(a) Base Case (b) High-$FSTI$ Case

Figure 5.12: Velocity rms, $\widetilde{u_{rms}}$, (m/s), at station 6 ($s/L_{ss} = 43.34\%$)

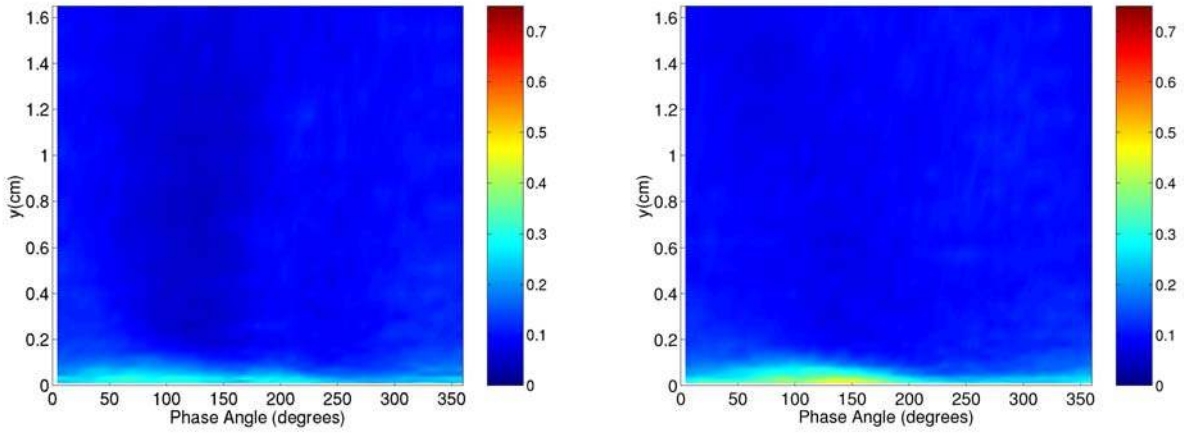

(a) Base Case

(b) High-$FSTI$ Case

Figure 5.13: Turbulence Intensity, $\widetilde{TI}$, at station 6 ($s/L_{ss} = 43.34\%$)

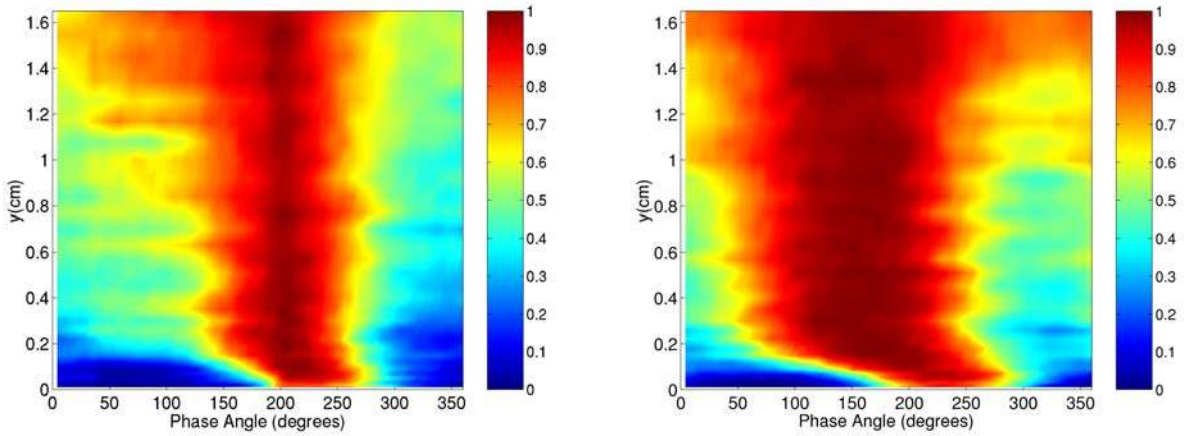

(a) Base Case

(b) High-$FSTI$ Case

Figure 5.14: Intermittency, $\tilde{\gamma}$, at station 6 ($s/L_{ss} = 43.34\%$)

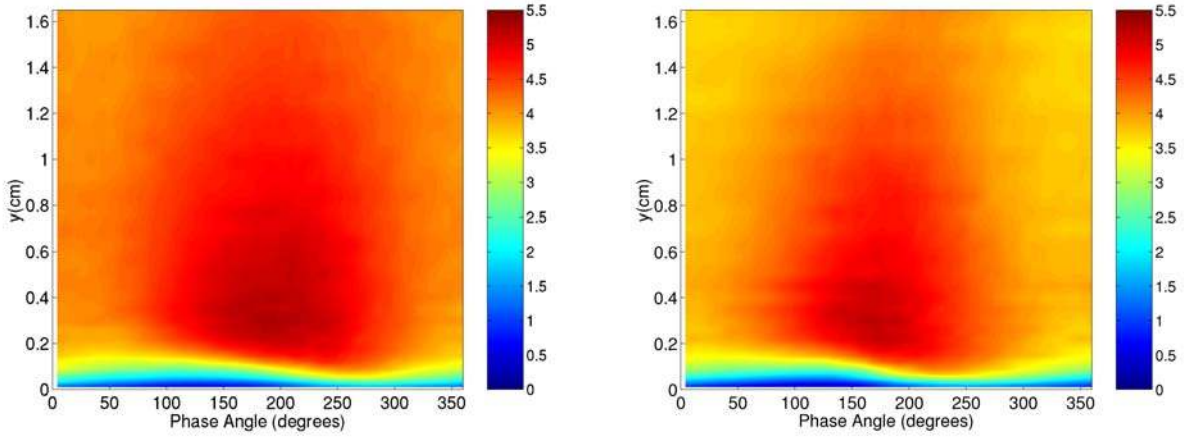

(a) Base Case

(b) High-$FSTI$ Case

Figure 5.15: Velocity, $\tilde{u}$, (m/s), at station 7 ($s/L_{ss} = 49.33\%$)

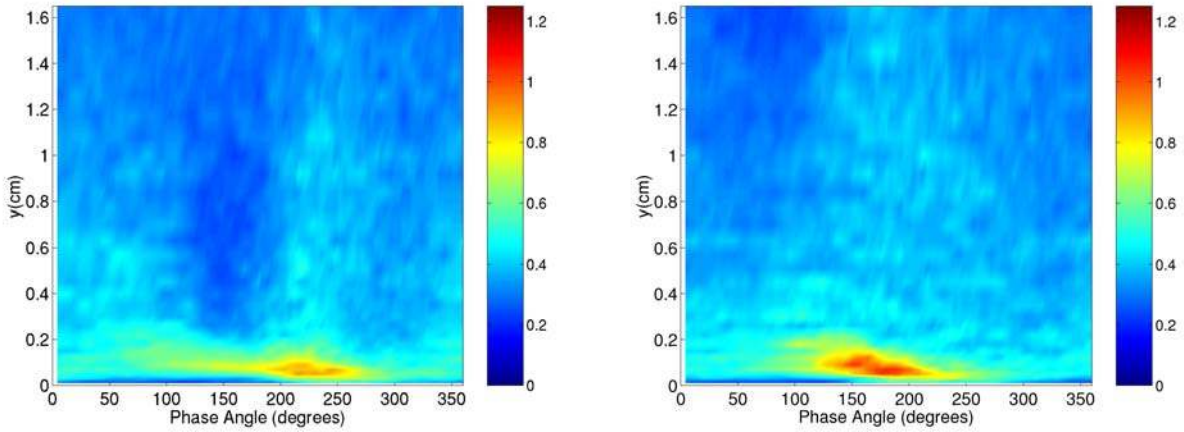

(a) Base Case

(b) High-$FSTI$ Case

Figure 5.16: Velocity rms, $\widetilde{u_{rms}}$, (m/s), at station 7 ($s/L_{ss} = 49.33\%$)

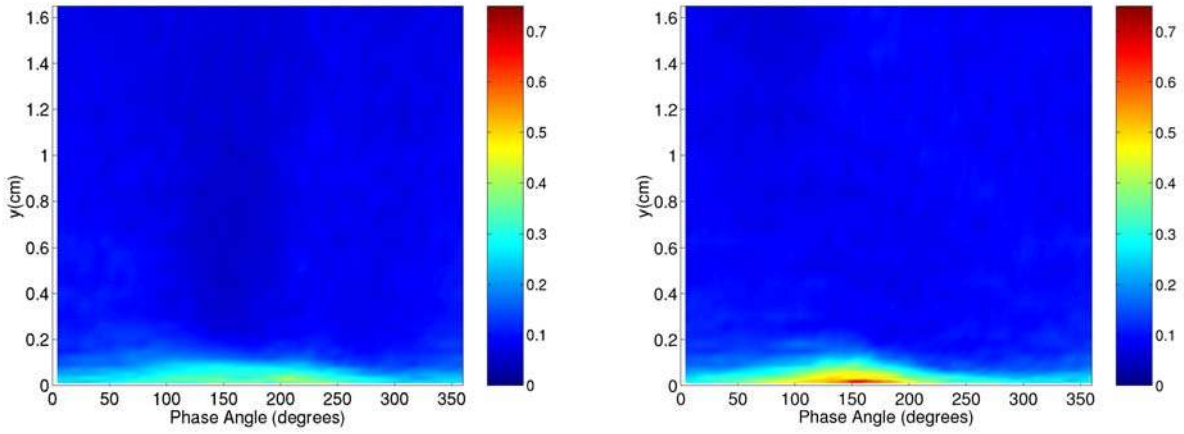

(a) Base Case

(b) High-$FSTI$ Case

Figure 5.17: Turbulence Intensity, $\widetilde{TI}$, at station 7 ($s/L_{ss} = 49.33\%$)

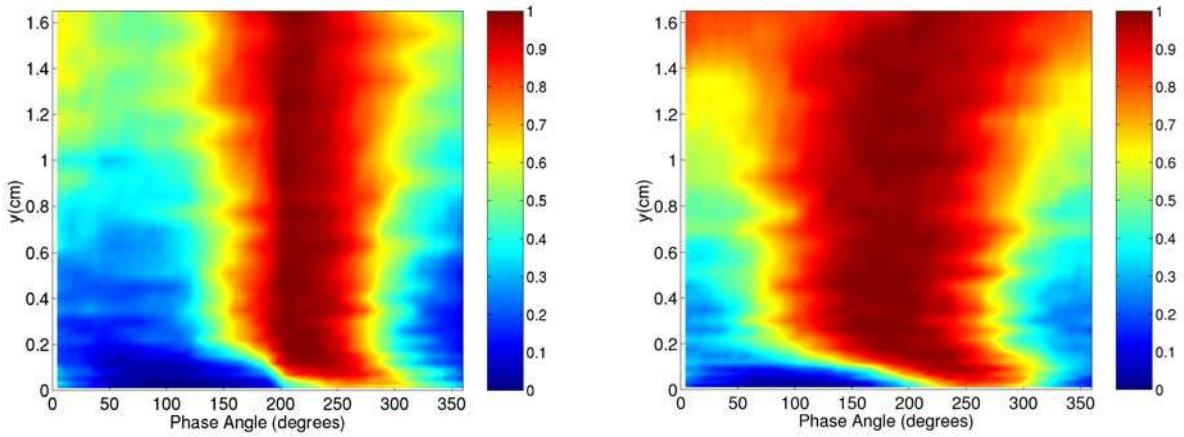

(a) Base Case

(b) High-$FSTI$ Case

Figure 5.18: Intermittency, $\tilde{\gamma}$, at station 7 ($s/L_{ss} = 49.33\%$)

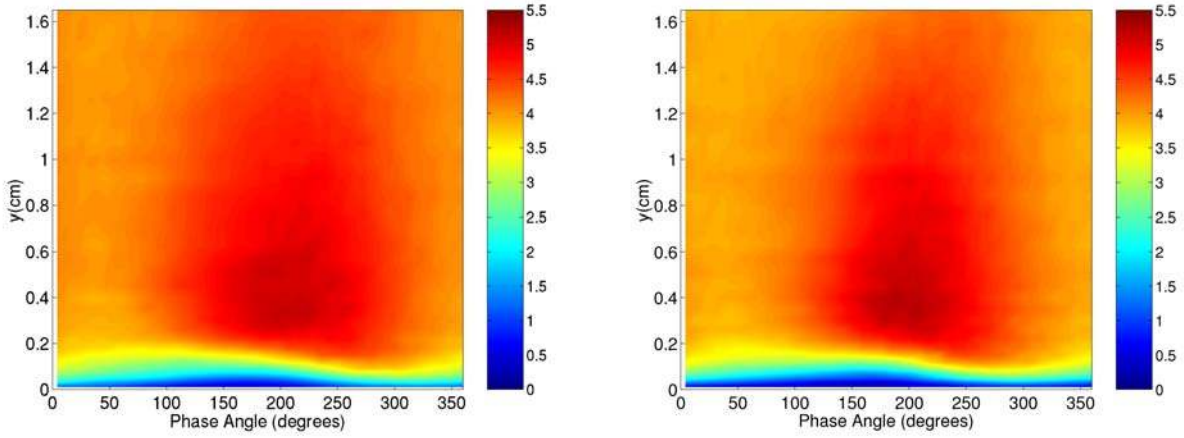

(a) Base Case

(b) High-$FSTI$ Case

Figure 5.19: Velocity, $\tilde{u}$, (m/s), at station 8 ($s/L_{ss} = 55.33\%$)

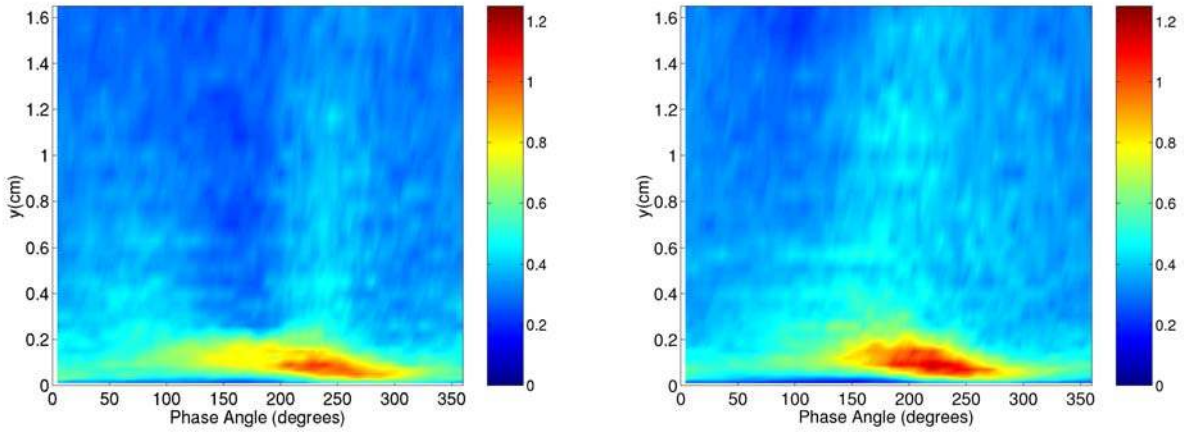

(a) Base Case

(b) High-$FSTI$ Case

Figure 5.20: Velocity rms, $\widetilde{u_{rms}}$, (m/s), at station 8 ($s/L_{ss} = 55.33\%$)

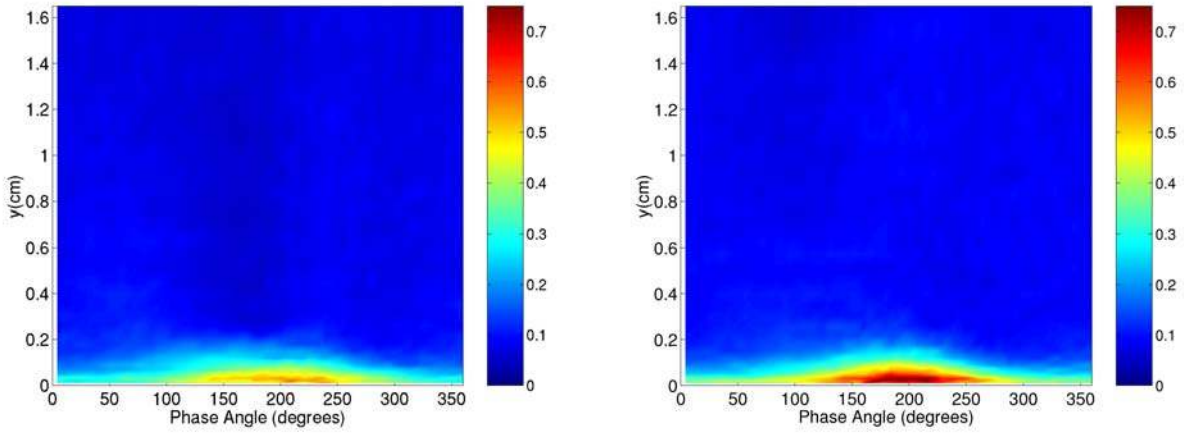

(a) Base Case

(b) High-$FSTI$ Case

Figure 5.21: Turbulence Intensity, $\widetilde{TI}$, at station 8 ($s/L_{ss} = 55.33\%$)

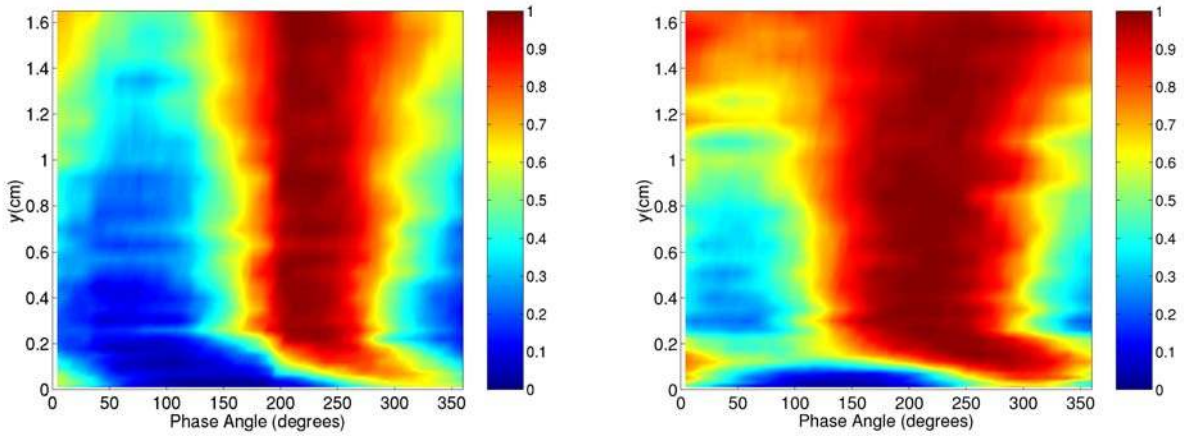

(a) Base Case

(b) High-$FSTI$ Case

Figure 5.22: Intermittency, $\tilde{\gamma}$, at station 8 ($s/L_{ss} = 55.33\%$)

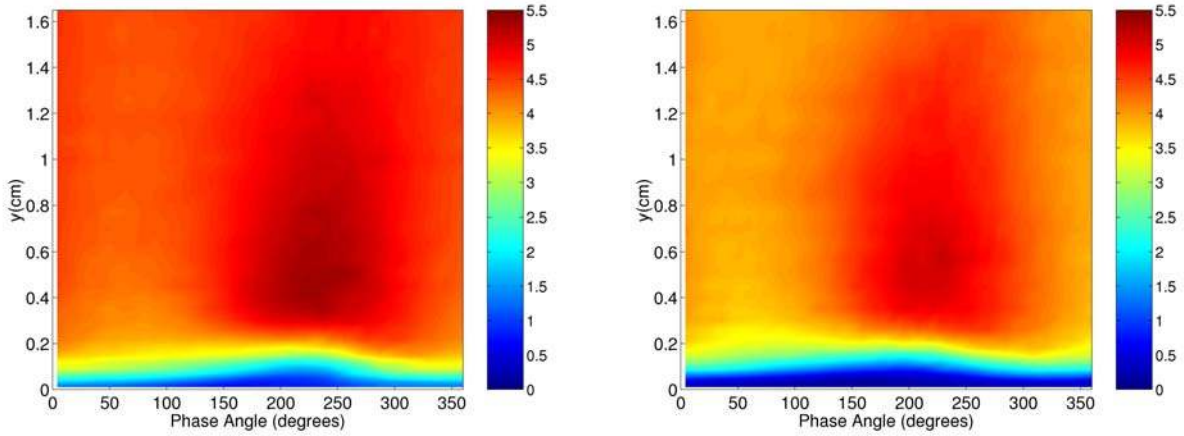

(a) Base Case (b) High-$FSTI$ Case

Figure 5.23: Velocity, $\tilde{u}$, (m/s), at station 9 ($s/L_{ss} = 61.32\%$)

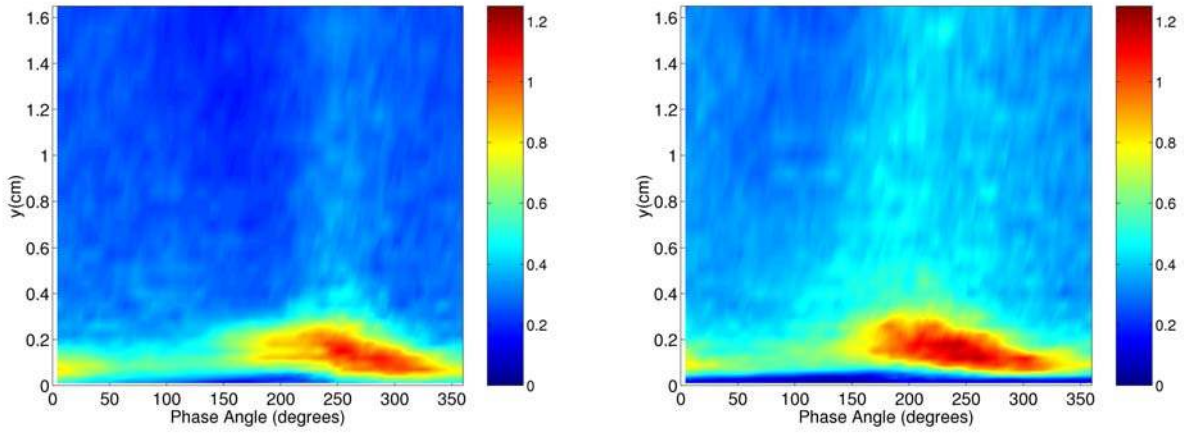

(a) Base Case (b) High-$FSTI$ Case

Figure 5.24: Velocity rms, $\widetilde{u_{rms}}$, (m/s), at station 9 ($s/L_{ss} = 61.32\%$)

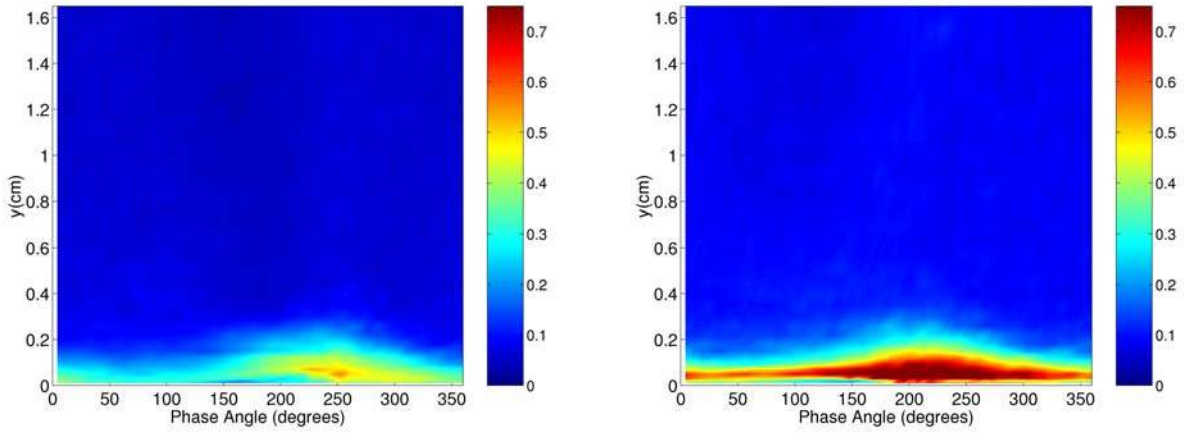

(a) Base Case

(b) High-$FSTI$ Case

Figure 5.25: Turbulence Intensity, $\widetilde{TI}$, at station 9 ($s/L_{ss} = 61.32\%$)

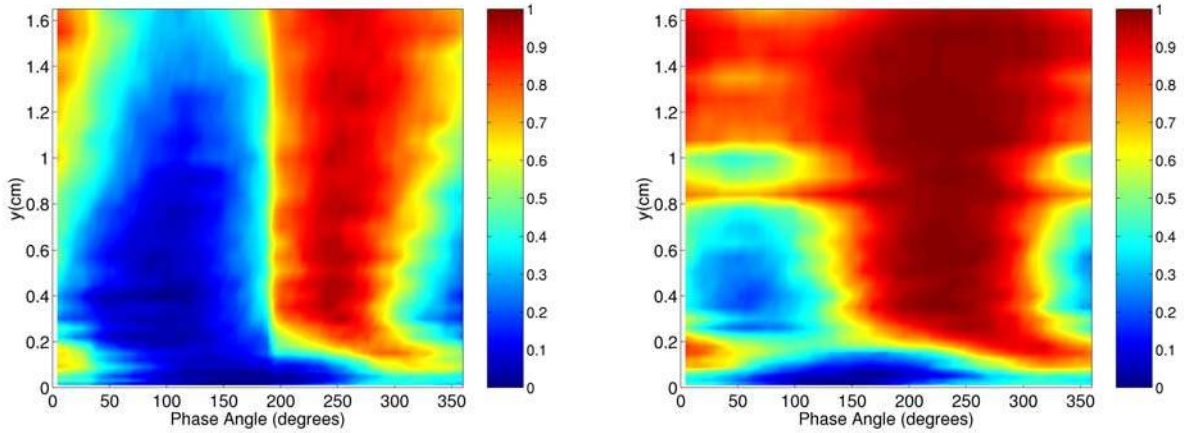

(a) Base Case

(b) High-$FSTI$ Case

Figure 5.26: Intermittency, $\tilde{\gamma}$, at station 9 ($s/L_{ss} = 61.32\%$)

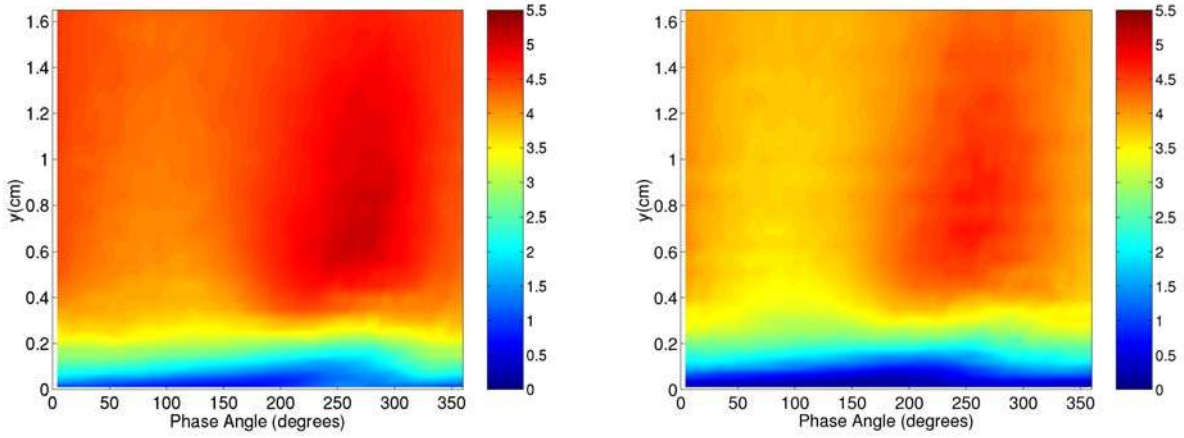

(a) Base Case (b) High-$FSTI$ Case

Figure 5.27: Velocity, $\tilde{u}$, (m/s), at station 10 ($s/L_{ss} = 70.31\%$)

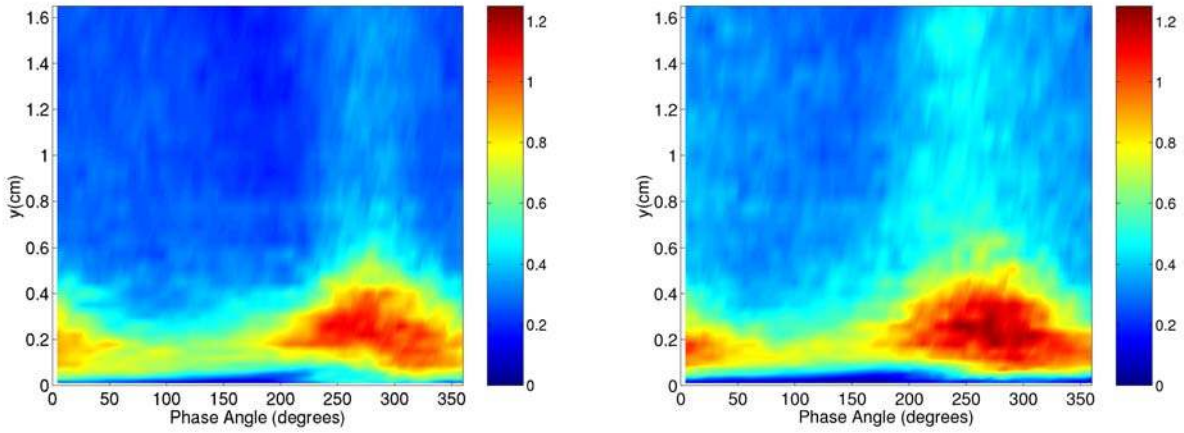

(a) Base Case (b) High-$FSTI$ Case

Figure 5.28: Velocity rms, $\widetilde{u_{rms}}$, (m/s), at station 10 ($s/L_{ss} = 70.31\%$)

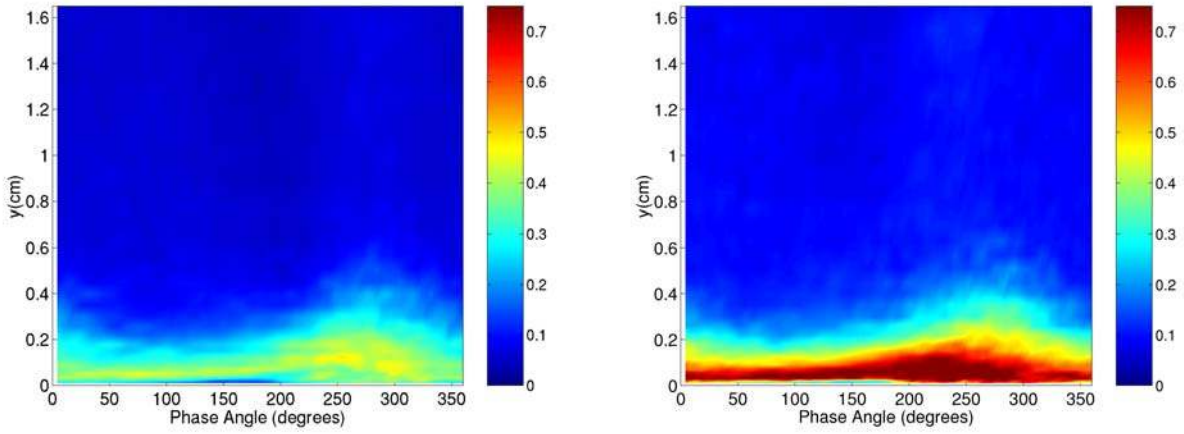

(a) Base Case

(b) High-$FSTI$ Case

Figure 5.29: Turbulence Intensity, $\widetilde{TI}$, at station 10 ($s/L_{ss} = 70.31\%$)

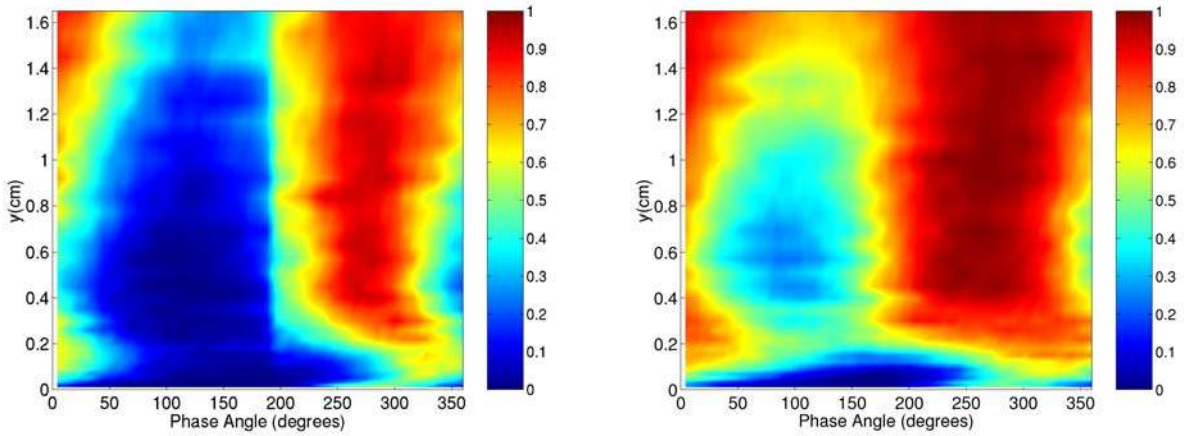

(a) Base Case

(b) High-$FSTI$ Case

Figure 5.30: Intermittency, $\tilde{\gamma}$, at station 10 ($s/L_{ss} = 70.31\%$)

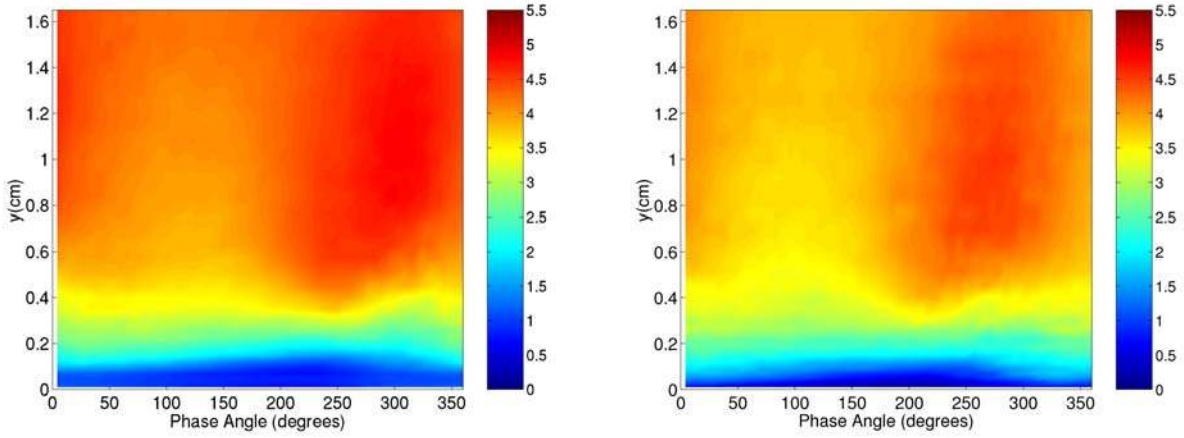

(a) Base Case (b) High-$FSTI$ Case

Figure 5.31: Velocity, $\tilde{u}$, (m/s), at station 11 ($s/L_{ss} = 76.11\%$)

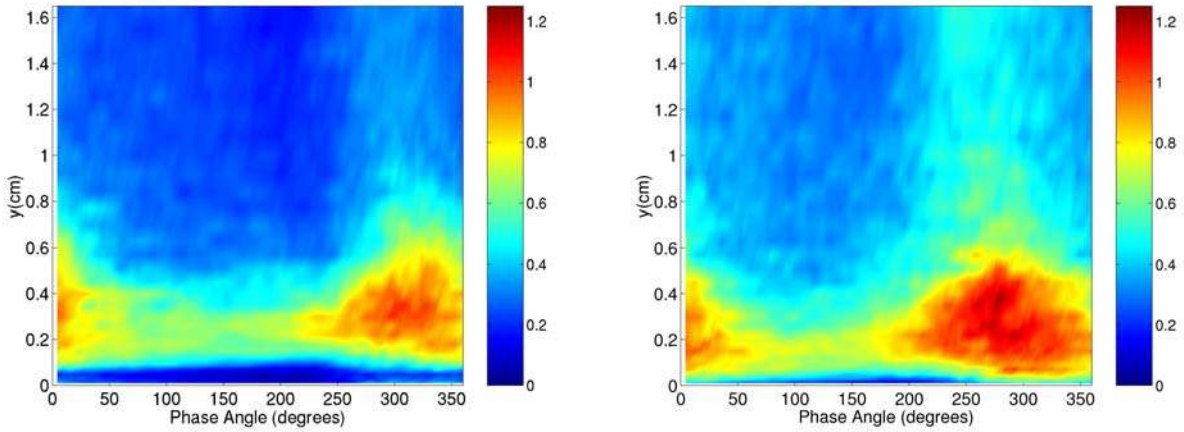

(a) Base Case (b) High-$FSTI$ Case

Figure 5.32: Velocity rms, $\widetilde{u_{rms}}$, (m/s), at station 11 ($s/L_{ss} = 76.11\%$)

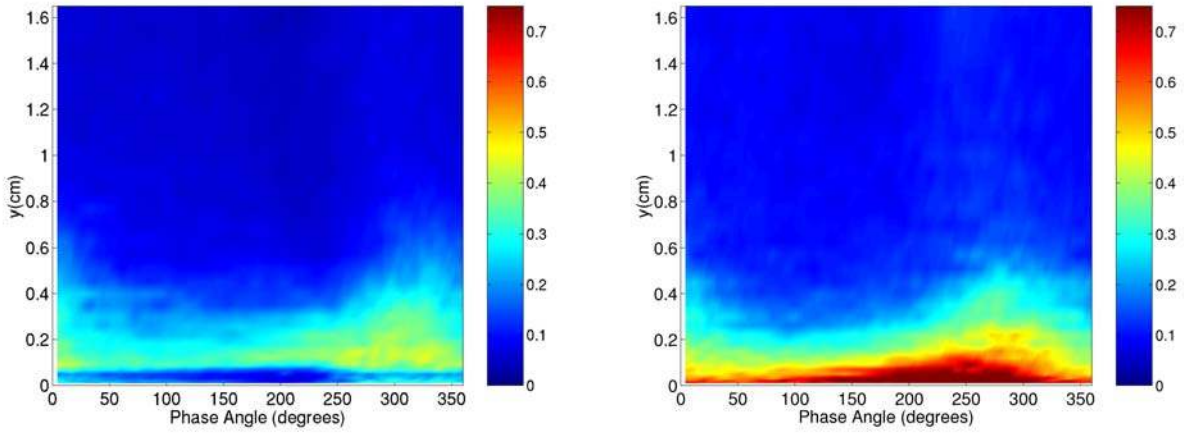

(a) Base Case

(b) High-$FSTI$ Case

Figure 5.33: Turbulence Intensity, $\widetilde{TI}$, at station 11 ($s/L_{ss} = 76.11\%$)

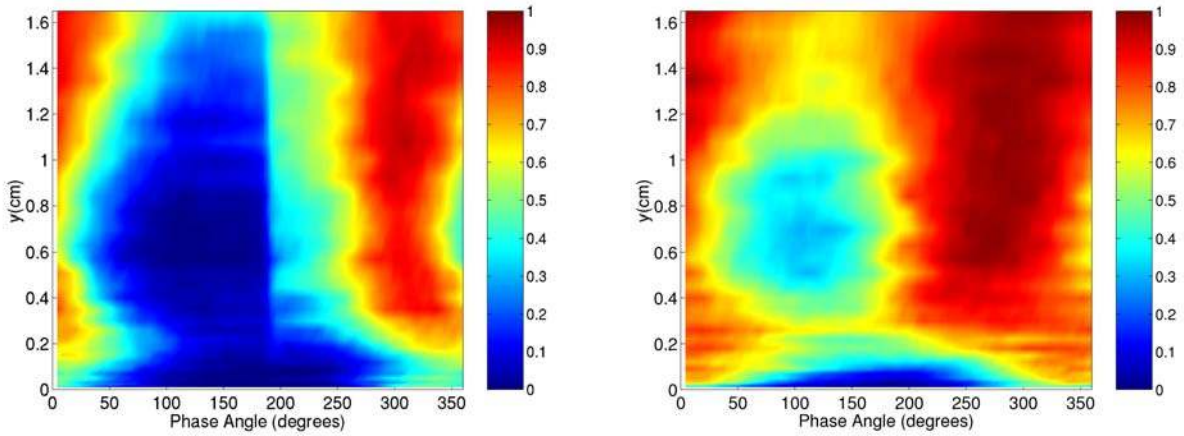

(a) Base Case

(b) High-$FSTI$ Case

Figure 5.34: Intermittency, $\tilde{\gamma}$, at station 11 ($s/L_{ss} = 76.11\%$)

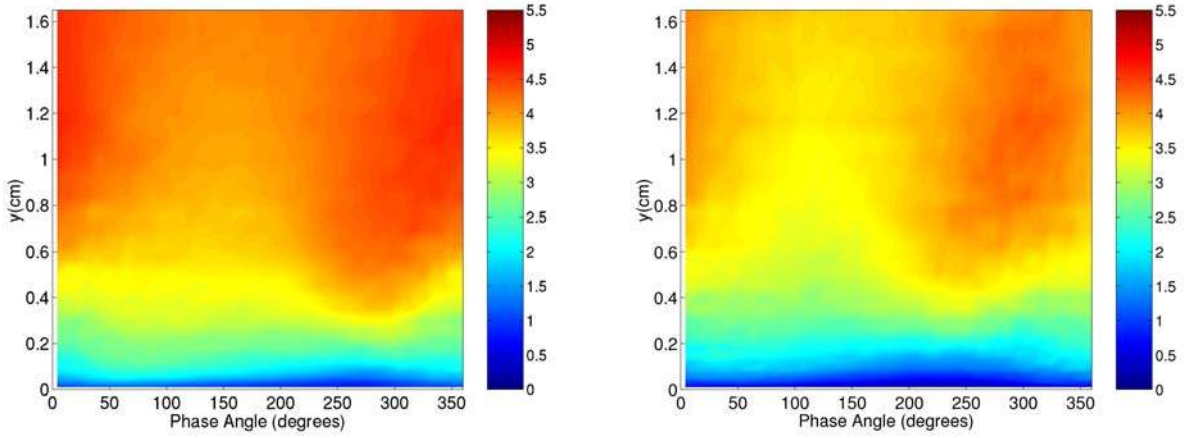

(a) Base Case (b) High-$FSTI$ Case

Figure 5.35: Velocity, $\tilde{u}$, (m/s), at station 12 ($s/L_{ss} = 84.00\%$)

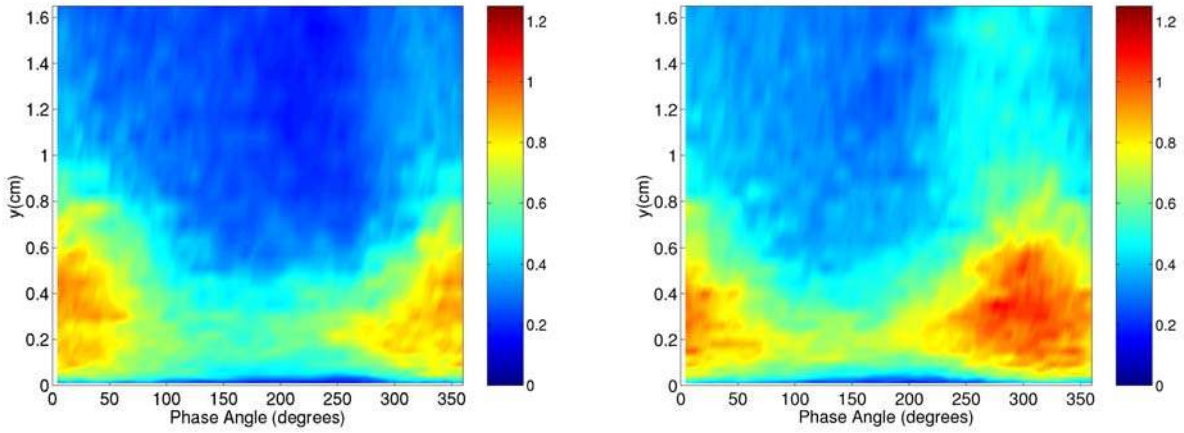

(a) Base Case (b) High-$FSTI$ Case

Figure 5.36: Velocity rms, $\widetilde{u_{rms}}$, (m/s), at station 12 ($s/L_{ss} = 84.00\%$)

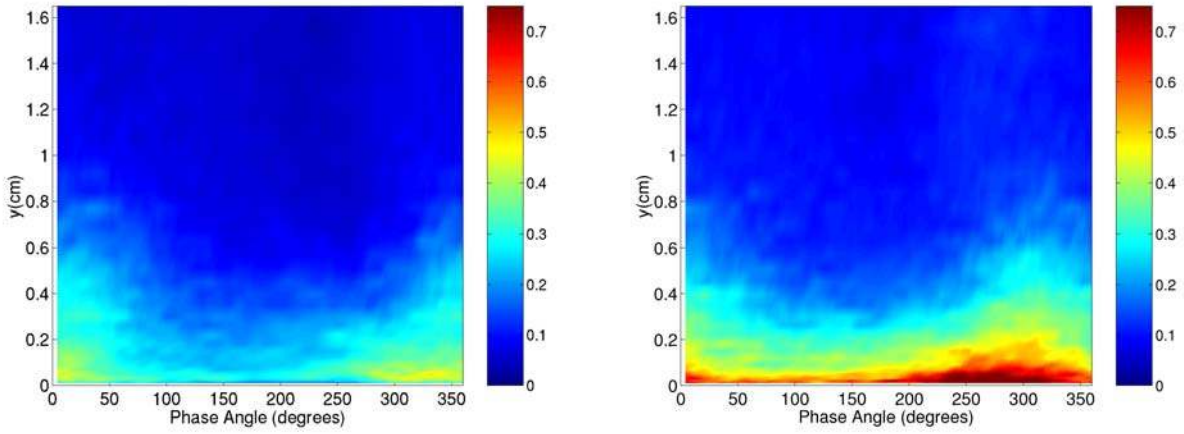

(a) Base Case

(b) High-$FSTI$ Case

Figure 5.37: Turbulence Intensity, $\widetilde{TI}$, at station 12 ($s/L_{ss} = 84.00\%$)

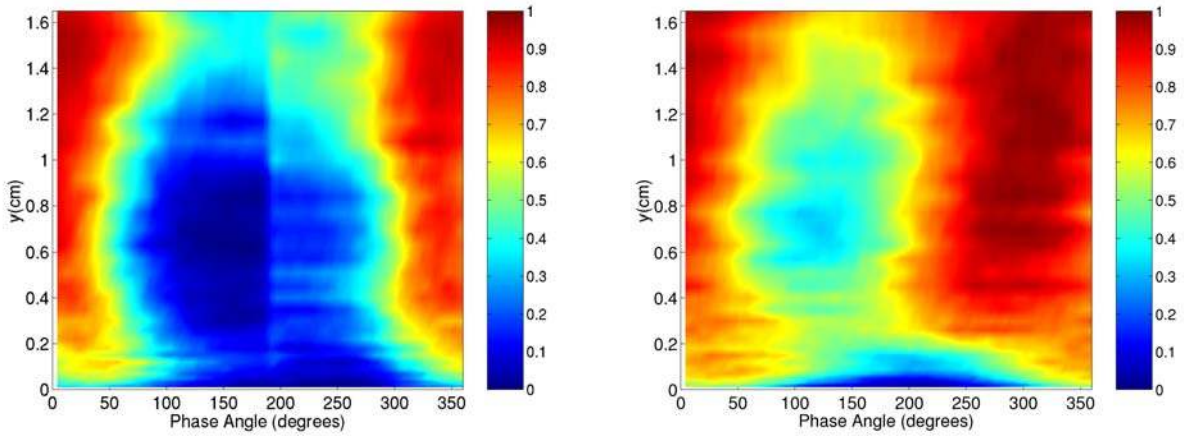

(a) Base Case

(b) High-$FSTI$ Case

Figure 5.38: Intermittency, $\tilde{\gamma}$, at station 12 ($s/L_{ss} = 84.00\%$)

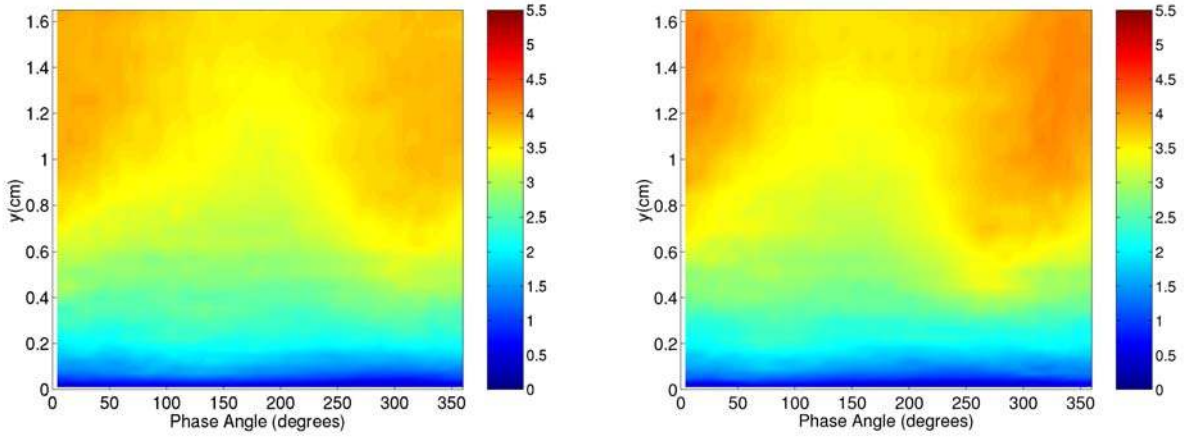

(a) Base Case

(b) High-$FSTI$ Case

Figure 5.39: Velocity, $\tilde{u}$, (m/s), at station 13 ($s/L_{ss} = 93.49\%$)

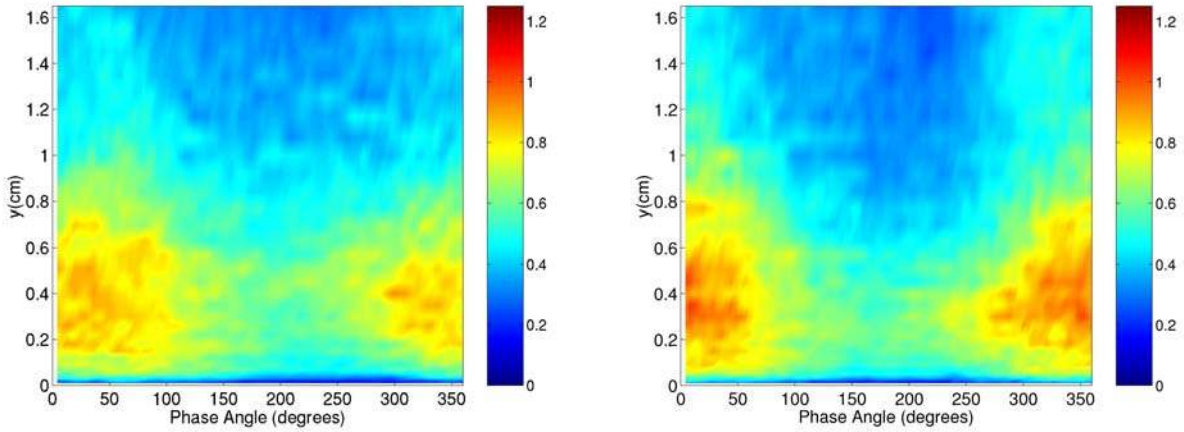

(a) Base Case

(b) High-$FSTI$ Case

Figure 5.40: Velocity rms, $\widetilde{u_{rms}}$, (m/s), at station 13 ($s/L_{ss} = 93.49\%$)

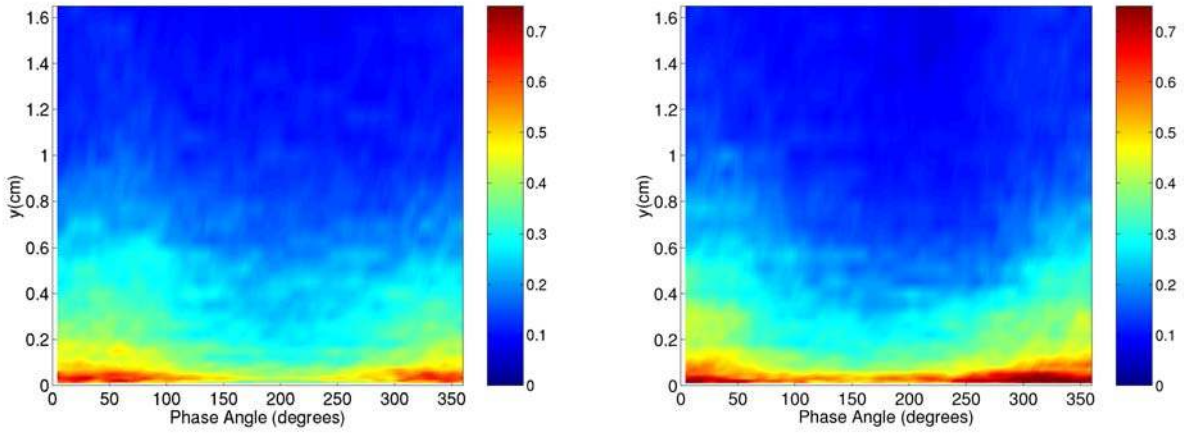

(a) Base Case

(b) High-$FSTI$ Case

Figure 5.41: Turbulence Intensity, $\widetilde{TI}$, at station 13 ($s/L_{ss} = 93.49\%$)

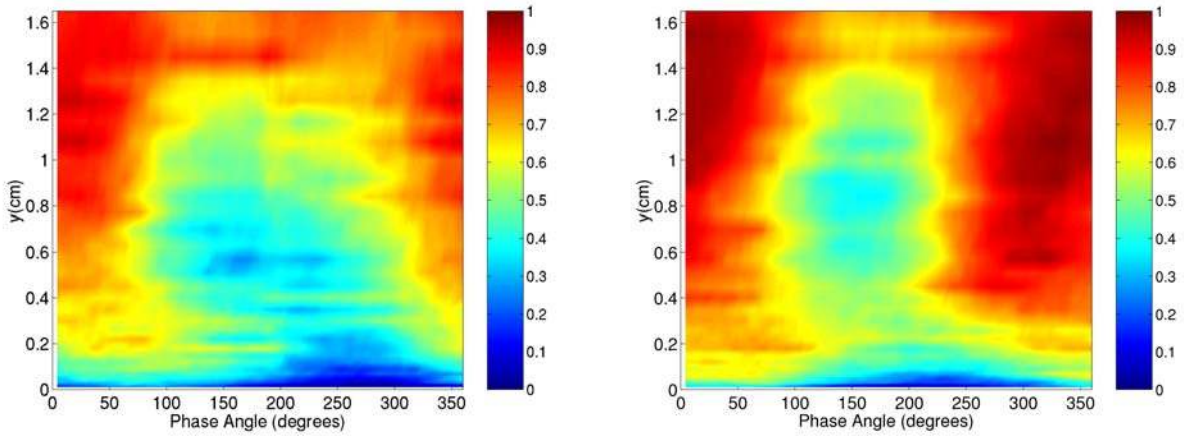

(a) Base Case

(b) High-$FSTI$ Case

Figure 5.42: Intermittency, $\tilde{\gamma}$, at station 13 ($s/L_{ss} = 93.49\%$)

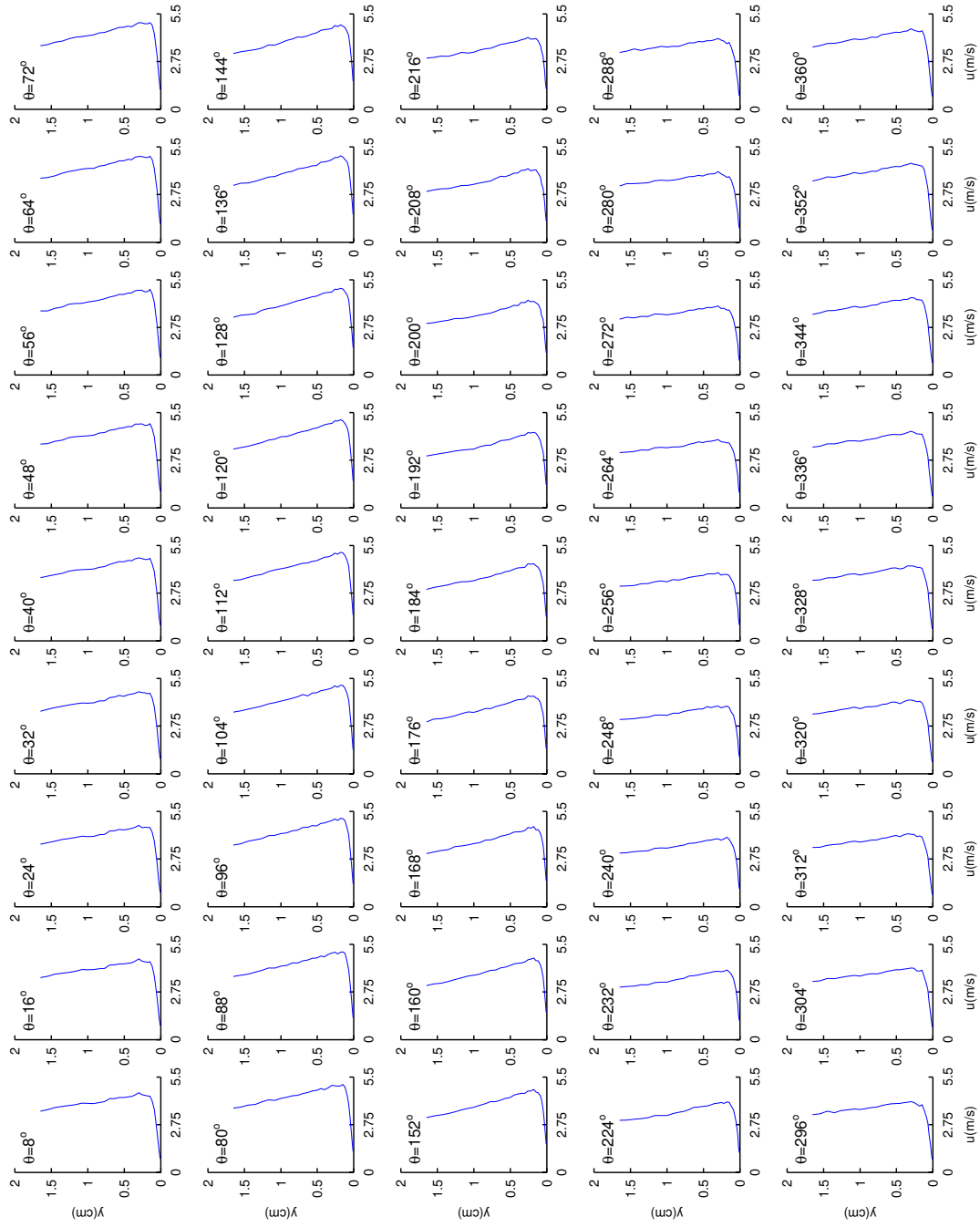

Figure 5.43: Phase average velocity $\tilde{u}(y, \theta)$ at station 4 ($s/L_{ss} = 31.36\%$), presented as a function of θ, high-$FSTI$ case.

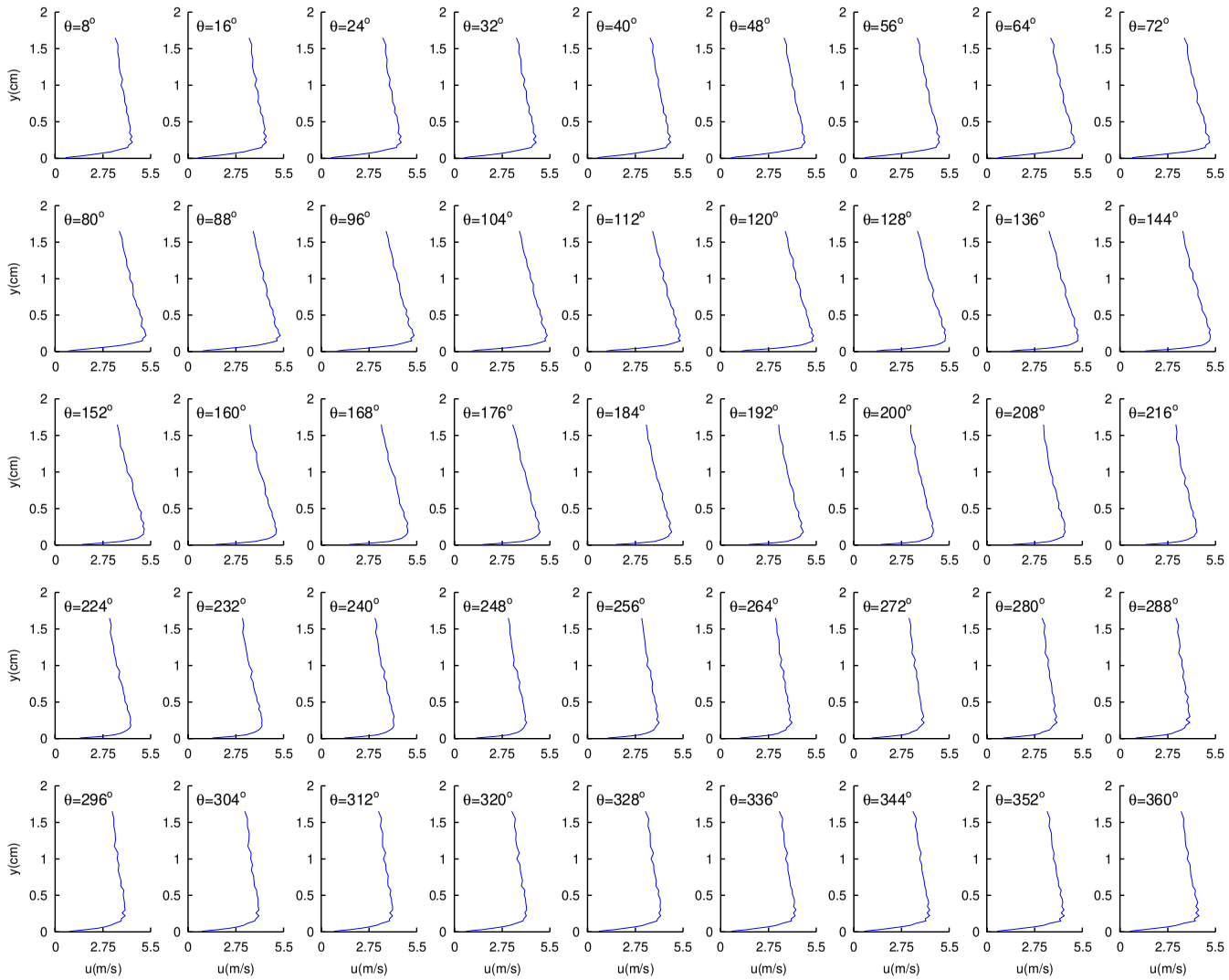

Figure 5.44: Phase average velocity $\tilde{u}(y, \theta)$ at station 5 ($s/L_{ss} = 37.35\%$), presented as a function of θ, high-$FSTI$ case.

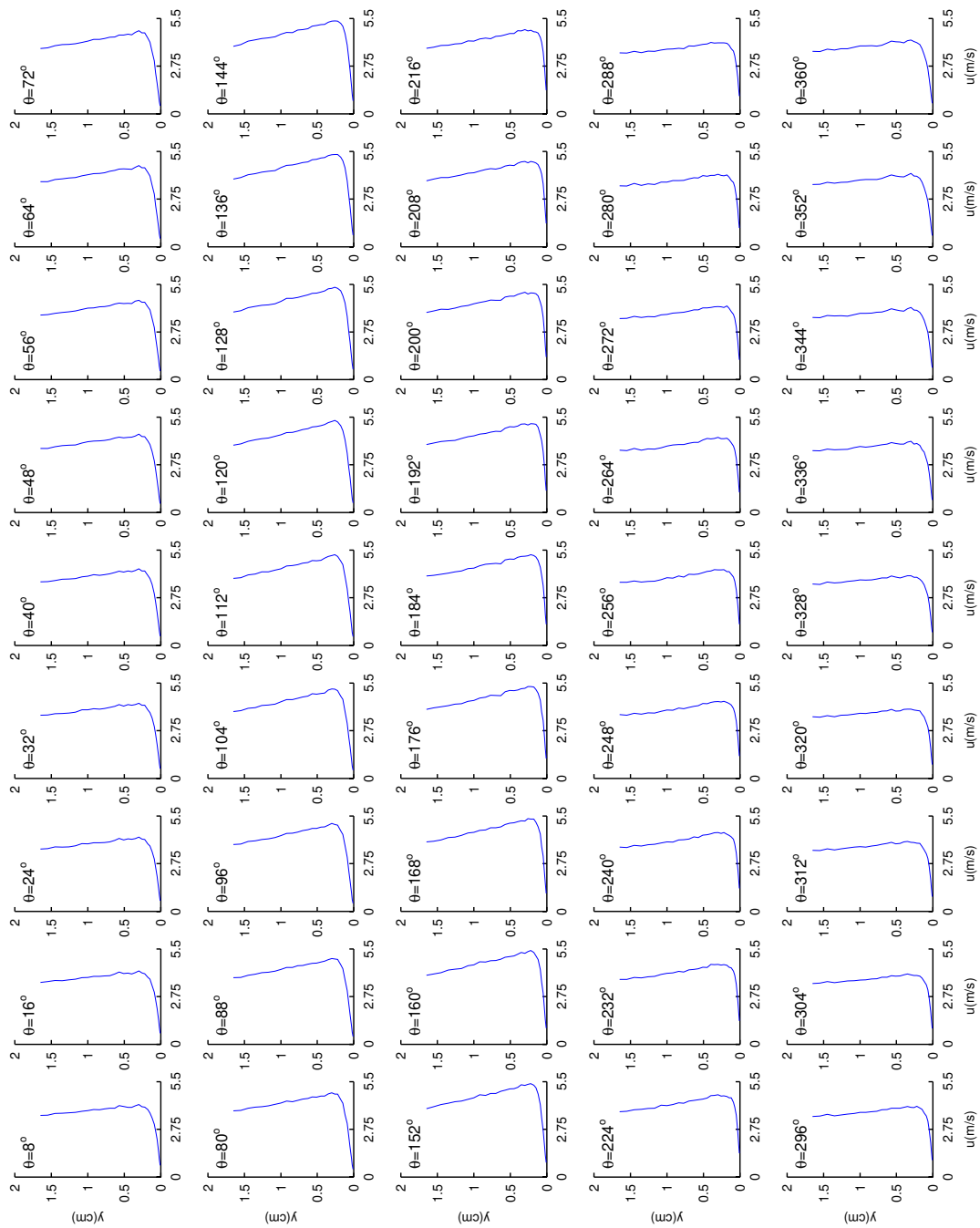

Figure 5.45: Phase average velocity $\tilde{u}(y, \theta)$ at station 6 ($s/L_{ss} = 43.34\%$), presented as a function of θ, high-$FSTI$ case.

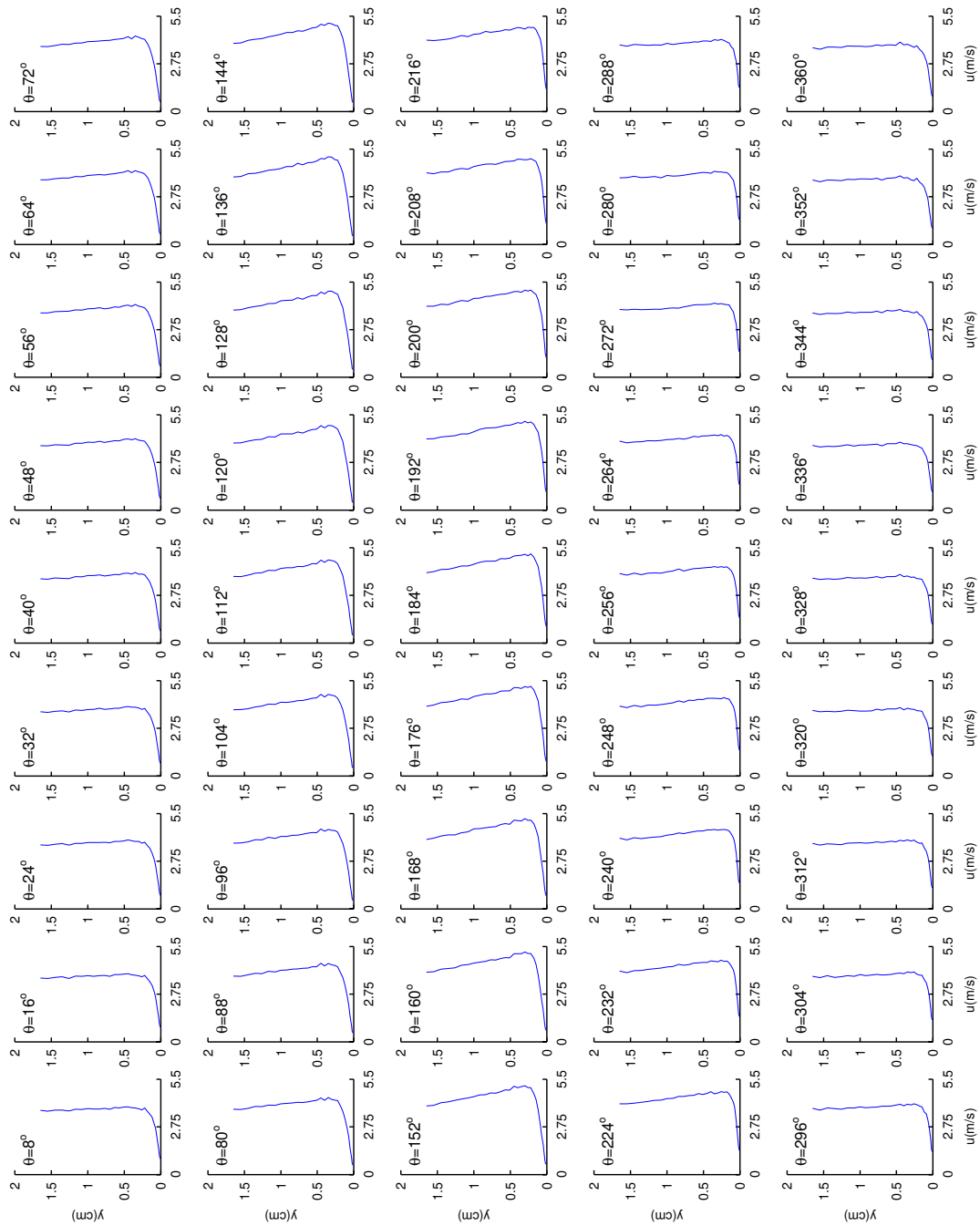

Figure 5.46: Phase average velocity $\tilde{u}(y,\theta)$ at station 7 ($s/L_{ss} = 49.33\%$), presented as a function of θ, high-$FSTI$ case.

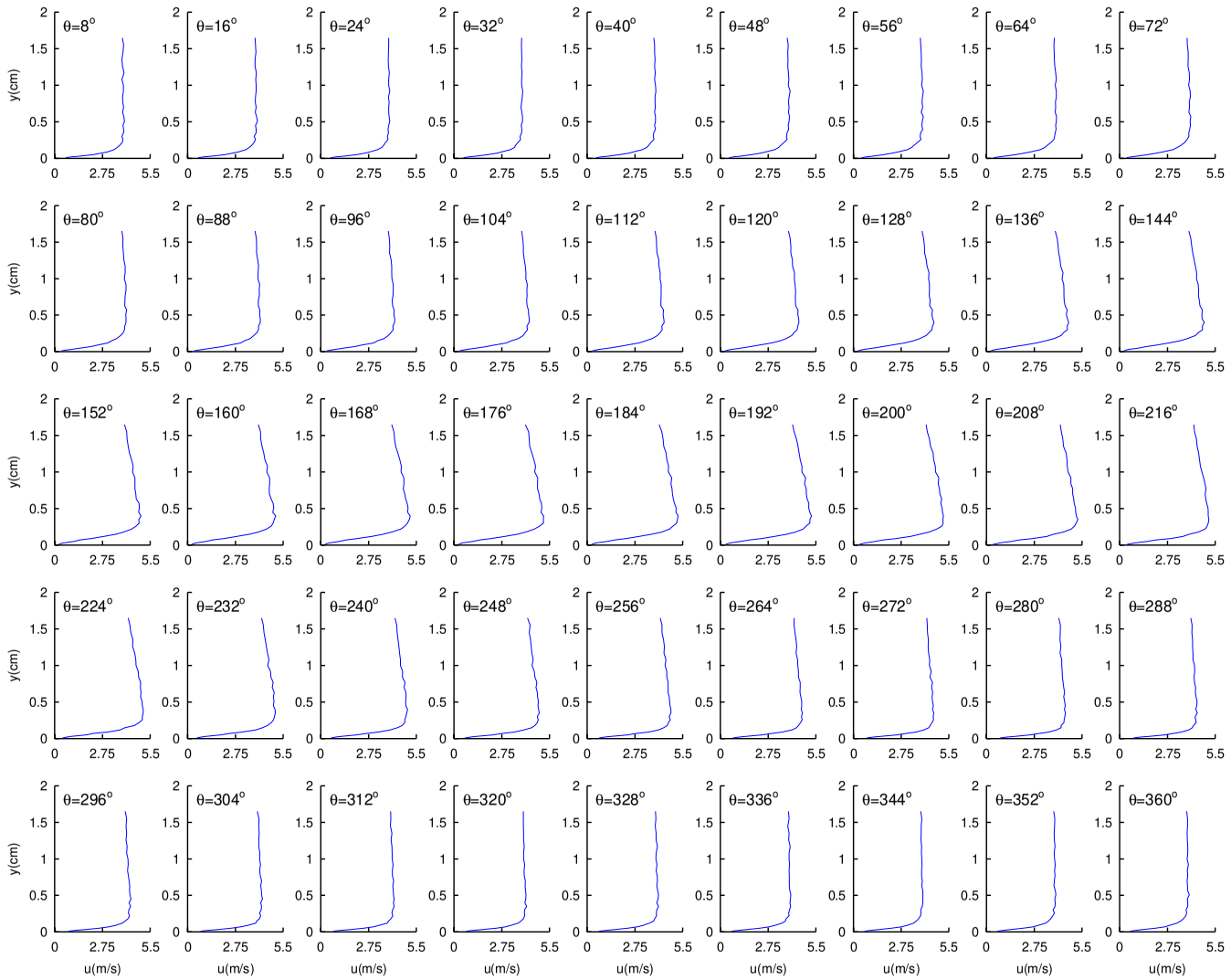

Figure 5.47: Phase average velocity $\tilde{u}(y, \theta)$ at station 8 ($s/L_{ss} = 55.33\%$), presented as a function of θ, high-$FSTI$ case.

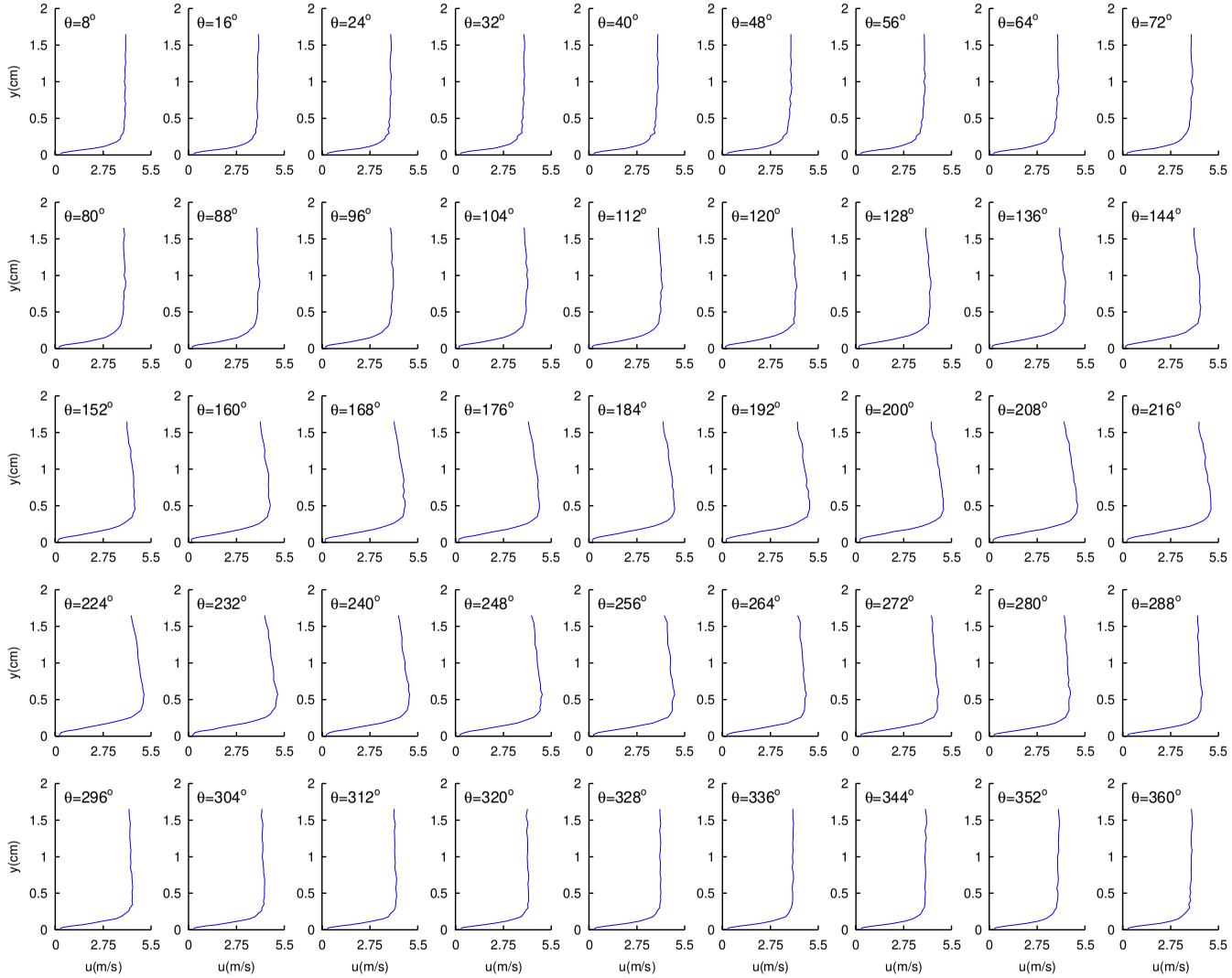

Figure 5.48: Phase average velocity $\tilde{u}(y, \theta)$ at station 9 ($s/L_{ss} = 61.32\%$), presented as a function of θ, high-$FSTI$ case.

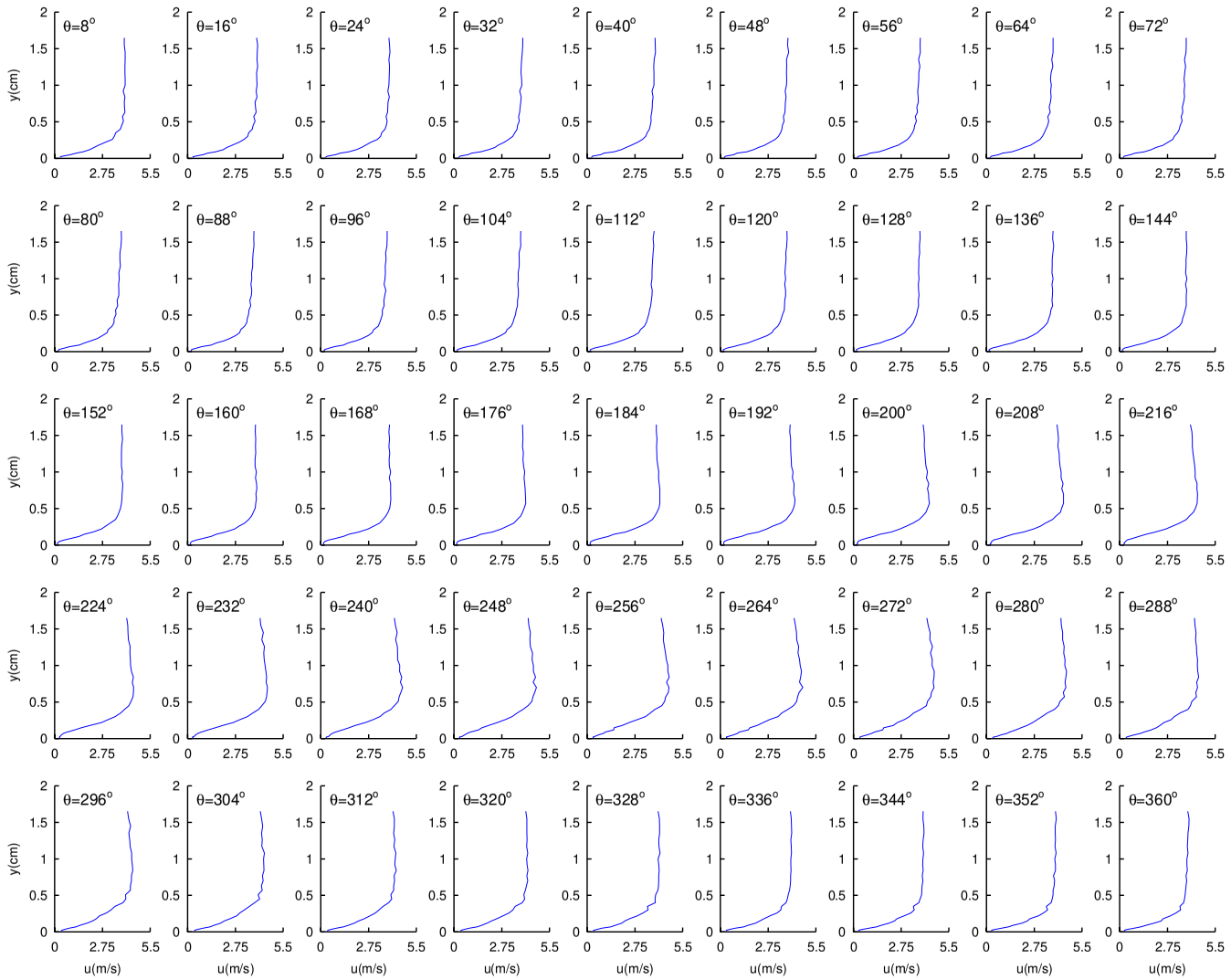

Figure 5.49: Phase average velocity $\tilde{u}(y, \theta)$ at station 10 ($s/L_{ss} = 70.31\%$), presented as a function of θ, high-*FSTI* case.

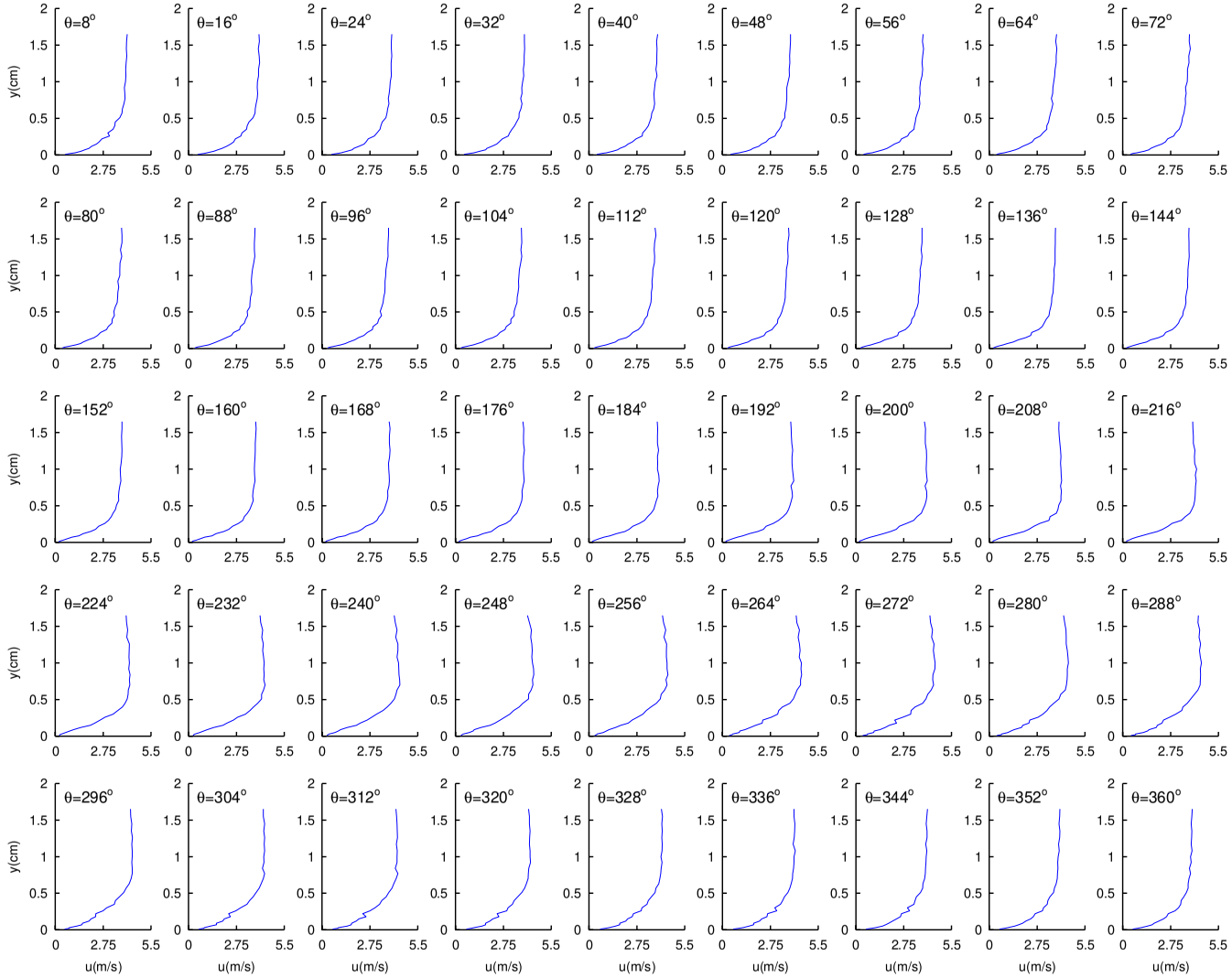

Figure 5.50: Phase average velocity $\tilde{u}(y, \theta)$ at station 11 ($s/L_{ss} = 76.11\%$), presented as a function of θ, high-$FSTI$ case.

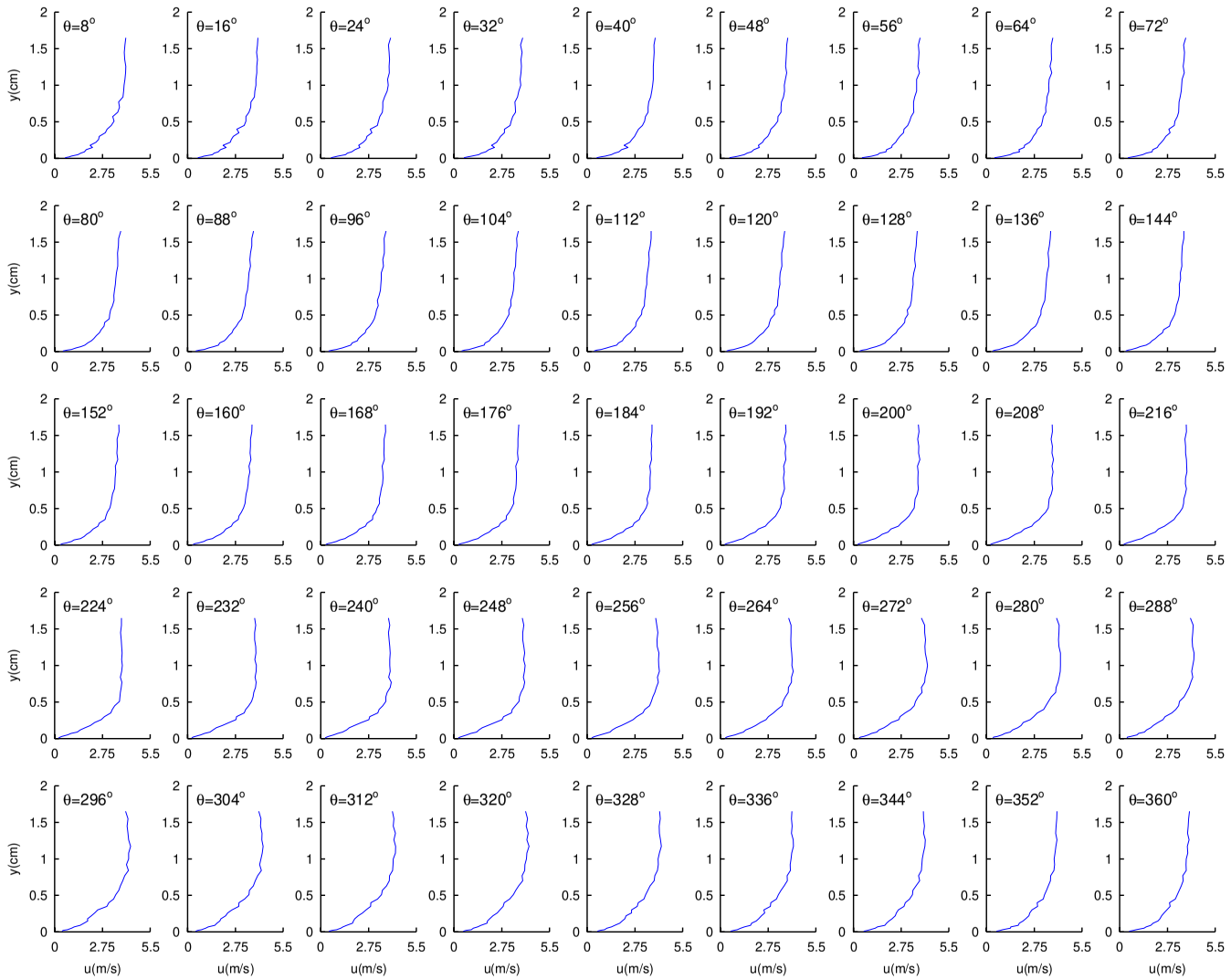

Figure 5.51: Phase average velocity $\tilde{u}(y, \theta)$ at station 12 ($s/L_{ss} = 84.00\%$), presented as a function of θ, high-*FSTI* case.

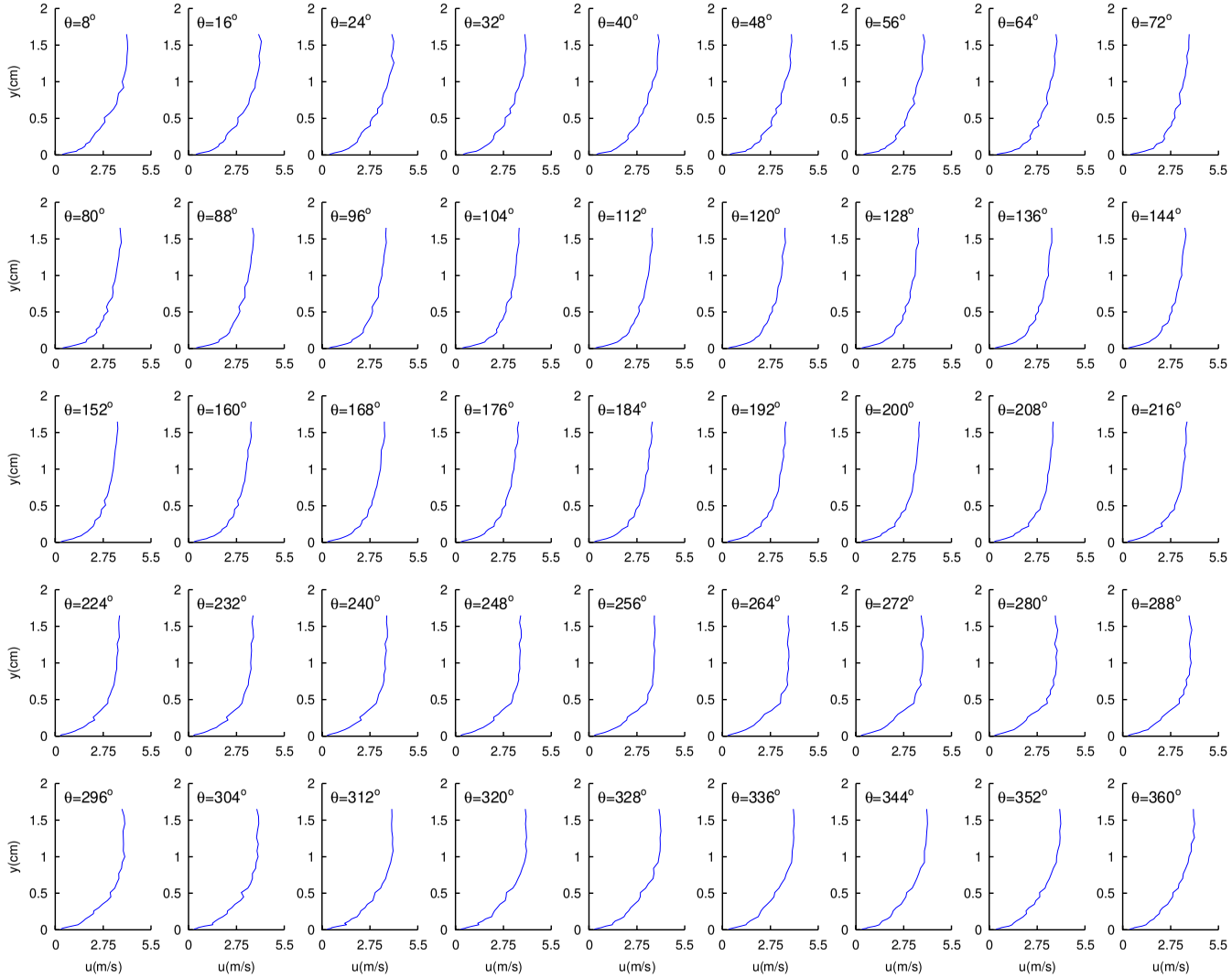

Figure 5.52: Phase average velocity $\tilde{u}(y, \theta)$ at station 13 ($s/L_{ss} = 93.49\%$), presented as a function of θ, high-$FSTI$ case.

Chapter 6

Conclusions

6.1 General Significance and Applicability of the Results

These results represent detailed documentation of the effects of increased wake spacing and elevated *FSTI* flow upon laminar-to-turbulent transition in a low-pressure turbine passage affected by passing wakes.

6.2 Specific Conclusions: Increased Wake Spacing Case

The basic flow field of the increased was spacing case is similar to the flow field of the base case described in Kaszeta and Simon (2002). However, the wider temporal spacing of the wakes allows a much longer period for the boundary layer to recover from the wakes' perturbations and allow the boundary layer to resume development that is more like that of the steady-flow case documented in Simon et al. (2000). This wider spacing produces some significant changes in the separation and transition processes occurring in the turbine passage:

1. As shown in section 4.2.2, the increased spacing flow separates upstream of the base case separation point. This appears to be caused by increased boundary layer growth that occurs in the longer between-wake period in the increased spacing case.

2. As shown in section 4.2.7, the longer between-wake period allows the development of a separation bubble which is significantly thicker than that seen in the base case.

More discussion about the increased wake spacing case can be found in Kaszeta et al. (2005).

6.3 Specific Conclusions: High-*FSTI* Case

The basic flow field of the high-*FSTI* case is similar to that shown for the base case documented in Kaszeta and Simon (2002). However, the increases in the overall level of turbulence and length scale have some significant effects on both separation and transition in the turbine passage:

1. As shown in section 5.2.1, the high-*FSTI* flow separates downstream of the base case separation point. The high turbulence intensity within the wakes and resulted high disturbance in the freestream are considered as the main reasons.

2. In the high-*FSTI* flow, the elevated *FSTI* present in the passage causes the flow to reattach earlier, as shown in section 5.2.6. The reattachment point change is far stronger than the separation point change. As a result, the high-*FSTI* flow has shorter, thinner separation bubble than that of the base case, suggesting higher aerodynamic efficiency than that documented in the base case.

3. As shown in section 5.2.2, the elevated *FSTI* appears to have its strongest effect on the transition process in the shear flow above the separation bubble in the period between wakes. This is mostly likely the strongest contributor to the earlier reattachment mentioned above.

More discussion of the increased FSTI case can be found in Kaszeta et al. (2005). The effects of temporal acceleration are further discussed in Jiang and Simon (2005).

6.4 Considerations for Further Study

Approximate surface shear stress maps computed from near-wall flow velocities were presented in this study. Previous measurements without wakes (Qiu and Simon, 1997; Simon et al., 2000) showed that separation and reattachment points taken from such shear stress distribution maps which were computed from near-wall flow velocities differed, somewhat, from the more reliable separation and reattachment measurements taken directly from surface shear direction measurements. The problem stems from the difficulty in deducing wall shear stress from near-wall velocity data in thin and rapidly-changing boundary layers. The

use of hot-wire anemometry to measure velocities means that for high-TI and reversing flow, the measured velocities (and hence the calculated shear stresses), have a high uncertainties. Furthermore, the relatively large size of the hot-wire probe with respect to the boundary layer thickness makes it difficult to determine the exact location of the wall. Thus, locations of separation and reattachment obtained from these approximate surface shear stress maps determined from in-flow measurements should be replaced by values measured directly at the wall.

References

Dietz, A. J., 1999. "Local Boundary-Layer Receptivity to a Convected Free-Stream Disturbance." *Journal of Fluid Mechanics*, vol. 378, pp. 291–317.

Dorney, D. J., Flitan, H. C., Ashpis, D. E., and Solomon, W. J., 2000. "Effects of Blade Count on Boundary Layer Development in a Low-Pressure Turbine." AIAA Paper 2000-0742.

Falco, R. E. and Gendrich, C. P., 1990. "The Turbulence Burst Detection Algorithm of Z. Zarić." In S. J. Kline and N. H. Afgan, editors, *Near-Wall Turbulence 1988 Z. Zarić Memorial Conference*, pp. 911–931. Hemisphere.

Halstead, D. E., Wisler, D. C., Okiishi, T. H., Walker, G. J., Hodson, H. P., and Shin, H.-W., 1997. "Boundary Layer Development in Axial Compressors and Turbines: Part 3 of 4: Low Pressure Turbines." *ASME Journal of Turbomachinery*, vol. 119, pp. 225–237. Also ASME Paper 95-GT-463.

Heitland, G., 2000. "Low Pressure Turbine Reynolds Number Effects: Small Engine Perspective." Presented at Minnowbrook III, 2000 Workshop on Boundary Layer Transition and Unsteady Aspects of Turbomachinery Flows, Blue Mountain Lake, New York.

Hinze, J. O., 1975. *Turbulence*. McGraw-Hill, New York, 2nd edn.

Howell, R. J., Hodson, H. P., Schulte, V., Schiffer, H. P., Haselbach, F., and Harvey, N. W., 2001. "Boundary Layer Development in the BR710 and BR715 LP Turbines -The Implementation of High Lift and Ultra High Lift Concepts." ASME Paper 2001-GT-0441.

Jiang, N. and Simon, T. W., 2003a. "Modeling Laminar-to-Turbulent Transition in a Low-Pressure Turbine Flow which is Unsteady due to Passing Wakes: Part I, transition onset." ASME Paper GT2003-38787, 2003 Int'l. Gas Turbine Conference, Atlanta, GA.

Jiang, N. and Simon, T. W., 2003b. "Modeling Laminar-to-Turbulent Transition in a Low-Pressure Turbine Flow which is Unsteady due to Passing Wakes: Part II Transition Path." ASME Paper GT2003-38963, 2003 Int'l. Gas Turbine Conference, Atlanta, GA.

Jiang, N. and Simon, T. W., 2003c. "The Influence of Unsteady Acceleration and Turbulence Intensity on Transition in low-Pressure Turbines." AIAA-2003-3630, AIAA Thermophysics Conference, Orlando, FL.

Jiang, N. and Simon, T. W., 2004. "Evaluation of Algebraic Transition Models for Application to Unsteady Flows in Low-Pressure Turbines." ASME Paper GT2004-54223, 2004 Int'l. Gas Turbine Conference, Vienna Austria.

Jiang, N. and Simon, T. W., 2005. "Transition in Low-Pressure Turbines: Effects of Unsteady Acceleration and Turbulence Intensity." *Journal of Thermophysics and Heat Transfer*, vol. 19, no. 2, pp. 148–155.

Kaszeta, R. W., 2000. *Experimental Investigation of Transition to Turbulence as Affected by Passing Wakes*. Ph.D. Thesis, University of Minnesota, Mechanical Engineering Department, Minneapolis, MN.

Kaszeta, R. W. and Simon, T. W., 2002. "Experimental Investigation of Transition to Turbulence as Affected by Passing Wakes." NASA Contractor Report NASA/CR-2002-212104.

Kaszeta, R. W., Simon, T. W., and Ashpis, D. E., 2001. "Experimental Investigation of Transition to Turbulence as Affected by Passing Wakes." Presented at the 2001 International Gas Turbine and Aeroengine Congress and Exposition, New Orleans, Louisiana. ASME Paper 2001-GT-195.

Kaszeta, R. W., Simon, T. W., Jiang, N., and Ottaviani, F., 2005. "The Influence of Wake Passing Frequency and Elevated Turbulence Intensity on Transition." *Journal of Thermophysics and Heat Transfer*, vol. 19, no. 2, pp. 137–147.

Kaszeta, R. W., Simon, T. W., Ottaviani, F., and Jiang, N., 2003. "The Influence of Wake Passing Frequency and Elevated Free Stream Turbulence Intensity on Transition in Low-Pressure Turbines." Presented at the 36th AIAA Thermophysics Conference, Orlando, Florida, June, 2003.

Mayle, R. E., 1991. "The Role of Laminar-Turbulent Transition in Gas Turbine Engines." *ASME Journal of Turbomachinery*, vol. 113, pp. 509–537. The 1991 IGTI Scholar Lecture, also presented as ASME Paper 91-GT-261.

Qiu, S., 1996. *An Experimental Study of Laminar to Turbulent Flow Transition with Temporal And Spatial Acceleration Effects*. Ph.D. Thesis, University of Minnesota, Department of Mechanical Engineering.

Qiu, S. and Simon, T. W., 1997. "An Experimental Investigation of Transition as Applied to Low Pressure Turbine Suction Surface Flows." Presented at the 1997 International Gas Turbine and Aeroengine Congress and Exposition, Orlando, Florida. ASME Paper 97-GT-455.

Schobeiri, M. T., Read, K., and Lewalle, J., 1995. "Effect of Unsteady Wake Passing Frequency on Boundary Layer Transition, Experimental Investigation and Wavelet Analysis." Presented at the 1995 International Gas Turbine and Aeroengine Congress and Exposition, Houston, Texas. ASME Paper 95-GT-437.

Simon, T. W. and Kaszeta, R. W., 2000. "Transition to Turbulence Under Low-Pressure Turbine Conditions." Proceedings of the International Symposium on Heat Transfer in Gas Turbine Systems, Cesme, Turkey, 13-18 August 2000, *Annals of the New York Academy of Sciences*.

Simon, T. W., Qiu, S., and Yuan, K., 2000. "Measurements in a Transitional Boundary Layer Under Low-Pressure Turbine Airfoil Conditions." NASA Contractor Report NASA/CR-2000-209957.

Suzen, Y. B. and Huang, P. G., 2000. "Modeling of Flow Transition Using an Intermittency Transport Equation." *Journal of Fluids Engineering*, vol. 123, no. 2.

Walker, G. J. and Solomon, W. J., 1992. "Turbulent Intermittency Measurement on an Axial Compressor Blade." In M. R. Davis and G. J. Walker, editors, *Eleventh Australasian Fluid Mechanics Conference*, pp. 1277–1280. Hobart, Australia.

Wills, J. A. B., 1962. "The Correction of Hot-Wire Readings for Proximity to a Solid Boundary." *Journal of Fluid Mechanics*, vol. 12, pp. 388–396.

Wolff, S., Brunner, S., and Fottner, L., 2000. "The Use Of Hot-Wire Anemometry to Investigate Unsteady Wake-Induced Boundary Layer Development on a High-Lift LP Turbine Cascade." Presented at the 2000 International Gas Turbine and Aeroengine Congress and Exposition, Munich, Germany.

Wu, X. and Durbin, P. A., 2000a. "Evidence of Longitudinal Vortices Evolved From Distorted Wakes in a Turbine Passage." Submitted to the *Journal of Fluid Mechanics*.

Wu, X. and Durbin, P. A., 2000b. "Numerical Simulation of Heat Transfer in a Transitional Boundary Layer with Passing Wakes." *ASME Journal of Heat Transfer*, vol. 122, pp. 248–257.

Yuan, K., 1999. *Simulation of Wakes: The Development of a Linear Cascade Wake Generator*. Master's Thesis, University of Minnesota. Department of Mechanical Engineering.

Appendix A

Facility Geometry

All of the important dimensions of the wake generator facility are shown in Figures A.1 and A.2. The dimensions themselves are listed in Table A.1.

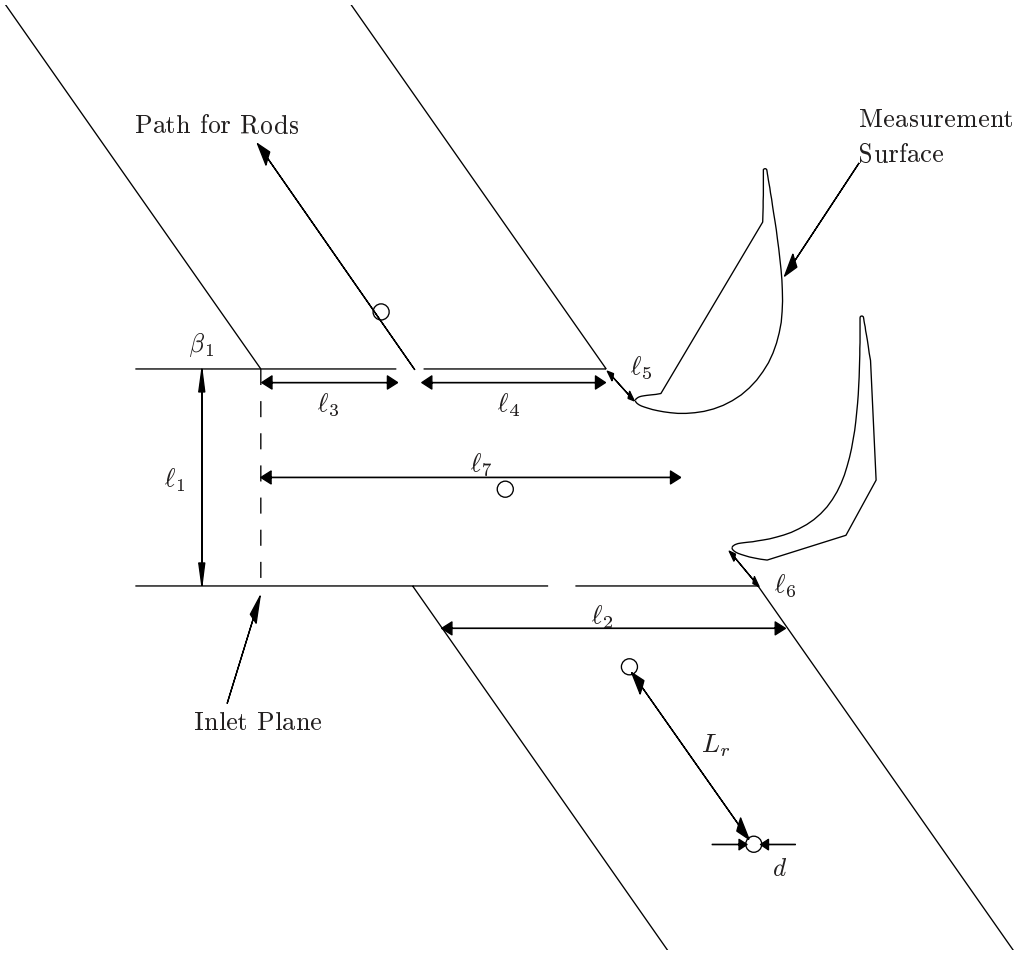

Figure A.1: Wake generator dimensions and geometry

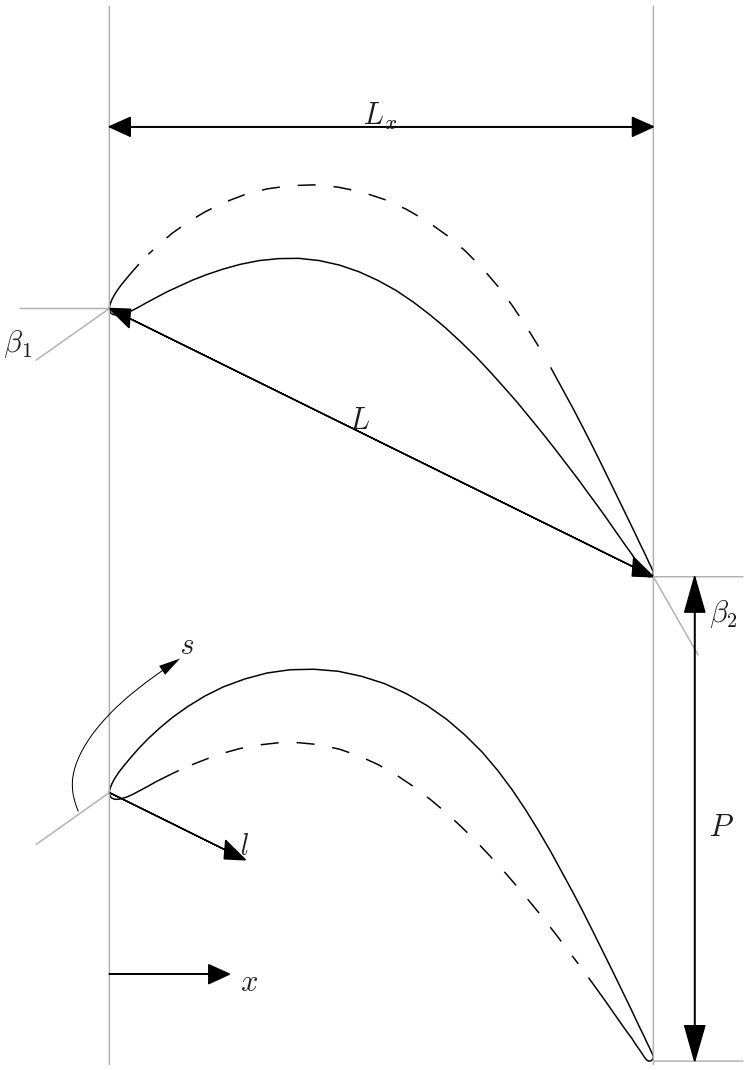

Figure A.2: Turbine passage dimensions and geometry

Table A.1: Wake generator and turbine passage dimensions

Dimension:	**Value:**
Chord length, L:	114.3 mm
Axial chord length, L_x:	103.57 mm
Suction surface length, L_{ss}:	152.76 mm
Axial chord to chord ratio, L_x/L:	0.906
Pitch to chord ratio, P/L:	0.8
Aspect ratio (span/chord), L_z/L:	6.0
Blade inlet angle, β_1:	35°
Blade outlet angle, β_2:	-60°
Rod diameter, d:	3.175 mm
Rod spacing, L_r, (Original Case):	91.44 mm
Rod spacing, L_r, (Increased Spacing Case) :	182.88 mm
Inlet channel width, ℓ_1:	114.3 mm
Wake generator streamwise length, ℓ_2:	142.24 mm
Wake generator upstream flap length, ℓ_3:	50.8 mm
Wake generator downstream flap length, ℓ_4:	79.375 mm
Suction surface bleed slot width, ℓ_5:	24.047 mm
Pressure surface bleed slot width, ℓ_6:	24.047 mm
Distance from the inlet plane to the point mid-span between the leading edges, ℓ_7:	182.25 mm

Appendix B

Source Code Listings

This appendix includes a number of programs, written in both C and MATLAB, used in collecting and processing the data. A description of each program is given in table B.1.

Table B.1: Included programs

Program	Language	Description
`automate2.c`	C	Data collection program for the single-wire anemometer and wake generator.
`p09.m`	MATLAB	Sample data reduction script which decomposes the velocity and photogate data into individual wakes and calculates ensemble-average velocity and turbulence intensity (base case).
`p09inter.m`	MATLAB	Sample data reduction script which calculates intermittency (base case).
`sp09.m`	MATLAB	Sample data reduction script which decomposes the velocity and photogate data into individual wakes and calculates ensemble-average velocity and turbulence intensity (increased wake spacing case).
`sp09inter.m`	MATLAB	Sample data reduction script which calculates intermittency (increaed wake spacing case).
`hp09.m`	MATLAB	Sample data reduction script which decomposes the velocity and photogate data into individual wakes and calculates ensemble-average velocity and turbulence intensity (high-$FSTI$ case).
`hp09inter.m`	MATLAB	Sample data reduction script which calculates intermittency (High-$FSTI$ case).
`lengthscale.m`	MATLAB	Sample script used to calculate power spectral densities and integral length scales.

B.1 automate2.c

```
#include<stdio.h>
#include<unistd.h>
#include<stdlib.h>
#include<ugpib.h>
#include<math.h>

/* Number of data points collected by the iotech */
#define DATAPOINTS 60000
/* Threshold voltage for determining photogate blockage */
#define THRESHOLD 2.5
/* Ideal length of each wake */
#define IDEALLENGTH 4520
/* Number of data points to shift waveform by */
#define LEADPOINTS 4125
/* Number of trials */
#define TRIALS 35
/* Gain on hotwire bridge */
#define GAIN 4.0

/* Platinum RTD Coefficients: */

#define R0 500.88
#define T0 0.0
#define alpha 0.003859

void main(int argc, char * argv[]) {
  int i,j;                        /* Counter Variables */

  int iotech1;                    /* Hotwire Iotech */
  int iotech2;                    /* Photogate Iotech */
  int dvm;                        /* Fluke DVM with Platinum RTD */
  int powersupply;                /* HP Power Supply */

  int opt;                        /* Command line option handling */

  FILE * velocitydatafile;        /* Velocity Data (whole record)*/
  FILE * photogatedatafile;       /* Photogate Data */

  FILE * calfile;                 /* Calibration data */
  char * calfilename;             /* The name of the calibration file */

  char mkdirhier[80];
  char banner[80];

  char trialdatafilename[120];    /* The name of the trial data file */
  char photogatedatafilename[120]; /* The name of the photogate data file */

  int pressurelocation;           /* Which pressure location are we at? */
  int ylocation;                  /* Which y-location are we at? */

  char resiststring[200];         /* String read from Fluke */
  double resist;                  /* Measured Resistance */

  double T_dry;                   /* dry temperature */
  double T_ref;                   /* Reference temperatures, stored in calfile */
  double T_sensor=250;            /* Sensor runs at 250 */
  double vcorr,volt;              /* Temperature correction */
  short velocitydata[DATAPOINTS]; /* Velocity Data in 16-bit integer format */
  short photogatedata[DATAPOINTS]; /* Photogate Data in 16-bit integer format */
  short flagdata[4];              /* 4 data points, one for each flag
                                     and two extras*/
  double m,b;                     /* Hotwire Calibration values */
  static double voltage[DATAPOINTS];
                                  /* The velocity voltage data, one channel */
```

```
static double u[DATAPOINTS];
                                /* The velocity data, one channel */
static double photogate[DATAPOINTS];
                                /* The photogate voltage data, one channel */

double startflagvoltage;        /* Photogate voltages */
double endflagvoltage;
double encoderflagvoltage;
int outcount;

/* Parse command line options */
calfilename="calfile.single";

/* Set Reasonable defaults */

pressurelocation=0;
ylocation=0;

while(1) {
  opt=getopt(argc,argv,"y:p:");
  if (opt == -1) break;
  switch (opt) {
  case 'y':                     /* Override default y location */
    ylocation=atoi(optarg);
    break;
  case 'p':                     /* Override default pressure tap location */
    pressurelocation=atoi(optarg);
    break;
  case ':':
    printf("missing argument\n");
    break;
  case '?':
    printf("Unknown option\n");
  }
}

/* Get calibration data */
calfile=fopen(calfilename,"r"); /* Open the calibration file for reading */
fscanf(calfile,"%lf",&T_ref); /* Get the reference temperature */
fscanf(calfile,"%lf %lf\n",&m,&b); /* get calib constants */

/* Find GPIB devices */
iotech1=ibfind("dev13");
iotech2=ibfind("dev14");
powersupply=ibfind("dev4");
dvm=ibfind("dev8");

/* Status report */
printf("Collecting Data at Pressure Location %d and Y location %d\n",
       pressurelocation, ylocation);

/* Find local temperature */
ibclr(dvm);                     /* Clear Fluke */
ibwrt(dvm,"*F4R0S0?",8);        /* Set to 4-wire mode */
sleep(4);                       /* Let it settle out */
ibrd(dvm,resiststring,40);      /* Read the resistance */
resist=atof(resiststring);
T_dry=(resist/R0-1)/alpha+T0;
printf("Temperature is %f degrees C\n",T_dry);

/* Set up velocity iotech.  This we only need to do once, since it never
   changes through the run */
ibclr(iotech1);                 /* Clear iotech */
ibtmo(iotech1,T30s);            /* Set a timeout */
ibwrt(iotech1,"M4X",3);         /* Clear Error Mask */
```

```
ibwrt(iotech1,"C1X", 3);        /* Use channel 1 only */
ibwrt(iotech1,"R2X", 3);        /* +/- 5 volts Range */
ibwrt(iotech1,"G11X", 4); /* set up binary little-endian transfer */
ibwrt(iotech1,"I0X", 3);        /* Set timing interval */
printf("Velocity Iotech set up\n"); fflush(stdout);

/* Set up photogate iotech.  This we only need to be careful with,
   since at some points in the code we read single points from
   single channels, other times we read a full sequence. */
ibclr(iotech2);                 /* Clear iotech */
ibtmo(iotech2,T30s);            /* Set a timeout */
ibwrt(iotech2,"M4X", 3);        /* Clear Error Mask */
ibwrt(iotech2,"G11X", 4);       /* set up binary little-endian transfer */
ibwrt(iotech2,"I0X", 3);        /* Set timing interval */
printf("Photogate Iotech set up\n"); fflush(stdout);

/* Turn off power supply */
printf("Turning off power..."); fflush(stdout);
ibwrt(powersupply,"2000",4);
printf("done (%d bytes written)\n",ibcnt); fflush(stdout);

/* Make storage directory */
sprintf(mkdirhier,"/bin/mkdir -p p%02d/velocity/y%02d\n",
        pressurelocation,ylocation);
printf("%s",mkdirhier);    fflush(stdout);
system(mkdirhier);
sprintf(mkdirhier,"/bin/mkdir -p p%02d/photogate/y%02d\n",
        pressurelocation,ylocation);
printf("%s",mkdirhier);    fflush(stdout);
system(mkdirhier);

/* Do each trial */
for(i=0;i<TRIALS;i++) {         /* Each trial */

  /* First determine that the return flag is triggered */
  ibwrt(iotech2,"C1,2,3,4X", 9); /* Use channels 1, 2, 3, and 4  only */
  ibwrt(iotech2,"R#1,2X", 6); /* +/- 5 volts Range */
  ibwrt(iotech2,"R#2,2X", 6); /* +/- 5 volts Range */
  ibwrt(iotech2,"R#3,2X", 6); /* +/- 5 volts Range */
  ibwrt(iotech2,"R#4,2X", 6); /* +/- 5 volts Range */
  ibwrt(iotech2,"N1X", 3);      /* Single data point */
  ibwrt(iotech2,"T6X", 3);      /* One-shot Trigger on talk */
  sleep(1);
  printf("Reading flags..."); fflush(stdout);
  ibrd(iotech2, (char *)flagdata, 8);
  printf("Done (%d bytes read)\n",ibcnt); fflush(stdout);

  encoderflagvoltage=(10.0/60000.0)*flagdata[0];
  startflagvoltage=(10.0/60000.0)*flagdata[2];
  endflagvoltage=(10.0/60000.0)*flagdata[1];

  printf("Flag Voltages:\nEncoder: %f\nStart: %f\nEnd: %f\n",
         encoderflagvoltage,startflagvoltage,endflagvoltage);

  /* Check flag status.  Start flag should be set, and
     end flag and encoder shouldn't be.  If error, exit. */
  if (!(( startflagvoltage<THRESHOLD)
       &&(endflagvoltage>THRESHOLD)
       &&(encoderflagvoltage>THRESHOLD))) {
    printf("FATAL PHOTOGATE ERROR.  Exiting...\007\n");
    fflush(stdout);
    exit(1);
  }

  /* Prepare both iotechs for work */
```

```
  ibwrt(iotech1,"N0X",3);      /* Put iotech in FIFO mode */
  ibwrt(iotech1,"T3X",3);      /* Trigger on falling external trigger */

  /* For second iotech, must reset channels, too */
  ibwrt(iotech2,"C1X",3);      /* Channel 1 only */
  ibwrt(iotech2,"R#1,2X", 6); /* +/- 5 volts Range */
  ibwrt(iotech2,"N0X",3);      /* Put iotech in FIFO mode */
  ibwrt(iotech2,"T3X",3);      /* Trigger on falling external trigger */

  /* Sleep */
  sleep(1);

  /* Turn on power */
  printf("Turning on power..."); fflush(stdout);
  ibwrt(powersupply,"2999",4);
  printf("done (%d bytes written)\n",ibcnt); fflush(stdout);

  /* Read both iotechs */
  printf("Reading %d bytes from velocity iotech ...",2*DATAPOINTS);
  fflush(stdout);
  ibrd(iotech1, (char *)velocitydata, DATAPOINTS*2);
  printf("done. (%d bytes read)\n",ibcnt); fflush(stdout);
  printf("Reading %d bytes from photogate iotech ...",2*DATAPOINTS);
  fflush(stdout);
  ibrd(iotech2, (char *)photogatedata, DATAPOINTS*2);
  printf("done. (%d bytes read)\n",ibcnt); fflush(stdout);

/* Recycle the wake generator */

/* First determine that the end flag is triggered */
  ibwrt(iotech2,"C1,2,3,4X", 9); /* Use channels 1, 2, 3, and 4  only */
  ibwrt(iotech2,"R#1,2X", 6); /* +/- 5 volts Range */
  ibwrt(iotech2,"R#2,2X", 6); /* +/- 5 volts Range */
  ibwrt(iotech2,"R#3,2X", 6); /* +/- 5 volts Range */
  ibwrt(iotech2,"R#4,2X", 6); /* +/- 5 volts Range */
  ibwrt(iotech2,"N1X", 3);     /* Single data point */
  ibwrt(iotech2,"T6X", 3);     /* One-shot Trigger on talk */
  sleep(1);
  printf("Reading flags ..."); fflush(stdout);
  ibrd(iotech2, (char *)flagdata, 8);
  printf("Done (%d bytes read)\n",ibcnt); fflush(stdout);

  encoderflagvoltage=(10.0/60000.0)*flagdata[0];
  startflagvoltage=(10.0/60000.0)*flagdata[2];
  endflagvoltage=(10.0/60000.0)*flagdata[1];

  printf("Flag Voltages:\nEncoder: %f\nStart: %f\nEnd: %f\n",
         encoderflagvoltage,startflagvoltage,endflagvoltage);

  /* Check flag status.  Start flag should be set, and
     end flag and encoder shouldn't be.  If error, exit. */
  if (!((startflagvoltage>THRESHOLD)
     &&(endflagvoltage<THRESHOLD)
     )) {
    printf("FATAL PHOTOGATE ERROR.  Exiting...\007\n");
    fflush(stdout);
    exit(1);
  }

  /* Prepare both iotechs for work */
  ibwrt(iotech1,"N0X",3);      /* Put iotech in FIFO mode */
  ibwrt(iotech1,"T3X",3);      /* Trigger on falling external trigger */

  /* For second iotech, must reset channels, too */
  ibwrt(iotech2,"C1X",3);      /* Channel 1 only */
```

```
    ibwrt(iotech2,"R#1,2X", 6); /* +/- 5 volts Range */
    ibwrt(iotech2,"N0X",3);     /* Put iotech in FIFO mode */
    ibwrt(iotech2,"T3X",3);     /* Trigger on falling external trigger */

    /* Sleep */
    sleep(1);

    /* Turn off power */
    printf("Turning off power...");  fflush(stdout);
    ibwrt(powersupply,"2000",4);
    printf("done (%d bytes written)\n",ibcnt);  fflush(stdout);

    /* Convert Binary Readings to voltages */
    for(j=0;j<DATAPOINTS;j++)   /* For each reading */
      {
        voltage[j]=((10.0/GAIN)/60000.0)*velocitydata[j];
        photogate[j]=(10.0/60000.0)*photogatedata[j];
      }

    /* Convert Voltage data to the effective velocity seen by each wire */
    vcorr=(T_sensor-T_ref)/(T_sensor-T_dry); /* 1st order
                                                temperature correction */
    for(j=0;j<DATAPOINTS;j++)   /* each datapoint */
      {
        volt=voltage[j]*voltage[j]*vcorr;
        u[j]=pow((b+m*volt),2.29885);
      }

    /* Form the filenames for the velocity and photogate data */
    sprintf(trialdatafilename,"p%02d/velocity/y%02d/p%02dy%02dt%03dvelocity",
            pressurelocation,ylocation,pressurelocation,ylocation,i);
    sprintf(photogatedatafilename,
            "p%02d/photogate/y%02d/p%02dy%02dt%03dphotogate",
            pressurelocation,ylocation,pressurelocation,ylocation,i);

    /* Write velocity data to file */
    printf("Writing u data to file %s...",trialdatafilename);  fflush(stdout);
    velocitydatafile=fopen(trialdatafilename,"w");
    outcount=fwrite(u,8,DATAPOINTS,velocitydatafile);
    fflush(velocitydatafile);fclose(velocitydatafile);
    printf("(%d records written)\n",outcount);  fflush(stdout);

    /* Write photogate data to file */
    printf("Writing photogate data to file %s...",
           photogatedatafilename);  fflush(stdout);
    photogatedatafile=fopen(photogatedatafilename,"w");
    fwrite(photogate,8,DATAPOINTS,photogatedatafile);
    fflush(photogatedatafile);fclose(photogatedatafile);
    printf("(%d records written)\n",outcount);  fflush(stdout);

    printf("Total number of trials: %d\n",i+1);
    sprintf(banner,"/usr/bin/figlet -c -f banner3 %d\n",i+1);
    system(banner);


    usleep(1750000);

  }
}
```

B.2 p09.m

```
clear;
clf;

leadpoints=3550;

%Sampling frequency
frequency=100000;
ideallength=4500;
trials=35;
rods=6;
pressurelocation=9;
phasesegments=90;
ystations=30;
ylocation=1;
y=[0.01 0.02 0.03 0.05 0.07 0.09 0.12 0.15 0.18 0.22 0.26 0.30 0.35 ...
   0.40 0.45 0.51 0.57 0.63 0.70 0.77 0.84 0.92 1.00 1.08 1.17 1.26 ...
   1.35 1.45 1.55 1.65];
wakes=rods*trials;
datapoints=60000;
pulsetime=zeros(1,50);
wakedata=zeros(wakes,ideallength);
uphase=zeros(phasesegments,ystations);
urmsphase=zeros(phasesegments,ystations);
tiphase=zeros(phasesegments,ystations);

% For each trial, we load in the photogate data and the velocity
% data. We find each state change in the photogate data, and use that
% to find the center of each wake. We then extract the wakes from
% each velocity data file

% For each y location
for ylocation=1:ystations,
  ylocation
  % For each trial
  for i=1:trials,
    velocityfilename=sprintf('p%02d/velocity/y%02d/p%02dy%02dt%03dvelocity',...
                             pressurelocation,ylocation,pressurelocation,...
                             ylocation,i-1);
    velocityfid=fopen(velocityfilename);
    velocitydata=fread(velocityfid,inf,'double');
    fclose(velocityfid);
    photogatefilename=sprintf('p%02d/photogate/y%02d/p%02dy%02dt%03dphotogate',...
                              pressurelocation,ylocation,...
                              pressurelocation,ylocation,i-1);
    photogatefid=fopen(photogatefilename);
    photogatedata=fread(photogatefid,inf,'double');
    fclose(photogatefid);
    % Find state changes
    pulses=0;
    lastpoint=5.0;
    for j=1:datapoints,
      if ((lastpoint>2.5)&(photogatedata(j)<2.5))
        pulsetime(pulses+1)=j;
        pulses=pulses+1;
      end
      if ((lastpoint<2.5)&(photogatedata(j)>2.5))
        pulsetime(pulses+1)=j;
        pulses=pulses+1;
      end
      lastpoint=photogatedata(j);
      if (pulses==28)
        break;
      end
    end
```

```
    % For each of the six wakes, take the ideallength points
    % around the center of the wake
    for j=1:6,
      thiswake=(i-1)*rods+j;
      centerpulse=pulsetime(7+4*(j-1));
      centerwake=centerpulse+leadpoints;
      wake=velocitydata((centerwake-ideallength/2):...
                        (centerwake+ideallength/2-1));
      wakedata(thiswake,:)=wake';
    end
  end
  % For each phase segment, find the mean velocity and the
      % rms fluctuation
  segmentlength=ideallength/phasesegments;
  for i=1:phasesegments,
    startsegment=(i-1)*(segmentlength*1)+1;
    endsegment=startsegment+segmentlength-1;
    segment=reshape(wakedata(:,[startsegment:endsegment]),1,...
                    segmentlength*wakes);
    uphase(i,ylocation)=mean(segment);
    urmsphase(i,ylocation)=std(segment);
  end
plot(uphase(:,[1:ylocation]));
pause(0.05);
end
tiphase=urmsphase./uphase;
phase=360*([1:phasesegments]/phasesegments);

savefilename=sprintf('p%02d.mat',pressurelocation);
save(savefilename,'uphase','urmsphase','tiphase','y',...
     'phase','pressurelocation');
```

B.3 p09inter.m

```
clear;
clf;

% Second pass---this one uses the profile results from the first pass
% calculate intermittency. (To calculate the windowing time and
% threshold values, we need to have a fairly decent estimate of the
% freestream velocity)

leadpoints=3550;

%Sampling frequency
frequency=100000;
ideallength=4500;
trials=35;
rods=6;
pressurelocation=9;
phasesegments=90;
ystations=30;
ylocation=1;
y=[0.01 0.02 0.03 0.05 0.07 0.09 0.12 0.15 0.18 0.22 0.26 0.30 0.35 0.40 ...
   0.45 0.51 0.57 0.63 0.70 0.77 0.84 0.92 1.00 1.08 1.17 1.26 1.35 1.45 ...
   1.55 1.65];
wakes=rods*trials;
datapoints=60000;
pulsetime=zeros(1,50);
uphase=zeros(phasesegments,ystations);
urmsphase=zeros(phasesegments,ystations);
tiphase=zeros(phasesegments,ystations);
rod1wakes=linspace(1, 205, 35);
rod2wakes=linspace(2, 206, 35);
rod3wakes=linspace(3, 207, 35);
```

```
rod4wakes=linspace(4, 208, 35);
rod5wakes=linspace(5, 209, 35);
rod6wakes=linspace(6, 210, 35);
uphase1=zeros(phasesegments,ystations);
urmsphase1=zeros(phasesegments,ystations);
tiphase1=zeros(phasesegments,ystations);
interphase1=zeros(phasesegments,ystations);
uphase2=zeros(phasesegments,ystations);
urmsphase2=zeros(phasesegments,ystations);
tiphase2=zeros(phasesegments,ystations);
interphase2=zeros(phasesegments,ystations);
uphase3=zeros(phasesegments,ystations);
urmsphase3=zeros(phasesegments,ystations);
tiphase3=zeros(phasesegments,ystations);
interphase3=zeros(phasesegments,ystations);
uphase4=zeros(phasesegments,ystations);
urmsphase4=zeros(phasesegments,ystations);
tiphase4=zeros(phasesegments,ystations);
interphase4=zeros(phasesegments,ystations);
uphase5=zeros(phasesegments,ystations);
urmsphase5=zeros(phasesegments,ystations);
tiphase5=zeros(phasesegments,ystations);
interphase5=zeros(phasesegments,ystations);
uphase6=zeros(phasesegments,ystations);
urmsphase6=zeros(phasesegments,ystations);
tiphase6=zeros(phasesegments,ystations);
interphase6=zeros(phasesegments,ystations);

interdata=zeros(wakes,ideallength);
interphase=zeros(phasesegments,ystations);
t=[0:(datapoints-1)]'/frequency;
deltat=1/frequency;
threshfactor=2.75;
ds=4e-6;
nu=15.75;

firststagefilename=sprintf('p%02d.mat',pressurelocation);

load(firststagefilename,'uphase');

% For each trial, we load in the photogate data and the velocity
% data.  We find each state change in the photogate data, and use that
% to find the center of each wake.  We then calculate the
% intermittency for each velocity trace, and use the photogate data to
% break this into wakes and ensemble average it like we did in the
% first pass

% For each y location
for ylocation=1:ystations,
  ylocation
        % Calculate correction factor
  ycur=y(ylocation)
  yscale=2*y(ylocation)*1e-2/ds
  if yscale<50,
          kw=0.9-7.2e-2*yscale+2.89e-3*yscale.^2-6.15E-5*yscale.^3 ...
              +6.51e-7*yscale.^4
  else
          kw=0.54-2.42e-2*yscale+5.01e-4*yscale.^2-5.36E-6*yscale.^3 ...
              +2.85e-8*yscale.^4
  end
  % For each trial
  for i=1:trials,
    i
    velocityfilename=sprintf( ...
      'p%02d/velocity/y%02d/p%02dy%02dt%03dvelocity',...
```

```
  pressurelocation,ylocation,pressurelocation,ylocation,i-1);
velocityfid=fopen(velocityfilename);
velocitydata=fread(velocityfid,inf,'double');
fclose(velocityfid);
photogatefilename=sprintf(...
  'p%02d/photogate/y%02d/p%02dy%02dt%03dphotogate',...
  pressurelocation,ylocation,pressurelocation,ylocation,i-1);
photogatefid=fopen(photogatefilename);
photogatedata=fread(photogatefid,inf,'double');
fclose(photogatefid);
% calcule u and du/dt
u=velocitydata;
dudt=[diff(u)./diff(t); 0];
% Calculate the criterion function and the threshold
criterion=u.*dudt;
threshold=threshfactor*std(criterion([3550:35050]));
criterion=abs(criterion);
threshline=threshold*ones(datapoints,1);
% Calculate the windowing time from the BL scale
delta=0.0165; % approximated BL thickness
Ufs=mean(uphase(:,30)); % approximated mean freestream velocity
tbl=delta/Ufs;
tw=tbl*2.5; % as suggested by Blair(1983)
% Initialize gamma, td, and jend
gamma=zeros(datapoints,1);
td=0;
jend=1;
j=1;
eventcontinues=1;
while j<(datapoints+1),
  % March through criterion, comparing each point to the threshold
  if (criterion(j)>threshold)
    td = (j-jend)*deltat;
  if (td>tw)
    % assume a new event is starting
    jstart=j;
  else
    % assume this is a continuation of a previous event
    jstart=jend;
  end
  while (eventcontinues>0),
          % Calculate average value of criterion since jstart
    criterionave=mean(criterion(jstart:j));
    if (criterionave>threshold) | (criterion(j)>threshold)
            eventcontinues=1;
    else
            jend=j;
      eventcontinues=0;
    end
          j=j+1;
  end
  td=(jstart-jend)*deltat;
  if (td<tw)
    gamma([jstart:j])=ones(j-jstart+1,1);
    jend=j;
  else
    jend=jstart;
      end
  end
        j=j+1;
end
      gamma2=ceil((criterion-threshold)/max(criterion));
% Find state changes
pulses=0;
lastpoint=5.0;
```

```
  for j=1:datapoints,
    if ((lastpoint>2.5)&(photogatedata(j)<2.5))
      pulsetime(pulses+1)=j;
      pulses=pulses+1;
    end
    if ((lastpoint<2.5)&(photogatedata(j)>2.5))
      pulsetime(pulses+1)=j;
      pulses=pulses+1;
    end
    lastpoint=photogatedata(j);
    if (pulses==28)
      break;
    end
  end
  % For each of the six wakes, take the ideallength points
  % of intermittency around the center of the wake
  for j=1:6,
    thiswake=(i-1)*rods+j;
    centerpulse=pulsetime(7+4*(j-1));
    centerwake=centerpulse+leadpoints;
    wake=velocitydata((centerwake-ideallength/2):...
                      (centerwake+ideallength/2-1));
    wakedata(thiswake,:)=wake';
    interwake=gamma((centerwake-ideallength/2):...
                    (centerwake+ideallength/2-1));
    interdata(thiswake,:)=interwake';
  end
% For each wake, calculate the velocity correction if required
if y<0.04,
wakedataraw=wakedata;
for i=1:wakes
  for j=1:ideallength
    if interdata(i,j)<1
            wakedata(i,j)=(wakedataraw(i,j).^0.45-...
                           ((nu/ds)^.45)*kw).^(1/.45);
    else
            wakedata(i,j)=0.84*(wakedataraw(i,j).^0.45-...
              ((nu/ds)^.45)*kw).^(1/.45)+0.16*wakedataraw(i,j);
    end
  end
end
end
end
% For each phase segment, find the mean velocity and the
      % rms fluctuation
segmentlength=ideallength/phasesegments;
for i=1:phasesegments,
  startsegment=(i-1)*(segmentlength*1)+1;
  endsegment=startsegment+segmentlength-1;
  segment=reshape(interdata(:,[startsegment:endsegment]),...
                  1,segmentlength*wakes);
  segment1=reshape(interdata(rod1wakes,[startsegment:endsegment]),...
                   1,segmentlength*wakes/6);
  segment2=reshape(interdata(rod2wakes,[startsegment:endsegment]),...
                   1,segmentlength*wakes/6);
  segment3=reshape(interdata(rod3wakes,[startsegment:endsegment]),...
                   1,segmentlength*wakes/6);
  segment4=reshape(interdata(rod4wakes,[startsegment:endsegment]),...
                   1,segmentlength*wakes/6);
  segment5=reshape(interdata(rod5wakes,[startsegment:endsegment]),...
                   1,segmentlength*wakes/6);
  segment6=reshape(interdata(rod6wakes,[startsegment:endsegment]),...
                   1,segmentlength*wakes/6);
  interphase(i,ylocation)=mean(segment);
  interphase1(i,ylocation)=mean(segment1);
```

```
    interphase2(i,ylocation)=mean(segment2);
    interphase3(i,ylocation)=mean(segment3);
    interphase4(i,ylocation)=mean(segment4);
    interphase5(i,ylocation)=mean(segment5);
    interphase6(i,ylocation)=mean(segment6);
    segment=reshape(wakedata(:,[startsegment:endsegment]),...
                    1,segmentlength*wakes);
    segment1=reshape(wakedata(rod1wakes,[startsegment:endsegment]),...
                    1,segmentlength*wakes/6);
    segment2=reshape(wakedata(rod2wakes,[startsegment:endsegment]),...
                    1,segmentlength*wakes/6);
    segment3=reshape(wakedata(rod3wakes,[startsegment:endsegment]),...
                    1,segmentlength*wakes/6);
    segment4=reshape(wakedata(rod4wakes,[startsegment:endsegment]),...
                    1,segmentlength*wakes/6);
    segment5=reshape(wakedata(rod5wakes,[startsegment:endsegment]),...
                    1,segmentlength*wakes/6);
    segment6=reshape(wakedata(rod6wakes,[startsegment:endsegment]),...
                    1,segmentlength*wakes/6);
    uphase(i,ylocation)=mean(segment);
    urmsphase(i,ylocation)=std(segment);
    uphase1(i,ylocation)=mean(segment1);
    urmsphase1(i,ylocation)=std(segment1);
    uphase2(i,ylocation)=mean(segment2);
    urmsphase2(i,ylocation)=std(segment2);
    uphase3(i,ylocation)=mean(segment3);
    urmsphase3(i,ylocation)=std(segment3);
    uphase4(i,ylocation)=mean(segment4);
    urmsphase4(i,ylocation)=std(segment4);
    uphase5(i,ylocation)=mean(segment5);
    urmsphase5(i,ylocation)=std(segment5);
    uphase6(i,ylocation)=mean(segment6);
    urmsphase6(i,ylocation)=std(segment6);
  end
end
tiphase=urmsphase./uphase;
tiphase1=urmsphase1./uphase1;
tiphase2=urmsphase2./uphase2;
tiphase3=urmsphase3./uphase3;
tiphase4=urmsphase4./uphase4;
tiphase5=urmsphase5./uphase5;
tiphase6=urmsphase6./uphase6;
phase=360*([1:phasesegments]/phasesegments);
fullphase=[phase,360+phase,720+phase,1080+phase,1440+phase,1800+phase];
ubyrod=[uphase1;uphase2;uphase3;uphase4;uphase5;uphase6];
urmsbyrod=[urmsphase1;urmsphase2;urmsphase3;...
           urmsphase4;urmsphase5;urmsphase6];
tibyrod=[tiphase1;tiphase2;tiphase3;tiphase4;tiphase5;tiphase6];
interbyrod=[interphase1;interphase2;interphase3;...
            interphase4;interphase5;interphase6];

%recalculate uphase, urmsphase, tiphase, and interphase
uphase=(uphase1+uphase2+uphase3+uphase4)/4;
urmsphase=(urmsphase1+urmsphase2+urmsphase3+urmsphase4)/4;
interphase=(interphase1+interphase2+interphase3+interphase4)/4;
tiphase=urmsphase./uphase;


savefilename=sprintf('p%02dfourrod.mat',pressurelocation);
save(savefilename,'interphase','uphase','urmsphase',...
     'tiphase','y','phase','pressurelocation','fullphase',...
     'ubyrod','urmsbyrod','tibyrod','interbyrod');
```

B.4 sp09.m

```
clear;
clf;

leadpoints=1500;

%Sampling frequency
frequency=100000;
ideallength=9000;
trials=35;
rods=3;
pressurelocation=9;
phasesegments=90;
ystations=30;
ylocation=1;
y=[0.01 0.02 0.03 0.05 0.07 0.09 0.12 0.15 0.18 0.22 0.26 0.30 0.35...
   0.40 0.45 0.51 0.57 0.63 0.70 0.77 0.84 0.92 1.00 1.08 1.17 1.26...
   1.35 1.45 1.55 1.65];
wakes=rods*trials;
datapoints=60000;
pulsetime=zeros(1,50);
wakedata=zeros(wakes,ideallength);
uphase=zeros(phasesegments,ystations);
urmsphase=zeros(phasesegments,ystations);
tiphase=zeros(phasesegments,ystations);

% For each trial, we load in the photogate data and the velocity
% data. We find each state change in the photogate data, and use that
% to find the center of each wake. We then extract the wakes from
% each velocity data file

% For each y location
for ylocation=1:ystations,
  ylocation
  % For each trial
  for i=1:trials,
    velocityfilename=sprintf(...
      'sp%02d/velocity/y%02d/sp%02dy%02dt%03dvelocity',...
      pressurelocation,ylocation,pressurelocation,ylocation,i-1);
    velocityfid=fopen(velocityfilename);
    velocitydata=fread(velocityfid,inf,'double');
    fclose(velocityfid);
    photogatefilename=sprintf(...
      'sp%02d/photogate/y%02d/sp%02dy%02dt%03dphotogate',...
      pressurelocation,ylocation,pressurelocation,ylocation,i-1);
    photogatefid=fopen(photogatefilename);
    photogatedata=fread(photogatefid,inf,'double');
    fclose(photogatefid);
    % Find state changes
    pulses=0;
    lastpoint=5.0;
    for j=1:datapoints,
      if ((lastpoint>2.5)&(photogatedata(j)<2.5))
        pulsetime(pulses+1)=j;
        pulses=pulses+1;
      end
      if ((lastpoint<2.5)&(photogatedata(j)>2.5))
        pulsetime(pulses+1)=j;
        pulses=pulses+1;
      end
      lastpoint=photogatedata(j);
      if (pulses==28)
        break;
      end
    end
```

```
    % For each of the four wakes, take the ideallength points
    % around the center of the wake
    for j=1:3,
      thiswake=(i-1)*rods+j;
      centerpulse=pulsetime(0+4+1+8*(j-1));
      centerwake=centerpulse+leadpoints;
      wake=velocitydata((centerwake-ideallength/2):...
        (centerwake+ideallength/2-1));
      wakedata(thiswake,:)=wake';
    end
  end
  % For each phase segment, find the mean velocity and the
      % rms fluctuation
  segmentlength=ideallength/phasesegments;
  for i=1:phasesegments,
    startsegment=(i-1)*(segmentlength*1)+1;
    endsegment=startsegment+segmentlength-1;
    segment=reshape(wakedata(:,[startsegment:endsegment]),...
      1,segmentlength*wakes);
    uphase(i,ylocation)=mean(segment);
    urmsphase(i,ylocation)=std(segment);
  end
plot(uphase(:,[1:ylocation]));
pause(0.01);
end
tiphase=urmsphase./uphase;
phase=360*([1:phasesegments]/phasesegments);

savefilename=sprintf('sp%02d.mat',pressurelocation);
save(savefilename,'uphase','urmsphase','tiphase','y',...
  'phase','pressurelocation');
```

B.5 sp09inter.m

```
clear;
clf;

% Second pass---this one uses the profile results from the first pass
% calculate intermittency. (To calculate the windowing time and
% threshold values, we need to have a fairly decent estimate of the
% freestream velocity)

leadpoints=1500;

%Sampling frequency
frequency=100000;
ideallength=9000;
trials=35;
rods=3;
pressurelocation=9;
phasesegments=90;
ystations=30;
ylocation=1;
y=[0.01 0.02 0.03 0.05 0.07 0.09 0.12 0.15 0.18 0.22 0.26 0.30...
   0.35 0.40 0.45 0.51 0.57 0.63 0.70 0.77 0.84 0.92 1.00 1.08...
   1.17 1.26 1.35 1.45 1.55 1.65];
wakes=rods*trials;
datapoints=60000;
pulsetime=zeros(1,50);
uphase=zeros(phasesegments,ystations);
urmsphase=zeros(phasesegments,ystations);
tiphase=zeros(phasesegments,ystations);
rod1wakes=linspace(1, 103, 35);
rod2wakes=linspace(2, 104, 35);
rod3wakes=linspace(3, 105, 35);
```

```
uphase1=zeros(phasesegments,ystations);
urmsphase1=zeros(phasesegments,ystations);
tiphase1=zeros(phasesegments,ystations);
interphase1=zeros(phasesegments,ystations);
uphase2=zeros(phasesegments,ystations);
urmsphase2=zeros(phasesegments,ystations);
tiphase2=zeros(phasesegments,ystations);
interphase2=zeros(phasesegments,ystations);
uphase3=zeros(phasesegments,ystations);
urmsphase3=zeros(phasesegments,ystations);
tiphase3=zeros(phasesegments,ystations);
interphase3=zeros(phasesegments,ystations);

interdata=zeros(wakes,ideallength);
interphase=zeros(phasesegments,ystations);
t=[0:(datapoints-1)]'/frequency;
deltat=1/frequency;
threshfactor=2.75;
ds=4e-6;
nu=15.75;

firststagefilename=sprintf('sp%02d.mat',pressurelocation);

load(firststagefilename,'uphase');

% For each trial, we load in the photogate data and the velocity
% data.  We find each state change in the photogate data, and use that
% to find the center of each wake.  We then calculate the
% intermittency for each velocity trace, and use the photogate data to
% break this into wakes and ensemble average it like we did in the
% first pass

% For each y location
for ylocation=1:ystations,
  ylocation
        % Calculate correction factor
  ycur=y(ylocation)
  yscale=2*y(ylocation)*1e-2/ds
  if yscale<50,
          kw=0.9-7.2e-2*yscale+2.89e-3*yscale.^2-6.15E-5*yscale.^3 ...
              +6.51e-7*yscale.^4
  else
          kw=0.54-2.42e-2*yscale+5.01e-4*yscale.^2-5.36E-6*yscale.^3 ...
              +2.85e-8*yscale.^4
  end
  % For each trial
  for i=1:trials,
    i
    velocityfilename=sprintf(...
                  'sp%02d/velocity/y%02d/sp%02dy%02dt%03dvelocity',...
                  pressurelocation,ylocation,pressurelocation,ylocation,i-1);
    velocityfid=fopen(velocityfilename);
    velocitydata=fread(velocityfid,inf,'double');
    fclose(velocityfid);
    photogatefilename=sprintf(...
                  'sp%02d/photogate/y%02d/sp%02dy%02dt%03dphotogate',...
                  pressurelocation,ylocation,pressurelocation,ylocation,i-1);
    photogatefid=fopen(photogatefilename);
    photogatedata=fread(photogatefid,inf,'double');
    fclose(photogatefid);
    % calcule u and du/dt
    u=velocitydata;
    dudt=[diff(u)./diff(t); 0];
    % Calculate the criterion function and the threshold
    criterion=u.*dudt;
```

```
threshold=threshfactor*std(criterion([3550:35050]));
criterion=abs(criterion);
threshline=threshold*ones(datapoints,1);
% Calculate the windowing time from the BL scale
delta=0.0165; % approximated BL thickness
Ufs=mean(uphase(:,30)); % approximated mean freestream velocity
tbl=delta/Ufs;
tw=tbl*2.5; % as suggested by Blair(1983)
% Initialize gamma, td, and jend
gamma=zeros(datapoints,1);
td=0;
jend=1;
j=1;
eventcontinues=1;
while j<(datapoints+1),
  % March through criterion, comparing each data point to the threshold
  if (criterion(j)>threshold)
    td = (j-jend)*deltat;
  if (td>tw)
    % assume a new event is starting
    jstart=j;
  else
    % assume this is a continuation of a previous event
    jstart=jend;
  end
  while (eventcontinues>0),
          % Calculate average value of criterion since jstart
    criterionave=mean(criterion(jstart:j));
    if (criterionave>threshold) | (criterion(j)>threshold)
            eventcontinues=1;
    else
            jend=j;
      eventcontinues=0;
    end
          j=j+1;
  end
  td=(jstart-jend)*deltat;
  if (td<tw)
    gamma([jstart:j])=ones(j-jstart+1,1);
    jend=j;
  else
    jend=jstart;
       end
  end
       j=j+1;
end
     gamma2=ceil((criterion-threshold)/max(criterion));
subplot(4,1,1)
plot(u)
subplot(4,1,2)
plot(abs(criterion))
hold on;
     plot(threshline);
     hold off;
subplot(4,1,3)
plot(gamma)
axis([0 datapoints -1 2]);
subplot(4,1,4)
plot(gamma2)
axis([0 datapoints -1 2]);
pause(0.001)
% Find state changes
pulses=0;
lastpoint=5.0;
for j=1:datapoints,
```

```
    if ((lastpoint>2.5)&(photogatedata(j)<2.5))
      pulsetime(pulses+1)=j;
      pulses=pulses+1;
    end
    if ((lastpoint<2.5)&(photogatedata(j)>2.5))
      pulsetime(pulses+1)=j;
      pulses=pulses+1;
    end
    lastpoint=photogatedata(j);
    if (pulses==28)
      break;
    end
  end
  % For each of the six wakes, take the ideallength points
  % of intermittency around the center of the wake
  for j=1:3,
    thiswake=(i-1)*rods+j;
    centerpulse=pulsetime(0+4+1+8*(j-1));
    centerwake=centerpulse+leadpoints;
    wake=velocitydata((centerwake-ideallength/2):...
      (centerwake+ideallength/2-1));
    wakedata(thiswake,:)=wake';
    interwake=gamma((centerwake-ideallength/2):...
      (centerwake+ideallength/2-1));
    interdata(thiswake,:)=interwake';
  end
% For each wake, calculate the velocity correction if required
if y<0.04,
wakedataraw=wakedata;
for i=1:wakes
  for j=1:ideallength
    if interdata(i,j)<1
      wakedata(i,j)=(wakedataraw(i,j).^0.45-((nu/ds)^.45)*kw).^(1/.45);
    else
      wakedata(i,j)=0.84*(wakedataraw(i,j).^0.45-...
        ((nu/ds)^.45)*kw).^(1/.45)+0.16*wakedataraw(i,j);
    end
  end
end
end
end
% For each phase segment, find the mean velocity and the
    % rms fluctuation
segmentlength=ideallength/phasesegments;
for i=1:phasesegments,
  startsegment=(i-1)*(segmentlength*1)+1;
  endsegment=startsegment+segmentlength-1;
  segment=reshape(interdata(:,[startsegment:endsegment]),...
    1,segmentlength*wakes);
  segment1=reshape(interdata(rod1wakes,[startsegment:endsegment]),...
    1,segmentlength*wakes/3);
  segment2=reshape(interdata(rod2wakes,[startsegment:endsegment]),...
    1,segmentlength*wakes/3);
  segment3=reshape(interdata(rod3wakes,[startsegment:endsegment]),...
    1,segmentlength*wakes/3);
  interphase(i,ylocation)=mean(segment);
  interphase1(i,ylocation)=mean(segment1);
  interphase2(i,ylocation)=mean(segment2);
  interphase3(i,ylocation)=mean(segment3);
  segment=reshape(wakedata(:,[startsegment:endsegment]),...
    1,segmentlength*wakes);
  segment1=reshape(wakedata(rod1wakes,[startsegment:endsegment]),...
    1,segmentlength*wakes/3);
  segment2=reshape(wakedata(rod2wakes,[startsegment:endsegment]),...
    1,segmentlength*wakes/3);
```

```
    segment3=reshape(wakedata(rod3wakes,[startsegment:endsegment]),...
      1,segmentlength*wakes/3);
    uphase(i,ylocation)=mean(segment);
    urmsphase(i,ylocation)=std(segment);
    uphase1(i,ylocation)=mean(segment1);
    urmsphase1(i,ylocation)=std(segment1);
    uphase2(i,ylocation)=mean(segment2);
    urmsphase2(i,ylocation)=std(segment2);
    uphase3(i,ylocation)=mean(segment3);
    urmsphase3(i,ylocation)=std(segment3);
  end
end
tiphase=urmsphase./uphase;
tiphase1=urmsphase1./uphase1;
tiphase2=urmsphase2./uphase2;
tiphase3=urmsphase3./uphase3;
phase=360*([1:phasesegments]/phasesegments);
fullphase=[phase,360+phase,720+phase];
ubyrod=[uphase1;uphase2;uphase3];
urmsbyrod=[urmsphase1;urmsphase2;urmsphase3];
tibyrod=[tiphase1;tiphase2;tiphase3];
interbyrod=[interphase1;interphase2;interphase3];

%recalculate uphase, urmsphase, tiphase, and interphase
uphase=(uphase1+uphase2+uphase3)/3;
urmsphase=(urmsphase1+urmsphase2+urmsphase3)/3;
interphase=(interphase1+interphase2+interphase3)/3;
tiphase=urmsphase./uphase;


savefilename=sprintf('sp%02dfourrod.mat',pressurelocation);
save(savefilename,'interphase','uphase','urmsphase','tiphase',...
  'y','phase','pressurelocation','fullphase','ubyrod','urmsbyrod',...
  'tibyrod','interbyrod');
```

B.6 hp09.m

```
clear;
clf;

leadpoints=3550;

%Sampling frequency
frequency=100000;
ideallength=4500;
trials=35;
rods=6;
pressurelocation=09;
phasesegments=90;
ystations=30;
ylocation=1;
y=[0.01 0.02 0.03 0.05 0.07 0.09 0.12 0.15 0.18 0.22 0.26 0.30 0.35...
   0.40 0.45 0.51 0.57 0.63 0.70 0.77 0.84 0.92 1.00 1.08 1.17 1.26...
   1.35 1.45 1.55 1.65];
wakes=rods*trials;
datapoints=60000;
pulsetime=zeros(1,50);
wakedata=zeros(wakes,ideallength);
uphase=zeros(phasesegments,ystations);
urmsphase=zeros(phasesegments,ystations);
tiphase=zeros(phasesegments,ystations);

% For each trial, we load in the photogate data and the velocity %
data. We find each state change in the photogate data, and use that %
to find the center of each wake. We then extract the wakes from u%
```

```
each velocity data file

% For each y location
for ylocation=1:ystations,
  ylocation
  % For each trial
  for i=1:trials,
    velocityfilename=sprintf(...
      'hp%02d/velocity/y%02d/hp%02dy%02dt%03dvelocity',...
      pressurelocation,ylocation,pressurelocation,ylocation,i-1);
    velocityfid=fopen(velocityfilename);
    velocitydata=fread(velocityfid,inf,'double');
    fclose(velocityfid);
    photogatefilename=sprintf(...
      'hp%02d/photogate/y%02d/hp%02dy%02dt%03dphotogate',...
      pressurelocation,ylocation,pressurelocation,ylocation,i-1);
    photogatefid=fopen(photogatefilename);
    photogatedata=fread(photogatefid,inf,'double');
    fclose(photogatefid);
    % Find state changes
    pulses=0;
    lastpoint=5.0;
    for j=1:datapoints,
      if ((lastpoint>2.5)&(photogatedata(j)<2.5))
        pulsetime(pulses+1)=j;
        pulses=pulses+1;
      end
      if ((lastpoint<2.5)&(photogatedata(j)>2.5))
        pulsetime(pulses+1)=j;
        pulses=pulses+1;
      end
      lastpoint=photogatedata(j);
      if (pulses==28)
        break;
      end
    end
    % For each of the six wakes, take the ideallength points
    % around the center of the wake
    for j=1:6,
      thiswake=(i-1)*rods+j;
      centerpulse=pulsetime(7+4*(j-1));
      centerwake=centerpulse+leadpoints;
      wake=velocitydata((centerwake-ideallength/2):...
        (centerwake+ideallength/2-1));
      wakedata(thiswake,:)=wake';
    end
  end
  % For each phase segment, find the mean velocity and the
      % rms fluctuation
  segmentlength=ideallength/phasesegments;
  for i=1:phasesegments,
    startsegment=(i-1)*(segmentlength*1)+1;
    endsegment=startsegment+segmentlength-1;
    segment=reshape(wakedata(:,[startsegment:endsegment]),...
      1,segmentlength*wakes);
    uphase(i,ylocation)=mean(segment);
    urmsphase(i,ylocation)=std(segment);
  end
plot(uphase(:,[1:ylocation]));
pause(0.05);
end
tiphase=urmsphase./uphase;
phase=360*([1:phasesegments]/phasesegments);

savefilename=sprintf('hp%02d.mat',pressurelocation);
```

```
save(savefilename,'uphase','urmsphase','tiphase','y',...
    'phase','pressurelocation');
```

B.7 hp09inter.m

```
clear;
clf;

% Second pass---this one uses the profile results from the first pass
% calculate intermittency.  (To calculate the windowing time and
% threshold values, we need to have a fairly decent estimate of the
% freestream velocity)

leadpoints=3550;

%Sampling frequency
frequency=100000;
ideallength=4500;
trials=35;
rods=6;
pressurelocation=09;
phasesegments=90;
ystations=30;
ylocation=1;
y=[0.01 0.02 0.03 0.05 0.07 0.09 0.12 0.15 0.18 0.22 0.26 0.30 0.35...
    0.40 0.45 0.51 0.57 0.63 0.70 0.77 0.84 0.92 1.00 1.08 1.17 1.26...
    1.35 1.45 1.55 1.65];
wakes=rods*trials;
datapoints=60000;
pulsetime=zeros(1,50);
uphase=zeros(phasesegments,ystations);
urmsphase=zeros(phasesegments,ystations);
tiphase=zeros(phasesegments,ystations);
rod1wakes=linspace(1, 205, 35);
rod2wakes=linspace(2, 206, 35);
rod3wakes=linspace(3, 207, 35);
rod4wakes=linspace(4, 208, 35);
rod5wakes=linspace(5, 209, 35);
rod6wakes=linspace(6, 210, 35);
uphase1=zeros(phasesegments,ystations);
urmsphase1=zeros(phasesegments,ystations);
tiphase1=zeros(phasesegments,ystations);
interphase1=zeros(phasesegments,ystations);
uphase2=zeros(phasesegments,ystations);
urmsphase2=zeros(phasesegments,ystations);
tiphase2=zeros(phasesegments,ystations);
interphase2=zeros(phasesegments,ystations);
uphase3=zeros(phasesegments,ystations);
urmsphase3=zeros(phasesegments,ystations);
tiphase3=zeros(phasesegments,ystations);
interphase3=zeros(phasesegments,ystations);
uphase4=zeros(phasesegments,ystations);
urmsphase4=zeros(phasesegments,ystations);
tiphase4=zeros(phasesegments,ystations);
interphase4=zeros(phasesegments,ystations);
uphase5=zeros(phasesegments,ystations);
urmsphase5=zeros(phasesegments,ystations);
tiphase5=zeros(phasesegments,ystations);
interphase5=zeros(phasesegments,ystations);
uphase6=zeros(phasesegments,ystations);
urmsphase6=zeros(phasesegments,ystations);
tiphase6=zeros(phasesegments,ystations);
interphase6=zeros(phasesegments,ystations);

interdata=zeros(wakes,ideallength);
```

```
interphase=zeros(phasesegments,ystations);
t=[0:(datapoints-1)]'/frequency;
deltat=1/frequency;
threshfactor=2.75;
ds=4e-6;
nu=15.75;

firststagefilename=sprintf('hp%02d.mat',pressurelocation);

load(firststagefilename,'uphase');

% For each trial, we load in the photogate data and the velocity
% data.  We find each state change in the photogate data, and use that
% to find the center of each wake.  We then calculate the
% intermittency for each velocity trace, and use the photogate data to
% break this into wakes and ensemble average it like we did in the
% first pass

% For each y location
for ylocation=1:ystations,
  ylocation
        % Calculate correction factor
  ycur=y(ylocation)
  yscale=2*y(ylocation)*1e-2/ds
  if yscale<50,
          kw=0.9-7.2e-2*yscale+2.89e-3*yscale.^2-6.15E-5*yscale.^3 ...
              +6.51e-7*yscale.^4
  else
          kw=0.54-2.42e-2*yscale+5.01e-4*yscale.^2-5.36E-6*yscale.^3 ...
              +2.85e-8*yscale.^4
  end
  % For each trial
  for i=1:trials,
    i
    velocityfilename=sprintf(...
      'hp%02d/velocity/y%02d/hp%02dy%02dt%03dvelocity',...
      pressurelocation,ylocation,pressurelocation,ylocation,i-1);
    velocityfid=fopen(velocityfilename);
    velocitydata=fread(velocityfid,inf,'double');
    fclose(velocityfid);
    photogatefilename=sprintf(...
      'hp%02d/photogate/y%02d/hp%02dy%02dt%03dphotogate',...
      pressurelocation,ylocation,pressurelocation,ylocation,i-1);
    photogatefid=fopen(photogatefilename);
    photogatedata=fread(photogatefid,inf,'double');
    fclose(photogatefid);
    % calcule u and du/dt
    u=velocitydata;
    dudt=[diff(u)./diff(t); 0];
    % Calculate the criterion function and the threshold
    criterion=u.*dudt;
    threshold=threshfactor*std(criterion([3550:35050]));
    criterion=abs(criterion);
    threshline=threshold*ones(datapoints,1);
    % Calculate the windowing time from the BL scale
    delta=0.0165; % approximated BL thickness
    Ufs=mean(uphase(:,30)); % approximated mean freestream velocity
    tbl=delta/Ufs;
    tw=tbl*2.5; % as suggested by Blair(1983)
    % Initialize gamma, td, and jend
    gamma=zeros(datapoints,1);
    td=0;
    jend=1;
    j=1;
    eventcontinues=1;
```

```
while j<(datapoints+1),
  % March through criterion, comparing each data point to the threshold
  if (criterion(j)>threshold)
    td = (j-jend)*deltat;
  if (td>tw)
    % assume a new event is starting
    jstart=j;
  else
    % assume this is a continuation of a previous event
    jstart=jend;
  end
  while (eventcontinues>0),
          % Calculate average value of criterion since jstart
    criterionave=mean(criterion(jstart:j));
    if (criterionave>threshold) | (criterion(j)>threshold)
            eventcontinues=1;
    else
            jend=j;
      eventcontinues=0;
    end
          j=j+1;
  end
  td=(jstart-jend)*deltat;
  if (td<tw)
    gamma([jstart:j])=ones(j-jstart+1,1);
    jend=j;
  else
    jend=jstart;
        end
  end
        j=j+1;
end
      gamma2=ceil((criterion-threshold)/max(criterion));
subplot(4,1,1)
plot(u)
subplot(4,1,2)
plot(abs(criterion))
hold on;
      plot(threshline);
      hold off;
subplot(4,1,3)
plot(gamma)
axis([0 datapoints -1 2]);
subplot(4,1,4)
plot(gamma2)
axis([0 datapoints -1 2]);
pause(0.01)
% Find state changes
pulses=0;
lastpoint=5.0;
for j=1:datapoints,
  if ((lastpoint>2.5)&(photogatedata(j)<2.5))
    pulsetime(pulses+1)=j;
    pulses=pulses+1;
  end
  if ((lastpoint<2.5)&(photogatedata(j)>2.5))
    pulsetime(pulses+1)=j;
    pulses=pulses+1;
  end
  lastpoint=photogatedata(j);
  if (pulses==28)
    break;
  end
end
% For each of the six wakes, take the ideallength points
```

```
    % of intermittency around the center of the wake
    for j=1:6,
      thiswake=(i-1)*rods+j;
      centerpulse=pulsetime(7+4*(j-1));
      centerwake=centerpulse+leadpoints;
      wake=velocitydata((centerwake-ideallength/2):...
        (centerwake+ideallength/2-1));
      wakedata(thiswake,:)=wake';
      interwake=gamma((centerwake-ideallength/2):...
        (centerwake+ideallength/2-1));
      interdata(thiswake,:)=interwake';
    end
  % For each wake, calculate the velocity correction if required
  if y<0.04,
  wakedataraw=wakedata;
  for i=1:wakes
    for j=1:ideallength
      if interdata(i,j)<1
              wakedata(i,j)=...
                (wakedataraw(i,j).^0.45-((nu/ds)^.45)*kw).^(1/.45);
      else
              wakedata(i,j)=0.84*(wakedataraw(i,j).^0.45...
                -((nu/ds)^.45)*kw).^(1/.45)+0.16*wakedataraw(i,j);
      end
    end
  end
  end
  end
  % For each phase segment, find the mean velocity and the
        % rms fluctuation
  segmentlength=ideallength/phasesegments;
  for i=1:phasesegments,
    startsegment=(i-1)*(segmentlength*1)+1;
    endsegment=startsegment+segmentlength-1;
    segment=reshape(interdata(:,[startsegment:endsegment]),...
      1,segmentlength*wakes);
    segment1=reshape(interdata(rod1wakes,[startsegment:endsegment]),...
      1,segmentlength*wakes/6);
    segment2=reshape(interdata(rod2wakes,[startsegment:endsegment]),...
      1,segmentlength*wakes/6);
    segment3=reshape(interdata(rod3wakes,[startsegment:endsegment]),...
      1,segmentlength*wakes/6);
    segment4=reshape(interdata(rod4wakes,[startsegment:endsegment]),...
      1,segmentlength*wakes/6);
    segment5=reshape(interdata(rod5wakes,[startsegment:endsegment]),...
      1,segmentlength*wakes/6);
    segment6=reshape(interdata(rod6wakes,[startsegment:endsegment]),...
      1,segmentlength*wakes/6);
    interphase(i,ylocation)=mean(segment);
    interphase1(i,ylocation)=mean(segment1);
    interphase2(i,ylocation)=mean(segment2);
    interphase3(i,ylocation)=mean(segment3);
    interphase4(i,ylocation)=mean(segment4);
    interphase5(i,ylocation)=mean(segment5);
    interphase6(i,ylocation)=mean(segment6);
    segment=reshape(wakedata(:,[startsegment:endsegment]),...
      1,segmentlength*wakes);
    segment1=reshape(wakedata(rod1wakes,[startsegment:endsegment]),...
      1,segmentlength*wakes/6);
    segment2=reshape(wakedata(rod2wakes,[startsegment:endsegment]),...
      1,segmentlength*wakes/6);
    segment3=reshape(wakedata(rod3wakes,[startsegment:endsegment]),...
      1,segmentlength*wakes/6);
    segment4=reshape(wakedata(rod4wakes,[startsegment:endsegment]),...
      1,segmentlength*wakes/6);
```

```
      segment5=reshape(wakedata(rod5wakes,[startsegment:endsegment]),...
        1,segmentlength*wakes/6);
      segment6=reshape(wakedata(rod6wakes,[startsegment:endsegment]),...
        1,segmentlength*wakes/6);
      uphase(i,ylocation)=mean(segment);
      urmsphase(i,ylocation)=std(segment);
      uphase1(i,ylocation)=mean(segment1);
      urmsphase1(i,ylocation)=std(segment1);
      uphase2(i,ylocation)=mean(segment2);
      urmsphase2(i,ylocation)=std(segment2);
      uphase3(i,ylocation)=mean(segment3);
      urmsphase3(i,ylocation)=std(segment3);
      uphase4(i,ylocation)=mean(segment4);
      urmsphase4(i,ylocation)=std(segment4);
      uphase5(i,ylocation)=mean(segment5);
      urmsphase5(i,ylocation)=std(segment5);
      uphase6(i,ylocation)=mean(segment6);
      urmsphase6(i,ylocation)=std(segment6);
    end
  end
tiphase=urmsphase./uphase;
tiphase1=urmsphase1./uphase1;
tiphase2=urmsphase2./uphase2;
tiphase3=urmsphase3./uphase3;
tiphase4=urmsphase4./uphase4;
tiphase5=urmsphase5./uphase5;
tiphase6=urmsphase6./uphase6;
phase=360*([1:phasesegments]/phasesegments);
fullphase=[phase,360+phase,720+phase,1080+phase,1440+phase,1800+phase];
ubyrod=[uphase1;uphase2;uphase3;uphase4;uphase5;uphase6];
urmsbyrod=[urmsphase1;urmsphase2;urmsphase3;urmsphase4;urmsphase5;urmsphase6];
tibyrod=[tiphase1;tiphase2;tiphase3;tiphase4;tiphase5;tiphase6];
interbyrod=[interphase1;interphase2;interphase3;...
  interphase4;interphase5;interphase6];

%recalculate uphase, urmsphase, tiphase, and interphase
uphase=(uphase1+uphase2+uphase3+uphase4)/4;
urmsphase=(urmsphase1+urmsphase2+urmsphase3+urmsphase4)/4;
interphase=(interphase1+interphase2+interphase3+interphase4)/4;
tiphase=urmsphase./uphase;


savefilename=sprintf('hp%02dfourrod.mat',pressurelocation);
save(savefilename,'interphase','uphase','urmsphase',...
  'tiphase','y','phase','pressurelocation','fullphase',...
  'ubyrod','urmsbyrod','tibyrod','interbyrod');
```

B.8 lengthscale.m

```
clear;
clf;

%Sampling frequency
freq=2000;

ufid=fopen('uraw');
vfid=fopen('vraw');
wfid=fopen('wraw');
u=fread(ufid,inf,'double');
v=fread(vfid,inf,'double');
w=fread(wfid,inf,'double');

ubar=mean(u);
vbar=mean(v);
wbar=mean(w);
```

```
urms=sqrt(var(u));
vrms=sqrt(var(v));
wrms=sqrt(var(w));

u=u-ubar;
v=v-vbar;
w=w-wbar;

% Calculate a -5/3 power law for comparison
fcompare=logspace(1.5,3);
PSDcompare=fcompare.^(-5/3);

%Choose appropriate windowing function:

window=boxcar(512);

%Calculate the PSDs

[Pu,fu]=psd(u,512,freq,window,'none');
[Pv,fv]=psd(v,512,freq,window,'none');
[Pw,fw]=psd(w,512,freq,window,'none');
W=norm(window)^2/sum(window)^2; % Normalize as per matlab email
Pu=4*Pu*W/(fu(2)-fu(1)); % Scale on df
Pv=4*Pv*W/(fv(2)-fv(1)); % Scale on df
Pw=4*Pw*W/(fw(2)-fw(1)); % Scale on df

loglog(fu,Pu,'r-',fu,Pv,'g--',fu,Pw,'b-.',fcompare,0.25*PSDcompare,'k--');
legend('uprime','vprime','wprime','-5/3 power relation');

%title('PSD of u\prime, v\prime, and w\prime, sampled at 2 kHz for 1049 seconds');
xlabel('frequency (Hz)');
ylabel('PSD');
hold off;

% Calculate Length Scales via the PSD
LambdauxPSD=ubar*Pu(1)/(4*(urms.*urms))
LambdavxPSD=ubar*Pv(1)/(4*(vrms.*vrms))
LambdawxPSD=ubar*Pw(1)/(4*(vrms.*vrms))
% Calculate Length Scales via the Autocorrelation
```

Appendix C can also be found in the ReadMe file on the accompanying CD–ROM.

Appendix C

CD Animations and Figures

Attached to this document is a CD containing digital copies of this report (in PDF format), ASCII-tabulated data of the ensemble-averaged results and a series of animations which allow better visualization of the experimental results. The animations are provided in both QUICKTIME (`.qt`) and WINDOWS MEDIA PLAYER (`.avi`) format. Note that the .qt files are of better resolution then the .avi files. The CD contents are described below.

C.1 Digital Copy of this Report

The text and figures of this report are included in digital format on the CD in PDF format, as NASA-CR-2007-214678.pdf, respectively.

C.2 ASCII-Tabulated Data

The ensemble-averaged distributions of $\tilde{u}(s, y, \theta)$, $\widetilde{u_{rms}}(s, y, \theta)$, $\widetilde{TI}(s, y, \theta)$ and $\tilde{\gamma}(s, y, \theta))$ are included on the CD as tab-delimited ASCII files for each pressure station, for all three cases investigated. In each file, each column represents a different wall-normal distance, y (in m), from the wall, while each row represents a different value of θ (in degrees). The quantities given are in floating point format double precision, and expressed in $^{m}/_{s}$. The y-values are used as column headings and the θ values are used as row labels, as shown in Figure C.1. The files are described in Table C.1.

C.3 Multidimensional Visualizations

The most convenient way to visualize the experimental results is to use a 3D visualization technique in which the quantity to be visualized ($\tilde{u}(s,y,\theta)$, $\widetilde{u_{rms}}(s,y,\theta)$, $\widetilde{TI}(s,y,\theta)$ or $\tilde{\gamma}(s,y,\theta)$) is represented as a 3D volume, with the three axes representing space (represented as s/L_{ss}, the fraction of the suction surface chord length), time (represented as t/T) and the wall-normal distance, y. The quantity being visualized is represented as varying colors. To completely show the distributions throughout the volume, animations were generated in which planes representing varying values of time, space and wall-normal distance are "dragged" through the visualization volume, creating movies.

The animations are named after the quantity being plotted, and the direction the visualization planes are being drawn in the volume. Lists of animations of the base case, increased wake spacing case and high-*FSTI* case are presented in Tables C.2, C.3 and C.4, respectively.

C.4 Case Comparison Visualizations

It is useful to visualize the effects of increased rod spacing and elevated *FSTI* by doing a side-by-side comparison of the data with the base case. Animations were generated comparing one measured quantity ($\tilde{u}(s,y,\theta)$, $\widetilde{u_{rms}}(s,y,\theta)$, $\widetilde{TI}(s,y,\theta)$ or $\tilde{\gamma}(s,y,\theta)$) in the base case with a syncronized movie showing the same quantity measured in either the increased wake spacing or high-*FSTI* case.

Like the previous animations, the visualizations are named by stating the quantity being plotted, and the direction the visualization planes are being drawn in the volume, with either the prefix 's' or 'h', indicating whether the animation shows a comparison with the the increased wake spacing or high-*FSTI* case, respectively. Lists of these animations are presented in Tables C.5, and C.6.

C.5 Wake Generator Movies

The files `upstream.{qt,avi}` and `overhead.{qt,avi}` show schematic animations of the wake generator in operation. Their titles refer to the direction in which the observer is viewing the wake generator.

	y_1	$\cdots$	y_{30}
θ_1	$\tilde{u}(y_1, \theta_1)$	$\cdots$	$\tilde{u}(y_{30}, \theta_1)$
$\vdots$	$\vdots$	$\ddots$	$\vdots$
θ_{90}	$\tilde{u}(y_1, \theta_{90})$	$\cdots$	$\tilde{u}(y_{30}, \theta_{90})$

Figure C.1: ACSII File Format

Table C.1: Description of ASCII data files

Filename:	**Description**:
`pXXu.txt`:	Distribution of $\tilde{u}(y, \theta)$ at station `pXX`, base case.
`pXXurms.txt`:	Distribution of $\widetilde{u_{rms}}(y, \theta)$ at station `pXX`, base case.
`pXXti.txt`:	Distribution of $\widetilde{TI}(y, \theta)$ at station `pXX`, base case.
`pXXgamma.txt`:	Distribution of $\tilde{\gamma}(y, \theta)$ at station `pXX`, base case.
`spXXu.txt`:	Distribution of $\tilde{u}(y, \theta)$ at station `pXX`, increased wake spacing case.
`spXXurms.txt`:	Distribution of $\widetilde{u_{rms}}(y, \theta)$ at station `pXX`, increased wake spacing case.
`spXXti.txt`:	Distribution of $\widetilde{TI}(y, \theta)$ at station `pXX`, increased wake spacing case.
`spXXgamma.txt`:	Distribution of $\tilde{\gamma}(y, \theta)$ at station `pXX`, increased wake spacing case.
`hpXXu.txt`:	Distribution of $\tilde{u}(y, \theta)$ at station `pXX`, high-$FSTI$ case.
`hpXXurms.txt`:	Distribution of $\widetilde{u_{rms}}(y, \theta)$ at station `pXX`, high-$FSTI$ case.
`hpXXti.txt`:	Distribution of $\widetilde{TI}(y, \theta)$ at station `pXX`, high-$FSTI$ case.
`hpXXgamma.txt`:	Distribution of $\tilde{\gamma}(y, \theta)$ at station `pXX`, high-$FSTI$ case.

Table C.2: Visualization animations, base case

Filename:	**Description**:
`usmovie.{qt,avi}`	Movie showing $\tilde{u}(s,y,\theta)$ at varying values of s/L_{ss}, base case.
`utmovie.{qt,avi}`	Movie showing $\tilde{u}(s,y,\theta)$ at varying values of t/T, base case.
`uymovie.{qt,avi}`	Movie showing $\tilde{u}(s,y,\theta)$ at varying values of y, base case.
`urmssmovie.{qt,avi}`	Movie showing $\widetilde{u_{rms}}(s,y,\theta)$ at varying values of s/L_{ss}, base case.
`urmstmovie.{qt,avi}`	Movie showing $\widetilde{u_{rms}}(s,y,\theta)$ at varying values of t/T, base case.
`urmsymovie.{qt,avi}`	Movie showing $\widetilde{u_{rms}}(s,y,\theta)$ at varying values of y, base case.
`tismovie.{qt,avi}`	Movie showing $\widetilde{TI}(s,y,\theta)$ at varying values of s/L_{ss}, base case.
`titmovie.{qt,avi}`	Movie showing $\widetilde{TI}(s,y,\theta)$ at varying values of t/T, base case.
`tiymovie.{qt,avi}`	Movie showing $\widetilde{TI}(s,y,\theta)$ at varying values of y, base case.
`gammasmovie.{qt,avi}`	Movie showing $\tilde{\gamma}(s,y,\theta)$ at varying values of s/L_{ss}, base case..
`gammatmovie.{qt,avi}`	Movie showing $\tilde{\gamma}(s,y,\theta)$ at varying values of t/T, base case.
`gammaymovie.{qt,avi}`	Movie showing $\tilde{\gamma}(s,y,\theta)$ at varying values of y, base case.

Table C.3: Visualization animations, increased wake spacing case

Filename:	**Description**:
`susmovie.{qt,avi}`	Movie showing $\tilde{u}(s,y,\theta)$ at varying values of s/L_{ss}, increased wake spacing case.
`sutmovie.{qt,avi}`	Movie showing $\tilde{u}(s,y,\theta)$ at varying values of t/T, increased wake spacing case.
`suymovie.{qt,avi}`	Movie showing $\tilde{u}(s,y,\theta)$ at varying values of y, increased wake spacing case.
`surmssmovie.{qt,avi}`	Movie showing $\widetilde{u_{rms}}(s,y,\theta)$ at varying values of s/L_{ss}, increased wake spacing case.
`surmstmovie.{qt,avi}`	Movie showing $\widetilde{u_{rms}}(s,y,\theta)$ at varying values of t/T, increased wake spacing case.
`surmsymovie.{qt,avi}`	Movie showing $\widetilde{u_{rms}}(s,y,\theta)$ at varying values of y, increased wake spacing case.
`stismovie.{qt,avi}`	Movie showing $\widetilde{TI}(s,y,\theta)$ at varying values of s/L_{ss}, increased wake spacing case.
`stitmovie.{qt,avi}`	Movie showing $\widetilde{TI}(s,y,\theta)$ at varying values of t/T, increased wake spacing case.
`stiymovie.{qt,avi}`	Movie showing $\widetilde{TI}(s,y,\theta)$ at varying values of y, increased wake spacing case.
`sgammasmovie.{qt,avi}`	Movie showing $\tilde{\gamma}(s,y,\theta)$ at varying values of s/L_{ss}, increased wake spacing case..
`sgammatmovie.{qt,avi}`	Movie showing $\tilde{\gamma}(s,y,\theta)$ at varying values of t/T, increased wake spacing case.
`sgammaymovie.{qt,avi}`	Movie showing $\tilde{\gamma}(s,y,\theta)$ at varying values of y, increased wake spacing case.

Table C.4: Visualization animations, high-$FSTI$ case

Filename:	**Description**:
`husmovie.{qt,avi}`	Movie showing $\tilde{u}(s,y,\theta)$ at varying values of s/L_{ss}, high-$FSTI$ case.
`hutmovie.{qt,avi}`	Movie showing $\tilde{u}(s,y,\theta)$ at varying values of t/T, high-$FSTI$ case.
`huymovie.{qt,avi}`	Movie showing $\tilde{u}(s,y,\theta)$ at varying values of y, high-$FSTI$ case.
`hurmssmovie.{qt,avi}`	Movie showing $\widetilde{u_{rms}}(s,y,\theta)$ at varying values of s/L_{ss}, high-$FSTI$ case.
`hurmstmovie.{qt,avi}`	Movie showing $\widetilde{u_{rms}}(s,y,\theta)$ at varying values of t/T, high-$FSTI$ case.
`hurmsymovie.{qt,avi}`	Movie showing $\widetilde{u_{rms}}(s,y,\theta)$ at varying values of y, high-$FSTI$ case.
`htismovie.{qt,avi}`	Movie showing $\widetilde{TI}(s,y,\theta)$ at varying values of s/L_{ss}, high-$FSTI$ case.
`htitmovie.{qt,avi}`	Movie showing $\widetilde{TI}(s,y,\theta)$ at varying values of t/T, high-$FSTI$ case.
`htiymovie.{qt,avi}`	Movie showing $\widetilde{TI}(s,y,\theta)$ at varying values of y, high-$FSTI$ case.
`hgammasmovie.{qt,avi}`	Movie showing $\tilde{\gamma}(s,y,\theta)$ at varying values of s/L_{ss}, high-$FSTI$ case..
`hgammatmovie.{qt,avi}`	Movie showing $\tilde{\gamma}(s,y,\theta)$ at varying values of t/T, high-$FSTI$ case.
`hgammaymovie.{qt,avi}`	Movie showing $\tilde{\gamma}(s,y,\theta)$ at varying values of y, high-$FSTI$ case.

Table C.5: Comparison animations, increased wake spacing case

Filename:	**Description**:
`scombousmovie.{qt,avi}`	Movie comparing $\tilde{u}(s,y,\theta)$ at varying values of s/L_{ss} in the base and increased wake spacing cases.
`scomboutmovie.{qt,avi}`	Movie comparing $\tilde{u}(s,y,\theta)$ at varying values of t/T in the base and increased wake spacing cases.
`scombouymovie.{qt,avi}`	Movie comparing $\tilde{u}(s,y,\theta)$ at varying values of y in the base and increased wake spacing cases.
`scombourmssmovie.{qt,avi}`	Movie comparing $\widetilde{u_{rms}}(s,y,\theta)$ at varying values of s/L_{ss} in the base and increased wake spacing cases.
`scombourmstmovie.{qt,avi}`	Movie comparing $\widetilde{u_{rms}}(s,y,\theta)$ at varying values of t/T in the base and increased wake spacing cases.
`scombourmsymovie.{qt,avi}`	Movie comparing $\widetilde{u_{rms}}(s,y,\theta)$ at varying values of y in the base and increased wake spacing cases.
`scombogammasmovie.{qt,avi}`	Movie comparing $\tilde{\gamma}(s,y,\theta)$ at varying values of s/L_{ss} in the base and increased wake spacing cases..
`scombogammatmovie.{qt,avi}`	Movie comparing $\tilde{\gamma}(s,y,\theta)$ at varying values of t/T in the base and increased wake spacing cases.
`scombogammaymovie.{qt,avi}`	Movie comparing $\tilde{\gamma}(s,y,\theta)$ at varying values of y in the base and increased wake spacing cases.

Table C.6: Comparison animations, high-$FSTI$ case

Filename:	**Description**:
`hcombousmovie.{qt,avi}`	Movie comparing $\tilde{u}(s, y, \theta)$ at varying values of s/L_{ss} in the base and high-$FSTI$ cases.
`hcomboutmovie.{qt,avi}`	Movie comparing $\tilde{u}(s, y, \theta)$ at varying values of t/T in the base and high-$FSTI$ cases.
`hcombouymovie.{qt,avi}`	Movie comparing $\tilde{u}(s, y, \theta)$ at varying values of y in the base and high-$FSTI$ cases.
`hcombourmssmovie.{qt,avi}`	Movie comparing $\widetilde{u_{rms}}(s, y, \theta)$ at varying values of s/L_{ss} in the base and high-$FSTI$ cases.
`hcombourmstmovie.{qt,avi}`	Movie comparing $\widetilde{u_{rms}}(s, y, \theta)$ at varying values of t/T in the base and high-$FSTI$ cases.
`hcombourmsymovie.{qt,avi}`	Movie comparing $\widetilde{u_{rms}}(s, y, \theta)$ at varying values of y in the base and high-$FSTI$ cases.
`hcombogammasmovie.{qt,avi}`	Movie comparing $\tilde{\gamma}(s, y, \theta)$ at varying values of s/L_{ss} in the base and high-$FSTI$ cases..
`hcombogammatmovie.{qt,avi}`	Movie comparing $\tilde{\gamma}(s, y, \theta)$ at varying values of t/T in the base and high-$FSTI$ cases.
`hcombogammaymovie.{qt,avi}`	Movie comparing $\tilde{\gamma}(s, y, \theta)$ at varying values of y in the base and high-$FSTI$ cases.

REPORT DOCUMENTATION PAGE

Form Approved
OMB No. 0704-0188

1. AGENCY USE ONLY (*Leave blank*)	2. REPORT DATE	3. REPORT TYPE AND DATES COVERED
	March 2007	Final Contractor Report

4. TITLE AND SUBTITLE

Experimental Investigation of Transition to Turbulence as Affected by Passing Wakes: Effects of High FSTI and Increased Rod Spacing

5. FUNDING NUMBERS

WBS 561581.02.08.03.02.01
NCC3–652

6. AUTHOR(S)

Richard W. Kaszeta, Terrence W. Simon, Nan Jiang, and Federico Ottaviani

7. PERFORMING ORGANIZATION NAME(S) AND ADDRESS(ES)

University of Minnesota
111 Church St. S.E.
Minneapolis, MN 55455

8. PERFORMING ORGANIZATION REPORT NUMBER

E–15814

9. SPONSORING/MONITORING AGENCY NAME(S) AND ADDRESS(ES)

National Aeronautics and Space Administration
Washington, DC 20546–0001

10. SPONSORING/MONITORING AGENCY REPORT NUMBER

NASA CR—2007-214678

11. SUPPLEMENTARY NOTES

Project manager, Dr. David Ashpis, Aeropropulsion Division, NASA Glenn Research Center, organization code RTT, e-mail: David.E.Ashpis@nasa.gov, 216–433–8317.

12a. DISTRIBUTION/AVAILABILITY STATEMENT

Unclassified - Unlimited
Subject Categories: 02, 07, and 34

Available electronically at http://gltrs.grc.nasa.gov

This publication is available from the NASA Center for AeroSpace Information, 301–621–0390.

12b. DISTRIBUTION CODE

13. ABSTRACT ***(Maximum 200 words)***

Experimental results from a study of the effects of passing wakes upon laminar-to-turbulent transition in a low-pressure turbine passage are presented. The test section geometry is designed to simulate the effects of unsteady wakes resulting from rotor-stator interaction upon laminar-to-turbulent transition in turbine blade boundary layers and separated flow regions over suction surfaces. Single-wire, thermal anemometry techniques are used to measure time-resolved and phase-averaged, wall-normal profiles of velocity, turbulence intensity and intermittency at multiple streamwise locations over the turbine airfoil suction surface. The Reynolds number based on suction surface length and stage exit velocity is 50,000. This study compares a previously documented base case flow having an approach flow turbulence intensity of 2.5 percent and a wake passing Strouhal number of 0.792 to two additional cases: one having an increased rod spacing case having a wake passing Strouhal number of 0.396, and another having an elevated approach flow turbulence intensity of 10 percent. From these data, the effects of increased rod spacing and elevated FSTI upon transition and separation processes in the near-wall flow are documented. The results show that a decreased wake passing Strouhal number results in an earlier separation with a larger separation bubble, while the elevated FSTI results in earlier separation, but with a shorter, thinner, separation bubble. The data and animations are included in an accompanying CD–ROM.

14. SUBJECT TERMS

Turbomachinery; Transition; Turbulence; Boundary layers; Turbulent spots; Heat transfer; Unsteady flow; Compressors; Turbines; Hot wire anemometry; Wakes; Low pressure turbine; Separation; Intermittency

15. NUMBER OF PAGES

189

16. PRICE CODE

17. SECURITY CLASSIFICATION OF REPORT	18. SECURITY CLASSIFICATION OF THIS PAGE	19. SECURITY CLASSIFICATION OF ABSTRACT	20. LIMITATION OF ABSTRACT
Unclassified	Unclassified	Unclassified	